Curso 2012/13
CIENCIAS Y TECNOLOGÍAS/8
I.S.B.N.: 978-84-15910-66-4

PEDRO ÁNGEL SALAZAR CARBALLO

Fabricación, optimización y caracterización «in vitro» e «in vivo» de biosensores amperométricos enzimáticos para determinar metabolitos energéticos (glucosa y lactato) en el sistema nervioso central

Directores
JOSÉ LUIS GONZÁLEZ MORA
ROBERT D. O'NEILL

SERVICIO DE PUBLICACIONES
UNIVERSIDAD DE LA LAGUNA

SOPORTES AUDIOVISUALES E INFORMÁTICOS
Serie Tesis Doctorales

A mi familia y amigos por darme su amistad y cariño.

Gracias a Miriam por abrirme la puerta.

Gracias a José Luis por dejarme entrar.

Gracias a Aydam y Nayma por haber nacido.

Agradecimientos:

Ahora, que reviso mi andadura y el trabajo realizado en los últimos años, me considero un hombre afortunado al haber dedicado todo este tiempo a la investigación, una de mis grandes pasiones. Sin duda, el afán por descubrir lo desconocido y el espíritu de superación me han ayudado en el desarrollo de la presente tesis. No siempre fue fácil, especialmente durante los primeros años, cuando todo era nuevo y la experiencia práctica y las publicaciones eran escasas. No imaginaba lo duro que era empezar un proyecto desde cero, donde el ensayo y error eran una tónica diaria. Me costó empezar y coger el impulso. Yo que estaba acostumbrado a trabajar con unidades bastante grandes: kg m^{-2} d^{-1}, Km^2, etc., me vi de repente trabajando con fibras de carbono de poco más de unas micras y haciendo craneotomías. Todavía recuerdo las conversaciones con José Luis cuando le mostré algunas publicaciones sobre un tinte (Azul de Prusia) que podía ayudarnos a detectar el peróxido de hidrógeno a potenciales inferiores a los empleados en el ámbito neuroquímico, y que podía sacarnos del punto muerto en el que nos encontrábamos hacía un tiempo. Sin duda, fue un acierto seguir por este camino, y fruto de esta idea loca hoy puedo presentar la presente memoria para obtener el grado de Doctor. Sin embargo, el tiempo dirá si hemos acertado, y si nuestros colegas creen oportuno utilizar los protocolos y aproximaciones aquí descritas.

Durante este período he podido cumplimentar mi formación como químico. Los conocimientos adquiridos en el ámbito de los biosensores, así como, la profundización en áreas tan diversas como la electroanalítica, neuroquímica y la fisiología me han ayudado a desarrollar la presente tesis, y sin duda son el fruto más preciado de estos años.

Sin duda alguna la curiosidad, las ganas de a prender y el espíritu de superación han sido las principales herramientas para finalizar la presente tesis. Sin embargo, parafraseando a uno de los mejores científicos de la historia (Sir Isaac Newton):"si he llegado tan lejos, es porque me he subido a hombros de gigantes". Han sido innumerables los artículos y revisiones leídas durante este tiempo, muchas más de las que aparecen en la bibliografía. Siempre ha habido un hueco para un "paper" en el coche, en la cama, en la cocina, en el salón, dando biberones (muchas veces rozando lo enfermizo). Muchos han sido los autores, si bien, le tengo especial cariño a algunos (Wang, Palleschi, Ricci, Moscone, Karyakin, Lowry, O'Neill, Pingarrón y colaboradores, Senthil-Kumar, Vittal). Gracias a todos ellos, sin su ayuda nunca habría podido realizar la presente tesis.

Gracias también a todos los contribuyentes, porque parte de la financiación de esta tesis ha salido de sus bolsillos.

Gracias a Informática y Equipamientos Médicos de Canarias S.L. por su apoyo a la investigación y por darme la oportunidad de poner en práctica los conocimientos adquiridos durante la elaboración de la presente tesis.

Gracias a Miriam por estar a mi lado y ayudarme a dar el salto, sé que los primeros años fueron difíciles, pero sin duda ha valido la pena. Gracias también por cederme parte de tu motivo de tesis.

Gracias a José Luis por acogerme en su laboratorio y por tratarme como a uno más desde el principio. Gracias también por darme carta blanca en la dirección que ha tomado la presente tesis y por poner a mi alcance los medios necesarios para finalizarla con éxito. He aprendido mucho estos años a su lado, y me ha brindado la oportunidad de aplicar mis conocimientos y mi entusiasmo a un área tan apasionante como la neuroquímica.

Thanks Robert, what started as a simple contact to resolve technical issues it became a fruitful collaboration. I've learned a lot over during these years and you've been my confidant scientist. Thanks for hundreds of mails and manuscript corrections (many of them during the holidays or during weekends). Your lessons and advice have always been very valuable. Now I know that I have a friend in the Emerald Island.

Gracias a Rossany, Meli, Ingrid, Francisco, Carlos, Óscar, Antonio y Cristian por su amistad y ayuda durante estos años.

Gracias a Pedro por sus numerosas conversaciones, consejos y palabras de ánimo.

Gracias a Bea, Pablo y Adrián (Departamento de Inorgánica) por ayudarme con los espectros de infrarrojos.

Gracias a José Luis y a Jonathan (Departamento de Química-Física) por dejarme utilizar la espectroscopía de impedancia.

Gracias a Tere y a María Jesús (Departamento de Analítica) por ser mis directoras de DEA y de Máster respectivamente.

Gracias a Jose Salazar, por tu amistad y por ser un ejemplo a seguir, tanto en el aspecto científico como en lo personal.

Gracias a Nemesio Pérez y Pedro Hernández por darme la oportunidad de hacer ciencia desde el segundo año de carrera y acogerme en su grupo al finalizar la misma.

Gracias también a mis antiguos compañeros del ITER (Gladys, Dácil, Noemi, Inés, Pablo, Rayco, Pepe, David, Eleazar…) con quienes compartí tan buenos momentos.

Gracias (Miriam, Rossany, José Luis y Pedro) por los consejos y revisiones de la presente tesis.

Muchas veces uno mismo es su peor crítico pensando que podía haber hecho más. Si bien es verdad que todo tiene un principio y un fin, y me he hecho de rogar hasta tener las publicaciones que he considerado suficientes para presentar esta humilde tesis. Ha llegado la hora de seguir el consejo que llevan dándome hace algún tiempo y cerrar este capítulo en mi vida.

Espero que en un futuro cercano pueda concluir las publicaciones que se han quedado en el tintero, y que los nuevos proyectos en los que estamos trabajando en el grupo den su fruto. Si algo he aprendido durante estos años es que nada cae del cielo, y que lo que obtienes está ligado al esfuerzo, a la astucia y al trabajo realizado, bueno algo de suerte siempre hay que tener.

Nuevamente, gracias a todos los que me han ayudado durante esta etapa. Espero que la presente tesis y las publicaciones que contienen puedan ayudar a otras personas que como yo disfrutan haciendo ciencia y no se quede en una estantería cogiendo polvo.

psalazar

Glosario de abreviaturas

^{13}C-NMR	.....	resonancia magnética nuclear de C-13
^{1}H-NMR	.....	resonancia magnética nuclear de protón
5-HT	.....	serotonina
A/P	.....	antero/posterior
AA	.....	ácido ascórbico
ADN	.....	ácido desoxirribonucleico
AFM	.....	microscopía de fuerzas atómica
ANLS	.....	Astrocyte-Neuron Lactate Shuttle
ATP	.....	adenosín trifosfato
AU	.....	ácido úrico
BHE	.....	barrera hematoencefálica
BSA	.....	serum de albumina bovina
C_{dl}	.....	capacidad de la doble capa
CFE	.....	electrodo de fibra de carbono
CMC	.....	concentración miscelar crítica
CNT	.....	nanotubos de carbono
CPA	.....	Amperometría a Potencial Constante
CPEs	.....	electrodos de pasta de carbono
CTA^+	.....	catión cetiltrimetilamonio
CTAB	.....	bromuro de cetiltrimetilamonio
CV	.....	Voltametría Cíclica
D/V	.....	dorsal/ventral
DA	.....	dopamina
DOPAC	.....	ácido 3,4-dihidroxifenilacético
DPV	.....	Voltamperometría Pulsada Diferencial
EIS	.....	espectroscopía de impedancia
ES	.....	complejo enzima-sustrato
FAD	.....	flavín adenín dinucleótido oxidado
$FADH_2$	.....	flavín adenín dinucleótido reducido
FCV	.....	Voltametría Cíclica Rápida
FIA	.....	Análisis por Inyección de Flujo
FMN	.....	flavín mononucleótido oxidado
$FMNH_2$	.....	flavín mononucleótido reducido
***f*MRI**	.....	resonancia magnética funcional
FSC	.....	flujo sanguíneo cerebral
GADPDH	.....	gliceraldehído-3-fosfato deshidrogenasa
GLAST (EAAT1)	.....	transportador de glutamato (tipo 1)
GLT-1 (EAAT2)	.....	transportador de glutamato (tipo 2)

GLUT1	.....	transportadores de glucosa (tipo 1)
GLUT3	.....	transportadores de glucosa (tipo 3)
GLUTs	.....	transportadores de glucosa
Gox	.....	glucosa oxidasa
h	.....	parámetro de Hill
H1000	.....	clorotrifluoroetileno (1000 cSt)
H200	.....	clorotrifluoroetileno (200 cSt)
H700	.....	clorotrifluoroetileno (700 cSt)
HV	.....	ácido homovanílico
i	.....	corriente
IUPAC	.....	Internacional Union of Pure and Applied Chemistry
J	.....	densidad de corriente
J_{max}	.....	densidad de corriente máxima
Kel-F	.....	policlorotrifluoroetileno
$\mathbf{K_M}$	.....	constante de Michaelis-Menten
$\mathbf{K_M(gluc)}$	.....	constante de Michaelis-Menten para la glucosa
$K_M(O_2)$	.....	constante de Michaelis-Menten para el oxígeno
Kps	.....	constante del producto de solubilidad
LDH1	.....	lactato deshidrogenasa (tipo 1)
LDH5	.....	lactato deshidrogenasa (tipo 5)
Lox	.....	lactato oxidasa
M/L	.....	medio/lateral
MCT	.....	transportador de monocarboxilatos
MCT1	.....	transportador de monocarboxilatos (tipo 1)
MCT2	.....	transportador de monocarboxilatos (tipo 2)
MCT4	.....	transportador de monocarboxilatos (tipo 4)
m-LDH	.....	lactato deshidrogenasa (mitocondrial)
***m*-PD**	.....	meta-fenilendiamina
$\mathbf{NAD^+}$	.....	nicotinamida adenín dinucleótido (oxidado)
NADH	.....	nicotinamida adenín dinucleótido (reducida)
NADPH	.....	nicotinamida adenina dinucleótido fosfato (reducida)
NE	.....	norepinefrina
NIRs	.....	Infrarrojo cercano
NO	.....	óxido nítrico
NPV	.....	voltametría normal pulsada
***o*-PD**	.....	orto-fenilendiamina
PANI	.....	polianilina
PB	.....	Azul de Prusia
PBS	.....	tampón fosfato (0.1M NaCl;0.027M KCL; pH=7.4)
PCTFE	.....	policlorotrifluoroetileno
PDMS	.....	polidimetilsiloxanos

PEI	.....	polietilenimina
PET	.....	tomografía por emisión de positrones
PG	.....	Verde de Prusia
PIM	.....	polímeroi de impresión molecular
PLL	.....	polilisina
P*m*PD	.....	meta-polifenilendiamina
PNA	.....	ácido nucleico peptídico
P*o*PD	.....	orto-polifenilendiamina
***p*-PD**	.....	para-fenilendiamina
P*p*PD	.....	para-polifenilendiamina
PPY	.....	popipirrol
PW	.....	Blanco de Prusia
$\mathbf{R_{ct}}$	.....	resistencia a la transferencia de carga
RL	.....	rango lineal
$\mathbf{R_S}$	.....	resistencia de la disolución
S	.....	sensibilidad analítica
SCE	.....	electrodo de calomelano saturado
SEGAI	.....	Servicio General de Apoyo a la Investigación
SEM	.....	microscopía electrónica de barrido
SGLTs	.....	co-transportadoras de Na^+ y glucosa
SNC	.....	sistema nervioso central
SPCE	.....	electrodos serigrafiados de pasta de carbono
TCA	.....	ciclo de los ácidos tricarboxílicos (ciclo de Krebs)
TCNQ	.....	tetracianoquinodimetano
TTF	.....	tetratiofulvaleno
ULL	.....	Universidad de La Laguna
VIS	.....	visible
VIS-Uv	.....	visible-ultravioleta
$\mathbf{V_{max}}$	.....	velocidad máxima de reacción
XRD	.....	difracción de rayos X
YSI	.....	Yellow Spring Instruments
Z_{im}	.....	impedancia imaginaria
Z_{re}	.....	Impedancia real
$\mathbf{Z_w}$	.....	impedancia de Warburg

Índice de tablas de figuras

Tabla 2.1.- Criterios de clasificación de los biosensores…….…….....**31**

Figura 1.1- Acoplamiento neurovascular. La posición intermedia de los astrocitos entre los vasos sanguíneos y las neuronas, evidencia la importancia que tienen dichos astrocitos en la regulación neurometabólica, permitiendo el suministro adecuado de nutrientes en función de la actividad neuronal (fuente: http://www.genomasur.com/BCH/BCH_libro/capitulo_09.htm)..….....…….....**6**

Figura 1.2.- Distribución de los transportadores de glucosa (GLUTs) y monocarboxilatos (MCT) en el cerebro. El alto grado de compartimentación cerebral favorece la expresión diferenciada de dichos transportadores (adaptada de Simpson et al., 2007)…….…….....**8**

Figura 1.3.- Modelo metabólico clásico: la glucosa y el oxígeno son liberados desde el vaso sanguíneo. El oxígeno difunde libremente a través de los tejidos, sin embargo, la glucosa debe atravesar cada uno de los compartimentos mediante transporte GLUTs específicos. En este modelo la glucosa es el combustible primario, tanto para las neuronas como para los astrocitos, siendo el lactato un mero subproducto metabólico que es desechado al intersticio. Se asume que las neuronas son capaces de controlar el suministro metabólico en función de su estado..…….....**10**

Figura 1.4.- La glucosa posee múltiples facetas metabólicas: puede ser almacenada como glucógeno para actuar de reserva energética, puede ser usada directamente para producir energía vía glicólisis o mediante el TCA, además, está conectada vía TCA en la síntesis de algunos neurotransmisores y sus intermediaros, también puede ser empleada en la biosíntesis de nucleótidos y NAPDH……...…….....**11**

Figura 1.5.- Hipótesis (ANLS) planteada por Pellerin y Magistretti (Pellegrin, 2003): La secuencia de eventos empezaría por la captación y regeneración del glutamato liberado en la hendidura sináptica (ciclo glutamato-glutamina), proceso acompañado por la entrada masiva de iones Na^+ al astrocito. Dicho mecanismo activaría la bomba de Na^+/K^+ produciendo un considerable descenso de las reservas energéticas astrocitarias. Para compensar dicha pérdida se activaría la glicólisis y/o glicogenolisis y el transporte de glucosa (GLUT1 45 kDa). Una consecuencia directa de la glicólisis astrocitaria es el aumento de piruvato y NADH citosólico. Como consecuencia podrían activarse varios procesos: (1) el TCA acoplado a la fosforilación oxidativa, generando ATP y regeneranto el NAD^+; (2) conversión de piruvato a lactato (LDH5), regenerando el NAD^+. Posteriormente, el lactato es transportado al intersticio vía MCT1 y MCT4. Una vez en el intersticio los transportadores MCT2 introducirían el lactato al interior de la neurona que seguidamente lo transformara a piruvato (LDH1) e incorpora al TCA acoplado a la fosforilación oxidativa……...…….....**16**

Figura 1.6.- Esquema de la hipótesis planteada por Cerdán (Cerdán et al., 2006). Dicho modelo enfatiza el transporte bidireccional que tiene el piruvato y el lactato entre la neurona y el astrocito. En dicho modelo existen dos fuentes de piruvato en la neurona y en la glía derivados del metabolismo de la glucosa o de los monocarboxilatos. La lanzadera lactato/piruvato es capaz de transferir continuamente lactato desde el astrocito a la neurona vía MCT, siendo metabolizado finalmente por la LDH1. Las altas concentraciones citosólicas de lactato en la neurona inhibe la glicólisis ya que disminuyen drásticamente los niveles de NAD^+ necesarios para la GAPDH, favoreciendo finalmente la oxidación del lactato extracelular. Posteriormente el piruvato es transportado hacia la glía, vía MCT, preparándose para un nuevo ciclo. ……**18**

Figura 1.7.- Esquema de la hipótesis planteada por Schurr (Schurr, 2006): La glicólisis citosólica produce piruvato, que posteriormente es reducido a lactato regenerando los niveles de NAD^+ citosólico. Posteriormente, dicho lactato es transportado, vía MCT, a la mitocondria donde es convertido en piruvato y entra en el TCA…….....**20**

Figura 1.8.- Comparación de las dimensiones de los electrodos de fibra de carbono (CFE), sonda de microdiálisis y el rango de tamaño de las neuronas. ……**26**

Figura 2.1.- Esquema de las partes fundamentales de un biosensor, así como el acoplamiento entre distintos sistemas de reconocimiento y sistemas de transducción……...**29**

Figura 2.2.- Fenómeno de la resonancia del plasmón de superficie. La resonancia del plasmón de superficie se produce por la reflexión total del haz de luz incidente al interaccionar con los plasmones por lo que se observa una reducción de la intensidad de la luz (fuente: Pérez, 2007)…….....**35**

Figura 2.4.- Esquema de las reacciones que ocurren en un biosensor de 1ª generación, basado en la detección amperométrica del H_2O_2 generado enzimáticamente……....**38**

Figura 2.5.- Esquema de las reacciones que ocurren en un biosensor de 2ª generación…….....**39**
Figura 2.6.- Esquema de las reacciones que ocurren en un biosensor de 3ª generación……...…..**40**
Figura 2.7- Métodos de inmovilización empleados en el desarrollo de biosensores, (adaptada de Sassolas et al., 2012)…….....……..……....**41**

Figura 2.8- Enlaces covalentes empleados sobre una superficie previamente aminada por acoplamiento mediante: (A) carboiimida (B) glutaraldehido (adaptada de Sassolas et al., 2012)…..……...……....**44**

Figura 3.1- Estructura zeolítica (cúbica centrada en las caras) propuesta para el PB (adapta a partir de: http://mslab.polymer.pusan.ac.kr/english/research.html). ..……..……..……..…….....**48**

Figura 3.2.- Esquema de reacciones acopladas en un biosensor de 1ª generación de glucosa, basado en la detección amperométrica del H_2O_2 con Azul de Prusia...……...……...…....**54**

Figura 3.3.- Histograma de publicaciones científicas referidas a las palabras claves: Prusian Blue y Prussian Blue-biosensors (fuente: http://www.sciencedirect.com). ……....…….…....**55**

Figura 5.1.- Fórmula (fuente: Wikipedia) y estructura del Nafion donde se observan los canales iónicos por donde existe libre flujo de moléculas de agua y cationes (fuente: http://www.intellectualism.org/questions/QOTD/dec03/20031209.php)….....**63**

Figura 5.2.- Posibles estructuras propuestas para el PoPD……...….....**66**

Figura 5.3.- a) Representación gráfica de la ecuación de Michaelis-Menten. **b)** Linearización de la ecuación de Michaelis-Menten por el método propuesto por Lineweaver-Burk……...…….……...**73**

Figura 5.4.- Esquema de un biosensor amperométrico enzimático de glucosa construido a partir de un microelectrodo de fibra de carbono de 8 µm de diámetro: PB (Azul de Prusia), Gox (glucosa oxidasa). La última capa de PoPD (poli-o-fenilendiamida), así como el PEI y el Nafion no han sido dibujados para facilitar la visualización del esquema…....……..……..…....**79**

Figura 5.5.- a) Variación del potencial aplicado durante CV **b)** Voltamperograma cíclico obtenido al ciclar un electrodo en presencia de un par redox…..…….....**92**

Figura 5.6.-a) Circuito de Randles, equivalente a una celda electroquímica convencional. **b)** Diagrama de Nyquist……...……...……...…....**97**

Índice

0.-Motivación…….. 2
1.-Metabolismo cerebral…….. 4
1.1-Zona de estudio: el sistema nervioso central…….. **4**
1.2.-Metabolismo cerebral: Glucosa……... **6**
1.3.-Metabolismo cerebral: Lactato……..... **12**
1.3.1.-Lanzadera de lactato: *Astrocite-Neuron-Lactate Shuttle Hypotesis*…….. **12**
1.3.2.-Nuevas hipótesis sobre el uso neuronal del lactato……... **17**
1.3.2.1.-Acoplamiento redox y actividad metabólica: *The redox-switch/redox-coupling hypothesis*…… **17**
1.3.2.2.-Transporte mitocondrial del lactato……..... **19**
1.4.- Metabolismo cerebral: técnicas instrumentales…… **21**
1.4.1.-Microdiálisis…… **22**
1.4.2.-Voltametría *in vivo*……... **22**
1.4.3.-Voltamperometría *vs.* Microdiálisis…….. **24**

2.- Biosensores…….. 28
2.1.-Definición……... **28**
2.2.-Los orígenes……... **29**
2.3.-Clasificación de los biosensores…….. **31**
2.3.1.-Clasificación en función del elemento de reconocimiento…... **32**
2.3.1.1.-Biosensores biocatalíticos……... **32**
2.3.1.2.-Biosensores de bioafinidad…… **33**
2.3.2.-Clasificación en función del tipo de transductor…… **33**
2.3.2.1.-Electroquímicos…… **34**
2.3.2.2.-Másicos, piezoeléctrico o acústicos……... **34**
2.3.2.3.-Térmicos……... **34**
2.3.2.4.-Ópticos…….. **35**
2.4.-Biosensores electroquímicos…… **35**
2.4.1.-Potenciométricos…… **36**
2.4.2.-Conductimétricos…….…….. **37**
2.4.3.-Amperométricos…… **37**
2.4.3.1.-Clasificación de los biosensores amperométricos…….. **37**
2.4.3.1.1.-Biosensores de 1ª generación…….. **37**
2.4.3.1.2.-Biosensores de 2ª generación……..... **39**
2.4.3.1.3.-Biosensores de 3ª generación……. **40**
2.5.-Técnicas de inmovilización enzimática…… **41**
2.5.1.-Métodos de inmovilización física……..... **42**
2.5.1.1.-Adsorción……..... **42**
2.5.1.2.-Atrapamiento……..... **42**
2.5.2.-Métodos de inmovilización química……..... **44**

2.5.2.1.-Enlace covalente……..... **44**
2.5.2.2.-Capa intermedia……..... **45**
2.5.2.3.-Entrecruzamiento…… **45**

3.-El Azul de Prusia…… 46
3.1.-Deposición de Azul de Prusia…… **50**
3.2.-Estabilidad de Azul de Prusia frente al pH…….. **51**
3.3.-Electrodeposición de PB en presencia de surfactantes catiónicos…. **52**
3.4.-Biosensores basados en Azul de Prusia…….. **54**

4.-Objetivos…….. 58

5.-Materiales y métodos…….... 61
5.1.-Reactivos…….. **61**
5.1.1.-Microelectrodos de fibra de carbono…… **61**
5.1.2.-Nafion……..... **62**
5.1.3.-Polietilenimina…… **63**
5.1.4.-Poli-*o*-fenilendiamina…….. **64**
5.1.5.-Glucosa oxidasa (*Gox*)……..... **66**
5.1.6.-Lactato oxidasa (*Lox)*…… ……. **67**
5.1.7.-Interferencias: El ácido ascórbico como prototipo de interferente endógeno……... **68**
5.2.- Enzimas y mecánica enzimática…… **69**
5.2.1.-Cálculo de los parámetros cinéticos enzimáticos……... **74**
5.2.2.-Déficit de oxígeno……... **75**
5.3.-Fabricación de los microbiosensores…… **78**
5.3.1.-Fabricación de los microelectrodos de fibra de carbono…….. **78**
5.3.2.-Modificación de los microelectrodos de fibra de carbono….. **78**
5.3.2.1.-Disminución del potencial de detección del H_2O_2……. **80**
5.3.2.2.-Reducción del déficit de oxígeno…….. **80**
5.3.2.3.-Incremento de la carga enzimática……..... **83**
5.3.2.4.-Mejora de la selectividad frente a los interferentes……..... **83**
5.3.2.5.-Optimización de las propiedades de biocompatibilidad…... **84**
5.3.3.-Microelectrodos centinela…… **86**
5.3.4.-Microelectrodos sensibles a oxígeno……..... **87**
5.4.-Voltamperometría……. **87**
5.4.1.-Procesos farádicos y no farádicos…… **87**
5.4.2.-Fenómenos de transporte…….. **89**
5.4.3.-Transferencia electrónica……... **90**
5.4.4.- Técnicas voltamperométricas……... **91**
5.4.4.1.-Voltamperometría a potencial constante……. **91**
5.4.4.2.-Voltamperometría cíclica.……..... **92**
5.5.- Otras técnicas instrumentales……. **94**

5.5.1.-Microscopía electrónica de barrido…….. **95**
5.5.2.-Espectroscopía de impedancia……. **96**
5.6.-Calibrado *in vitro*…….. **98**
5.7.-Animales y método quirúrgico…….. **99**
5.8.-Registro *in vivo* …… **100**
5.8.1.-Implantación del sistema electroquímico……... **100**
5.8.2.-Estudio farmacológico……... **101**
5.8.3.-Estimulación eléctrica…… **101**
5.9.-Instrumentación electroquímica y tratamiento de datos…… **102**

6.-Resultados y discusiones…… 104

6.1.-Desarrollo de un microelectrodo de fibra de carbono modificado con PB como transductor selectivo para biosensores de 1ª generación, aplicaciones en el ámbito neuroquímico…… **104**

6.2.-Microbiosensores sensibles a glucosa, basados en microelectrodos de carbono modificados con PB: Aplicaciones *in vivo* en el sistema nervioso central…… **108**

6.3.-Aplicaciones fisiológicas de microbiosensores sensibles a glucosa basados en microelectrodos de carbonos modificados con PB……... **112**

6.4.-Electrodeposición de PB sobre electrodos de carbono mediada por surfactantes: mejoras en la estabilidad, en las propiedades electroquímicas y aplicación en microbiosensores sensibles a lactato…. **117**

6.5.-Optimización y caracterización de electrodos serigrafiados de carbono modificados con PB en presencia de surfactantes: detección de H_2O_2 a bajos potenciales……... **122**

6.6.-Desarrollo de un microbiosensor basado en fibras de carbono modificado con PB para medir lactato en el espacio extracelular del tejido cerebral…… **127**

7.-Conclusiones…… 133
8.-Trabajo futuro……... 136
9.-Anexo I: Publicaciones…….. 138
10.-Anexo II: Otras publicaciones……..... 203
11.-Bibliografía…… 223

INTRODUCCIÓN

0.- Motivación

Durante la última década se ha generado un importante debate sobre la regulación de la respuesta metabólica del cerebro frente a la actividad neuronal. Las células cerebrales son altamente dependientes y necesitan un suministro continuo de energía. Todos los datos disponibles sugieren que la glucosa, bajo condiciones fisiológicas normales, es el principal combustible energético. Debido a que el cerebro tiene muy pocas reservas, necesita un suministro vascular continuo de glucosa y oxígeno. Así, a los 20 segundos de ausencia de flujo sanguíneo cerebral (FSC) se pierde el conocimiento; la glucosa, el glucógeno y el ATP existentes en el medio son consumidos entre 3 y 5 minutos, pudiéndose producir lesiones neuronales irreversibles en el caso de no revertir el proceso.

Históricamente, el lactato se había considerado un subproducto metabólico derivado de la glucólisis o un signo de hipoxia (derivado del metabolismo anaeróbico celular). Sin embargo, en los últimos 20 años se han publicado una gran cantidad de trabajos que indican que el lactato puede ser producido en muchos tejidos bajo condiciones aeróbicas. Así, algunos autores señalan que el lactato podría ser utilizado como combustible complementario, e incluso, han sugerido que puede ser el substrato energético preferido por las neuronas durante estados de activación. Basándose en estos resultados, se han planteado nuevas hipótesis sobre el metabolismo neuronal, el acoplamiento neurovascular, etc. *Pellerin* y *Magistretti* (1994) han propuesto una hipótesis "*Astrocyte-Neuron Lactate Shuttle*" (ANLS) según la cual la activación neuronal producida por el glutamato (principal neurotransmisor y responsable del 90% de las sinapsis) conduce a la captación de glucosa por parte de los astrocitos, posteriormente su glucólisis genera lactato que es exportado al compartimiento extracelular donde es captado por las neuronas. Esta idea ha dividido a la comunidad científica en dos

escuelas y ha generado un intenso debate durante los últimos 20 años. La mayor parte de las evidencias de ANLS se basan en experimentos *in vitro*, en la disposición espacial de la glía entre los vasos sanguíneos y las neuronas, en la presencia de algunas enzimas y en la expresión de ciertos transportadores específicos.

El desarrollo de nuevos métodos para cuantificar y estudiar la evolución de glucosa y lactato de forma más precisa y localizada, así como, su relación con el consumo de oxígeno y el FSC podría ayudarnos a entender mejor dichos procesos neurometabólicos, teniendo en cuenta que todos los mecanismos que acompañan a la sinapsis ocurren en una escala temporal muy corta, milisegundos.

En las últimas décadas, los microbiosensores han resultado ser un instrumento con un gran potencial en la investigación biomédica y en aplicaciones neurometabólicas. Su reducido tamaño, así como, su alta resolución temporal y espacial los convierten en una alternativa a otras técnicas más costosas y con un alto grado de especialización.

Es por ello, que la presente memoria está orientada hacia la construcción y caracterización de microbiosensores amperométricos sensibles a la glucosa y al lactato. Dispositivos lo suficiente pequeños, sensibles y selectivos para ser empleados en animales de experimentación para cuantificar concentraciones basales del analito de interés en el espacicio extracelular. Y que a posteriori, puedan ser empleados en estudios neurometabólicos, farmacológicos, etc., tanto a nivel de experimentación animal como humana.

1.-Metabolismo cerebral

1.1- Zona de estudio: el sistema nervioso central

El sistema nervioso central (SNC), formado por el encéfalo y la médula espinal, posee una naturaleza heterogénea conformada por una multitud de células más o menos especializadas. El cerebro, el cual supone un 80%de la masa del encéfalo y un 2-3% del peso corporal, recibe el 15% del flujo cardíaco en reposo (*Sokoloff, 1960; Guyton y Hall, 2011*). A su vez, es uno de los órganos con mayor demanda energética, gastando el 20% del oxígeno y el 25% de la glucosa consumida por el organismo (*Siesjo, 1978; Fox et al., 1988; Clarke y Sokoloff 1999*). Debido a este consumo y a que el cerebro posee pocas reservas energéticas, la regulación neurometabólica debe ser rápida y eficaz, generalmente, mediante el correcto suministro de metabolitos a través del FSC.

El FSC en humanos presenta un valor medio de 750 ml/min (57 ml/100 g/min) (*Serrá et al., 2005*). A presiones normales está regulado casi exclusivamente por mecanismos intrínsecos locales, miógenos y metabólicos, permitiendo así una tasa de flujo constante (*Fox, 2004*). Al igual que sucede en otros tejidos del organismo el FSC está muy relacionado con el metabolismo tisular circundante. Según se cree, varios son los factores metabólicos que contribuyen a la regulación del FSC: (1) concentración de CO_2, (2) pH, (3) concentración de O_2, (4) sustancias liberadas por los astrocitos (*Guyton y Hall, 2011*), (5) otros. Esta precisa regulación permite mantener un suministro continuado de glucosa y O_2, así como, la eliminación de productos metabólicos generados durante la actividad cerebral (CO_2 y H_2O).

En estado de reposo, el cerebro consume una considerable energía (10% de la glucosa en sangre), empleada en su mayor parte en mantener los potenciales de membrana celulares y las condiciones homeostáticas óptimas para una adecuada transmisión nerviosa. En términos comparativos el consumo energético del cerebro

podría ser comparado con el de una bombilla de 20 W (*McKenna et al., 2006*). Aproximadamente el 75% de dicha energía es consumida en procesos relacionados con la transmisión nerviosa (*ciclo glutamato-glutamina, potencial de acción, receptores postsinápticos, etc.)*, mientras que el 25% restante es empleada en funciones esenciales tales como: *síntesis y degradación proteica, estabilización de los gradientes eléctricos e iónicos transmembrana, transporte axoplasmático, intercambio de nucleótidos y lípidos*. (*McKenna et al., 2006*).

Cuando se estudia el funcionamiento del cerebro se suele enfocar desde una óptica neuronal. Las neuronas (~10^{11}) son células altamente excitables que permiten el procesamiento de información en el cerebro mediante la transmisión de señales eléctricas complejas, siendo así, la unidad funcional por excelencia. No obstante, más de la mitad del volumen cerebral está ocupado por células muy poco excitables, que pese a su elevado número, solo consumen entre un 15 y un 30% del balance energético total. Menospreciadas durante varias décadas, la neuroglía constituye la población mayoritaria, destacando en este grupo los astrocitos o astroglía. Su localización estratégica entre los vasos sanguíneos y las neuronas (**Figura 1.1**), así como, la expresión de receptores y transportadores específicos frente a ciertos neurotransmisores, ha llevado a postular su participación en la función metabólica y sináptica de las neuronas. Hoy en día, a parte de su papel homeostático se considera que son células que se comunican entre sí y con las neuronas de una manera dinámica y cooperativa (*Lòpez-Bayghen et al., 2007 Lòpez-Bayghen y Ortega, 2010*).

1.2.- Metabolismo cerebral: Glucosa

Años de investigación en el campo del metabolismo cerebral han culminado con la aceptación de algunas ideas que actualmente son difícilmente cuestionables, y que sin duda, han generado un gran debate dentro de la comunidad científica. Dichas ideas se resumen a continuación: (1) La glucosa es inequívocamente el combustible energético y el único substrato disponible para sustentar la actividad neuronal (*Siesjo, 1978*). (2) Además, se asume que la mayor parte de la glucosa empleada se consume por vía oxidativa, tanto en condiciones basales como en estados activados (*Sokoloff et al, 1977*). (3) El consumo energético es predominantemente debido a la actividad neuronal (80-95%) frente a la actividad de otras células como la glía (5-20%) (*McKenna et al., 2006*). (4) El consumo y suministro de glucosa está perfectamente acoplado a la actividad sináptica (*Sokoloff et al, 1977; Barret et al., 2003; McKenna et al., 2006*).

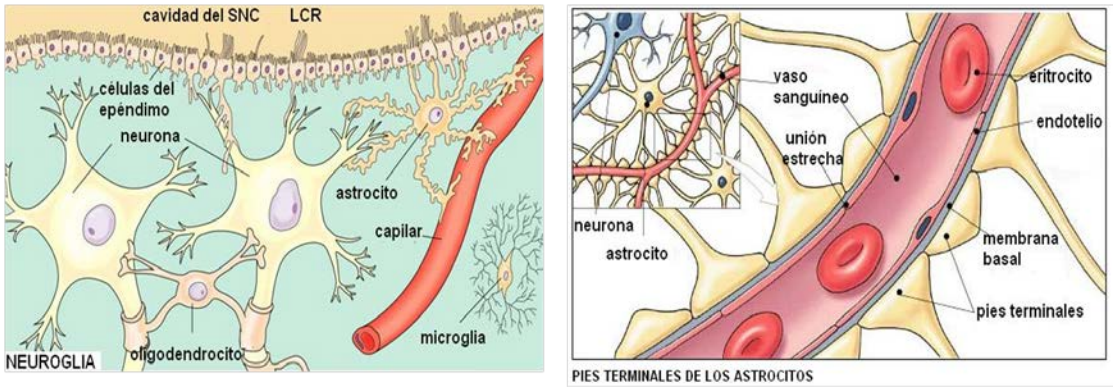

Figura 1.1- *Acoplamiento neurovascular. La posición intermedia de los astrocitos entre los vasos sanguíneos y las neuronas, evidencia la importancia que tienen dichos astrocitos en la regulación neurometabólica, permitiendo el suministro adecuado de nutrientes en función de la actividad neuronal (fuente: http://www.genomasur.com/BCH/BCH_libro/capitulo_09.htm).*

En este modelo, la energía consumida durante los procesos de activación neuronal proviene de la glucosa y del O_2 liberados directamente desde los vasos sanguíneos hacia el espacio extracelular (*intersticio*). De esta manera, se propone un conjunto de mecanismos (*metabólicos* y *miógenos*) de autorregulación energética (vía

neurotransmisores y *vasodilatadores*) que permiten a las neuronas disponer de un suministro energético acorde a sus necesidades funcionales. Un aumento de la actividad neuronal produce y libera neurotransmisores y sustancias vasoactivas que conducen finalmente a un incremento del FSC, y por ende, a un incremento en la concentración y liberación de metabolitos energéticos. Es decir, existe un acoplamiento dinámico entre la actividad neural y el FSC.

Si bien, el transporte de O_2 es por simple difusión a través de los tejidos y de las membranas celulares, el transporte de glucosa en las células de los mamíferos está facilitado por dos familias de proteínas: (1) transportadores de glucosa, GLUTs (*Joost y Thorens, 2001; Joost et al., 2002*) y (2) co-transportadores de Na^+ y glucosa, SGLTs (*Wood y Trayhurn, 2003*). Los GLUTs son principalmente expresados en: (1) el SNC (vaso, células gliares, neuronas) y (2) los eritrocitos, favoreciendo el paso de glucosa por transporte pasivo, sin consumo de energía y a favor del gradiente de concentración (*Joost y Thorens, 2001; Joost et al., 2002; Bermúdez et al., 2007*). Dicho mecanismo imposibilita la acumulación celular de glucosa, y en el caso de acumularla debe hacerse en su forma polimérica (*glucógeno*), únicamente en los astrocitos.

En la actualidad se conocen 13 transportadores GLUTs (*Joost y Thorens, 2001; Wood y Trayhurn, 2003*), sin embargo, los transportadores GLUT1 y GLUT3 son expresados mayoritariamente en el SNC (**Figura 1.2**) (*Rayner et al., 1994; Vannucci et al., 1997; Vannucci et al., 1998*). La capacidad de transportar glucosa de los GLUTs depende de varios factores, principalmente: (1) expresión y concentración en los distintos tejidos y (2) propiedades cinéticas intrínsecas.

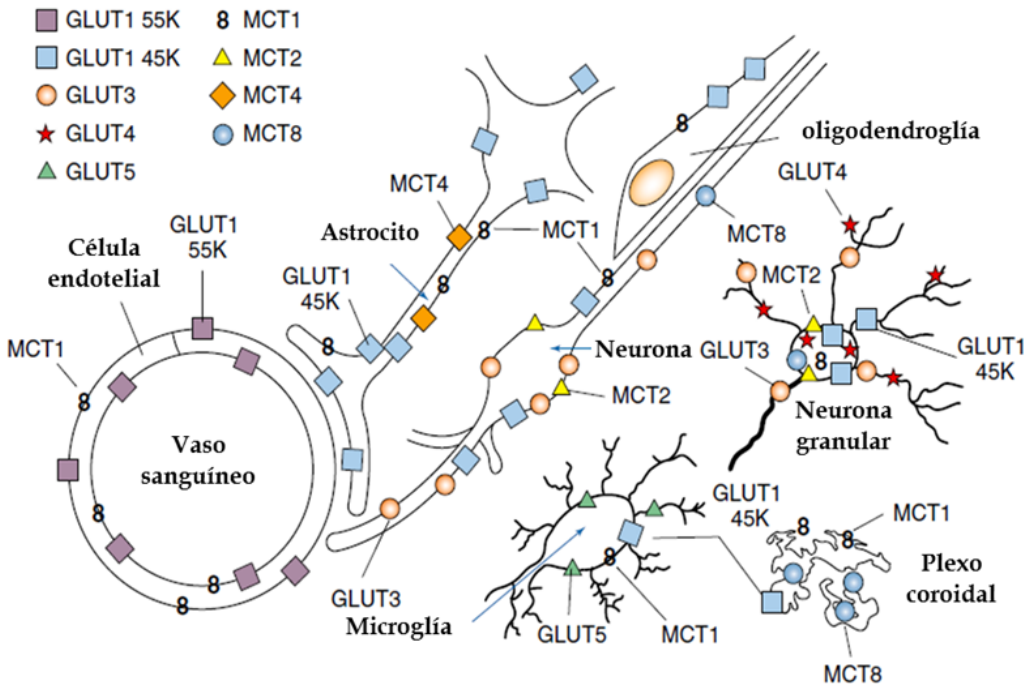

Figura 1.2.- *Distribución de los transportadores de glucosa (GLUTs) y monocarboxilatos (MCT) en el cerebro. El alto grado de compartimentación cerebral favorece la expresión diferenciada de dichos transportadores (adaptada de Simpson et al., 2007).*

Para acceder al parénquima cerebral la glucosa requiere atravesar las membranas celulares del endotelio, que en el SNC constituyen la *barrera hematoencefálica* (BHE) (*Cremer et al., 1979; Bradbury, 1993*), siendo en última instancia el transporte mediado por los GLUTs (**Figura 1.3**). Cada una de las diferentes isoformas de los GLUTs tienen expresión y características cinéticas propias, adaptadas a las necesidades metabólicas de los distintos tejidos del organismo (*Doege et al., 2000*). La isomorfa GLUT1 presenta dos conformaciones proteicas diferentes. Ambas son glicoproteínas de 45 o 55 kDa con doce dominios transmembrana en estructura α hélice (*Baldwin y Lienhard, 1989*). La GLUT1 (55 kDa), altamente glicosilada, se encuentra en las células endoteliales que conforman la BHE (*Harik et al, 1990; Farrell y Pardridge, 1991; Maher et at., 1993*), mientras que la isoforma de GLUT1 (45 kDa) parece estar asociada a las células gliales o astrocitos (*Bondy et al., 1992; Maher et al, 1993*). Por último, el GLUT3 se encuentra mayoritariamente expresado en las neuronas (*Maher et al. 1993; Nagamatsu et al., 1993*).

Ambos transportadores GLUT1 y GLUT3, poseen una alta afinidad por la glucosa (*Bermúdez et al., 2007*), con una K_M = 1-2 mM, muy por debajo de la concentración de glucosa sanguínea (~ 5 mM). Dichos transportadores son capaces de transportar glucosa al interior de las células de una manera estable y continua. Siendo de gran importancia en células con una alta dependencia energética como: tejido nervioso y eritrocitos (*Bermúdez et al., 2007*). Las concentraciones cerebrales para dichos transportadores (GLUTs) estimadas por varios autores son: GLUT1 (45 kDa): 6.9-7.7 pmol mg^{-1} de proteína; GLUT1 (55 kDa): 2.3-2.5 pmol mg^{-1} de proteína; GLUT3: 8-11 pmol mg^{-1} de proteína (*Maher y Simpson, 1994; Vannucci et al., 1997; Choeri et al 2005; Simpson et al 2007*). A su vez, se ha demostrado que la constante catalítica (k_{cat}) para GLUT3 es unas 6-7 veces mayor que para GLUT1, lo que pone de manifiesto que los transportadores neuronales son muchos más rápidos y efectivos que los gliares (*Lowe y Walmsley, 1986; Maher et al., 1996*). Por otro lado, estudios recientes realizados con microscopía confocal revelan que el glutamato (principal neurotransmisor cerebral y responsable del 80-90% de las sinapsis) inhibe los transportadores neuronales GLUT3, mientras que estimula el transporte de glucosa en los GLUT1 (45 kDa) astrocitarios (*Loaiza et al., 2003; Porras et al., 2004*). Otro dato interesante, es el desacoplamiento temporal observado entre el consumo de O_2, el flujo sanguíneo local y el consumo de glucosa durante periodos de activación descrito por algunos autores (*Fox y Raichle 1986; Fox et al., 1988*).

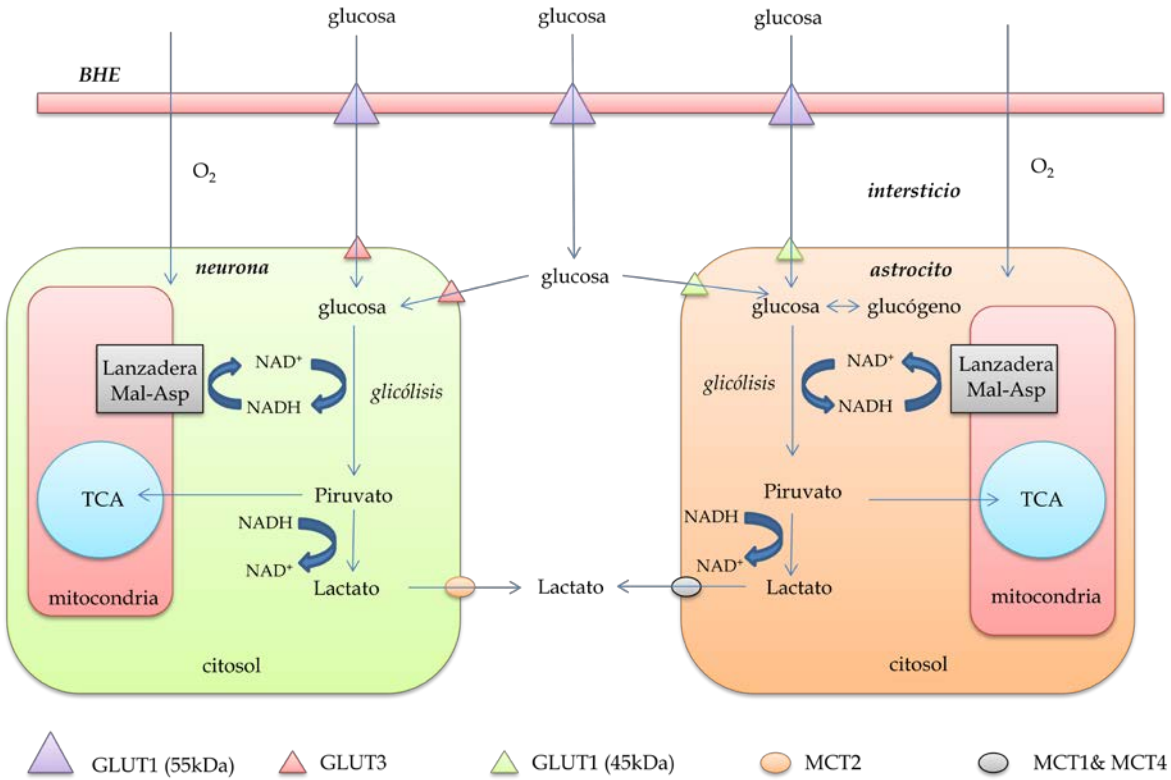

Figura 1.3.- *Modelo metabólico clásico: la glucosa y el oxígeno son liberados desde el vaso sanguíneo. El oxígeno difunde libremente a través de los tejidos, sin embargo, la glucosa debe atravesar cada uno de los compartimentos mediante transportadores GLUTs específicos. En este modelo la glucosa es el combustible primario, tanto para las neuronas como para los astrocitos, siendo el lactato un mero subproducto metabólico que es desechado al intersticio. Se asume que las neuronas son capaces de controlar el suministro metabólico en función de su estado.*

Por último, es importante matizar que la glucosa en el cerebro no funciona únicamente como sustrato energético [vía ciclo de los ácidos tricarboxílicos (TCA)], sino que cumple varias funciones (**Figura 1.4**), como pueden ser la de sustrato para la biosíntesis de inositol y glucógeno. Además, su esqueleto de carbono puede ser incorporado a la acetilcolina, lactato, glutamato, glutamina, aspartato y alanina. En el cerebro desarrollado, el metabolismo a través del ciclo de la pentosa fosfato es particularmente importante ya que proporciona ribosa-5-fosfato para la síntesis de nucleótidos y la NADPH necesarios para la biosíntesis de lípidos (*Tabernero et al., 1996*).

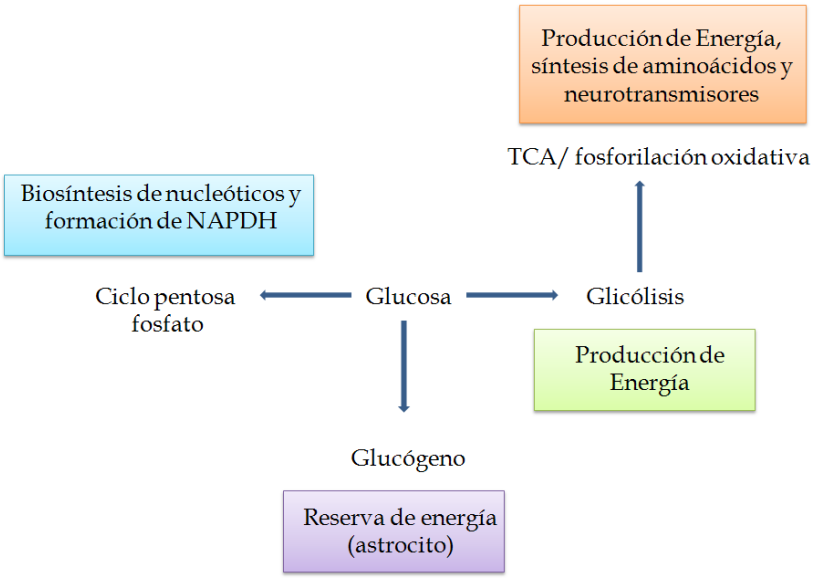

Figura 1.4.- *La glucosa posee múltiples facetas metabólicas: puede ser almacenada como glucógeno para actuar de reserva energética, puede ser usada directamente para producir energía vía glicólisis o mediante el TCA, además, está conectada vía TCA en la síntesis de algunos neurotransmisores y sus intermediaros, también puede ser empleada en la biosíntesis de nucleótidos y NAPDH.*

1.3.- Metabolismo cerebral: Lactato

Recientemente, se ha demostrado que el *lactato* podría ser algo más que un mero subproducto energético, y que éste, puede ser utilizado como fuente de energía por las células de la retina (*Poitry-Yamate, 1995*), en neuronas en el cerebro adulto *(Larrabee, 1995; Hu y Wilson, 1997; Schurr et al., 1999*) y en general por cualquier tejido en condiciones fisiológicas normales (*Brooks, 1987; Haljamae, 1987*). Incluso, dicho consumo puede ser preferencial frente a la glucosa en determinadas condiciones (*Pellerin y Magistretti, 1994*).

Por otro lado, es bien conocido que la tasa de transporte y el metabolismo oxidativo de la glucosa es muy bajo en el cerebro en desarrollo (*período posnatal*), y éste aumenta con la madurez del SNC (*Vannucci et al., 1997; Dwye et al., 2002; Vannucci y Simpson, 2003*). Dicho proceso está relacionado con el desarrollo progresivo de algunos transportadores y lanzaderas específicas del TCA, necesarios para metabolizar la glucosa a nivel celular (*McKenna et al., 2006*). Debido a esta inmadurez temporal del SNC, varios ácidos monocarboxílicos, incluyendo el lactato y otros cuerpos cetónicos como el acetoacetato y el *β*-hidroxibutirato, son empleados como sustratos energéticos. Estos compuestos también son incorporados en los lípidos, aminoácidos y las proteínas en el cerebro en desarrollo (*Cremer, 1982; Nehlig, 2004*). Según estos datos, el lactato parece tener un papel importante durante el período postnatal, tanto como fuente de energía, como sustrato primario para la biosíntesis de intermediarios metabólicos (*Medina, 1985*), siendo este hecho consistente con la alta concentración de grasas en la leche materna (*Vannucci y Simpson, 2003*).

1.3.1.- Lanzadera de lactato: *Astrocite-Neuron-Lactate Shuttle Hypotesis*

A partir de las observaciones citadas anteriormente y otros datos recogidos en la bibliografía (*Pellerin et al., 1998*; *Pellerin, 2003*), Pellerin y Magistretti (*Pellerin y Magistretti, 1994*) han propuesto un modelo (*Astrocite-Neuron-Lactate Shuttle,* ANLS), mediante el cual el

lactato producido en el astrocito es usado como fuente de energía por las neuronas. Dicha hipótesis supone una secuencia temporal de sucesos y mecanismos acoplados, que dan lugar finalmente a la liberación de lactato en el espacio extracelular y a su recaptación por parte de la neurona (**Figura 1.5**). Esta hipótesis ha sido avalada por un número importante de datos y observaciones fisiológicas (*Schurr et al. 1997a; Schurr et al. 1997b; Schurr et al. 1999; Pellerin 2003*).

Los astrocitos desempeñan un papel fundamental en el flujo de sustratos energéticos a las neuronas debido a su localización estratégica y a su versatilidad metabólica (*Magistretti y Pellerin, 1996; Lòpez-Bayghen et al., 2007; Lòpez-Bayghen y Ortega, 2010*). La morfología particular de los astrocitos, con sus terminaciones alrededor de los capilares sanguíneos, hace que los astrocitos sean la primera barrera celular que la glucosa ha de atravesar para penetrar en el SNC. Esta localización privilegiada, así como, la existencia de transportadores específicos (GLUT1 (55 kDa) en las células endoteliales y GLUT1 (45 kDa) en los pies astrocitarios), apoyan el papel que desempeñan los astrocitos en la distribución de nutrientes desde la sangre hasta otras células cerebrales (*Magistretti y Pellerin, 1999a; Magistretti y Pellerin, 1999b*)

Los astrocitos tienen la capacidad de detectar la actividad sináptica mediante receptores y/o transportadores específicos en la hendidura sináptica (*Pellerin y Magistretti, 1994*). Por otro lado, recientes investigaciones han demostrado que la captación de glutamato, vía transportadores GLT-1 (EAAT2) y GLAST (EAAT1) (*Araque et al., 1999; Pellerin, 2003*), estimula la glucólisis aeróbica astrocitaria (*Pellerin y Magistretti, 1994; Takahashi et al., 1995; Hamai et al., 1999*).

El transporte de glutamato en los astrocitos está dirigido por un gradiente electroquímico de Na^+: una molécula de glutamato es cotransportada con tres iones Na^+

hacia el interior celular y como consecuencia, un ión K^+ sale al exterior. Esto genera un incremento en la concentración intracelular de Na^+, que es equilibrado a través de la Na^+/K^+-ATPasa. Este proceso consume ATP e implica la activación de la glicólisis y la producción de lactato (*Pellerin y Magistretti, 1994;, Takahashi et al., 1995; Pellerin y Magistretti, 1997; Magistretti y Pellerin, 1999a; Magistretti y Pellerin, 1999b*). Un gran número de evidencias experimentales apoyan que dicho mecanismo no es activado por los receptores glutamatérgicos, sino por los transportadores EAAT1 y EAAT2 (*Pellerin y Magistretti, 1994; Takahashi et al., 1995; Pellerin y Magistretti, 1997*). Teniendo en cuenta que la oxidación de piruvato por el TCA es la vía más eficiente para obtener ATP, la razón por la cual los astrocitos favorecen la formación de lactato no ha sido entendida completamente (*Pellerin, 2005*).

Durante un proceso glicolítico continuado los niveles elevados de NAD^+ citosólico, esenciales durante la reacción catalizada por la gliceraldehído-3-fosfato deshidrogenasa (GADPDH) en la glucólisis (segunda fosforilación), se reducen drásticamente (ver ***Figura 1.5***). Pellerin y colaboradores han propuesto que dicha reserva citosólica de NAD^+ podría ser regenerada de forma eficiente por la conversión (reducción) piruvato-lactato mediante la lactato deshidrogenasa astrocitaria (LDH5) (*Pellerin, 2005*). Recientemente, han sido presentados argumentos adicionales que sugieren que los astrocitos poseen una reducida capacidad de regenerar los niveles de NAD^+ a partir del NADH citosólico mediante la lanzadera *malato-aspartato* (*Ramos et al., 2003*). De esta manera, todo parece indicar que la conversión piruvato-lactato podría tener un papel adicional, no solo de suministro metabólico, sino también regenerando los niveles de NAD^+ citosólicos indispensables en la glucólisis astrocitaria.

Una vez generado el lactato en el citosol astrocitario, es necesario su transporte mediante transportadores especializados. En este caso, Pellerin y colaboradores se apoyan en las diferentes propiedades cinéticas de dichos transportadores, así como, en la distribución

diferenciada de los mismo en el SNC (*Pellerin y Magistretti, 1999a; Pellerin 2003; Pellerin; 2005*). Los astrocitos expresan en su membrana celular transportadores monocarboxilatos **(**MCT1 y MCT4) que favorecen el transporte de lactato al intersticio. Por otro lado, las neuronas expresan transportadores monocarboxilatos tipo MCT2 que favorecen la captación neuronal de lactato. Finalmente, la presencia de isomorfas de lactato deshidrogenasa (LDH1) en el citosol neuronal favorecen la conversión (oxidación) lactato-piruvato, siendo este último, transportado al interior de las mitocondrias (vía transportadores monocarboxilatos) donde continúa el TCA acoplado a la fosforilación oxidativa (*Pellerin y Magistretti, 1999a; Pellerin 2003; Pellerin; 2005*).

Sin duda, dicho hipótesis y su evolución a lo largo del tiempo han generado un intenso debate entre partidarios y detractores (*Hertz, 1999; Bliss et al., 2001; Bouzier-Sore et al., 2002; Bouzier-Sore et al., 2003; Chih y Roberts, 2003; Bergersen, 2007*). En 2011 Pellerin ha presentado una nueva revisión con el sugerente título "*Sweet sixteen for ANLS*" donde se hace una nueva revisión de los conceptos e ideas fundamentales (*Pellerin y Magistretti; 2011*).

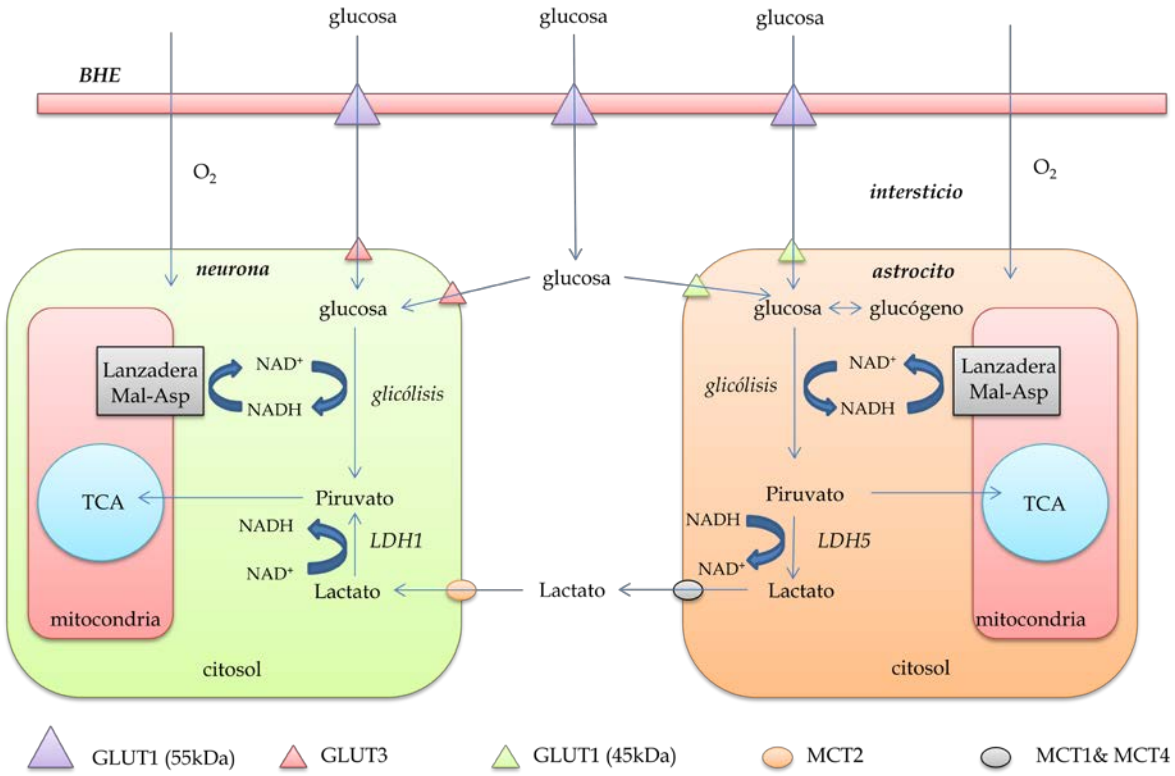

Figura 1.5.- *Hipótesis (ANLS) planteada por Pellerin y Magistretti (Pellegrin, 2003): La secuencia de eventos empezaría por la captación y regeneración del glutamato liberado en la hendidura sináptica (ciclo glutamato-glutamina), proceso acompañado por la entrada masiva de iones Na^+ al astrocito. Dicho mecanismo activaría la bomba de Na^+/K^+ produciendo un considerable descenso de las reservas energéticas astrocitarias. Para compensar dicha pérdida se activaría la glicólisis y/o glicogenolisis y el transporte de glucosa (GLUT1 45 kDa). Una consecuencia directa de la glicólisis astrocitaria es el aumento de piruvato y NADH citosólico. Como consecuencia, podrían activarse varios procesos: (1) el TCA acoplado a la fosforilación oxidativa, generando ATP y regeneranto el NAD^+; (2) conversión de piruvato a lactato (LDH5), regenerando el NAD^+. Posteriormente, el lactato es transportado al intersticio vía MCT1 y MCT4. Una vez en el intersticio los transportadores MCT2 introducirían el lactato al interior de la neurona que seguidamente lo transformara a piruvato (LDH1) e incorpora al TCA acoplado a la fosforilación oxidativa.*

1.3.2.- Nuevas hipótesis sobre el uso neuronal del lactato

1.3.2.1.- Acoplamiento redox y actividad metabólica: *The redox-switch/redox-coupling hypothesis*

Recientemente, se han postulado nuevos mecanismos para describir el acoplamiento neurona-astrocito (*Cerdán et al., 2006, Rodrigues et al., 2009*). Dichos autores proponen que las neuronas y los astrocitos pueden intercambiar reversiblemente lactato y piruvato vía MCT (**Figura 1.6**). Dicho mecanismo se basa en la inhibición de la glicólisis vía GADPDH en condiciones reductoras (bajas concentraciones de NAD^+ citosólico) así como, en la compartimentación subcelular del piruvato y el intercambio reversible de monocarboxilatos entre la neurona y la glía. Dicha compartimentación permite a la neurona y la glía elegir su sustrato metabólico (*glucosa o lactato*) en función de: (1) el estado redox citosólico ("*redox switch*", relación NAD^+/NADH), (2) de las concentraciones extracelulares relativas de lactato y glucosa.

Cerdán y colaboradores sugieren que durante la captación de glutamato por la glía se incrementa su actividad glicolítica y la actividad del TCA, produciendo una importante reducción de la relación NAD^+/NADH citosólica en la glía (*Cerdán et al., 2006*). Posteriormente se transfieren equivalentes reductores a la neurona reduciendo los niveles de NAD^+/NADH y provocando la inhibición (*switch off*) de la glicólisis neuronal y favoreciendo el transporte (vía MCT) y oxidación del lactato extracelular (vía LDH1 y TCA) para generar piruvato (recuperando los niveles de NAD^+ citosólico). Finalmente, este piruvato acumulado en exceso en el citosol neuronal, podría entrar al TCA o volver al espacio extracelular. Posteriormente el piruvato podría entrar en la glía (vía MCT), recuperando así los niveles redox basales (*Ramírez et al., 2007*) y comenzar un nuevo ciclo lactato/piruvato entre la neurona y la glía.

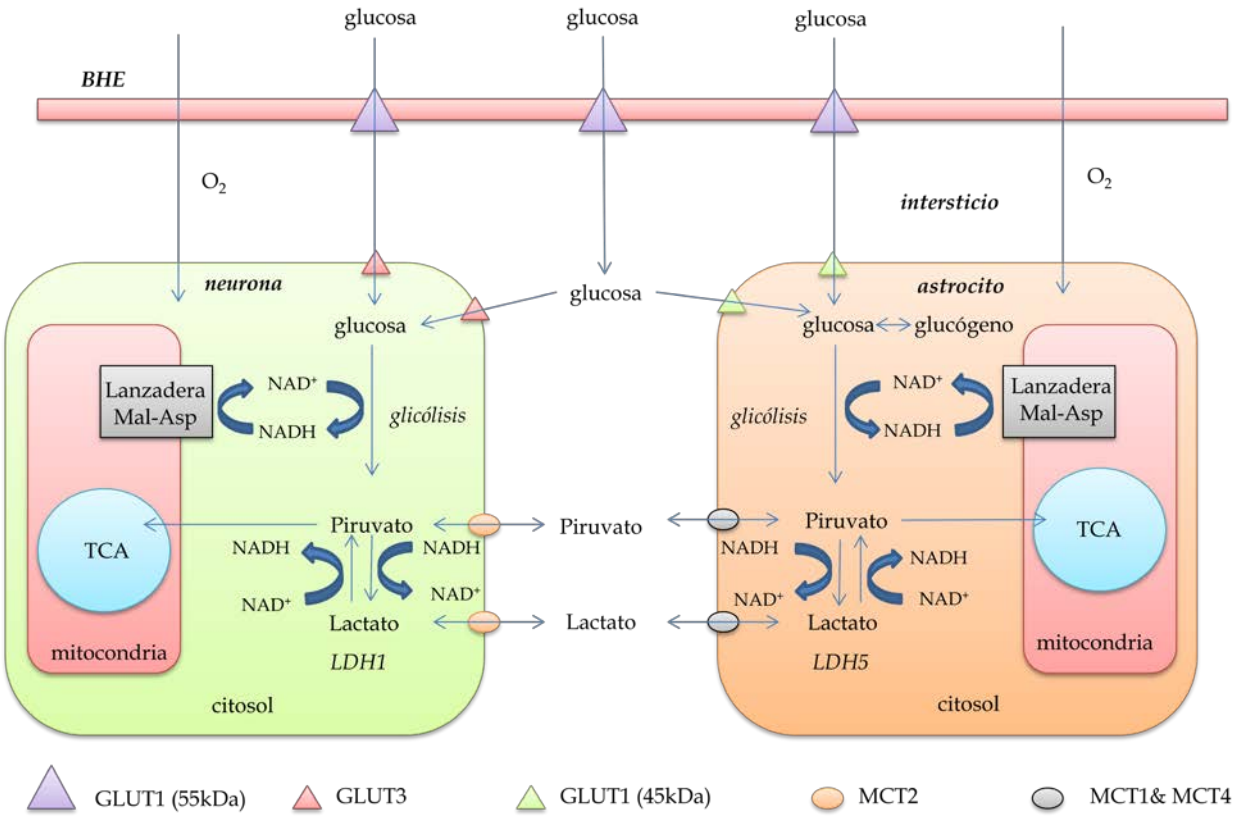

Figura 1.6.- *Esquema de la hipótesis planteada por Cerdán (Cerdán et al., 2006). Dicho modelo enfatiza el transporte bidireccional que tiene el piruvato y el lactato entre la neurona y el astrocito. En dicho modelo existen dos fuentes de piruvato en la neurona y en la glía derivados del metabolismo de la glucosa o de los monocarboxilatos. La lanzadera lactato/piruvato es capaz de transferir continuamente lactato desde el astrocito a la neurona vía MCT, siendo metabolizado finalmente por la LDH1. Las altas concentraciones citosólicas de lactato en la neurona inhibe la glicólisis ya que disminuyen drásticamente los niveles de NAD^+ necesarios para la GAPDH, favoreciendo finalmente la oxidación del lactato extracelular. Posteriormente el piruvato es transportado hacia la glía, vía MCT, preparándose para un nuevo ciclo.*

1.3.2.2.- Transporte mitocondrial del lactato

Nuevas investigaciones han sugerido que el lactato puede ser metabolizado directamente en el interior de la mitocondria y no necesariamente en el citoplasma neuronal (*Schurr, 2006*). Este hecho parece ser confirmado por: (1) existencia de transportadores MCT en la membrana mitocondrial, (2) presencia de formas isomorfas LDH localizadas en la membrana interna mitocondrial de las neuronas (m-LDH) (*Hashimoto et al, 2008*).

Esta hipótesis alternativa (**Figura 1.7**) sugiere que el lactato y no el piruvato, es el producto final de la glicólisis en todos los tipos de tejidos y en cualquier condición: aeróbica o anaeróbica (*Schurr, 2006; Schurr y Payne, 2007)*. Bajo esta suposición, la glicólisis citosólica siempre conduce a la formación de lactato, principalmente para regenerar el NAD^+ que se consume durante glicólisis. Finalmente, si la producción de lactato se produce en condiciones aeróbicas, es transportado a través de la membrana mitocondrial vía transportadores monocarboxilatos (MCT1 y MCT2) y convertido en piruvato (vía m-LDH). Una vez en esta forma, entraría al TCA acoplado a la fosforilación oxidativa para obtener ATP. Avalando dicha hipótesis se encuentran los estudios de Hashimoto y colaboradores realizados en 2008, que demuestran la presencia de transportadores MCT1 y MCT2 en la membrana mitocondrial, así como, la presencia de m-LDH en su interior (*Hashimoto et al, 2008*). Finalmente, ese mismo año estudios paralelos confirmaron la presencia de transportadores MCTs mitocondriales no solo en las neuronas sino también en células gliares (*Lemire et al., 2008*).

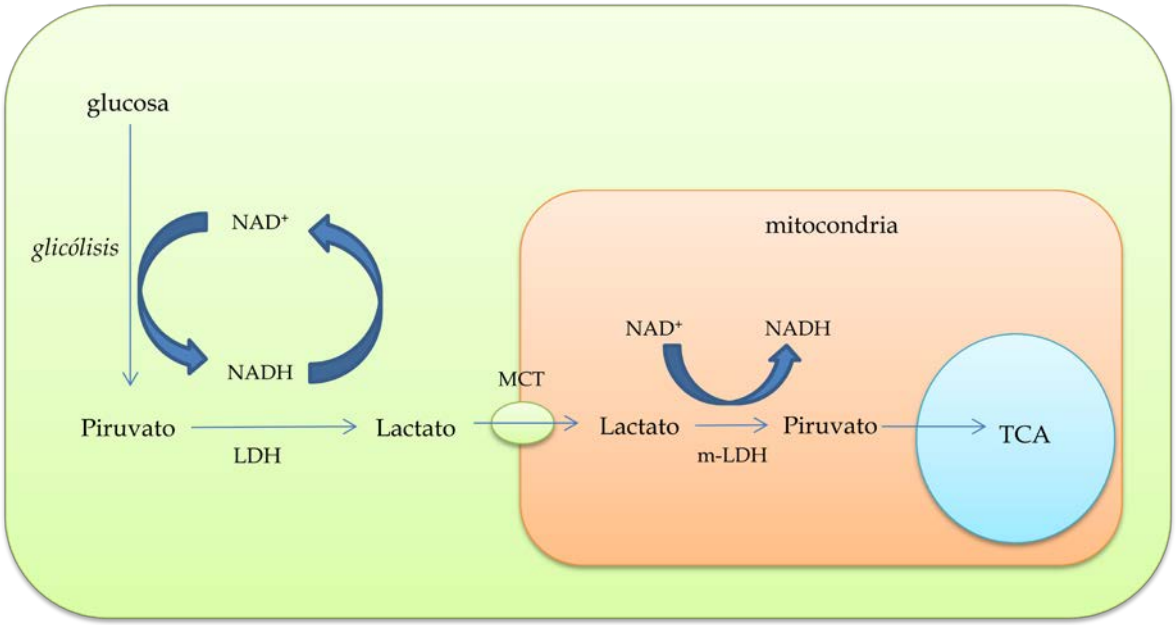

Figura 1.7.- *Esquema de la hipótesis planteada por Schurr (Schurr, 2006): La glicólisis citosólica produce piruvato que posteriormente es reducido a lactato, regenerando los niveles de NAD⁺ citosólico. Seguidamente, dicho lactato es transportado, vía MCT, a la mitocondria donde es convertido en piruvato y entra en el TCA.*

.

1.4.- Metabolismo cerebral: técnicas instrumentales

Actualmente, existe un gran interés por el estudio y conocimiento de las funciones cerebrales (lenguaje, memoria, plasticidad, emociones), así como, su modificación en procesos neurodegenerativos (Alzhéimer, Párkinson, Huntington), procesos adictivos, etc. Ello ha propiciado que hoy en día existan un gran número de técnicas instrumentales, empleadas en dilucidar aspectos concretos del comportamiento, funcionamiento y metabolismo cerebral. Algunas de estas técnicas son costosas y aparatosas como: resonancia magnética funcional (*f*MRI), tomografía por emisión de positrones (PET), técnicas de fluorescencia, espectroscopía de protón (^{1}H-NMR) y C-13 (^{13}C-NMR); y otras más sencillas y económicas como: microdiálisis, técnicas espectroscópicas en el infrarrojo cercano (NIRs) y en el visible (VIS), sensores, biosensores etc.

El desarrollo de las modernas técnicas de análisis neuroquímico, ha dado lugar a un avanzado grado de especialización, sin embargo cada técnica presenta sus propias restricciones inherentes. Por ejemplo, las técnicas espectroscópicas como el NIRs (*infrarrojo cercano*) dependen del poder de penetración de los fotones en los tejidos, la resonancia magnética (^{1}H-NMR y ^{13}C-NMR) no permite una resolución (resolución del *vóxe*l) menor del cm^{2}, llevando a una imprecisión en la localización (espacio intra y extracelular) de los metabolitos estudiados, especialmente cuando los modelos compartimentales han sido aceptados como doctrina (*McKenna et al., 2006*). Esto ha llevado a que los métodos invasivos de análisis (microdiálisis, voltametría *in vivo,* electroforesis capilar etc.), con una mayor resolución espacial, hayan sido usados más frecuentemente en modelos animales.

1.4.1.- Microdiálisis

La *microdiálisis cerebral* es un método analítico que utiliza un sistema cerrado en el cual una sonda de doble luz, con una membrana de diálisis (Ø~250-500 μm) en uno de sus extremos, se inserta en una región determinada del cerebro. A través de dicha membrana se produce una difusión pasiva y a favor del gradiente de concentración de analitos y/o fármacos, entre el líquido de perfusión y el medio extracelular (*Benveniste et al., 1990*). La técnica fue desarrollada en la década de los 60 y 70 por varios grupos (*Bito et al., 1966; Delgado et al., 1972*) y empleada en el estudio de distintos analitos en diversos tejidos, incluyendo el cerebro (*Bito et al., 1966; Delgado et al., 1972*). Pese a que inicialmente presentaba ciertas limitaciones, la técnica fue perfeccionada y aplicada a nivel cerebral por otros grupos de investigadores (*Ungerstedt y Pycock, 1974; Mas et al., 1995a; Mas et al., 1995b*). Esta técnica permite estimar *in vivo* la liberación de neurotransmisores y metabolitos, y a su vez, estudiar los cambios inducidos en ellos por drogas y fármacos perfundidos a través de la sonda de diálisis o administrados por vía sistémica (*Ungersted, 1991*).

1.4.2.- Voltametría *in vivo*

Aproximadamente cincuenta años después del nacimiento de las técnicas voltamperométricas (1922) a cargo del premio Nobel Jaroslav Heyrovsky, apareció un interés generalizado por el estudio de distintos compuestos electroactivos en el SNC. Los primeros estudios que aparecen usando técnicas voltamperométricas se remontan a los años 50, cuando Clark y colaboradores midieron O_2 y ácido ascórbico en el cerebro (*Clark et al., 1958; Clark y Lyons, 1965*). Sin embargo, Ralph Adams fue el primero en aplicar dichas técnicas en el SNC de forma generalizada, y hoy en día es

considerado como el principal impulsor de las técnicas voltamperométricas en el estudio del SNC (*Kissinger et al., 1973*).

En la década de los 70 y 80 se empezó a estudiar la electrooxidación de fenoles, catecoles y catecolaminas en sistemas *in vivo* (*Gonon et al., 1981; O'Neill et al., 1983; Sharp et al., 1983; González-Mora et al., 1988; González-Mora et al., 1989*). Varios grupos de investigación sugirieron la posibilidad de implantar pequeños electrodos en el SNC y estudiar diferentes neurotransmisores catecolaminérgicos [dopamina (DA, norepinefrina (NE)] y sus metabolitos [ácido homovanílico (HV) y ácido 3,4-dihidroxifenilacético (DOPAC)] *(Gonon et al., 1981; O'Neill y Fillenz, 1985; González-Mora et al., 1988; Wightman et al., 1988; González-Mora et al., 1989; González-Mora et al., 1990; Mas et al., 1990; Louilot et al., 1991*).

Los primeros electrodos utilizados en voltamperometría *in vivo* fueron electrodos de pasta de carbono (CPEs) *(O'Neill et al., 1982*), aunque rápidamente Gonon y colaboradores establecieron el uso de electrodos de fibra de carbono (CFEs), mucho más versátiles y con reducidas dimensiones (~µm) (*Gonon et al., 1981; Mas et al., 1989; Mas et al., 1995a; Mas et al., 1995b*).

Inicialmente, los problemas encontrados en dichos dispositivos fueron: (1) baja selectividad frente a otros compuestos electroactivos presentes en el SNC (*ácido ascórbico* (AA), *ácido úrico* (AU), (2) pasivación de la superficie del electrodo por agentes floculantes (*lípidos* y *proteínas*), (3) agresividad del medio de trabajo (*respuesta inmunológica*). Para solventar estos problemas se recurrió al empleo de dos estrategias distintas: (1) Pretratamiento electroquímico de las fibras de carbono (*Gonon et al., 1981*), dicho tratamiento alteraba la superficie del electrodo y permitía detectar a diferentes potenciales AA y distintos catecoles. (2) Recubrimiento del electrodo con polímeros

polianiónicos como el Nafion (*Gerhard et al., 1984*). (3) Deconvolución matemática mediante algoritmos no lineales (*Mas et al., 1989; González-Mora et al., 1991*).

Con el devenir de los tiempos se ha incrementado el interés por mejorar las propiedades antiinterferentes y la sensibilidad de estos métodos electroquímicos. Sin duda, gran parte del éxito actual se debe a la gran diversidad de las técnicas voltamperométricas existentes [Voltametría Cíclica (CV), Amperometría a Potencial Constante (CPA), Voltametría Cíclica Rápida (FCV), Voltamperometría Pulsada Diferencial (DPV)] (*Mas et al., 1990; Louilot et a., 1991; Guadalupe et al., 1992; Mas et al., 1995a; Mas et al., 1995b*) y a la utilización de nuevos materiales poliméricos y electrocatalíticos, que permiten no solo mejorar la selectividad, sino proporcionar mejores condiciones de trabajo (sensibilidad, estabilidad, potencial de trabajo, límite de detección, etc.) (*Lowry et al., 1998; Breccia et al., 2002; Li et al., 2002; Qian et al., 2004; Killoran y O'Neill, 2008; O'Neill et al 2008; Rothwell et al., 2008*).

Finalmente, el uso de los métodos voltamperométricos ha permitido el estudio de una gran variedad de procesos y mecanismos neuroquímicos y neurofisiológicos (*Kozminski et al., 1998, Colliver et al., 2000, Pothos et, al 2000; Avshalumov et al., 2003; Stuber et al., 2005a; Stuber et al., 2005b*)

1.4.3.- Voltamperometría *vs.* Microdiálisis

Pese a que desde la década de los 60 se desarrollaban electrodos electroquímicos para un número razonable de analitos, el salto tecnológico que permitió su adecuación para realizar estudios en el cerebro fue, la *miniaturización*. En la décadas de los 80-90 se introdujeron los CPEs (Ø~250 μm) *(O'Neill et al., 1982*) y los CFEs (Ø ~10μm) (*Gonon et al., 1981; González-Mora et al., 1988; Wightman et al., 1988; González-Mora et al., 1989; González-Mora et al., 1990 ;Mas et al., 1990; Louilot et a., 1991; Mas et al., 1991; Guadalupe et*

al., 1992; Mas et al., 1995a; Mas et al., 1995b), los cuales redujeron significativamente el tamaño de tales dispositivos. Gracias a este reducido tamaño (~µm), sobre todo los CFEs, ofrecían ventajas analíticas (*gran resolución espacial y temporal*) frente a otras técnicas convencionales (*microdiálisis, electroforesis capilar, etc.*), **Figura 1.8**.

La inserción de la sonda de recogida de muestra (*microdiálisis*) produce alteraciones del medio de estudio (*cerebro*), debidas principalmente, a sus grandes dimensiones (Ø~250-500 µm). Como consecuencia, aparecen alteraciones fisiológicas y anatómicas en la región de estudio (*rotura de vasos sanguíneos, pérdida de la integridad de la barrera hematoencefálica, cambios en la microcirculación local, edema, consumo extra de glucosa, producción de citoquinas, eventual proliferación de células gliales, etc.*) que se pueden extender hasta 1 mm de la zona de implantación (*Benveniste et al., 1987; O'Neill et al., 1991; Fumero et al., 1994; Mas et al., 1995a Zhou et al., 2001; Khan y Michael, 2003*). Estudios recientes con FCV han demostrado alteraciones en la liberación y recaptación de DA en el tejido próximo a la sonda de microdiálisis (Ø~220µm) (*Borland et al., 2005*).

Por otro lado, debido la dilución del analito en la disolución de perfusión, no se mide la concentración real del espacio extracelular, sino una concentración menor que depende de: (1) la tasa de reparto a través de la membrana de microdiálisis, (2) la velocidad de perfusión, (3) tamaño de poro, (4) las características estructurales de la molécula, etc. Esto hace difícil o al menos laboriosa la obtención del valor de fondo (*nivel basal*) del analito (*Zero Net Flux method*) (*Lönnroth et al., 1987*). Dicha dilución puede incluso enmascarar los cambios fisiológicos acontecidos cuando este se presenta a bajas concentraciones como es el caso del glutamato (concentración basal ~ 20 µM (*Oldenziel et al., 2006; Oldenziel et al., 2007*).

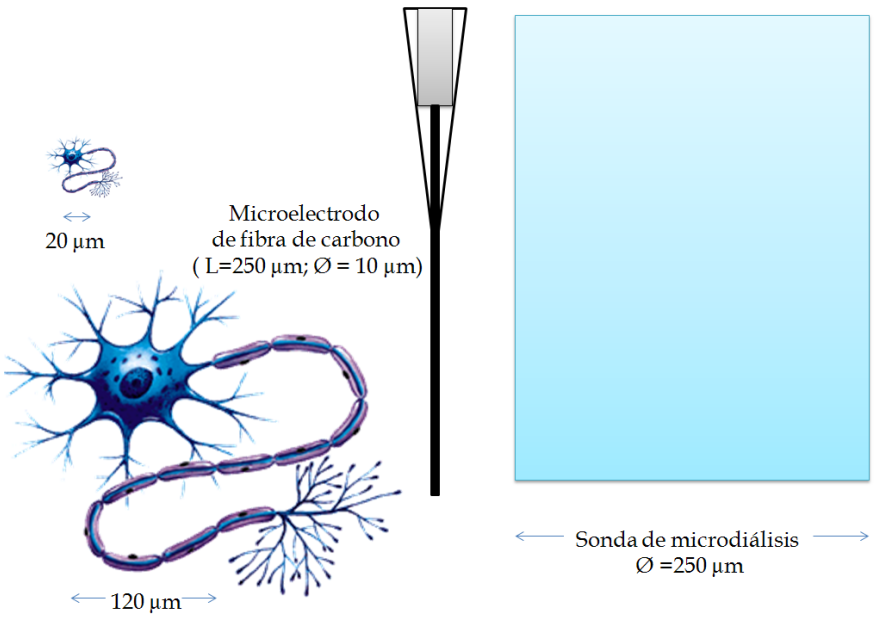

Figura 1.8.- *Comparación de las dimensiones de los electrodos de fibra de carbono (CFE), sonda de microdiálisis y el rango de tamaño de las neuronas.*

La principal ventaja de la microdiálisis es que puede determinar varios analitos simultáneamente, especialmente cuando se combinan con técnicas cromatográficas y sistemas de detección adecuados (*Kaul et al., 2011*). Sin embargo, ello lleva consigo el aumento de la resolución temporal (velocidad de muestreo: 5-8 muestras/hora, separación cromatográfica: 15-20 minutos). Una forma de disminuir dicho tiempo es hacer pasar el líquido de perfusión con el analito por una celda de reacción donde se pueda monitorizar los cambios del analito acoplando un sensor electroquímico o un biosensor al sistema (*Moscone y Mascini, 1992; Steinkuh et al., 1996; Ricci et al., 2007*). Sin embargo, dicha aproximación no disminuye el tiempo necesario de perfusión del líquido a través de todo el sistema de muestreo, obteniéndose así, una resolución de 15-20 muestras/hora (*Yao y Yano, 2004*).

Gracias al pequeño tamaño de los microelectrodos las lesiones ocasionadas por su inserción son reducidas notablemente y además, aparecen nuevas característica (*pequeñas corrientes de medida*, *modificación de la técnica voltamperométrica, resolución temporal, etc.)*, que hacen que los microelectrodos sean adecuados para realizar estudios a nivel fisiológico. Sin duda, la mayor ventaja es que miden directamente en el espacio extracelular, sin necesidad de utilizar métodos de extracción Por otro lado, la elevada relación señal/ruido permite alcanzar bajos límites de detección y una elevada resolución temporal.

Las pequeñas corrientes generadas en el microelectrodo (~*pA*), hacen que sea posible medir en medios con una alta resistencia, como son los medios biológicos (SNC). La resolución temporal es muy corta (<*1s*) (*Robinson et al., 2003; Cheer et al., 2004*), debido principalmente a dos factores: (1) *dinámico*, al disminuir el tamaño del electrodo disminuye también la capa difusiva circundante, incrementando así la velocidad de transporte de masa desde y hacia el electrodo; y (2) *eléctrico*, al disminuir la superficie del electrodo la *corriente capacitiva* decrece exponencialmente, mientras que la *corriente farádica* disminuye linealmente, luego la razón i_{far}/i_{cap} aumenta al disminuir las dimensiones, permitiendo reducir el tiempo necesario para alcanzar el estado estacionario (*Yáñez-Sedeño y Pigarrón, 2001*).

Por último, la posibilidad de modificar dichos microelectrodos adecuadamente ha permitido la determinación de metabolitos no electroactivos: glucosa (*Moscone y Mascini, 1992; Steinkuh et al., 1996; Fillenz y Lowry 1998; Lowry et al., 1998; Ricci et al., 2007*); lactato (*Shram et al., 1998; Yao y Yano, 2004; Burmeister et al., 2005*), glutamato (*Kulagina et al., 1999; Kasai et at., 2001; Kasai et at., 2002; Oldenziel et al., 2006; Oldenziel et al., 2007*), piruvato (*Yao y Yano, 2004*), etc., incrementando así su interés metodológico en el ámbito neuroquímico.

2.- Biosensores

2.1.- Definición

La detección de especies electroactivas como el ácido ascórbico (*O'Neill et al., 1983*), ácido úrico (*O'Neill, 1990*), ácido homovanílico (*O'Neill y Fillenz, 1985*) y oxígeno (*Lowry et al., 1996; Bolger y Lowry, 2005*) han sido realizadas con éxito mediante electrodos no modificados. Sin embargo, la detección de especies no electroactivas, tales como aminoácidos (glutamato), metabolitos energéticos (glucosa, lactato, piruvato), etc. requieren el empleo de biosensores (*Moscone y Mascini, 1992; Steinkuh et al., 1996; Shram et al., 1998; Yao y Yano, 2004; Burmeister et al., 2005; Oldenziel et al., 2006; Oldenziel et al., 2007; Ricci et al., 2007*).

De acuerdo con la definición que da la *IUPAC* (*Internacional Union of Pure and Applied Chemistry*) (*Thévenot et al., 1999; Thévenot et al., 2001*), un ***biosensor*** es un dispositivo analítico que incorpora un elemento biológico (ácido nucleico, enzima, anticuerpo, receptor, tejido, célula), o biomimético (PIMs, aptámeros, PNAs), íntimamente asociado a un transductor fisicoquímico (**Figura 2.1**), que en presencia del analito, produce una señal discreta o de carácter continuo (pH, transferencia de electrones, de calor, cambio de potencial, de masa, variación de las propiedades ópticas, etc.), proporcional a la cantidad de analito presente en la matriz en la que se encuentra.

Las características más importantes de los biosensores y que los convierten en herramientas analíticas competitivas con las técnicas clásicas de análisis (microdiálisis, electroforesis,…) son: *especificidad, alta sensibilidad, corto tiempo de análisis, uso en sistemas de Análisis por Inyección de Flujo (FIA), facilidad de automatización, capacidad de trabajar en tiempo real, bajo coste de fabricación, etc. (Prodromidis y Karayannis, 2002; D'Orazio, 2003; Mehrvar y Abadi, 2004; D'Orazio, 2011*).

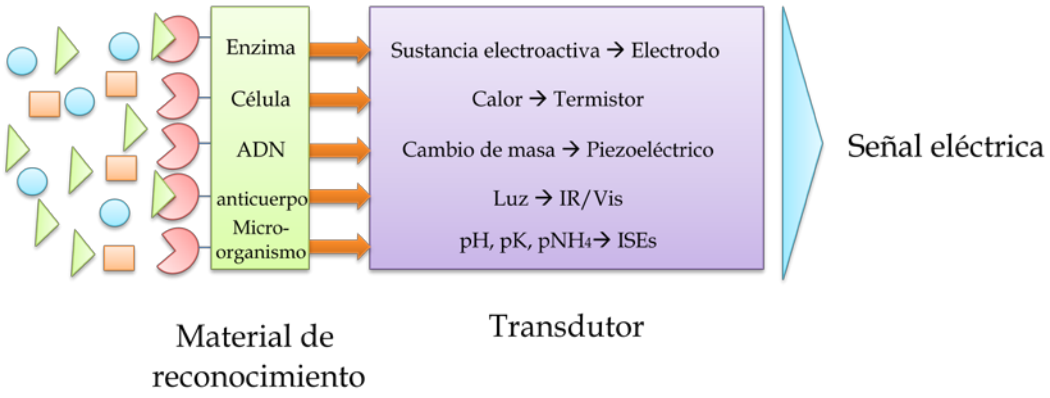

Figura 2.1.- *Esquema de las partes fundamentales de un biosensor, así como, el acoplamiento entre distintos sistemas de reconocimiento y sistemas de transducción.*

2.2.- Los orígenes

El nacimiento de los biosensores se puede atribuir a *Leland C. Clark Jr.* (*Clark y Lyons, 1962*), quien sugirió por primera vez la posibilidad de modificar un electrodo de oxígeno para estudiar una reacción enzimática que consumiera dicho reactivo. De esta forma, la enzima (*Glucosa oxidasa, Gox*) fue retenida mediante una membrana semipermeable de diálisis en la superficie de un electrodo de oxígeno. Clark observó que la respuesta de este nuevo dispositivo era proporcional a la concentración de glucosa: la enzima oxidaba la glucosa y como consecuencia, se producía un descenso proporcional en la concentración de oxígeno en la superficie del electrodo. En estas primeras publicaciones Clark y Lyons acuñaron el término "*electrodo enzimático*" a su nuevo invento (*Clark y Lyons, 1962*).

Posteriormente, este diseño fue implementado (*Updike y Hicks, 1967*). Dichos autores emplearon dos electrodos de oxígeno (uno recubierto con enzima y otro no). Dicha modificación permitió corregir las variaciones de oxígeno en el medio (*efecto matriz*). En 1973, Guilbault y Lubrano desarrollaron un electrodo enzimático para

determinar glucosa en sangre mediante la detección amperométrica (*anódica*) del peróxido de hidrógeno generado durante la reacción enzimática (*Guilbault y Lubrano,* 1973). En 1975, empezó la comercialización de este dispositivo por la empresa *Yellow Spring Instruments* (analizador YSI modelo 23) (*Magner, 1998*). Ese mismo año, Divis desarrolló un dispositivo para determinar etanol que utilizaba microorganismos como elemento de reconocimiento (*Divis, 1975*). A partir de este momento el término "*biosensor*" empezó a ser usado.

En las últimas décadas, el diseño y las aplicaciones de los biosensores en distintos campos de la química analítica han continuado creciendo. El desarrollo de los biosensores ha estado centrado principalmente en el campo del diagnóstico clínico (biosensores sensibles a glucosa) (*Wang, 2001; D'Orazio, 2003; Wilson, 2005; D'Orazio, 2011*). Sin embargo, han aparecido muchas aplicaciones en el ámbito medioambiental, agroalimentario, químico, farmacéutico y militar (*Mason, 1988; Kulys et al., 1989; Ramsay, 1998; Castillo et al., 2004*). El número de publicaciones científicas, revisiones y patentes sobre biosensores desarrollados en los últimos años es muy elevado, lo que refleja el gran interés que despiertan estos dispositivos en la comunidad científica (*Wang, 2001; Castillo et al., 2004; D'Orazio, 2011*). A su vez, el empleo de nuevos materiales (*nanopartículas, nanotubos de carbono, grafenos, etc.*) y elementos de reconocimiento (*anticuerpos, receptores iónicos, compuesto biomiméticos*) han mejorado sus características analíticas. Por último, los biosensores ofrecen una excelente versatilidad, pudiéndose fabricar a la carta y con características específicas a su ámbito de aplicación.

2.3.- Clasificación de los biosensores

Los biosensores pueden clasificarse atendiendo a diferentes criterios (**Tabla 2.1**). Así, podemos clasificarlos según el *tipo de interacción* entre el analito y el material biológico, el *método de detección*, la naturaleza del *material biológico de reconocimiento* o la naturaleza del *sistema de transducción* empleado (*Thévenot et al., 1999; Thévenot et al., 2001*).

Tipo de interacción	***Detección de la interacción***
Biocatalítico	Directo
Bioafinidad	Indirecto
Elemento de reconocimiento	***Sistema de transducción***
Enzima	Electroquímicos
Orgánulo, tejido	Ópticos
Receptor biológico	Piezoeléctricos
Anticuerpo	Termométricos
Ácidos nucleicos	Nanomecánicos
PIM (polímeros de impresión)	
Aptámeros	

Tabla 2.1.- *Criterios de clasificación de los biosensores.*

Sin duda, las clasificaciones más extendidas son: (1) en función del tipo de interacción que existe entre el elemento de reconocimiento y el analito: *biocatalítico* (enzimas, células, orgánulos) y *bioanifidad* (anticuerpo, lectinas, receptores biológicos, ácidos nucleicos); (2) según el sistema de transducción empleado para seguir la reacción de biorreconocimiento.

2.3.1.- Clasificación en función del elemento de reconocimiento

Las moléculas utilizadas en los biosensores como elementos de reconocimiento deben cumplir ciertos requisitos fundamentales para poder ser empleadas como unidades sensoras: (1) tienen que poseer afinidad hacia el elemento objeto del reconocimiento; (2) dicho reconocimiento deberá ser lo suficientemente selectivo para reconocer a este elemento en presencia de otros compuestos (interferentes); y (3) deberá permanecer estable a lo largo del tiempo (*Thévenot et al., 1999; Thévenot et al., 2001*).

El reconocimiento molecular puede dar lugar a un enlace entre el elemento receptor y la molécula de interés (*antígeno-anticuerpo*), o bien, a una interacción de naturaleza catalítica (*enzima-sustrato-producto*). Este es el principal criterio que se utiliza para clasificar los biosensores como *biocatalíticos* o de *bioafinidad*

2.3.1.1.- Biosensores biocatalíticos

Se basan en la utilización de catalizadores biológicos que participan en una reacción química (*Mason, 1988; Kulys et al., 1989; Ramsay, 1998; Castillo et al., 2004*). Una vez finalizado el proceso, el biocatalizador se regenera y puede ser usado en un nuevo ciclo catalítico.

Estos biocatalizadores pueden ser enzimas aisladas o en paquetes multienzimáticos que actúan de modo encadenado en orgánulos celulares, células completas y tejidos animales o vegetales. Entre las enzimas disponibles comercialmente, las más utilizadas son las correspondientes a la familia de las óxido-reductasas (*glucosa oxidasa, xantina oxidasa, lactato oxidasa, glutamato oxidasa*, etc.). Se trata de enzimas muy estables que catalizan reacciones de oxido-reducción y que pueden acoplarse a distintos sistemas de transducción.

Las principales ventajas del uso de enzimas en la construcción de biosensores son: (1) elevada selectividad, (2) rápida respuesta, (3) simplicidad del método de detección, (4) capacidad de autoregenerarse y (4) extensa disponibilidad comercial *(Prodromidis y Karayannis, 2002; D'Orazio, 2003; Mehrvar y Abdi, 2004; D'Orazio, 2011*).

2.3.1.2.- Biosensores de bioafinidad

Los biosensores de bioafinidad se basan en la interacción del analito con el elemento de reconocimiento sin que medie transformación catalítica alguna. La interacción conlleva la aparición y/o modificación de un equilibrio analito-receptor.

Para cuantificar dicha interacción, puede recurrirse a métodos directos, de tipo: *sándwich*, *de desplazamiento* y *competitivos*. Dado que en la interacción no se consumen sustratos ni se generan productos de reacción, se recurre al marcaje del receptor implicado en la interacción, o bien, al de un elemento que compita con el analito por la unión al receptor. Como marcadores se utilizan compuestos fluorescentes, nanopartículas o enzimas que intervengan en una reacción complementaria transducible.

En la actualidad se emplean distintos receptores de bioafinidad como: anticuerpos (*Abad y Montoya, 1994; Abad et al., 1997; López y Ortega et al., 1998; López y Ortega, 2002; Manclús et al, 2004; Yu et al., 2006*), lectinas (*Xi et al., 2001; Shao et al., 2010; Xue et al., 2010*), ácidos nucleicos (*Loiza et al., 2007; Loiza et al., 2008, Martínez-Paredes et al., 2010; Ortiz et al., 2011*), etc.

2.3.2.-Clasificación en función del tipo de transductor

El sistema de transducción, o más conocido como *transductor,* es el elemento y generalmente el soporte del material biológico. Transforma las variaciones de las propiedades físico-químicas, que se producen debido a la interacción específica

analito-sistema de reconocimiento, en una señal que puede ser registrada, amplificada y almacenada. Dicha señal proporciona información cuantitativa o semicuantitativa del analito determinado. Para el adecuado funcionamiento del biosensor, el elemento de reconocimiento y el sistema de transducción deben estar en contacto directo. En función de la naturaleza del sistema de transducción podemos distinguir distintos sistemas:

2.3.2.1.-Electroquímicos

Los transductores electroquímicos transforman la señal que se produce por la interacción entre el sistema de reconocimiento y el analito en una señal eléctrica (*Wang, 2001; Castillo et al., 2004; Grieshaber et al., 2008*). Dicha señal nos proporciona información analítica cuantitativa del analito que la origina..

2.3.2.2.- Másicos, piezoeléctrico o acústicos

Los sistemas de transducción piezoeléctrica, miden cambios directos de masa inducidos por la formación del complejo receptor-analito sobre la superficie del electrodo (cristal). Puesto que la frecuencia de oscilación del cristal viene determinada por su masa, de acuerdo con la ecuación de Sauerbrey, esta frecuencia variará cuando se produzca dicha interacción, pudiendo ser relacionada con la concentración de analito (*Skladal, 2003; Pohanka y Skladal, 2005; Kreutz, 2006; Pohanka et al., 2007;*).

2.3.2.3.- Térmicos

Los transductores termométricos (generalmente termistores) son capaces de medir cambios de calor originados por reacciones enzimáticas. Esta variación de temperatura puede ser relacionada con la concentración de analito (*Lammers y Scheper, 1999; Ramanathan et al., 1999; Demchenko et al., 2007*).

2.3.2.4.- Ópticos

Los transductores ópticos se basan en la medida de las variaciones de las propiedades de la luz (absorción, fluorescencia, luminiscencia, dispersión o índice de refracción) como consecuencia de la interacción física o química entre el analito y el biosensor (*Mansouri y Schultz, 1984; Marvin y Hellinga, 1998; Russell et al., 1999; Ballerstadt y Schultz, 2000; Pickup et al., 2005*). La introducción a principios de los 90 de una nueva tecnología de biosensores basadas en el fenómeno de resonancia de plasmón de superficie (SPR) ha permitido el estudio en tiempo real del proceso de interacción entre biomoléculas.

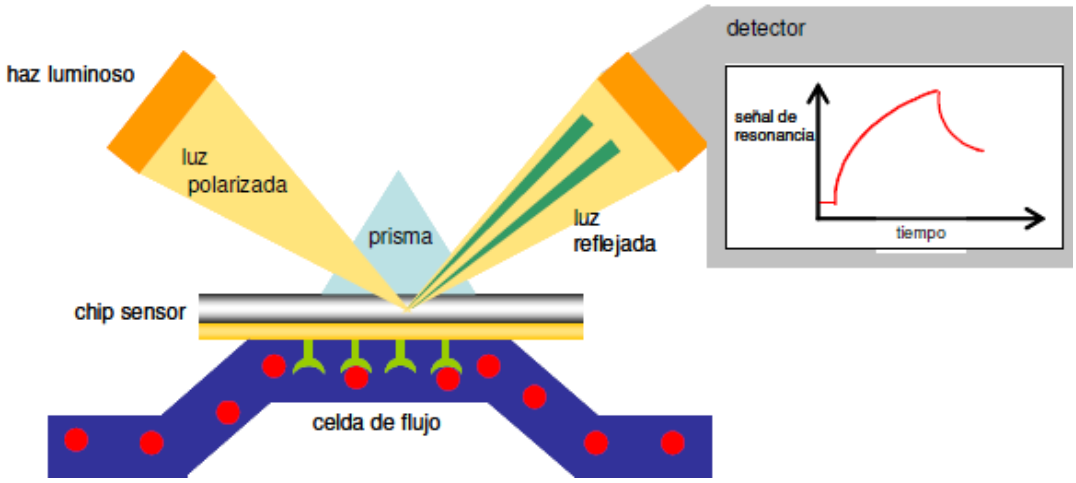

Figura 2.2.- *Fenómeno de la resonancia del plasmón de superficie. La resonancia del plasmón de superficie se produce por la reflexión total del haz de luz incidente al interaccionar con los plasmones por lo que se observa una reducción de la intensidad de la luz (fuente: Pérez, 2007).*

2.4.- Biosensores electroquímicos

Los *transductores electroquímicos* transforman la señal que se produce por la interacción entre el sistema de reconocimiento y el analito en una señal eléctrica (*Wang, 2001; D'Orazio, 2003; Castillo et al., 2004; Grieshaber et al., 2008; D'Orazio, 2011*). Las técnicas electroanalíticas son capaces de proporcionar límites de detección excepcionalmente bajos y abundante información sobre los sistemas estudiados:

estequiometría, velocidad de transferencia de carga, velocidad de transferencia de masa, constante de velocidad y constante de equilibrio.

En el campo de los biosensores el uso de transductores electroquímicos presentan numerosas ventajas: (1) se necesitan volúmenes pequeños, incluso del orden de nanolitros; (2) la señal obtenida es eléctrica, (3) los límites de detección que se obtienen normalmente son adecuados para la detección de muchos analitos interesantes, incluso a nivel biológico; (4) son susceptibles a la miniturización; (5) relativa simplicidad en su funcionamiento y bajo coste de la instrumentación analítica; (6) los dispositivos son especialmente apropiados para la monitorización en tiempo real.

Atendiendo a como ocurra este proceso de transducción, existen tres tipos de biosensores electroquímicos: *potenciométricos, conductimétricos, y amperométricos* (*Thévenot et al., 1999; Thévenot et al., 2001; D'Orazio, 2003; Grieshaber et al., 2008*).

2.4.1.- Potenciométricos

Este método se basa en la medida de la diferencia de potencial eléctrico entre dos electrodos (*indicador* y *referencia*) en ausencia de corriente. Las variaciones en la medida del potencial de celda vienen determinadas por la ecuación de Nernst, siendo proporcional a la concentración de algún ion generado durante la reacción enzimática (*Chumbimuni-Torres et al., 2006; Chumbimuni-Torres et al., 2009; Zhang et al., 2009a; Wang et al., 2010*). Un biosensor de este tipo podría ser un sensor selectivo a NH_4^+ modificado con ureasa. Durante la reacción, dicha enzima descompone la urea (**Ecuación 2.1**) en dos iones: amonio y carbonato (*D'Orazio, 2003*), siendo el primero cuantificado por dicho electrodo.

$$Urea + 2H_2O \xrightarrow{Ureasa} 2NH_4^+ + CO_3^{2-} \qquad \textbf{Ecuación 2.1}$$

2.4.2.- Conductimétricos

Este tipo de transductores mide los cambios de conductividad debida a la interacción con el analito (*Gallardo-Soto et al., 2001; Roach et al., 2003; Zhang et al., 2009b*), ya sea en la disolución de medida o en una membrana selectiva dispuesta en la superficie del electrodo conductimétrico. El ejemplo más característico lo constituye el biosensor de urea, donde la generación de iones carbonato y amonio (**Ecuación 2.1**) produce un aumento en la conductividad del medio (*D'Orazio, 2003*).

2.4.3.- Amperométricos

Se basan en la medida de la corriente generada por el intercambio electrónico entre el material de biorreconocimiento y el transductor (*Garguilo, 1996; Ferri et al., 2001; Fiorito y Córdoba de Torresi, 2001; D'Orazio, 2003; Mitala, 2006*). La posibilidad de poder incorporar en el transductor otros componentes, como mediadores redox, cofactores y otras biomoléculas, confiere a este tipo de biosensores una gran versatilidad de uso.

2.4.3.1.- Clasificación de los biosensores amperométricos

Durante las reacciones de oxidación-reducción se transfieren electrones entre reactivos y productos. Desde el punto de vista enzimático, el resultado final es la transferencia de uno o varios electrones desde la enzima a la superficie del transductor (*Habermüller et al., 2000*). Teniendo en cuenta dicho proceso de transferencia electrónica existen tres tipos o generaciones de biosensores:

2.4.3.1.1.- Biosensores de 1ª generación

Están basados en hacer reaccionar el analito con una enzima específica (**Ecuación 2.2**) y en la medida de un producto (**Ecuación. 2.3**) o de un cosustrato (**Ecuación 2.4**) de

la reacción enzimática (*Karyakin et al., 2002; Li et al., 2008; Tseng et al., 2009*). Fueron los primeros que se desarrollaron, el electrodo de Clark modificado con *Gox*, antes mencionado, pertenece a este grupo (*Clark y Lyons, 1962*).

El inconveniente de medir algunos cosustratos o productos de reacción es la necesidad de aplicar sobrepotenciales muy elevados y la aparición de fenómeos de interferencia. A su vez, a estos potenciales se puede producir la polimerización de los productos de reacción, que suelen pasivar la superficie del electrodo. Todo ello ha dado lugar a: (1) el empleo de membranas permeoselectivas que impiden la llegada de interferentes a la superficie activa del transductor (*Garjonyte et al., 1999a; Rothwell et al., 2010*), (2) detección catalítica de los intermedios de reacción (H_2O_2) (*Karyakin et al., 2002*) y (3) uso de mediadores redox artificiales, que reducen el potencial aplicado (dando lugar a la segunda generación de biosensores amperométricos).

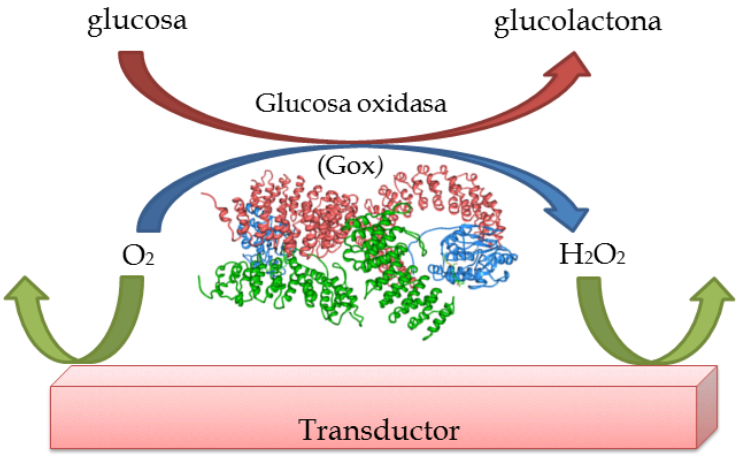

Figura 2.4.- *Esquema de las reacciones que ocurren en un biosensor de 1ª generación, basado en la detección amperométrica del H_2O_2 generado o el O_2 consumido enzimáticamente.*

$$\text{glucosa} + O_2 \xrightleftharpoons{Gox} \text{gluconolactona} + H_2O_2 \qquad \textbf{Ecuación 2.2}$$

$$H_2O_2 \Leftrightarrow 2\,H^+ + O_2 + 2e^- \quad (+0.7\ \text{V vs. SCE}) \qquad \textbf{Ecuación 2.3}$$

$O_2 + 4\,H^+ + 4\,e^- \quad \Leftrightarrow \quad 2\,H_2O \quad$ (-0.65 V vs. SCE)

Ecuación 2.4

2.4.3.1.2.- Biosensores de 2ª generación

Los biosensores de segunda generación utilizan un mediador que transfiere los electrones puestos en juego en el centro activo enzimático hacia la superficie del transductor (*Schuhmann et al., 1990; Palmisano et al., 2000; Chaubey y Malhotra, 2002; Mao et al., 2003*). De esta manera, sustituyen al cosustrato natural empleado por la enzima. El mediador debe poseer unas características determinadas para favorecer dicho proceso: (1) debe transferir los electrones rápidamente para evitar la competencia de los cosustratos naturales de la enzima; (2) debe tener un potencial redox próximo a cero, para evitar la interacción con otros analitos que pueden actuar como interferentes.

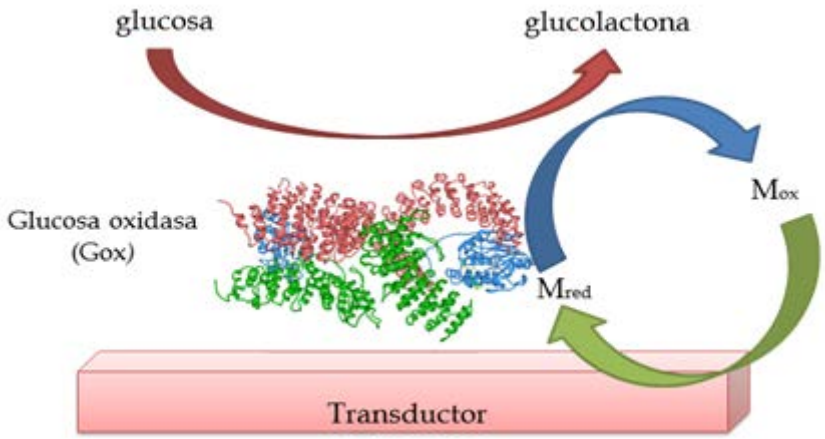

Figura 2.5.- *Esquema de las reacciones que ocurren en un biosensor de 2ª generación.*

Los mediadores más usados, tanto libres como inmovilizados en un hidrogel, son el par ferro/ferricianuro, ferroceno y sus derivados, 1,4-benzoquinonas, azul de metileno, rojo neutro, y algunos complejos de osmio y rutenio (*Ryabov et al., 1995; Castillo, 2004*). Los principales problemas asociados a dichos biosensores incluyen la competencia de los cosustratos naturales y la pérdida de la estequiometría de la

reacción, así como, pérdida del mediador (*potencialmente tóxico*) por difusión y contaminación de la muestra (*Schumann et al., 1990*).

2.4.3.1.3.- Biosensores de 3ª generación

En esta ocasión la enzima es conectada directamente con la superficie del transductor (*Ruzgas et al., 1996; Godet et al., 1999; Ryabova et al., 1999; Xiao et al., 2003; Cano et al., 2008*), evitando el uso de cualquier intermedio de reacción (cosustrato o mediador redox). Este tipo de biosensores presenta una mayor selectividad, ya que trabaja a potenciales próximos a los intrínsecos de la enzima. Según la *teoría de Marcus,* la espontaneidad de que ocurra dicho proceso de transferencia electrónica entre la enzima y el electrodo va a depender de lo accesible que sea el centro activo de la enzima (*Marcus y Sutin, 1985; Marcus, 1993*).

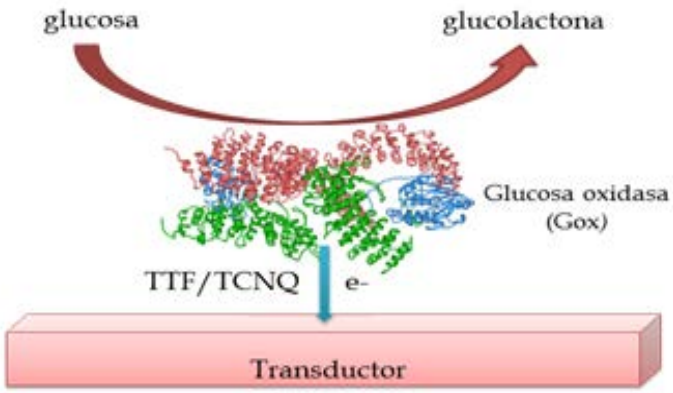

Figura 2.6.- *Esquema de las reacciones que ocurren en un biosensor de 3ª generación.*

Una de las enzimas más viables para su utilización en este tipo de biosensores es el HRP (peroxidasa de rábano), ya que su centro activo no se encuentra en el interior de la enzima (*Ruzgas et al., 1996*). Sin embargo, la mayoría de enzimas son sistemas muchos más complejos y poseen su centro activo mucho más protegido. Ejemplos evidentes de esta aproximación son los biosensores que incluyen en su estructuración

sales orgánicas conductoras tales como: tetratiofulvaleno (TTF) y/o tetracianoquinodimetano (TCNQ) (*Cano et al., 2008*).

2.5.- Técnicas de inmovilización enzimática

El buen funcionamiento de un biosensor depende de la adecuada inmovilización del sistema de reconocimiento sobre el transductor. El objetivo de dicha inmovilización es favorecer un íntimo contacto entre el biorreceptor y el transductor. El componente biológico de un biosensor tiene que ser incorporado en el dispositivo de manera que no se altere su actividad si posee propiedades catalíticas, o bien, que el sitio de unión en el que se produce la interacción con el analito se encuentre accesible al mismo (*Hermanson et al., 1992; Cao et al., 2005; Mateo et al., 2007; Minteer et al., 2011*).

La inmovilización puede realizarse mediante *métodos físicos*, fundamentalmente por adsorción o por atrapamiento, y *métodos químicos*, mediante la formación de enlaces covalentes, capas intermedias (*afinidad*) o por entrecruzamiento (*crosslinking*) (*Choi, 2004; Choi et al., 2005; Andreescu y Marty, 2006; Arya et. al; 2008*).

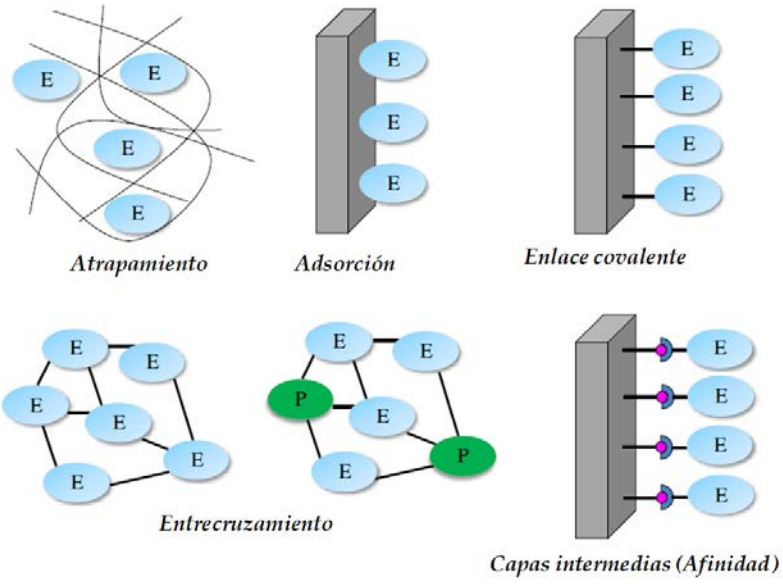

Figura 2.7- *Métodos de inmovilización empleados en el desarrollo de biosensores, (adaptada de Sassolas et al., 2012).*

Como ventajas del empleo de enzimas inmovilizadas se pueden destacar (1) el aumento de la estabilidad de la enzima; (2) la posible reutilización del biosensor, por lo que disminuye los costes del proceso y (3) la posibilidad de diseñar un reactor enzimático de fácil manejo y control, adaptado a la aplicación de la enzima inmovilizada (*Sassolas et al., 2012*). Por el contrario, los principales inconvenientes del proceso de inmovilización son: (1) alteración de la conformación de la enzima respecto a su estado nativo; (2) gran heterogeneidad del sistema enzima-soporte, donde pueden existir distintas fracciones de proteínas inmovilizadas con un diferente número de uniones al soporte; (3) pérdida de actividad enzimática durante la inmovilización (*Sassolas et al., 2012*).

2.5.1.- Métodos de inmovilización física

2.5.1.1.- Adsorción

Representa el método más sencillo para la inmovilización de proteínas y otras biomoléculas, por lo que suele resultar la alternativa más simple (*Sassolas et al., 2012*). No obstante, presenta el inconveniente de su reversibilidad y variabilidad, que pueden representar un problema cuando las condiciones ambientales fluctúan (pH, fuerza iónica, disolventes empleados, etc.). Además, la densidad de moléculas inmovilizadas sobre la superficie suele ser inferior a otros métodos de inmovilización alternativos. Sin embargo, dada su simplicidad la inmovilización física goza todavía de gran popularidad para la inmovilización de numerosas moléculas sobre superficies sensoras (*Chaubey et al., 2000; Liu et al., 2007; Xu et al., 2008; Wang et al., 2009*).

2.5.1.2.- Atrapamiento

Consiste en la retención física del elemento de reconocimiento en las cavidades interiores de una matriz sólida porosa, constituida generalmente por pasta de carbono *(Rubianes et al., 2003; Antiochia et al., 2007; Odaci et al., 2008)*, polímeros del tipo poliuretano (*Puig-Lleixa et al., 2001; Fritzen-García et al., 2009*), poliacrilatos, poliacrilamidas, polimetacrilatos, poliestireno, alcohol polivinílico, etc. (*Sassolas et al., 2012*). En general, este método de inmovilización puede llevarse a cabo de maneras distintas, como la polimerización interfacial, la simple evaporación del disolvente, el atrapamiento en una matriz polimérica y la retención mediante membranas. Se han utilizado distintas membranas semipermeables como medio de atrapamiento: acetato de celulosa, policarbonatos, teflón, Nafion (*Gogol et al., 2000*) y poliuretano (*Puig-Lleixa et al., 2001; Fritzen-García et al., 2009*). Estas membranas presentan la ventaja de preservar la configuración y actividad de las moléculas inmovilizadas, aunque introducen barreras difusionales que normalmente afectan a los tiempos de respuesta de los sensores.

En los biosensores electroquímicos se emplean además otras alternativas, como el atrapamiento mediante *electropolimerización* y generación de membranas poliméricas (popipirrol PPY, polianilina PANI, *orto-*, *meta-* y *para-* polifenilendiamina P*o*PD, P*m*PD, P*p*PD) (*Mazeikiene y Malinauskas, 2002; Langer et al., 2004; Mathebe et al., 2004; Guerrieri et al., 2006; Li et al., 2007*). Se puede recurrir a polímeros conductores, como el PPY y la PANI. Por otro lado, el *o*-PD, *m*-PD, *p*-PD pueden generar películas poliméricas (P*o*PD, P*m*PD, P*p*PD) conductora o no, en función de las condiciones de trabajo (*Li et al., 2002*). En el último caso, las propiedades aislantes dan lugar a un crecimiento limitado y generan películas poliméricas extremadamente delgadas (~10-30 nm) con mejores propiedades difusivas (*Li et al., 2002; Killoran y O'Neill, 2008; O'Neill et al., 2008; Rothwell et al., 2008*). Durante el proceso de inmovilización enzimática se suele añadir

otra enzima sin actividad (ej: BSA) que evita que se produzca un alto grado de compactación y en definitiva, pérdida de la actividad catalítica.

2.5.2.- Métodos de inmovilización química

2.5.2.1.- Enlace covalente

En las reacciones químicas utilizadas en la inmovilización covalente generalmente intervienen los grupos nucleófilos de las moléculas como: grupos amina (-NH_2) (*Wu et al., 1994; Ferreira et al., 2003*), grupos carboxílicos (-COOH) (*Delvaux M y Demoustier-Champagne S, 2003*), alcoholes (-OH) (*Sassolas et al., 2012*), tioles (-SH) y grupos imidazol (*Sassolas et al., 2012*). Las vías principales de reacción son: (1) activación de ácidos carboxílicos en ésteres mediante carbodiimida y N-hidroxisuccinimida, (2) formación de una base de Schiff entre una amina nucleófila y un aldehído, (3) sustituciones nucleofilicas entre aminas primarias o tioles y grupos electrófilos con un elemento saliente, como un éster activado o un halogenuro de ácido (*Sassolas et al., 2012*).

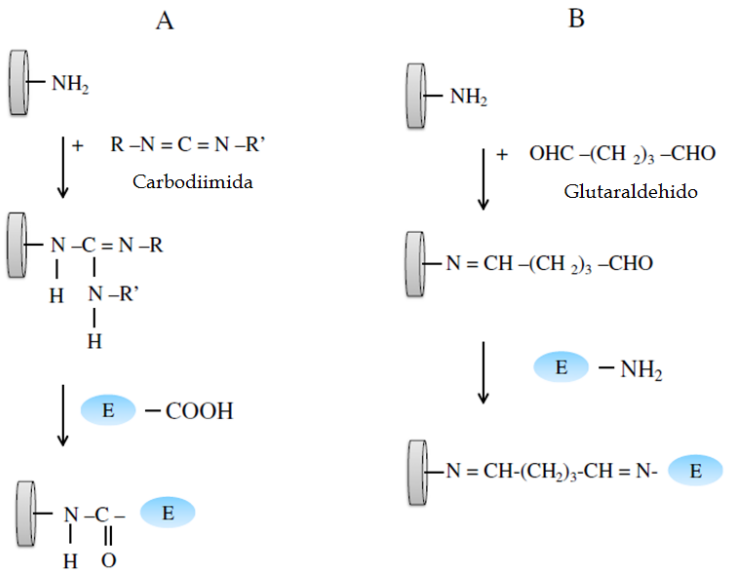

Figura 2.8- *Ejemplos de enlaces covalentes sobre una superficie previamente aminada por acoplamiento mediante: (A) carboiimida (B) glutaraldehido (adaptada de Sassolas et al., 2012).*

2.5.2.2.- Capa intermedia

Otra vía de inmovilización consiste en generar un sedimento de moléculas que formen un enlace selectivo de bioafinidad entre dicho sedimento (lectina, avidina, quelatos metálico) (*Andreescu et al., 2001*) y las moléculas de reconocimiento (enzimas, anticuerpos, DNA). Este método permite controlar la orientación de la biomolécula con el fin de evitar la desactivación enzimática y/o bloqueo del centro activo. Las capas intermedias más empleadas son: proteína A, concanavalina A (*Bucur et al., 2004*), proteína G y avidina (*Sassolas et al., 2012*).

2.5.2.3.- Entrecruzamiento

El método de entrecruzamiento o *cross-linking* se basa en crear enlaces intermoleculares irreversibles entre las enzimas (o material biológico de reconocimiento) usando polímeros con grupos bi y multifuncionales (dialdehídos, diiminoésteres, diisocianatos, sales de bisdiazonio) (*Gogol et al., 2000; Berezhetskyy et al., 2008; Luo et al., 2008; Kong et al., 2009; Sassolas et al., 2012*). Este método es atractivo debido a su simplicidad y a la fortaleza del enlace químico producido. El principal inconveniente es la pérdida de actividad debido a distorsiones en la conformación enzimática y/o a las alteraciones químicas del sitio activo durante la reticulación. Proteínas sin actividad enzimática como el BSA, rico en residuos de lisina, suele ser correticulada con el receptor biológico para disminuir dichos efectos disfuncionales (*Gogol et al., 2000; Pei et al. 2004; Berezhetskyy et al., 2008; Yonemori et al., 2009*).

3.- El Azul de Prusia

El Azul de Prusia (*Prussian Blue, PB*), $Fe_4[Fe(CN)_6]_3$, pertenece a la familia de los hexacianometalatos metálicos, $\{X_n[Y(CN)_6]_m\}$, donde X e Y son sustituidos por átomos de hierro (*Karyakin, 2001; Abbaspour y Kamyabi, 2005; Giménez-Romero et al., 2007*). Es el compuesto de coordinación más antiguo conocido y utilizado como tinte desde el siglo XVIII (*Kraft, 2008*). Sus propiedades electroquímicas se conocen desde la década de los setenta, cuando Neff informó de la deposición de una fina capa de PB sobre una lámina de platino (*Neff, 1978*). A partir de este momento, aparecieron un gran número de publicaciones estudiando sus propiedades electrocrómicas (*Ellis et al., 1981; Rajan et al., 1982; Mortimer y Rosseinsky, 1983; Mortimer y Rosseinsky, 1984; Koncki et al., 2001; Koncki, 2002*) y electroquímicas (*Itaya et al., 1986; Feldman et al., 1987; Dostal et al., 1995*). Desde un punto de vista práctico, el PB ha sido empleado con éxito en el campo de los biosensores (*Garjonyte y Malinauskas, 2000a; Guan et al., 2004; Haghighi et al., 2004*) e inmunosensores (*Jiang et al., 2010; Liu et al., 2010; Wang et al., 2011*). A su vez, se han descrito multitud de métodos para optimizar su deposición (*química, fotoquímica* o *electroquímica*) y estabilidad (*Ricci y Palleschi, 2005*).

Hoy en día, su comportamiento electroquímico se entiende bastante bien. Los electrodos modificados con PB muestran, mediante CV, dos picos característicos (*Ellis et al., 1981; Rajan et al., 1982; Itaya et al., 1984a; Itaya et al., 1984 b; Ohzuku et al., 1985; Itaya et al., 1986*). El primero corresponde a la interconversión entre el Blanco de Prusia (*Prussian White, PW*) y el PB (**Ecuación 3.1**), mientras que el segundo, corresponde a la transición entre PB y el Verde de Prusia (*Prussian Green, PG*), (**Ecuación 3.2**). Las

reacciones de transferencia de electrones en presencia de KCl como electrolito soporte se pueden formular de la siguiente manera (ecuaciones 3.1 y 3.2):

$$(PB)\ Fe^{III}_4[Fe^{II}(CN)_6]_3 + 4e^- + 4K^+ \rightarrow (PW)\ K_4Fe^{II}_4[Fe^{II}(CN)_6]_3 \qquad \textbf{Ecuación 3.1}$$

$$(PB)\ Fe^{III}_4[Fe^{II}(CN)_6]_3 + 3Cl^- \rightarrow (PG)\ Fe^{III}_4[Fe^{III}(CN)_6]_3Cl_3 + 3e^- \qquad \textbf{Ecuación 3.2}$$

Donde los potenciales para dichas transiciones se sitúan a +0.1 y +0.9 V frente SCE respectivamente (*Ellis et al., 1981; Itaya et al., 1982a; Itaya et al., 1982b; Itaya et al., 1982c; Rajan et al., 1982; Ohzuku et al., 1985; Karyakin, 2001*). Sus propiedades electroquímicas, tales como: potencial formal, sensibilidad, estabilidad y constantes de velocidad de transferencia electrónica de las conversiones PB/PW y PB/PG dependen del: método de deposición, pH, naturaleza y concentración de electrolito soporte, etc. (*Itaya et al., 1982a, Itaya et al., 1986; García-Jareño et al., 1998*).

La estructura *zeolítica* del PB (**Figura 3.1**), cuya celda unitaria posee una estructura tridimensional cúbica centrada en las caras con una celda unitaria de 10.2 Å y un diámetro de canal aproximado de 1.6 Å (*Ludi y Gudel, 1973; Herren et al., 1980*), define en gran medida las propiedades electrocatalíticas y electroquímicas del PB, permitiendo así, la libre difusión a través de su estructura cristalina de moléculas de bajo peso molecular (como el O_2 y H_2O_2) y de ciertos iones (*Itaya et al., 1986*). Las reacciones de oxido/reducción son acompañadas por la difusión de cationes (K^+) y aniones (Cl^-) que permiten compensar la carga de las distintos estados redox (**Ecuación 3.1** y **Ecuación 3.2**). Por ello dichas interconversiones, PW/PB y PB/PG, son muy influenciadas por el electrolito soporte, que debe difundir a través de su estructura cristalina (*Itaya et al., 1982a, Itaya et al., 1986; García-Jareño et al., 1998; Ricci y Palleschi, 2005*).

Debido a este mecanismo (**Ecuación 3.1**), sólo cationes con radios hidratados pequeños, tales como K^+ (1.25 Å), NH_4^+ (1.25 Å), Rb^+ (1.28 Å) y Cs^+ (1.19 Å), pueden difundir libremente por la estructura del PB y compensar las cargas durante la interconversión PW/PB. Por otro lado, Na^+ (1.35 Å), Ca^{2+} (1.56 Å), Mg^{2+} (1.61 Å), debido a sus radios hidratados mayores no pueden difundir tan libremente en la estructura tridimensional del PB, dificultando y/o inhibiendo la interconversión PW/PB y viceversa.

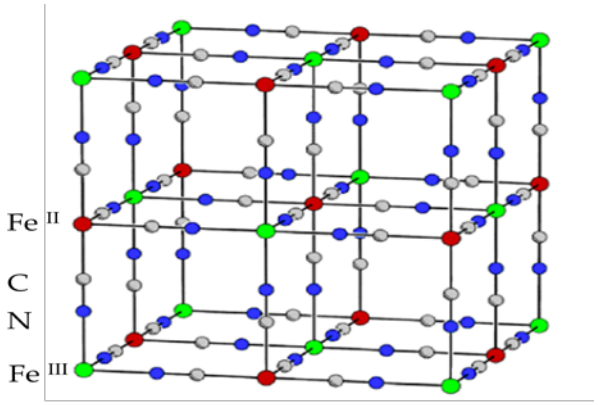

Figura 3.1- *Estructura zeolítica (cúbica centrada en las caras) propuesta para el PB (adapta a partir de: http://mslab.polymer.pusan.ac.kr/english/research.html).*

Durante muchos años, la estructura del PB y la relación con su comportamiento electroquímico y sus propiedades electrocatalíticas ha sido fuente de controversia. Los primeros intentos por resolver dicha estructura, o más bien su estequiometría se remontan al siglo XVII y XIX, cuando químicos tan prestigiosos como: Priestley, Scheele, Bertholet, Gay-Lussac y Berzelius intentaron elucidar la composición química del PB (*Kraft et al., 2008*). En 1782 Scheele descubrió que se formaba cianuro de hidrógeno al calentar el PB en una disolución diluida de ácido sulfúrico, mientras que en 1811 la determinación estequiométrica de Gay-Lussac del cianuro de hidrógeno concluyó con la hipótesis de que el PB contenía cianuros en su estructura (*Kraft et al.*,

2008). Debido a la falta de técnicas analíticas adecuadas, los detalles estructurales e incluso su composición estequiométrica solo pudo ser resuelta parcialmente. En la década de los 30 del siglo pasado, Keggin y Miles (*Keggin y Miles, 1936*) estudiaron su estructura mediante rayos X. Dichos autores distinguieron dos formas diferentes de PB que llamaron desafortunadamente: *soluble* e *insoluble*. Estos términos, usados en la industria textil de la época no se refieren a la solubilidad en agua, sino más bien indican la facilidad con la que los iones potasio se introducen en la estructura del PB. La inadecuada aplicación de estos términos ha sido debatida por muchos autores, siendo demostrado finalmente que ambas conformaciones son muy insoluble (Kps = 10^{-40}) (*Ellis et al., 1981; Mortimer y Rosseinsky, 1984*).

De acuerdo con Keggin y Miles, la forma "*soluble*" del PB $\{KFe^{III}Fe^{II}(CN)_6\}$ tiene una estructura cúbica en las que el hierro (II) y el hierro (III) se encuentran en una cara cúbica centrada en las caras, donde el hierro (II) está rodeado por átomos de carbono y el hierro (III) está rodeado por átomos de nitrógeno coordinados octaédricamente. Por otro lado, la forma "i*nsoluble*" $\{Fe^{III}_4[Fe^{II}(CN)_6]_3\}$ presenta un exceso de iones férricos, que remplazan a los iones potasio de la forma soluble en las posiciones intersticiales (*Keggin y Miles, 1936; Mortimer y Rosseinsky, 1984*). Posteriores trabajos (*Ludi y Gudel, 1973; Buser et al., 1977; Herren et al., 1980*) mostraron algunas discrepancias con la forma insoluble del PB propuesta por Keggin y Miles. Dichos autores encontraron una estructura más desordenada, donde una cuarta parte de los sitios ocupados por el anión ferrocianuro estaban desocupados, a su vez, encontraron la presencia de 14 a 16 moléculas de agua en cada celda unitaria. Una porción de estas moléculas de agua estaban ocupando los sitios vacíos de nitrógeno del grupo ferrocianuro, mientras que el resto ocupaba posiciones intersticiales en forma de agua no coordinada. Por otra parte, dichos autores no encontraron hierro (III) en sitios intersticiales. Estos resultados

también han sido confirmados por espectroscopia Mossbauer e infrarrojo (*Duncan y Wrigley, 1963; Robin y Day, 1967*).

Hay que destacar que la incertidumbre encontrada y las distintas estructuras propuestas para el PB pueden atribuirse al hecho de que el PB es una designación química genérica de un material mucho más complejo con estequiometría variable (*Itaya et al., 1986*). Siendo la estructura definitiva función de los materiales de partida y del procedimiento de cristalización, que podría generar estructuras con: iones coprecipitados, distinto contenido en agua coordinada y no coordinada, distinto grado de defectos y vacantes en el retículo cristalino, presencia de ferrocianuro hidrolizado, etc.

3.1.- Deposición de Azul de Prusia

La mayoría de los depósitos de PB se obtienen mediante el empleo de técnicas electroquímicas, ya que permiten un control exacto de la extensión de la deposición (cantidad y espesor del depósito). Entre estas, destaca la *técnica galvanostática* en la que el electrodo a modificar se introduce en una disolución que contiene iones ferricianuro y cloruro férrico y se aplica un potencial adecuado y constante durante un tiempo determinado *(Karyakin et al., 1996; Karyakin et al., 1998; Garjonyte y Malinauskas, 1999b; Karyakin et al., 2000; Garjonyte y Malinauskas, 2000b*). La CV también ha sido usada con éxito, donde la cantidad de PB depositado depende de la velocidad de barrido, los límites del ciclado y el número de ciclos empleados (*Garjonyte y Malinauskas, 1999b*).

La electrodeposición es seguida generalmente por una etapa de activación (*transición de la forma insoluble a la soluble*) del depósito mediante CV, donde los electrodos modificados con PB son ciclados en la disolución electrolítica soporte hasta que el CV permanece constante (30-50 ciclos). Posteriormente, el depósito es

estabilizado (pérdida del agua de solvatación) mediante una etapa de calentamiento (100 ºC durante 1-1.5 h).

La *deposición química* ha demostrado ser una alternativa útil y cada vez es más empleada, sobre todo para modificar tintas de impresión para electrodos serigrafiados (*Moscone et al., 2001; Ricci et al., 2003a; Ricci et al., 2003b*). Dicha técnica consiste en hacer reaccionar Fe^{3+} con $Fe^{II}(CN)_6^{4-}$ o Fe^{2+} con $Fe^{III}(CN)_6^{3-}$ dando lugar a una suspensión coloidal de color azul, que posteriormente se mezcla con los materiales empleados en la construcción de electrodos serigrafiados.

3.2.- Estabilidad de Azul de Prusia frente al pH

La desventaja principal de PB es su solubilidad a pH neutro y básico. Dicha solubilidad está relacionada con la formación de hidroxo-complejos de hierro y la precipitación de $Fe(OH)_3$ a partir de pH 6.4 (*Feldman y Murray, 1987; Stilwell et al., 1992*), que en definitiva, producen la ruptura de los enlaces CN-Fe-CN (*Karyakin y Karyakina, 1999*). Diferentes estudios de estabilidad indican que el depósito de PB puede ser estabilizado en medio neutro y básico modificando el procedimiento de deposición (*Moscone et al., 2001; Ricci et al., 2003a*), aunque existen numerosas variaciones más o menos laboriosas, las etapas claves se pueden resumir en: (1) electrodeposición en medio ácido 0.1 M de KCl y HCl, (2) activación por ciclado a potencial controlado, (3) estabilización térmica.

Otros métodos propuestos consisten en modificar ligeramente su estructura química, así como su estructura tridimensional para evitar la libre difusión de grupos OH^- a través del cristal (*Moscone et al., 2001; Haghighi et al., 2004*). Sin embargo, un enfoque más práctico utiliza el recubrimiento y/o codeposición de PB con diversos polímeros como: Nafion, PPY, PANI y P*o*PD, mejorando así, su estabilidad operativa y

selectividad frente diversas sustancias electroactivas (*Karyakin y Chaplin, 1994; Chi y Dong, 1995; Karyakin et al., 1995; García-Jareño et al., 1996; Karyakin et al., 1996; Garjonyte y Malinauskas, 2000a; Garjonyte y Malinauskas, 2000b; Lukachova et al., 2002*). Lukachova y colaboradores han descrito un electrodo modificado con PB recubierto con PoPD con una sensibilidad moderada H_2O_2 (0.3 A M^{-1} cm^{-2}), una elevada selectividad (~600) frente el AA y una excelente estabilidad operativa (~20 h) (*Lukachova et al., 2003*).

3.3.- Electrodeposición de PB en presencia de surfactantes catiónicos

Recientemente ha sido descrita la electrodeposición de PB y otros hexacianoferratos en presencia de bromuro de cetiltrimetilamonio (CTAB) (*Vittal et al., 1999; Vittal et al., 2000; Vittal et al., 2001; Senthil-Kumar y Chandrasekara-Pillai, 2006a; Vittal et al., 2006; Vittal et al., 2008*). Según está recogido en la bibliografía, las reacciones en condiciones normales de formación del PB son:

$$Fe^{3+} + e^- \rightarrow Fe^{2+} \qquad \textbf{Ecuación 3.3}$$

$$Fe^{3+} + Fe^{2+} + [Fe^{III}(CN)_6]^{3-} \rightarrow Fe^{3+}_{1/3}Fe^{3+}\,[Fe^{II}(CN)_6]^{4-} \qquad \textbf{Ecuación 3.4}$$

Donde $Fe^{3+}_{1/3}Fe^{3+}[Fe^{II}(CN)_6]^{4-}$ es la forma insoluble del PB (*Senthil-Kumar y Chandrasekara- Pillai, 2006b*). De acuerdo con estos autores, la presencia de CTAB en la disolución de trabajo durante la formación del PB puede facilitar la electrodeposición sobre la superficie del electrodo al interactuar positivamente con los componentes de la disolución y la superficie del transductor. Según el mecanismo propuesto, cuando el catión CTA^+ se encuentra en disolución a su CMC (*Critical Miscellar Concentration*), la superficie del electrodo (interfase agua/electrodo) estaría totalmente recubierta por iones CTA^+ perfectamente orientados, favoreciendo así, la interacción electrostática entre los grupos $[Fe^{III}(CN)_6]^{3-}$ y CTA^+. De esta forma, no solo se incrementa el número de grupos $[Fe^{III}(CN)_6]^{3-}$ en la superficie del electrodo (recordemos que las funciones -

$COOH/COO^-$ comunes en electrodos de carbono pueden dificultar la adsorción del anión $[Fe^{III}(CN)_6]^{3-}$), sino que también favorece una orientación adecuada del ferricianuro que posteriormente reacciona con los iones Fe^{2+} y Fe^{3+} (**Ecuación 3.4**) (*Senthil-Kumar y Chandrasekara-Pillai, 2006b*).

Por otro parte, si se emplea la CV como método de electrodeposición, a partir de 0.9 V vs. SCE el PB adquiere carga negativa, favorenciendo la formación de una nueva capa de CTA^+ sobre el depósito de PB recién formado, y favoreciendo la electrodeposición de una nueva capa de PB. Mediante dicho proceso, se van alternando capas de PB y CTA^+ dando lugar a una estructura híbrida PB/CTAB (muy irregular y porosa) que puede continuar creciendo virtualmente hasta que se agoten los reactivos en la disolución de trabajo o se ralentice su aporte hacia superficie del electrodo (*Senthil-Kumar y Chandrasekara-Pillai, 2006b*).

Con esta metodología se ha conseguido además del incremento significativo del depósito y de la sensibilidad frente a H_2O_2, una mejora en la rapidez y eficacia del transporte iónico (*Vittal et al., 2006; Vittal et al., 2008*). Por otro lado, y de suma importancia para la aplicación del PB en biosensores que operan en condiciones fisiológicas, se ha obtenido una muy buena estabilidad de los depósitos de PB a pH neutro y ligeramente básico. Dicha estabilidad se puede atribuir a varios factores: (1) el CTAB, así como otros surfactantes catiónicos, posee en su estructura amonios cuaternarios con propiedades ácidas, creando un microentorno ligeramente ácido que puede anular el efecto de los iones OH^-; (2) la estabilización electrostática entre capas catiónicas (CTA^+) y aniónicas (PB) ofrece una estabilización adicional y evita su disolución (*Senthil-Kumar y Chandrasekara-Pillai, 2006a*).

3.4.- Biosensores basados en Azul de Prusia

Pese a que en 1984 Itaya y colaboradores (*Itaya et al., 1984a; Itaya et al., 1984b*) demostraron que la forma reducida de la PB (PW) mostraba actividad catalítica frente a la reducción selectiva de O_2 y H_2O_2 a un potencial próximo a -0.250 y 0 V frente a SCE respectivamente, no fue hasta 1994 cuando Karyakin y colaboradores (*Karyakin et al, 1994*) propusieron el primer biosensor de glucosa que aprovechaba dichas propiedades para detectar el H_2O_2 generado enzimáticamente por la *glucosa oxidasa* (**Figura 3.2**). En 1995, dicho autor optimizó su diseño alcanzando un límite de detección de 10^{-6} M y un rango lineal hasta una concentración de 5 mM (*Karyakin et al., 1995*). En ese mismo año Chi y Dong, consiguieron depositar la *Gox* durante la electrodeposición del PB (*Chi y Dong, 1995*), añadiendo posteriormente un recubrimiento con Nafion. Este biosensor presentó una rápida respuesta, un límite de detección de $2 \cdot 10^{-6}$ M y un rango de concentración lineal de 0.01-3 mM.

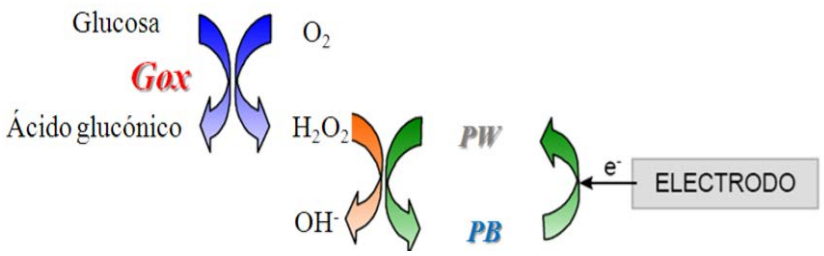

Figura 3.2.- *Esquema de reacciones acopladas en un biosensor de 1ª generación de glucosa, basado en la detección amperométrica del H_2O_2 con Azul de Prusia.*

El interés de la comunidad científica por el PB ha ido creciendo, en especial debido a sus propiedades electrocatalíticas y electrocrómicas. Este avance se muestra en la **figura 3.3,** donde se observa un continuado aumento en el número de publicaciones científicas, mostrando un incremento notable a partir de 2005, donde se triplica el número de publicaciones anuales.

El ámbito más generalizado de aplicación ha sido el desarrollo de biosensores sensibles a glucosa (*Karyakin et al., 1994; Chi y Dong, 1995; Karyakin et al., 1995; Garjonyte y Malinauskas, 2000a; Garjonyte y Malinauskas, 2000b; Li et al., 2008*). Sin embargo, muchas otras enzimas han sido empleadas: lactato oxidasa (*Garjonyte et al., 2001; Ricci et al., 2003c*), colesterol oxidasa (*Li et al, 2003; Vidal et al, 2004*), aminoácido oxidasa (*Chi y Dong, 1995*), etanol oxidasa (*Karyakin et al, 1996*), glutamato oxidasa (*Karyakin y Karyakina, 2000*), lisina oxidasa (*Ricci et al. 2003b*) y oxalato oxidasa (*Fiorito y Córdoba de Torresi, 2004*).

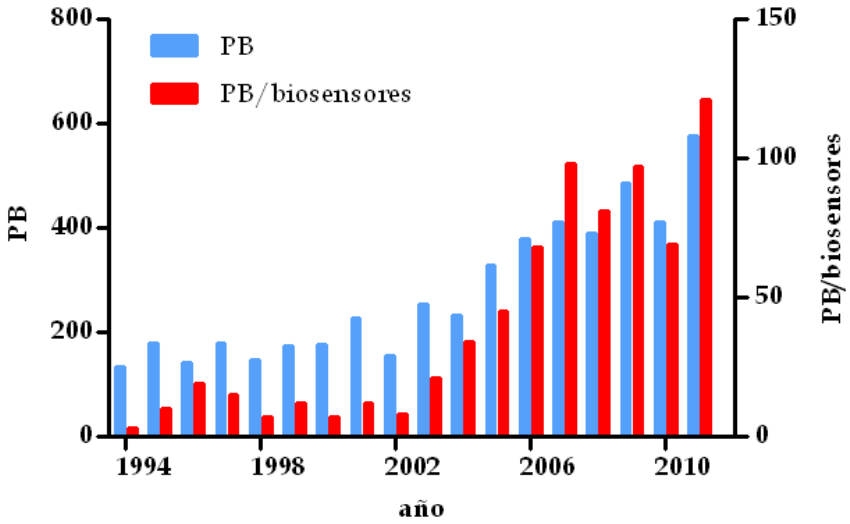

Figura 3.3.- *Histograma de publicaciones científicas referidas a las palabras claves: Prusian Blue y Prussian Blue-biosensors* (fuente: http://www.sciencedirect.com).

Pese al gran número de aplicaciones del PB en el ámbito de los biosensores (*Ricci y Palleschi, 2005*), el desarrollo de microbiosensores modificados con PB y su aplicación en el ámbito neuroquímicoy neurofisilógico no ha sido explorado hasta la presente tesis. Fruto del presente trabajo se han publicado 7 artículos en revistas científicas indexadas, así como numerosas presentaciones en congresos nacionales e internacionales.

OBJETIVOS

4.-Objetivos

El objetivo de esta tesis es el diseño y caracterización (*in vitro* e *in vivo*) de biosensores que puedan medir glucosa y lactato en el sistema nervioso central (SNC). Debido a las restricciones espaciales inherentes a dicho estudio, como punto de partida se han empleado electrodos de fibra de carbono de ~ 10 μm de diámetro. Estas pequeñas dimensiones aseguran una perfecta resolución espacial y evita que se produzcan alteraciones considerables del medio (espacio extracelular cerebral), tales como: pérdida de integridad de la barrera hematoencefálica, rotura de vasos sanguíneos, cambios en la microcirculación local, edemas etc.

El desarrollo de la presente memoria ha estado orientado hacia la elaboración de biosensores *electroquímicos* que *a posteriori* puedan ser usados en resolver uno de los debates más importantes que hoy en día se plantean en el área de la neurociencia: *el estudio del metabolismo energético cerebral*. El enfoque electroquímico ha sido elegido por ser una técnica versátil, económica, de fácil uso y una herramienta complementaria a otras técnicas empleadas en el laboratorio de Neuroquímica y Neuroimagen de la Universidad de La Laguna (RMN, microdiálisis, técnicas espectroscópicas, etc.).

Por otro lado, se ha modificado el enfoque convencional: empleo de transductores de Pt, Pt/Ir ($\Phi \sim 100$ μm) y detección amperométrica a + 0.70 V, por un nuevo sistema de transducción basado en fibras de carbono modificadas con PB, capaz de seguir la reacción enzimática a un potencial próximo a 0 V. Evitando así, el posible efecto que el potencial aplicado pueda ejercer sobre la exitabilidad neuronal.

Dicha aproximación resulta novedosa, tanto por las propiedades electrocatalíticas que ofrece el PB, como por el hecho de que hasta el momento no se han encontrado evidencias bibliográficas del uso del PB en el diseño de microbiosensores para medir glucosa y lactato en el SNC.

A continuación, se resumen los objetivos principales que se han marcado como fundamentales en el desarrollo del presente trabajo:

1) Construción y modificación de microelectrodos de fibra de carbono con PB.
2) Optimización de la electrodeposición, estabilidad y sensibilidad del depósito PB mediante el uso de surfactantes catiónicos.
3) Construcción de microbiosensores de glucosa y lactato con sensibilidad, selectividad y resolución temporal y espacial adecuados para trabajar en el SNC.
4) Empleo de una amplia gama de polímeros con el fin de optimizar: i) la operatividad a bajas concentraciones de oxígeno ii) la sensibilidad analítica iii) la biocompatibilidad y iv) la selectividad de los microbiosensores frente a los interferentes biológicos más comunes.

5) Optimización de los protocolos de modificación enzimática con *Gox* y *Lox* para adecuar la sensibilidad y selectividad de los microbiosensores desarrollados a las condiciones del entorno de trabajo.
6) Diseño y elaboración de experimentos, *in vitro* e *in vivo* de validación que demuestren la utilidad de los microbiosensores desarrollados en la presente tesis en el ámbito neuroquímico y neurofisiológico.

MATERIALES Y MÉTODOS

5.-Materiales y métodos

5.1.-Reactivos

Todos los reactivos han sido suministrados por la compañía *Sigma-Aldrich* y usados sin previa modificación y/o purificación. Cada reactivo ha sido almacenado en las condiciones recomendadas por la casa comercial. Todas las disoluciones fueron preparadas con agua ultrapura (*Milli-Q/Millipore*) y conservadas en nevera mientras no eran usadas. Las disoluciones de reactivos poco estables (H_2O_2, *o*-PD, interferentes, glutaraldehido, etc.) se prepararon previo uso. Las disoluciones enzimáticas y el calibrado de los microbiosensores han sido realizadas en tampón fosfato salino 0.01M (sigma [P4417]: 0.01 M tampón fosfato, 0.135 M NaCl, 0.027 M KCl, pH=7.4).

Las fibras de carbono y los capilares de vidrio usados en la construcción de los microbiosensores fueron suministrados por la empresa *World Precission Instrument y Union Carbide*, mientras que el alambre de cobre de 0.25 mm fue suministrado por *RS*. La resina epoxi empleada para sellar los extremos de los microbiosensores ha sido resina comercial de uso cotidiano. Los electrodos serigrafiados de pasta de carbono (SPCE) modelo DRP-110 fueron suministrado por la empresa española *Dropsens*.

A continuación, se describen brevemente los principales reactivos empleados en la construcción y validación de los microbiosensores:

5.1.1.-Microelectrodos de fibra de carbono

Las fibras de carbono son relativamente inertes y tienen excelentes propiedades mecánicas y eléctricas, además son ideales para realizar registros electrofisiológicos y electroquímicos con un tamaño micrométrico.

Los CFEs fueron introducidos en la década de los 70 por *François Gonon* y colaboradores (*Gonon et al., 1981*). En sus primeros experimentos Gonon y colaboradores midieron la corriente de oxidación de dopamina (DA) utilizando técnicas como la voltametría normal pulsada (NPV) y la CV. Dichos trabajos concluyeron que los CFEs tenían un límite de detección mejor que los CPEs. Por otro lado, dependiendo del método electroquímico aplicado los compuestos con picos de oxidación y reducción solapados podían ser resueltos adecuadamente.

Los CFEs han demostrado ser muy adecuados para la detección electroquímica *in vivo* de distintas catecolaminas (*Ponchon et al., 1979*) y otras especies oxidables, incluyendo óxido nítrico (NO) (*Malinski y Taha, 1992*). La inmovilización de moléculas de ADN o de nanotubos de carbono (CNT) (*Zhang et al., 2007*) sobre los CFEs ha abierto nuevas vías en la detección electroquímica de especies de importancia biológica.

5.1.2.-Nafion

El Nafion *es un polímero polianiónico* descubierto por la empresa *DuPont* en 1966. Dicho polielectrolito es un polímero perflurado (con átomos de flúor en vez de hidrógeno) compuesto por cadenas, tipo teflón, de las que derivan cadenas laterales con grupos iónicos (sulfonatos, SO_3^-). Los protones de los grupos HSO_3 (ácido

sulfónico) pueden saltar a un grupo SO_3^- adyacente mediante un mecanismo conocido como *hopping*, actuando como un excelente transportador de protones. Su estructura porosa con canales con un tamaño comprendido entre 10 y 50 Å permite el movimiento no solo de cationes, sino también de otras pequeñas moléculas como: H_2O, CH_3OH, H_2O_2.

Sin embargo, su naturaleza aniónica impide el paso de aniones a través de su estructura (*expulsión Donnan*). Tradicionalmente, en el ámbito biomédico ha sido empleado como recubrimiento externo en microelectrodos para detectar distintos neurotransmisores y metabolitos en el SNC en presencia de interferentes de naturaleza aniónica (Gerhardt et al., 1984; *O'Neill et al., 2008*). Por otro lado, también ha sido empleado para disminuir los procesos de biofloculación sobre la superficie sensora *(Oldenziel et al., 2006*). De esta forma, microelectrodos modificados con Nafion presentan repulsiones electroestáticas frente a compuestos aniónicos como el AA, AU, lípidos, etc., mientras que permite el paso de neurotransmisores catiónicos (DA y serotonina (5-HT)) con un coste temporal mínimo (*Gogol et al., 2000; Choi et al., 2005; O'Neill et al., 2008; Tseng et al., 2009*).

El proceso de recubrimiento consiste en sumergir el electrodo varias veces en una disolución comercial de Nafion al 5% en alcohol, y dejarlo secar a temperatura ambiente o en la estufa a 180 º C.

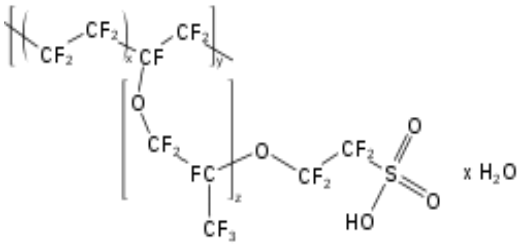

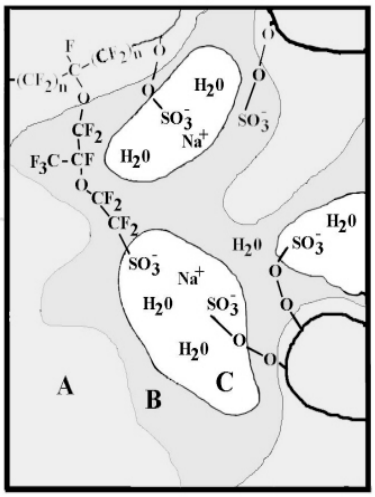

Figura 5.1.-*Fórmula (fuente: Wikipedia) y estructura del Nafion donde se observan los canales iónicos por donde existe libre flujo de moléculas de agua y cationes (fuente: http://www.intellectualism.org/questions/QOTD/dec03/20031209.php).*

5.1.3.- Polietilenimina

La Polietilenimina (PEI) es un polímero catiónico obtenido a partir de monómeros de etilenimina. Según su estructura molecular, dicho polímero puede ser lineal o ramificado. El PEI contiene una gran cantidad de grupos amino que pueden ser primarios, secundarios o terciarios. Debido a su alto contenido en dichos grupos funcionales, tanto la polietilenimina lineal como la ramificada han despertado un gran interés en la industria aeronáutica para capturar y almacenar CO_2.

Al igual que otros policationes (derivados de polilisina, PLL) es empleado en terapia génica en procesos de *transfección celular* (*Garnett, 1999*), protegiendo al ADN de la degradación en el compartimento endosomal, durante la maduración del endosoma a lisosoma, y facilitando el tránsito intracelular del ADN hacia el núcleo celular.

Por otro lado, debido a su carácter policatiónico puede ser empleado para acumular y estabilizar enzimas con punto isoeléctrico inferior al pH fisiológico sobre la superficie del transductor. Incrementando la actividad y la carga enzimática en la superficie del biosensor (*Breccia et al 2002; Qian et al., 2004*), y en consecuencia aumentando la sensibilidad y disminuyendo el límite de detección del mismo (*O'Neill et al 2008*).

5.1.4.- Poli-*o*-fenilendiamina

En los últimos años ha incrementado el interés de los polímeros no conductores, en especial su aplicación en el desarrollo de sensores y biosensores electroquímicos. Su

limitado crecimiento debido a su naturaleza no conductora permite generar capas muy delgadas (10-30 nm), con buenas propiedades difusivas, tiempos de respuesta rápidos y con excelentes propiedades antiinterferentes (*Li et al., 2002; Killoran y O'Neill, 2008; O'Neill et al., 2008; Rothwell et al., 2008*). Por otro lado, presentan buena biocompatibilidad y permiten inmovilizar enzimas en su estructura (*Lowry et al., 1998*). Otra ventaja importante, es que el proceso de autosellado permite que la electropolimerización sea mucho más reproducible y con menores defectos estructurales, obteniéndose un recubrimiento más homogéneo sin huecos o surcos estructurales (*pin-holes*).

Los monómeros más comunes empleados en la síntesis de películas no conductoras son derivados del benceno, tales como: fenol, *o*- y *p*-aminophenol, *o*-, *m*- y *p*-diaminobenceno (*fenilendiamina*) y *o*- y *p*-dihidroxibenceno (*Mazeikiene y Malinauskas, 2002; Langer et al., 2004; Mathebe et al., 2004; Guerrieri et al., 2006; Li et al., 2007*). En los últimos años el interés por la síntesis de membranas poliméricas basadas en la *o*-fenilendiamina (*o*-PD) se ha incrementado, sobre todo en el ámbito fisiológico. En condiciones de neutralidad el monómero se polimeriza en su forma no conductora, formando una membrana químicamente inerte, extremadamente fina (10-30 nm) y reproducible. Dicha membrana posee excelentes propiedades difusivas frente a pequeñas moléculas como el H_2O_2 y el O_2. Sin embargo, debido a su denso empaquetamiento presenta excelentes propiedades antiinterferentes (impidiendo la difusión de moléculas de mayor tamaño que el monómero).

Por otro lado, presenta pocos problemas frente a fenómenos de biofloculación proteica e interacción con el sistema inmune, pudiendo ser mejorada al incorporar heparina o BSA a la disolución de electropolimerización. La adición de BSA disminuye el grado de compactación de la capa de P*o*PD y disminuye la pérdida de sensibilidad

debido a las nuevas restricciones difusivas de los analitos, cofactores y productos enzimáticos a través dicha membrana. A su vez, disminuye el número de desactivaciones de los centros activos enzimáticos debido a fenómenos estéricos.

Todavía no ha sido resuelta la estructura de la P*o*PD debido a que su limitado grosor dificulta su estudio mediante técnicas instrumentales convencionales como el microscopio de barrido electrónico. Sin embargo, existen diversos autores que sugieren la existencia de dos estructuras plausibles: estructura tipo escalera (*Chiba et al., 1987*) y estructura abierta (*Yano, 1995*).

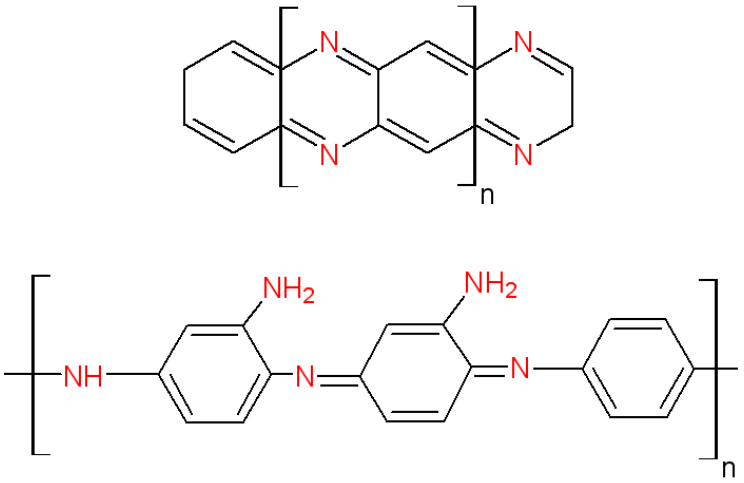

Figura 5.2.- *Posibles estructuras propuestas para el PoPD.*

Las propiedades permeoselectivas de los derivados de la fenilendiamina (*o-*, *m-* y *p-)* así como, las condiciones óptimas para su síntesis (CV, CPA, potencial de deposición, fuerza iónica del medio, naturaleza iónica del medio, etc.) han sido revisadas y discutidas ampliamente en publicaciones recientes (*Killoran et al; 2007; Rothwell et al 2009; Rothwell et al., 2010; Rothwell y O'Neill, 2011*) justificando sin duda, el empleo de la P*o*PD como membrana permeoselectiva en el desarrollo de la presente tesis.

5.1.5.- Glucosa oxidasa (*Gox*)

La *Glucosa oxidasa* (*Gox*) es una flavoproteína que cataliza la oxidación de la β-D-glucosa en ácido glucónico con la utilización del oxígeno como aceptor último de electrones (*Wang, 2008; Wang 2011*). Durante la reacción se produce H_2O_2 como subproducto. La *Gox* es una de las enzimas mejor estudiadas, puesto que presenta numerosas ventajas con respecto a otras enzimas: alta constante de velocidad, excelente selectividad, buena estabilidad térmica y con el pH, bajo coste de obtención, etc. La enzima está constituida por dos subunidades idénticas y una única molécula de flavín adenín dinucleótido (FAD) como grupo prostético. La *Gox* posee un peso molecular de 186,000 g/mol y unas dimensiones de 70 Å x 55 Å x 80 Å.

El grupo prostético en su estado FAD se encuentra en la forma oxidada y para pasar a su forma reducida ($FADH_2$) necesita la adición de dos átomos de hidrógenos que toma del sustrato (glucosa). Ambos pares son electroquímicamente reversibles en presencia de cofactores como el O_2. La estructura cristalina de la *Gox* ha revelado recientemente que el tamaño de la hendidura enzimática presenta una apertura inicial de 10 Å x 10 Å y que solo puede modificar su tamaño en unos pocos angstroms. Esto permite que la glucosa entre al sitio activo y pueda ser oxidada de manera específica.

5.1.6.- Lactato oxidasa (*Lox)*

La enzima *Lactato oxidasa* (*Lox*) pertenece también al grupo de las flavoenzimas. En este caso, el grupo prostético es el grupo flavín mononucleótido (FMN) (*Chaubey et al., 2000; Garjonyte et., 2001; Burmeister et al., 2005*). La Lox y otras enzimas similares catalizan la oxidación de α-hidroxoácidos sin generar intermedios de reacción. El mecanismo de reacción de la *Lox,* así como la de otros miembros de la misma familia (*Glicolato oxidasa, Flavocitocromo* B_2), se produce mediante un proceso carbaniónico. El proceso de oxidación comienza cuando un protón α del sustrato es abstraído por una

base del centro activo y los electrones resultantes del carbanión formado son transferidos al grupo flavín. Se cree que la interacción (iónica) inicial ocurre entre un grupo carboxilato y un residuo de arginina en la *cara si* del centro activo.

Pese la estructura cristalina de la Lox no ha sido resuelta todavía, la estructura de enzimas de la misma familia es bien conocida. La secuencia de aminoácidos de dichas enzimas presenta una estructura coherente entre ellas y coherentes con el mecanismo carbaniónico propuesto anteriormente. La reacción de oxidación del lactato por la Lox viene recogida en la **ecuación 5.1**, donde el grupo prostético, inicialmente en el estado oxidado (FMN), reacciona con el lactato para dar piruvato y pasar a su forma reducida ($FMNH_2$). Posteriormente, en presencia de O_2 molecular (*cofactor*), el $FMNH_2$ se reoxida a su forma original y queda preparado para reaccionar con otra molécula de lactato, **ecuación 5.2**.

$$Lactato + Lox(FMN) \rightarrow piruvato + Lox(FMNH_2) \qquad \textbf{Ecuación 5.1}$$

$$Lox(FMNH_2) + O_2 \rightarrow Lox(FMN) + H_2O_2 \qquad \textbf{Ecuación 5.2}$$

5.1.7.- Interferencias: El ácido ascórbico como prototipo de interferente endógeno

Existen multitud de compuestos biológicos (neurotransmisores, metabolitos, etc.) que pueden ser oxidados o reducidos en la superficie de un electrodo (*compuestos electroactivos).* Dichos procesos de oxido-reducción generan corrientes eléctricas que se suman o restan a la respuesta del biosensor y que puede producir errores en la interpretación de los resultados, tanto en la corriente de fondo (*concentración basal del analito*), como frente a la respuesta de estímulos fisiológicos y electrofisiológicos.

El ácido ascórbico (AA) es el mayor interferente en biosensores de 1ª generación, debido principalmente a: (1) su alta concentración en el SNC de mamíferos: 200-400 μM (en el mismo rango o superior que muchos analitos de interés), y (2) por el hecho de

que es oxidado en un amplio rango de potencial ($E_{1/2}$ entre -100 y +400 mV frente a SCE) (*O'Neill et al., 1998*). Es por ello que el AA ha sido usado como prototipo de interferente endógeno en procesos de validación y en test de interferencias en el ámbito de los biosensores. Por otro lado, en los estudio de validación frente a interferentes se han empleado otras muchas sustancias que potencialmente podían actuar como interferentes (*ver artículos adjuntos*).

5.2.- Enzimas y mecánica enzimática

Durante el desarrollo del presente trabajo el empleo de enzimas oxido-reductasa (*Gox, y Lox*) ha sido fundamental, pues es el material biológico que permite la detección y cuantificación de *glucosa y lactato* en el SNC. Con el fin de entender mejor el funcionamiento de los microbiosensores (*calibrado, sensibilidad, selectividad, interferencias,...)* se introducen a continuación algunos conceptos básicos. Sin embargo para una lectura y estudio en profundidad del *apartado 5.2* se recomienda consultar: (*Mathews et al., 1999; Lehninger et al., 2005*)

Las enzimas son *altamente selectivas* al sustrato, su característica principal es que *incrementan la velocidad* de la reacción sin que esta sea consumida, es decir, se *regeneran* durante la misma reacción enzimática, quedando lista para reaccionar con otra molécula de sustrato. Estas dos propiedades son las que hacen que las enzimas sean los materiales biológicos más empleados en el desarrollo de biosensores.

La estructura tridimensional de la enzima es la responsable de la mayor parte de las propiedades enzimáticas, incluida la selectividad al sustrato. Generalmente, son estructuras que consisten en largas cadenas de aminoácidos unidas por enlaces peptídicos empaquetadas en estructuras secundarias, terciarias y cuaternarias por

puentes de azufre, interacciones hidrofóbicas y puentes de hidrógenos. Esta macroestructura tridimensional es la que da lugar a la aparición del centro activo de la enzima, altamente selectivo al sustrato.

Los estudios sistemáticos sobre la actividad enzimática comenzaron a finales del siglo XIX. Ya en 1882 se introdujo el concepto de *complejo enzima-sustrato* (ES) como intermediario del proceso de catálisis enzimática. En 1913, *Leonor Michaelis y Maud Menten*, desarrollaron esta teoría y propusieron una ecuación de velocidad que explica el comportamiento cinético de las enzimas. Para explicar la relación observada entre la velocidad inicial (v_0) y la concentración inicial de sustrato ($[S]_0$) Michaelis y Menten propusieron que las reacciones catalizadas enzimáticamente ocurrían *en dos etapas*: En la primera etapa ocurre la *formación del complejo ES* (etapa rápida, **ecuación 5.3**) y en la segunda, el complejo ES da lugar a la *formación del producto* (P, paso lento de la reacción), liberando así a la enzima para realizar un nuevo ciclo catalítico:

$$E + S \underset{k_{-1}}{\overset{k_1}{\longleftrightarrow}} ES \xrightarrow{k_2} E + P \qquad \textbf{Ecuación 5.3}$$

En este esquema, k_1, k_{-1} y k_2 son las constantes cinéticas individuales de cada proceso y reciben el nombre de *constantes microscópicas de velocidad*. Según esto, se puede afirmar que:

$$v_1 = k_1 [E] [S] \qquad \textbf{Ecuación 5.4}$$

$$v_{-1} = k_{-1} [ES] \qquad \textbf{Ecuación 5.5}$$

$$v_2 = k_2 [ES] \qquad \textbf{Ecuación 5.6}$$

Donde: *[E]*, *[S]* y *[ES]* son las concentraciones de enzima libre, de sustrato y del complejo enzima-sustrato respectivamente. La concentración total de enzima, $[E_T]$, (que es constante a lo largo de la reacción) es:

$$[E_T] = [E] + [ES] \qquad \textbf{Ecuación 5.7}$$

Reordenando queda:

$$[E] = [E_T] - [ES] \qquad \textbf{Ecuación 5.8}$$

Sustituyendo **5.8** en **5.4** se puede expresar v_1 de la siguiente forma:

$$v_1 = k_1[S][E_T] - k_1[S][ES] \qquad \textbf{Ecuación 5.9}$$

Adoptando la *hipótesis del estado estacionario*, según la cual la concentración del complejo ES es pequeña y constante a lo largo de la reacción (*d[ES]/dt* =0), se tiene que:

$$\frac{d[ES]}{dt} = v_1 - v_{-1} - v_2 = (k_1[S][E_T] - k_1[S][ES]) - k_{-1}[ES] - k_2[ES] = 0$$

Ecuación 5.10

Reordenando queda:

$$k_1[S][E_T] - k_1[S][ES] = k_{-1}[ES] + k_2[ES] \qquad \textbf{Ecuación 5.11}$$

Despejando *[ES]* resulta:

$$[ES] = (k_1[S][E_T]) / (k_1[S] + k_{-1} + k_2) \qquad \textbf{Ecuación 5.12}$$

Operando:

$$[ES] = \frac{[S][E_T]}{[S]+[(k_{-1} + k_2) / k_1)]} \qquad \textbf{Ecuación 5.13}$$

Finalmente se obtiene:

$$[ES] = \frac{[S][E_T]}{[S]+K_M} \qquad \textbf{Ecuación 5.14}$$

Donde K_M es la *constante de Michaelis-Menten*:

$$[(k_{-1} + k_2) / k_1)] = K_M \qquad \textbf{Ecuación 5.15}$$

Como *[ES]* es constante, y k_2 es el paso lento de la reacción enzimática, la velocidad de formación de los productos es constante, y dependerá tan solo de *[ES]*, luego la velocidad macroscópica del proceso es:

$$v = v_2 = k_2 [ES] = cte \qquad \textbf{Ecuación 5.16}$$

Por lo tanto, en el estado estacionario, la velocidad de formación del producto es:

$$v = k_2 \frac{[S][E_T]}{[S] + K_M} \qquad \textbf{Ecuación 5.17}$$

Para cualquier reacción enzimática, $[E_T]$, k_2 y K_M son constantes. Considerando dos casos extremos:

- *A concentraciones de sustrato pequeñas* ($[S] << K_M$) $v = (k_2 [E_T]/K_M) [S]$. Como los términos entre paréntesis son constantes, pueden englobarse en una nueva constante, k_{obs}, de forma que la expresión queda reducida a: $v = k_{obs} [S]$, con lo cual la reacción es un *proceso cinético de primer orden*.

- *A concentraciones de sustrato elevadas* ($[S] >> K_M$), $v = k_2 [E_T]$. La velocidad de reacción es independiente de la concentración del sustrato y por tanto, la reacción es un *proceso cinético de orden cero*. Además, tanto k_2 como $[E_T]$ son constantes pudiéndose definir un nuevo parámetro, la *velocidad máxima de la reacción* (V_{max}), siendo $V_{max} = k_2 [E_T]$, que es la velocidad que se alcanzaría cuando todo el enzima disponible se encuentra unida al sustrato (*saturación enzimática*).

Introduciendo el parámetro V_{max} en la ecuación general de la velocidad, se obtiene la expresión más conocida de la *ecuación de Michaelis-Menten*:

$$v = \frac{[S]}{K_M + [S]} \cdot V_{max} \qquad \textbf{Ecuación 5.18}$$

La representación gráfica de la ecuación de Michaelis-Menten (v frente a $[S]$) es una curva hiperbólica (**Figura 5.3a**). V_{max} corresponde al valor máximo al que tiende la curva experimental y K_M corresponde a la concentración de sustrato a la cual la velocidad de la reacción es la mitad de la V_{max} .

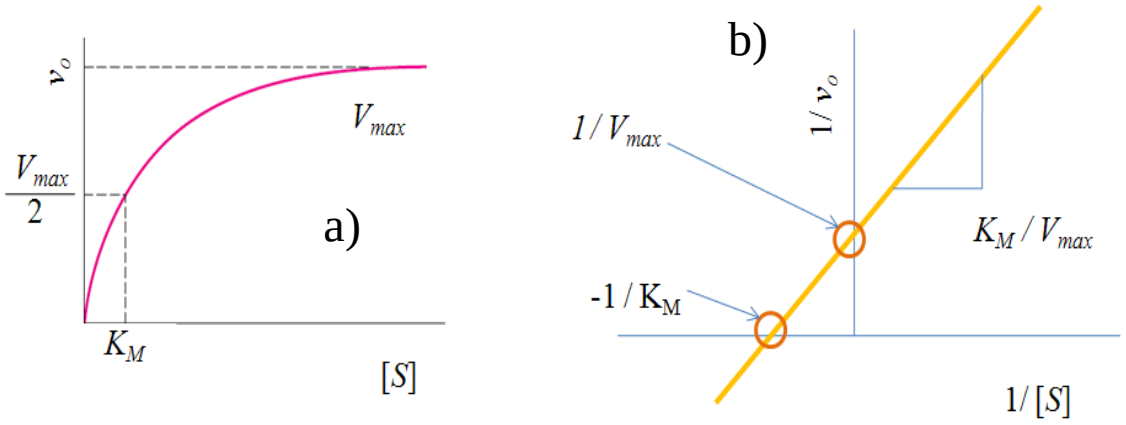

Figura 5.3.- ***a)*** *Representación gráfica de la ecuación de Michaelis-Menten.* ***b)*** *Linealización de la ecuación de Michaelis-Menten por el método propuesto por Lineweaver-Burk.*

K_M es un parámetro cinético importante por varias razones:

1) La razón V_{max}/K_M ~ sensibilidad analítica en el tramo inicial.
2) El valor de K_M da una idea de la afinidad del enzima por el sustrato:
    1. *a menor* K_M $\rightarrow$ *mayor afinidad*
    2. *a mayor* K_M $\rightarrow$ *menor afinidad*

Este hecho tiene fácil explicación si se tiene en cuenta la **ecuación 5.3**, donde el complejo *ES* se forma y disocia en las reacciones [(1)] y [(*2)* y (*-1)*] respectivamente. Así, si K_M es grande, $(k_{-1} + k_2) >> k_1$ (ver **ecuación 5.15**) predomina la disociación del complejo *ES* (poca afinidad hacia el sustrato). En el otro extremo, se tiene que para valores pequeños de K_M, $(k_{-1} + k_2) << k_1$ predomina la formación del complejo *ES* (gran afinidad hacia el sustrato).

Hay enzimas que no obedecen la ecuación de Michaelis-Menten, siguiendo así, una cinética no Michaeliana. Esto ocurre con las *enzimas alostéricos*, cuya gráfica v_o frente a *[S]* no es una hipérbola, sino una sigmoide. En la *cinética sigmoidea*, pequeñas variaciones en la *[S]* en una zona crítica (cercana a la K_M) se traducen en grandes variaciones en la velocidad de reacción. Esta cinética, es característica de procesos donde más de una molécula de sustrato reacciona con una molécula de enzima. Si cada centro activo de la enzima es similar e independiente de la respuesta previa de un centro activo cercano, aparece un comportamiento hiperbólico, si por el contrario, existe un aumento en la afinidad por parte del centro activo vecino debido a la presencia de una molécula de sustrato previo, aparece dicho comportamiento sigmoideo, conocido como "*efecto cooperativo*".

5.2.1.- Cálculo de los parámetros cinéticos enzimáticos

El cálculo de los parámetros cinéticos se realizó utilizando los datos de intensidad de corriente (*i*) de los microbiosensores en el estado estacionario. Partiendo de una disolución de PBS pH= 7.4, se añadieron distintos volúmenes de una disolución de analito (*glucosa* y *lactato*) de concentración conocida y se construyó la curva de calibrado *i* vs. [*S*].

Antes de calcular las constantes cinéticas y las características analíticas de la curva de calibrado, es necesario verificar que la reacción enzimática que tiene lugar sobre la superficie del transductor obedece a una cinética del tipo *Michaelis-Menten*. Para ello, se calcula el parámetro "h" de la *ecuación linealizada de Hill*, que proporciona una medida del grado de desviación de una cinética de *Michaelis*-Menten. Dicha ecuación es:

$$log\ \left[\left(\frac{i_{max}}{i}\right) - 1\right] = log\ K_M - h\ log\ [S] \quad \textbf{Ecuación 5.19}$$

Para reacciones enzimáticas con una cinética de Michaelis-Menten el valor de "h" es próximo a 1, presentando así, una cinética hiperbólica. Valores de "h" próximos a 2 aparecen cuando existe una cinética sigmoidea.

Una vez calculado el parámetro "h", se procedió al cálculo de los parámetros cinéticos. Para determinar gráficamente los valores de K_M y V_{max} es más sencillo utilizar la representación doble recíproca o *Lineweaver-Burk* ($1/v$ frente a $1/[S]$), ya que muestra dependencia lineal (**Figura 5.3b**). Dicha recta posee las siguientes características:

1. La pendiente es K_M / V_{max}
2. La abscisa en el origen ($1/v = 0$) es $-1/K_M$
3. La ordenada en el origen ($1/[S] = 0$) es $1/V_{max}$

Desde el punto de vista analítico, a medida que se obtiene un biosensor con una K_M más elevada, la sensibilidad de dicho dispositivo disminuye, pero aumenta el rango de linealidad de trabajo. Sin embargo, un biosensor con un valor menor de K_M daría lugar a un biosensor mucho más sensible al analito, pero con un menor rango lineal.

De esta forma, controlando los parámetros cinéticos se ajusta la respuesta del biosensor a las necesidades específicas del campo de aplicación.

5.2.2.- Déficit de oxígeno

El mecanismo enzimático para la G*ox*, que es similar para otras muchas oxidasas-reductasas, se puede escribirse de acuerdo a las ecuaciones **5.20** y **5.21** (*Dixon et al., 2002; McMahom et al., 2005*):

$$\text{glucosa} + \text{Gox/FAD} \rightarrow \text{Gox/FADH}_2 + \text{gluconolactona} \qquad \textbf{Ecuación 5.20}$$

$$\text{Gox/FADH}_2 + O_2 \rightarrow \text{Gox/FAD} + H_2O_2 \qquad \textbf{Ecuación 5.21}$$

Donde FAD y $FADH_2$ son la forma oxidada y reducida respectivamente del grupo prostético, *flavín adenín dinucleótido (FAD)*.

El llamado *déficit de oxígeno*, pone de manifiesto la dependencia de la actividad enzimática frente a la concentración del cosustrato natural (O_2). La función de dicho cosustrato es regenerar el grupo prostético de la enzima tras reaccionar con la glucosa. Sin embargo, en ausencia o a baja concentración de O_2 la enzima no puede volver a su estado inicial. De esta forma, la generación de H_2O_2 que es detectado y que es un índice del avance de la reacción y en definitiva de la concentración de glucosa, se ve limitada por la capacidad de regeneración de la enzima, y deja de ser proporcional a la concentración de glucosa (*limitación estequiométrica*).

Cuando la concentración del sustrato y del cosustrato (ej: glucosa y O_2) no es constante con el tiempo es necesario un modelo cinético con dos sustratos (*Leypoldt y Gough, 1984*). Sin embargo, cuando la concentración de uno de ellos es constante, se simplifica a un modelo cinético de un sustrato (**ecuación 5.22**) de acuerdo al mecanismo propuesto por *Michaelis-Menten* (*McMahom et al., 2005*).

$$J_{gluc} = J_{max}\left(1 + \frac{K_M(G)}{[G]}\right)^{-1} \qquad \textbf{Ecuación 5.22}$$

Donde la corriente o más correctamente la densidad de corriente (*J*), corriente normalizada con respecto al área del electrodo, es una medida de la velocidad global de la reacción enzimática y J_{max} es el valor de *J* (J_{gluc}) cuando la enzima se encuentra saturada con el sustrato, glucosa (*G*). De esta forma distintos valores de J_{max}, determinados en las mismas condiciones, reflejan diferencias en la actividad enzimática y distintos valores para la constante de Michelis-Menten (K_M) o más correctamente, de la constante aparente de Michaelis-Menten [$K_M(G)$]. Alternativamente, si la concentración de sustrato (glucosa) es fija y la concentración del cosustrato (O_2) es variable se puede modificar la ecuación general y escribirla acorde a:

$$J_{gluc} = J'_{max}\left(1 + \frac{K_M(O_2)}{[O_2]}\right)^{-1} \qquad \textbf{Ecuación 5.23}$$

Esta nueva ecuación puede ser usada para evaluar la dependencia de J_{gluc} con respecto a la concentración de O_2 (*Dixon et al., 2002*), donde J'_{max} es la respuesta máxima para una concentración fija de glucosa, y $K_M(O_2)$ es la constate aparente de Michaelis-Menten para el O_2. La opción de usar una única ecuación con dos sustratos como han empleado otros autores (*Leypoldt y Gough, 1984*) y de la cual se puede derivar la verdadera K_M, no ha sido empleada en la presente tesis, debido a que la constante aparente de Michaelis-Menten [K_M(gluc) o $K_M(O_2)$] definida separadamente es analíticamente más sencilla y útil para definir el rango lineal (*RL*) para ambos sustratos individualmente [RL ~ $1/2K_M$] y para saber la influencia de los parámetros cinéticos en la sensibilidad analítica *(S)*, $S \sim J_{max}/K_M$ (*McMahom et al., 2005*).

5.3.- Fabricación de los microbiosensores

Previa elaboración de los microbiosensores es necesario fabricar un transductor con las dimensiones y características adecuadas para trabajar en el SNC.

5.3.1.- Fabricación de los microelectrodos de fibra de carbono

La fabricación de los microelectrodos de fibra de carbono (CFEs) constituye ya de por sí un trabajo laborioso y meticuloso, debido a que es necesario elaborar microelectrodos con una gran reproducibilidad y tamaño adecuado. Las fibras de carbono de 8 μm de diámetro se montan y fijan mediante una pintura conductora de plata sobre un cable eléctrico de 0.25 mm de diámetro. Posteriormente, son secadas en estufa a 60 ^{o}C durante media hora e introducidas en un capilar de borosilicato previamente estirado (estirador de pipetas *Kopf 750*). Una vez la fibra salga por el orificio anterior, ésta es cortada a un tamaño de 250 μm de longitud. El dispositivo es fijado por ambos extremos con una resina epoxi no conductora y secado en estufa durante una hora. Finalmente, se suelda un pin chapado en oro al extremo del cable con el fin de ofrecer un buen contacto eléctrico. Posteriormente, los electrodos pueden

ser sometidos a un proceso de limpieza sumergiendo la punta en distintas disoluciones: acetona, agua, ácido sulfúrico, agua, y secado en estufa una hora.

5.3.2.- Modificación de los microelectrodos de fibra de carbono

Una vez construidos los CFEs, el siguiente paso es la modificación del transductor con el material biológico de reconocimiento, en nuestro caso con *Gox* o *Lox*. Con el fin de optimizar la respuesta de los microbiosensores se han empleado en el diseño distintos compuestos (surfactantes, compuestos electrocatalíticos, polímeros, etc.) que han permitido: (1) disminuir el potencial de detección del H_2O_2; (2) reducir el déficit de oxígeno; (3) incrementar la carga enzimática y la sensibilidad, así como reducir el límite de detección; (4) evitar los fenómenos de interferencia; (5) mejorar la biocompatibilidad de la superficie del microbiosensor.

A continuación, se resumen las etapas de modificación de los microbiosensores amperométricos acorde a los ítems anteriormente enumerados (ver **figura 5.4** para detalles de la configuración). Sin embargo, hay que tener en cuenta que dicho proceso ha sido modificado a lo largo del desarrollo de la presente tesis con el fin de optimizar los resultados (*ver detalles en los artículos adjuntos*).

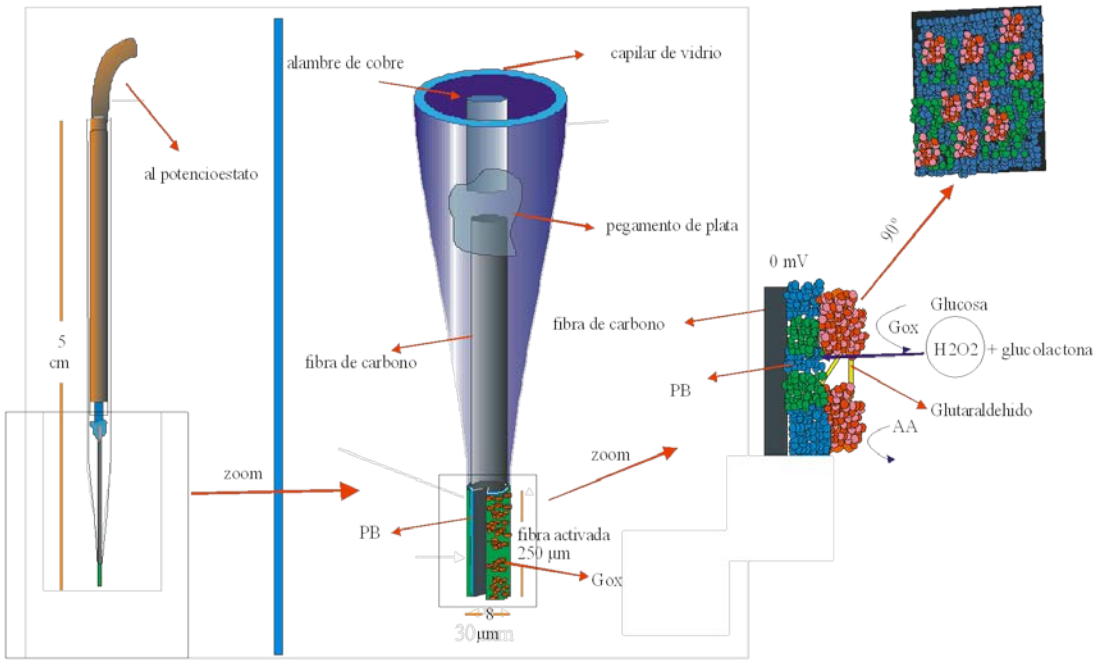

Figura 5.4.- *Esquema de un biosensor amperométrico enzimático de glucosa construido a partir de un microelectrodo de fibra de carbono de 8 µm de diámetro: PB (Azul de Prusia), Gox (glucosa oxidasa). La última capa de PoPD (poli-o-fenilendiamida), así como, el PEI y Nafion no han sido dibujados para facilitar la visualización del esquema.*

5.3.2.1.- Disminución del potencial de detección del H_2O_2

Para disminuir el potencial de detección de H_2O_2 se ha electrodepositado una capa de PB. Generalmente se ha empleado una etapa de electrodeposición mediante CV, otra de activación ciclando en la disolución de electrolito soporte, y finalmente un proceso de estabilización térmica (1h a 80-100ºC) para eliminar el agua de solvatación de la estructura cristalina. Por otra parte las condiciones de electrodeposición: método de electrodeposición, límites en los potenciales de ciclado, velocidad de barrido, pH de la disolución de trabajo, adición de surfactante como mediador de la electrodeposición,

tratamiento térmico, han sido estudiadas en detalle y constituyen buena parte del grueso de la presente tesis.

Con el fin de estudiar en detalle la optimización y la electrodeposición del PB, sobre todo en presencia de distintitos surfactantes, se han empleado tarjetas serigrafiadas de carbono (*DRP-110*) suministradas por la empresa española *Dropsens*. La elección de dichos electrodos ha sido para simplificar y ahorrar tiempo en la tediosa fabricación de un número ingente de microelectrodos, así como para asegurar la reproducibilidad y el fácil manejo de los electrodos durante el estudio.

5.3.2.2.- Reducción del déficit de oxígeno

Las limitaciones estequimétricas derivadas de las fluctuaciones del cosustrato es un problema importante en el ámbito de aplicación por tres razones primordiales: (1) la concentración de O_2 en el espacio extracelular en el cerebro es de aproximadamente 50 µM (cinco veces menor que en una disolución aireada) (*Nair et al., 1987; Murr et al., 1994, Zauner et al., 1995*); (2) este nivel puede fluctuar de manera significativa en condiciones fisiológicas y/o dependiendo de las condiciones experimentales (estrés, efecto de algunos anestésicos, hipoxia inducida, acción farmacológica) (*Dixon et al., 2002; Bolger y Lowry, 2005; Bazzu et al., 2009*); (3) la elevada concentración de algunos metabolitos (glucosa ~0.5-1 mM (*McNay et al., 2001; O'Neill et al., 2008*), lactato ~ 0.4 mM (*Goodman et al., 1996; Demestre et al., 1997; Shram et al., 1998*) frente a la concentración del O_2 en el espacio extracelular.

Con el fin de superar dicha problemática y minimizar sus efectos se han aplicado distintas estrategias, entre las que se incluyen: (1) el uso de distintas configuraciones (*Dixon et al., 2002; McMahom et al., 2006; McMahom et al., 2007*) y transductores con diferentes geometrías y tamaños que optimicen la llegada de O_2 a la superficie del

biosensor (*McMahom y O'Neill, 2005*); (2) la inclusión de una barrera de difusión que permita el libre paso del O_2 y dificulte la llegada del sustrato, aumentando así la relación *O_2/sustrato* en la superficie del biosensor; (3) la optimización de la carga enzimática (*McMahom et al., 2007*), para mejorar la sensibilidad y el rango lineal del biosensor; (4) el uso de polímeros que presenten una gran solubilidad para el O_2 y que actúen de reservorio interno (*Wang y Lu, 1998; Wang et al., 2000a; Wang et al., 2001; Wang et al., 2002*).

Si bien en la presente memoria se han empleado las aproximaciones (2) y (3), también se ha estudiado el uso de diversas fuentes o reservorios de O_2. Para ello se han empleado distintos fluorocarbonos (Nafion, H700), debido a que dichos polímeros poseen una notable solubilidad para el O_2.

Durante los últimos años, los fluorocarbonos han sido empleados en electrodos de pasta de carbono para desarrollar biosensores que pudiesen trabajar en ausencia o a bajas concentraciones de O_2 (*Wang y Lu, 1998*). Además, debido a su notable solubilidad para el O_2 han sido empleados como sustitutos sanguíneos y transportadores de O_2 en animales y humanos (*Wang et al., 2000a*). Algunos de estos flurocarbonos son polímeros de bajo peso molecular, derivados del clorotrifluoroetileno, $-(CF_2CFCl)_n-$, donde *n* varía entre 2 y 8. Compuestos como: (1) H200, H700, H1000 (nombres comerciales) (*Wang et al., 2000a*), (2) Kel-F (policlorotrifluoroetileno, PCTFE) (*Wang y Lu, 1998; Wang et al., 2000a; Wang et al., 2001; Wang et al., 2002*) y (3) Nafion (derivado sulfonado del tetrafluoretileno) (*Wang y Lu, 1998*) han sido usados con éxito. Por otro lado, los polidimetilsiloxanos (PDMS) han sido incorporados en biosensores de glucosa, manteniendo la reacción enzimática en ausencia de O_2 durante más de 15 horas (*Wang et al., 2002*).

Pese a que dicho enfoque ha sido empleado con éxito en macrobiosensores, especialmente en electrodos de pasta de carbono, los estudios en microbiosensores y en en aplicaciones fisiológicas han sido nulos o al menos muy limitados (no existe constancia de referencias bibliográficas). Por ello, se han seleccionado dos de ellos: (1) Nafion y (2) H700 para estudiar sus propiedades y la capacidad para mitigar los efectos de trabajar a bajas concentraciones de O_2.

El proceso de modificación ha consistido en la inmersión del transductor en una disolución alcohólica de Nafion al 5% o H700. Dicho proceso se realiza sumergiendo rápidamente 15 veces el CFE/PB y dejándolo secar a temperatura ambiente durante 30 minutos.

Resultados parciales de dicho estudio se han presentado durante la redacción de la presente memoria en el *14th International Conference on In Vivo Methods* organizado por la *Internationl Society for Monitoring Molecules in Neuroscience* que tuvo lugar en Londres entre el 16 y 20 de septiembre de 2012. A su vez, se está redactando una publicación a falta de realizar los estudios en modelos animales (*ver Anexo II: otras publicaciones*).

5.3.2.3.- Incremento de la carga enzimática

Con el fin de incrementar la cantidad de enzima retenida en la superficie del microbiosensor se realizan 15 inmersiones rápidas en PEI (2.5% w/v) y se seca a temperatura ambiente. Posteriormente, se realizan 30 inmersiones rápidas en la disolución enzimática (*Gox* (300 U/mL) o *Lox* (100 U/mL)) y 5 minutos después se sumergen 5 veces en una disolución de glutaraldehido en PBS [*glutaraldehido* (0.1% w/v)/BSA (1% w/v)], dejando entrecruzar durante 1-2 horas a temperatura ambiente

al aire. Posteriormente, los microbiosensores son guardados en la nevera en seco hasta el día siguiente.

El protocolo descrito anteriormente corresponde al método optimizado, sin embargo, durante el proceso de optimización también se ha empleado PEI al 1 y al 5 % w/v, se ha modificado el protocolo de inmersión alternándolo enzima y PEI, y se ha estudiado como afecta el tiempo de secado (hidratación del PEI) en la carga enzimática final.

5.3.2.4.- Mejora de la selectividad frente a los interferentes

Pese a que las interferencias son reducidas bastante debido al bajo potencial de trabajo, se ha empleado una capa protectora (P*o*PD) que impide el acceso del AA y otros interferentes al interior de microbiosensor. El protocolo empleado consistió en la electrodeposición de una capa de P*o*PD mediante CPA durante aproximadamente 15-20 minutos. La disolución (PBS) para la electrodeposición ha sido desoxigenada previamente (20 minutos bajo burbujeo de N_2). Posteriormente, se disolvió el monómero (*o*PD) a una concentración de 300 mM sonicando durante 15 minutos y se añadió BSA a una concentración de 5mg/mL para disminuir la desactivación enzimática debido al alto grado de compactación del polímero.

Cuando la disolución de monómero está lista se introducen los electrodos (biosensor, auxiliar y referencia) en la disolución y se aplica un potencial de ~ 0.7 V durante 15-20 minutos. El P*o*PD (en su forma no conductora) presenta una alta resistencia eléctrica, propiedad que hace que el crecimiento de la membrana polimérica esté autolimitado. De esta manera, a medida que aumenta el grosor de dicha capa, disminuye la intensidad de corriente (disminuye la electropolimerización) y aumenta el grado de compactación del entramado polimérico (impidiendo así, la llegada de más

moléculas de monómero). Pasado un tiempo determinado (función de la concentración de monómero, potencial aplicado, método de electro-deposición elegido, etc.), la corriente se estabiliza, indicando la finalización del proceso de electropolimerización.

5.3.2.5.- Optimización de las propiedades de biocompatibilidad

Los biosensores usados en neuroquímica, especialmente en métodos *in vivo*, tienen que solventar los problemas inherentes que aparecen en sistemas biológicos y que surgen debido a la interacción electrodo-matriz, siendo los más significativos: (1) respuesta a sustancias endógenas electroactivas, *interferentes*; (2) degradación de la superficie del sensor como consecuencia de que el organismo reconoce al mismo como un elemento externo (*respuesta inflamatoria debida a problemas de inmunidad o de reacción a un cuerpo extraño*).

Las interacciones adversas entre la superficie del dispositivo implantado (*biosensor*) y el medio biológico de implantación (SNC) no afectan solo al biosensor, sino también al entorno de estudio (*Wilson y Gifford, 2005*). De esta forma se ha tener en cuenta un enfoque más amplio a la hora de definir operacionalmente la *biocompatibilidad* (*Williams, 1989*). Para los biosensores, esto se traduce en tres consideraciones: (1) influencia de la respuesta inflamatoria inicial (debida a lesiones durante la inserción), y adsorción de biomoléculas en la superficie del electrodo, (2) modificación de las condiciones fisiológicas locales debido al implante del mismo, las cuales pueden modificar la concentración y difusión del analito de interés y (3) degradación de biosensor (*Reichert y Sharkawy, 1999*).

Las alteraciones más evidentes sobre el entorno son fisiológicas y anatómicas debido al tamaño del dispositivo de medida (*rotura de vasos sanguíneos, pérdida de la integridad de la barrera hematoencefálica, cambios en la microcirculación local, edema, consumo*

extra de glucosa, producción de citoquinas, eventual proliferación de células gliales, etc.) que se pueden extender hasta 1 mm de la zona de implantación (*Benveniste et al., 1987; O'Neill et al, 1991; Zhou et al., 2001; Khan y Michael, 2003*). Todo ello ha dado lugar a una reducción de las dimensiones del dispositivo a implantar.

Por otro lado, un diseño adecuado de la superficie del biosensor puede reducir su degradación paulatina, debido a la acción inflamatoria que ocurre a su alrededor. En contanto con la sangre (por hemorragia o al introducir el biosensor en un catéter) la principal fuente de complicación surge debido a la contaminación por depósito de la superficie del electrodo por proteínas y compuestos de coagulación que finalmente conducen a la formación de trombos, causando un importante riesgo para la salud. Es por ello, que la implantación subcutánea de biosensores ha sido elegida como una alternativa que reduce las complicaciones (interacción electrodo-proteínas) y riesgos para la salud (*Wang, 2008*).

Una excelente descripción de la respuesta inflamatoria a los dispositivos implantados es recogida por Anderson (*Anderson, 1993*). La respuesta aguda se inicia inmediatamente después de que el biosensor se ha implantado. Durante la respuesta inicial, las proteínas plasmáticas y células inflamatorias migran al sitio del cuerpo extraño (biosensor). Las proteínas son adsorbidas inicialmente, y posteriormente las células fagocitarias (neutrófilos, monocitos, y macrófagos) rodean el biosensor con el fin de destruirlo mediante la liberación de especias reactivas de oxígeno (H_2O_2, O^{2-}, NO, OH^-) y lisoenzimas. Sin embargo, debido a las dimensiones del biosensor esta tarea es prácticamente imposible. El momento exacto, la acción y la intensidad del proceso dependen de la naturaleza del cuerpo extraño (tamaño, forma, y propiedades físicas y químicas de su superficie). Dicha respuesta aguda dura unos 3 días, después de la cual comienza una respuesta inflamatoria en la cual el cuerpo extrañó es cubierto

por una cápsula fibrosa que lo aísla del entorno, y por ende, disminuye el flujo de reactantes a la superficie del biosensor (*Mas et al., 1995a*).

Con el fin de mejorar la biocompatibilidad de los biosensores se ha estudiado proteger su superficie externa con: (1) revestimientos poliméricos (acetato de celulosa, poliuretano, derivados del polietilenglicol, óxidos de polietileno, Nafion, electropolimerización de o-PD y compuestos análogos que presentan una baja adsorción de proteínas (*Moussy et al., 1993; Quinn et al., 1997; Chapman et al 2001*); (2) co-inmovilización de sustancias anticoagulantes como la heparina (*Wang et al., 2000b*); (3) modificación de la superficie externa con sustancias que liberen NO, un eficaz inhibidor de la adhesión plaquetaria y bacterianas (*Shin et al., 2004; Gifford et al., 2005; Oh et al., 2005; Frost y Meyerhoff, 2006*).

En la presente memoria la metodología empleada ha sido aprovechar las buenas propiedades de biocompatibilidad que presentan el P*o*PD.

5.3.3.- Microelectrodos centinela

Con el fin de comprobar el efecto de los interferentes y el origen de las respuestas fisiológicas registradas se han construido microelectrodos centinelas. Su diseño ha sido el mismo que rige la construcción de los microbiosensores, excluyendo la adición de la enzima que actúa como receptor biológico. De esta forma, se puede evaluar la contribución del entorno de trabajo a la respuesta total del sistema de medida (contribución no farádica, interferentes, etc.).

5.3.4.- Microelectrodos sensibles a oxígeno

Los CFEs también han sido empleados para construir microelectrodos sensibles a oxígeno. Su fabricación, mucho más sencilla, ha consistido en el recubrimiento de la

fibra de carbono con P*o*PD. Posteriormente se han polarizado a -0.65 V para medir el O_2 tanto en condiciones *in vitro* como *in vivo*.

5.4.- Voltamperometría

Las *técnicas potenciostáticas* o *voltamperométricas* estudian los procesos de transferencia de carga entre el electrodo de trabajo y el analito que se encuentra en disolución aplicando un potencial controlado. Abarcan un grupo de métodos electroanalíticos en los que la información sobre el analito se deduce de la medida de la intensidad de corriente en función del potencial aplicado, en condiciones que favorezcan la polarización total de un electrodo indicador, o de trabajo. Para una lectura más detallada tanto para el *apartado 5.4* como el *apartado 5.5* se recomienda: (*Wang, 2000c*).

5.4.1.- Procesos farádicos y no farádicos

El objetivo de las técnicas con potencial controlado es obtener una corriente relacionada con la concentración del analito de interés. Por esta razón, se mide la transferencia electrónica durante el proceso redox que sufre dicho analito en la superficie del electrodo de trabajo:

$$O + n\,e^- \leftrightarrow R \qquad \textbf{Ecuación 5.24}$$

Donde ***O*** es la forma oxidada del par redox, ***R*** es la forma reducida del par redox y ***n*** es el números de electrones que son puestos en juego.

La corriente resultante del cambio de estado de oxidación del analito genera una corriente eléctrica que por seguir las leyes de Faraday se denomina *corriente farádica* (*la oxidación o reducción de 1 mol de sustancia produce un cambio de 96.487 culombios*). Sin embargo, cuando se aplica un potencial a un electrodo pueden

generarse otras corrientes de naturaleza diferente, *no farádicas*, debidas principalmente a que en la interfaz electrodo-disolución se genera una *doble capa eléctrica* donde aparecen fenómenos de adsorción y desorción asociados al trasporte de carga.

Por otra parte, las concentraciones de reactantes y productos existentes vendrán especificados por la *ecuación de Nernst:*

$$E = E^o + \frac{RT}{nF} ln\left(\frac{C_O}{C_R}\right) \qquad \textbf{Ecuación 5.25}$$

Donde $\boldsymbol{E}$ es el potencial aplicado, $\boldsymbol{E^o}$ es el potencial estándar, $\boldsymbol{R}$ es la constante de los gases ideales, $\boldsymbol{T}$ es la temperatura en grados Kelvin, $\boldsymbol{F}$ es la constate de Faraday, $\boldsymbol{C_O}$ es la concentración de la especie oxidada, $\boldsymbol{C_R}$ es la concentración de la especie reducida.

La corriente $(\boldsymbol{i_z})$ registrada durante un experimento voltamperométrico representa la velocidad (v_z) de reacción a la cual el analito es oxidado/reducido en la interfase electrododo-disolución y viene expresada como:

$$v_z = \frac{i_z}{nF} \qquad \textbf{Ecuación 5.26}$$

Generalmente dicha velocidad es normalizada con respecto a la superficie $(\boldsymbol{A})$ del electrodo de trabajo (*mol* s^{-1} cm^{-2}) quedando:

$$J_z = \frac{i_z}{A} = \frac{i_z}{nFA} \qquad \textbf{Ecuación 5.27}$$

La corriente o velocidad de reacción está controlada por: (1) *transferencia de masa* del analito y sus productos de reacción hacia y desde la superficie del electrodo, (2) velocidad de *transferencia electrónica* sobre la superficie del electrodo. A continuación se define brevemente cada uno de ellos.

5.4.2.- Fenómenos de transporte

Para que la sustancia electroactiva se oxide o reduzca en la superficie del electrodo es necesario que el analito, que se encuentra en el seno de la disolución, alcance de alguna manera dicha superficie. El transporte del analito en el seno de la disolución se efectúa mediante tres mecanismos distintos de transporte de masa, los cuales influyen de manera distinta en la velocidad con que los reactivos y productos son transportados desde y hacia la superficie del electrodo. Tales procesos son: *difusión, migración y convección*.

En sistemas fisiológicos, como el espacio extracelular del SNC, la contribución del término convectivo se puede despreciar. Por otra parte, el líquido cefalorraquídeo actúa como *electrolito inerte o soporte* ya que está compuesto por una gran cantidad de especies iónicas electroquímicamente inertes (Na^+, K^+, Ca^{2+}, HCO^-_3). Estos electrolitos no reactivos hacen que la *corriente capacitiva* no se vea alterada por la variación de la concentración del analito, de tal forma que la contribución migratoria también puede ser despreciada.

5.4.3.- Transferencia electrónica

El proceso de transferencia electrónica (**ecuación 5.24**) consiste en la transferencia de *n* electrones entre la banda de conducción del electrodo de trabajo y un orbital molecular de las especie oxidada o reducida (orbitales HOMO y LUMO respectivamente). La expresión de la velocidad de reacción *directa* (reducción) v_d presenta una cinética de primer orden:

$$v_d = k_d\, C_O \qquad \textbf{Ecuación 5.28}$$

Mientras que la reacción *inversa* (oxidación), también de primer orden, v_i es:

$$v_i = k_i\, C_R \qquad \textbf{Ecuación 5.29}$$

Donde k_d y k_i son las constantes de velocidad directa e inversa respectivamente. Estas constantes dependen de las condiciones experimentales de acuerdo a:

$$k_d = k^o exp\left[-\frac{\alpha nF(E-E^o)}{RT}\right] \qquad \textbf{Ecuación 5.30}$$

$$k_i = k^o exp\left[\frac{(1-\alpha)nF(E-E^o)}{RT}\right] \qquad \textbf{Ecuación 5.31}$$

Donde k^o es la *constante de velocidad estándar* y α es el *coeficiente de transferencia electrónico*. El valor de k^o (cm/s) indica la velocidad de reacción entre la superficie del electrodo y el reactivo. El valor de α (comprendido entre 0 y 1) informa sobre la simetría de la curva de energía libre (respecto a reactivos y productos). Para sistemas simétricos α será muy próximo a 0.5, de esta forma α es una medida de la fracción de energía puesta en el sistema para reducir la energía de activación

5.4.4.- Técnicas voltamperométricas

Hoy en día existen un gran número de técnicas que difieren en la forma en que el potencial es aplicado, y en definitiva, en la forma que la corriente es medida. Durante el desarrollo de la presente tesis se han empleado, rutinariamente, dos de estos métodos: *(1)* Voltamperometría a potencial constante *(CPA)* o Amperometría y *(2)* Voltamperometría cíclica *(CV)*. Estos métodos han sido empleados tanto en la modificación y caracterización *in vitro* de los microbiosensores como en su aplicación *in vivo*.

5.4.4.1.- Voltamperometría a potencial constante

El potencial de trabajo se fija a un potencial donde ocurre la oxidación/reducción del analito de interés en régimen difusivo (*sin agitación mecánica y en presencia de una gran concentración de electrolito inerte*). Bajo estas condiciones, la corriente registrada alcanza un valor máximo (*corriente límite* i_L), proporcional a la concentración del analito.

Al aplicar un potencial constante inicialmente aparece una *contribución no farádica* que cae a cero rápidamente. Una vez pasado estos momentos iniciales la corriente generada es función última de la concentración de analito. Admitiendo que la i_L es de origen difusivo y que poca cantidad de analito es consumida durante el proceso de medida (concentración del analito constante), se puede asumir que se alcanza el estado estacionario (*steady-state*). Este hecho y la excelente resolución temporal hacen que esta técnica sea ideal para el estudio de sistemas "*in vivo*". Normalmente, esta técnica permite la detección de moléculas o iones a concentraciones próximas a 10^{-9} M.

Bajo las condiciones de estado estacionario la i_L es directamente proporcional al coeficiente de difusión y concentración del sustrato:

$$i_L = \frac{nFACD}{r}\, G \qquad \textbf{Ecuación 5.32}$$

Donde ***C*** es la concentración de analito, ***D*** es el coeficiente de difusión, ***r*** es el radio del electrodo y ***G*** es un factor geométrico

5.4.4.2.- Voltamperometría cíclica

En CV, el potencial aplicado varía linealmente (**Figura 5a**) con el tiempo desde un valor inicial (E_i) hasta un valor final (E_f). Cuando se ha alcanzado este valor, el sentido de barrido se invierte y el potencial vuelve generalmente a su valor original. El intervalo de potenciales elegido para un experimento dado, es aquel en el que tiene lugar la oxidación o reducción del analito de interés. Las condiciones de trabajo al igual que en amperometría son las necesarias para que la llegada del analito a la superficie del electrodo esté controlada por difusión. La dependencia entre la velocidad de barrido y amplitud del pico explica el papel de la *adsorción*, *difusión* y *reacciones químicas acopladas* dentro del proceso en estudio.

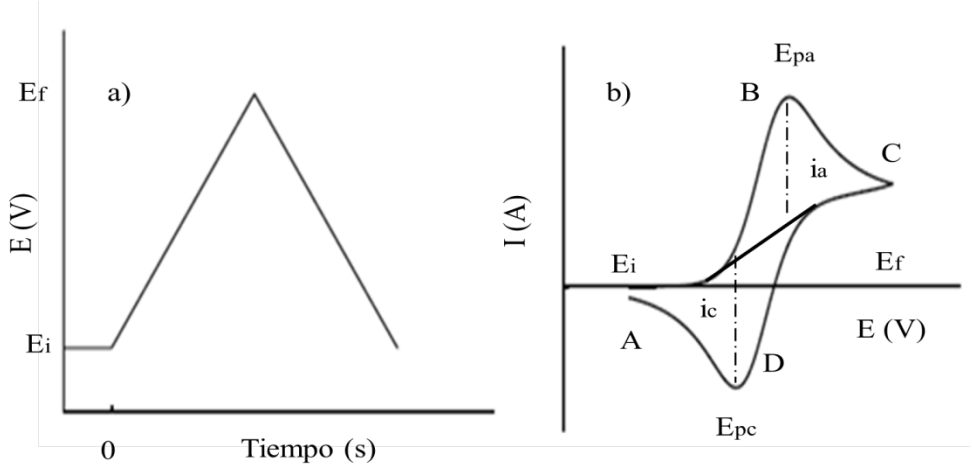

Figura 5.5.- a) *Variación del potencial aplicado durante CV* ***b)*** *Voltamperograma cíclico obtenido al ciclar un electrodo en presencia de un par redox.*

La **figura 5.5b** muestra la respuesta para un sistema reversible, en la cual se indican distintos parámetros característicos: potencial del pico catódico (E_{pc}), potencial del pico anódico (E_{pa}), intensidad del pico catódico (i_{pc}) e intensidad del pico anódico (i_{pa}). Al comenzar la CV no se observa intensidad de corriente apreciable (A), ya que no hay especies oxidables en esa zona de potencial. Cuando el potencial alcanza valores próximos a E_{pa} se desarrolla una intensidad anódica debida a la oxidación de *R* en la superficie del electrodo. La intensidad del pico (i_{pa}) es debida a dos componentes: (1) la

intensidad inicial necesaria para ajustar la concentración superficial de reactivo a su concentración de equilibrio dada por la ecuación de Nernst y (2) la *intensidad controlada por difusión*. La primera, disminuye rápidamente a medida que la capa de difusión se extiende hacia el exterior de la superficie del electrodo. Por lo tanto, la altura de pico viene determinada en última instancia por el proceso difusivo. Como este es incapaz de suministrar reactivo suficiente, llegado un momento ocurre la caída de corriente posterior a i_{pa}, alcanzando así la región (C). La intensidad catódica (i_{pc}) resultante de la reducción de *O* que se ha acumulado cerca de la superficie del electrodo durante el barrido directo y el potencial catódico (E_{pc}), pueden explicarse del mismo modo para el barrido inverso. De esta forma, la corriente catódica genera un pico y después disminuye a medida que se consume la especie *R* acumulada en la superficie del electrodo. Para un sistema reversible se tiene que $I_{pc}/I_{pa} \sim 1$.

Por otro lado, la separación entre dichos picos es función del número de electrones que entran en juego en la reacción de óxido/reducción, de acuerdo a la siguiente ecuación:

$$E_{pa} - E_{pc} = 59/n\ (mV) \qquad \textbf{Ecuación 5.33}$$

La ecuación matemática que cuantifica la intensidad de pico (asumiendo difusión plana), es la ecuación de *Randles-Sevcik*, que a 25 ^{o}C se escribe como:

$$i_p = 2.69 \cdot 10^5\, n^{3/2}\, A\, C\, D^{1/2}\, v^{1/2} \qquad \textbf{Ecuación 5.34}$$

Donde ν es la velocidad de barrido. Como se puede observar, la intensidad del pico de corriente es proporcional a la concentración de la especie electroactiva, a la raíz cuadrada de la velocidad de barrido y del coeficiente de difusión de analito.

5.5.- Otras técnicas instrumentales

Durante el desarrollo de la presente memoria se han empleado diversas técnicas instrumentales para caracterizar las modificaciones realizadas sobre el transductor. Algunas de estas técnicas han sido usadas en el laboratorio de Neuroquímica y Neuroimagen (CPA, CV, espectroscopía visible-ultravioleta), mientras que otras han sido realizadas usando las infraestructuras del Departamento de Química Inorgánica (espectroscopía de infrarrojo) y del Departamento de Química-Física (espectroscopía de impedancia) de la ULL. A su vez, técnicas más específicas fueron sido realizadas en el Servicio de Microscopía Electrónica (SEGAI).

A continuación, se describen brevemente las técnicas más relevantes y menos conocidas: microscopía electrónica de barrido y espectroscopía de impedancia, prestando especial atención a esta última puesto que es una herramienta muy útil en la caracterización y estudio de superficies.

5.5.1.- Microscopía electrónica de barrido

La microscopía electrónica de barrido (SEM) proporciona información sobre la morfología y topografía de la superficie de los sólidos, aunque también puede ser empleada para estudiar la composición del material analizado. Tiene la ventaja de tratarse de una técnica no destructiva que sirve de complemento en el análisis de la muestra a través de otras técnicas como la difracción de rayos X (XRD) o la microscopía de fuerzas atómica (AFM).

El funcionamiento del SEM se basa en el bombardeo de una superficie mediante electrones a gran velocidad generados por un filamento de wolframio sometido a un alto voltaje y a una temperatura elevada. Dicho haz de electrones se colima utilizando diferentes lentes y bobinas magnéticas hasta hacerlo incidir en la muestra que se encuentra bajo vacío. Finalmente, los electrones que interaccionan con la muestra se recogen en diferentes sensores dependiendo del análisis a realizar. De todas las formas de radiación resultantes de la interacción del haz incidente y la muestra, hay dos realmente fundamentales en microscopía de barrido: los electrones secundarios y los electrones retrodispersados. Los primeros son electrones de baja energía (decenas de eV) que resultan de la emisión por parte de los átomos constituyentes de la muestra (los más cercanos a la superficie) debido a la colisión con el haz incidente. Los electrones retrodispersados, por otra parte, son electrones del haz incidente que han interaccionado (colisionado) con los átomos de la muestra y han sido reflejados. La intensidad de ambas emisiones varía en función del ángulo que forma el haz incidente con la superficie del material, es decir, depende de la topografía de la muestra. Finalmente, de la señal producida por los electrones secundarios se obtiene una imagen tridimensional de la muestra.

5.5.2.- Espectroscopía de impedancia

La espectroscopía de impedancia (EIS) es una técnica electroquímica empleada para medir la respuesta eléctrica de los materiales en función de la frecuencia de la señal de excitación, generalmente sinousoidal. La impedancia de un material no es más que la resistencia (R) de dicho material al paso de una corriente eléctrica (I) cuando se trabaja en corriente alterna (CA). En un circuito en corriente continua (CC) la resistencia (R) viene dada por la *ley de Ohm*:

$$R = \frac{E}{I} \qquad \textbf{Ecuación 5.35}$$

Donde E se mide en voltios, I se mide en amperios y R se mide en ohmios.

En el caso de una señal alterna la expresión equivalente sería la siguiente:

$$Z = \frac{E}{I} \qquad \textbf{Ecuación 5.36}$$

Siendo Z la impedancia del circuito, también en ohmios.

La principal diferencia entre la resistencia de un circuito en *CC* y la impedancia de un circuito en *CA*, es que esta última depende de la frecuencia (en Hz) de la señal de excitación. Es una técnica relativamente nueva, pero muy útil, que permite caracterizar muchas de las propiedades eléctricas y los procesos físico-químicos de los materiales y su interfase. A través de este tipo de análisis electroquímico se puede obtener información sobre la cinética, los mecanismos de formación y modificación de superficies. Esta técnica tiene numerosas aplicaciones que van desde el estudio del transporte de masa, velocidades medias de difusión, corrosión y propiedades eléctricas hasta el estudio de defectos microestructurales. Se puede usar para el estudio de sistemas tan variados como sensores químicos, biosensores, inmunosensores, componentes de pilas de combustión, o para investigar el comportamiento de las membranas en células vivas o tejidos.

Para poder estudiar el comportamiento de una célula electroquímica (en nuestro caso constituida por un electrodo de referencia, un auxiliar y un electrodo de trabajo), se representa el sistema en estudio mediante un modelo o circuito equivalente (*circuito de Randles*). El circuito se describe como sigue: la resistencia R_{ct} está en serie con un

elemento Z_w y en paralelo con un condensador C_{dl}. A su vez, este conjunto está en serie con una segunda resistencia R_S, tal como se muestra en la **figura 5.6a**.

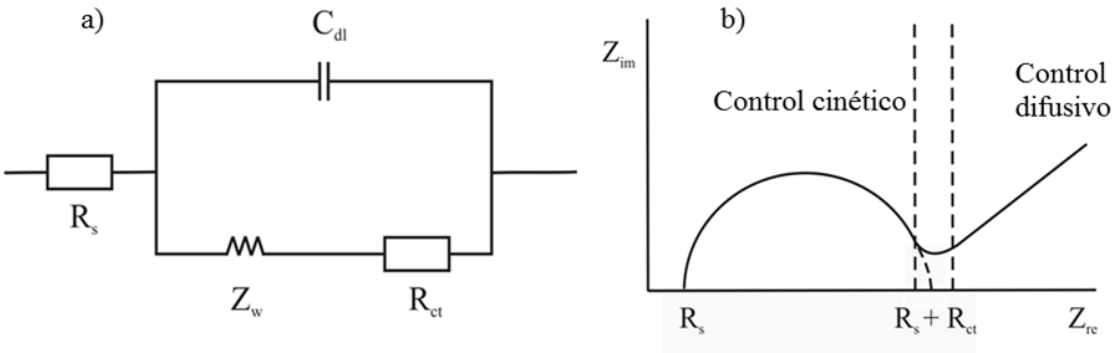

Figura 5.6.- a) *Circuito de Randles, equivalente a una celda electroquímica convencional.* ***b)*** *Diagrama de Nyquist.*

Los elementos R_S y Z_w representan las propiedades de la disolución del electrolito y la difusión de la especie redox en la disolución respectivamente. Estos parámetros no se ven afectados por las transformaciones químicas que ocurren en la superficie del electrodo. Por otro lado, los elementos C_{dl} y R_{ct}, dependen de las características de la interfase electrodo/electrolito, proporcionando información sobre la existencia de cambios en las propiedades de la superficie del electrodo al inmovilizar o acoplar materiales sobre la interfase estudiada.

La representación más empleada en EIS es el diagrama de Nyquist, donde se representa en el plano complejo las componentes imaginarias (Z_{im}) frente a las componentes reales (Z_{re}) de la impedancia obtenida a varias frecuencias. En la **figura 5.6b** se muestra esta representación para el circuito de Randles. Dicho diagrama presenta una zona semicircular a altas frecuencias, característica de un proceso limitado por transferencia electrónica, mientras que a bajas frecuencias aparece un tramo lineal de pendiente uno, asociado a un proceso puramente difusivo.

5.6.- Calibrado in vitro

Todos los calibrados se han realizado en un vaso de precipitado con 25 mL de PBS a temperatura ambiente, utilizando como electrodo de referencia un electrodo de calomelano saturado (SCE) comercial (*Crison Instruments S.A.)* y como auxiliar un alambre de platino o de acero inoxidable. El potencial de detección en los estudios amperométricos ha sido 0.0 V frente a SCE para los microelectrodos de fibra de carbono y de -0.05 V frente al electrodo de pseudoreferencia interno de plata para las tarjetas serigrafiadas.

Las calibraciones de glucosa y de lactato han sido realizadas en PBS, previa estabilización de la corriente de fondo. Posteriormente, se han añadido distintos volúmenes de disolución patrón (glucosa o lactato) y se ha agitado la disolución durante 10 segundos. Finalmente, se ha dejado que la corriente alcance el estado estacionario.

Las calibraciones con H_2O_2 se han realizado de forma análoga mediante agitación constante utilizando el medio electrolítico empleado durante la electrodeposición del PB. La disolución patrón de H_2O_2 (10 mM) ha sido preparada en agua bidestilada antes de las calibraciones.

Los estudios relacionados con el *déficit de oxígeno* han sido realizados con disoluciones previamente desoxigenadas con N_2 durante 20 minutos. En los estudios donde la concentración de O_2 ha sido modificada durante la medida, se ha fijado la concentración de glucosa (0.5, 1, 2, 5 mM) y se han modificado los niveles de O_2 mediante el suministro de aire o N_2 puro, todo ello en una celda de trabajo aislada. Para correlacionar la respuesta del biosensor con la concentración de O_2 se ha

monitorizado la concentración del mismo mediante el uso de un electrodo sensible a O_2 según se describe en el **apartado 5.3.4**.

5.7.- Animales y método quirúrgico

Los animales utilizados en la realización de la presente memoria han sido ratas Sprargue-Dawley macho, con un peso aproximado de 350 gramos. Para los experimentos *in vivo* los animales han sido anestesiados mediante inyección intraperitoneal de uretano (1.25 g/Kg).

Una vez anestesiado, el animal se posiciona en un estereotáxico y es mantenido a 36.5-37 ^{o}C. La fijación de la cabeza ha sido realizada por acoplamiento de los incisivos en la cavidad anterior, quedando 3.3 mm por debajo del eje horizontal (*Paxinos y Watson, 1986*). La fijación terminó mediante la introducción de las barras laterales en el canal auditivo, de forma que la cabeza del animal quedó totalmente inmovilizada.

La operación quirúrgica comienza con una incisión cutánea longitudinal en sentido anteroposterior en la línea media de la piel iniciada desde la línea ocular hasta la base posterior del cráneo. A continuación se cortan los tejidos blandos de la superficie del cráneo hasta dejar perfectamente visibles las suturas craneales y su unión en los puntos Bregma y Lambda (puntos de corte entre suturas craneales). Una vez preparada la superficie se procede a su perforación mediante el uso de un taladro eléctrico que permite realizar un hueco de unos 10 mm de diámetro, siempre teniendo cuidado en no dañar las membranas meníngeas ni los vasos sanguíneos circundantes. Una vez terminado el orificio y limpio de restos y material óseo se procede a la retirada con una aguja estéril y unas pinzas quirúrgicas de una porción de duramadre en la zona de inserción para facilitar la introducción del microbiosensor. La zona de trabajo se ha localizado siguiendo el atlas estereotáxico de Paxinos y Watson (*Paxinos y Watson,*

1986), seleccionando el cortex prefrontal como zona de estudio: *A/P +2.7 de Bregma, M/L +1.2 y D/ V -0.5 de Dura.*

5.8.- Registro in vivo

Para poder medir analitos en el SNC de la rata es necesario contar con una celda electroquímica completa en la zona de estudio. Para ello es necesario disponer de:

(1) *un electrodo de trabajo* (microbiosensor).

(2) *un electrodo de referencia* (alambre de plata clorurada, Ag/AgCl). Dicho electrodo se fabricó utilizando hilo de plata de 0.2 mm de diámetro cubierto con teflón y despojado de dicha cubierta por ambos extremos. A uno de los extremos se soldó un conector chapado en oro y se conectó al potenciostato. El otro extremo se modificó mediante un tratamiento de cloración en una cubeta de HCl 1M aplicando un potencial de +0.8 V hasta que adquiere una tonalidad oscura (AgCl).

(3) *un electrodo auxiliar* (acero inoxidable o alambre de platino).

5.8.1.- Implantación del sistema electroquímico

Los electrodos de referencia y auxiliar son colocados en la superficie del cráneo (cerca de la zona de trabajo). Para facilitar una buena conducción eléctrica con el líquido extracelular ambos electrodos son envueltos en una tira de gelatina purificada y esterilizada, *Espongostán*®, e impregnados con PBS. Esta zona es humedecida continuamente con PBS para mantener una buena conducción. De esta forma, se mantiene el contacto eléctrico con el microbiosensor implantado en el córtex prefrontal y el resto de componentes de la celda electroquímica. Alternativamente, también se ha optado por el recubrimiento del sistema con agar, siendo este último una opción más cómoda y segura, debido a que mantiene la zona húmeda durante más tiempo.

5.8.2.- Estudio farmacológico

Los estudios farmacológicos se han diseñado con el objeto de caracterizar y comprender la respuesta de los microbiosensores y no para investigar los procesos fisiológicos que acontecen en detalle. En estos estudios se han empleado distintas aproximaciones: (1) inyección local e (2) inyección intraperitoneal, (3) administración de gases, etc.

Para realizar las inyecciones locales se ha diseñado un sistema de inyección que proporciona un volumen controlado en el entorno de acción del microbiosensor. Este dispositivo consiste en un soporte de aluminio modificado. El microbioensor se introduce en dicho soporte que actúa como cánula guía. Por el lateral de la cánula se colocó una aguja de acero unida al exterior del soporte con cemento dental y por cuyo interior se hace pasar un tubo de polimicro de 76 μm de diámetro interno que termina en el entorno de la punta del microbiosensor (200 μm de la fibra de carbono).

5.8.3.- Estimulación eléctrica

La estimulación eléctrica local ha sido empleada con el objetivo de estudiar el consumo y liberación de glucosa y lactato durante los procesos de activación neuronal. Dicha estimulación ha sido generada por un estimulador bipolar Grass, modelo S-8800 conectado un electrodo bipolar. Este electrodo consiste en 2 fibras de carbono de 30 micras de diámetro o dos alambres de tungsteno de aproximadamente 150 μm (afilados por corrosión electroquímica hasta presentar unas pocas micras de diámetro en la punta) y separados una distancia de 500 μm. El estimulador ha sido colocado en las proximidades del microbiosensor, aproximadamente a 100 μm. La corriente aplicada ha sido de 400 a 1500 μA y se ha modificado tanto la duración (0.1-5 s) como la frecuencia (5-60 Hz) de la misma.

5.9.- Instrumentación electroquímica y tratamiento de datos

Todas las medidas *in vitro* e *in vivo*, así como las modificaciones y la caracterización electroquímica de las distintas etapas de construcción han sido realizadas con un potenciostato Quadstad 164 (*EDAQ*). Los datos han sido almacenados y tratados mediante una unidad e-corder 401 de la misma casa comercial usando el software: *Echem v 2.0* o *Chart v 5.0*, en función de las necesidades de cada momento. Las tarjetas serigrafiadas fueron modificadas y caracterizadas con un potenciostato *DRP-STAT200 y* el software *DropView* (Dropsens).

Los datos experimentales han sido tratados con los softwares específicos de cada casa comercial, permitiendo obtener los parámetros electroquímicos necesarios para el análisis posterior: carga acumulada, potenciales de oxidación y reducción, altura de los picos catódicos y anódicos, intensidad de corriente, etc.

Por otro lado, las representaciones gráficas y el cálculo de los parámetros cinéticos, analíticos y enzimáticos han sido calculados con el programa *GraphPad Prism v 5.0*.

RESULTADOS Y DISCUSIONES

6.-Resultados y discusiones

6.1.- Desarrollo de un microelectrodo de fibra de carbono modificado con PB como transductor selectivo para biosensores de 1ª generación, aplicaciones en el ámbito neuroquímico

Extraído de:

> ***Salazar*** *P, Martín M, Roche R, O'Neill RD, González Mora JL. Prussian Blue-modified microelectrodes for selective transduction in enzyme-based amperometric microbiosensors for in vivo neurochemical monitoring.* ***Electrochimica Acta*** *55 (**2010**) 6476-6484.*
>
> Índice de impacto: 4.039 (5 últimos años)

En la presente publicación hemos desarrollado y demostrado la idoneidad de un microelectrodo de fibra de carbono modificado previamente con PB para detectar H_2O_2. Las principales ventajas del diseño han sido sus pequeñas dimensiones ($\Phi \sim 10$ μm) y el bajo potencial de detección del H_2O_2 (0 V frente a SCE). La electrodeposición ha sido realizada mediante CV en un rango de potencial entre -0.2 y +0.4 V frente $Ag/AgCl_{sat}$ (v= 0.1 V/s). Durante el ciclado del microelectrodo se observa un

crecimiento paulatino en la intensidad del pico anódico y catódico, correspondiente a la transición PW/PB, demostrándose así la satisfactoria electrodeposición del PB sobre la fibra de carbono. Posteriormente, dichos electrodos fueron activados ciclándolos 50 veces en la disolución electrolítica soporte y sometidos a tratamiento térmico (80 ^{o}C, 1 h). Los depósitos fueron caracterizados mediantes espectroscopía IR y Vis-UV. Los datos del IR mostraron un pico agudo en 2067cm^{-1} relacionado con el estiramiento del enlace de Fe-CN, donde los grupos CN están unidos a un Fe^{2+} con carácter iónico. Por otro lado, mediante espectroscopía Vis-UV se observó la banda de absorción a 672 nm asociada a la transferencia de carga entre el Fe^{3+} y Fe^{2+}, y que igualmente ha sido utilizada como prueba irrefutable de la formación del depósito de PB.

Con el fin de optimizar las condiciones de deposición se estudió, por CV y CPA, la respuesta del transductor modificado frente a la adición de H_2O_2, así como el efecto que ejercen distintos electrolitos soportes en el mecanismo de oxidación del par PW/PB, y por ende, en la sensibilidad para el H_2O_2. La respuesta (CV) frente a la adición de H_2O_2 fue evidente, observándose el característico comportamiento electrocatalítico al incrementarse la concentración de H_2O_2 (reducción del pico anódico e incremento del pico catódico). Por otro lado, se encontró un incremento en la sensibilidad frente al H_2O_2 (CPA) a medida que disminuye el radio hidratado del catión empleado como electrolito soporte, dicho hallazgo se encontró también bien documentado en la bibliografía. Dicho fenómeno tiene su explicación en la transferencia iónica subyacente durante la reacción de reducción/oxidación del PB. Durante la interconversión del par PW/PB es necesario un flujo catiónico, de o desde la disolución soporte, para compensar el balance de cargas asociados al cambio del estado de oxidación del átomo de hierro. Es por ello que, en presencia de iones con

pequeño volumen hidratado (Cs^+, K^+) la sensibilidad para el H_2O_2 es mayor, puesto que se favorece dicho flujo catiónico en el interior de la estructura cristalina.

En el presente trabajo se ha optimizado el potencial de trabajo, así como las posibles interferencias con el O_2, otro compuesto que puede ser detectado mediante el empleo de electrodos modificados con PB. Los resultados mostraron que el potencial óptimo para detectar H_2O_2 en presencia de O_2 se encuentran en el rango de +0.1 a -0.2 V frente SCE, y que en igualdad de condiciones el PB es dos órdenes de magnitud más sensible al H_2O_2. Dichos resultados están de acuerdo con los datos presentados por otros grupos y con que la forma PW, presente a potenciales < +0.1 V, es la que cataliza la reducción del H_2O_2. Finalmente, se obtuvo una sensibilidad y un límite de detección de 1.00 ± 0.04 A M^{-1} cm^{-2} y $1\ 10^{-8}$ M respectivamente.

Con el fin de optimizar la estabilidad y selectividad se procedió a realizar el recubrimiento del microelectrodo (CFE/PB) con distintos polímeros: Nafion, PoPD y una configuración híbrida (Naf/PoPD). El resultado más evidente ha sido la pérdida de casi el 50% de sensibilidad para la configuración (CFE/PB/PoPD), atribuida a fenómenos difusivos. Las otras dos configuraciones presentaron una disminución de la sensibilidad (70-80%), que puede ser debida tanto a procesos difusivos como a una menor electrodeposición de PB sobre el transductor modificado previamente con Nafion (CFE/Naf/PB/PoPD). Finalmente, la configuración óptima fue seleccionada en base a la selectividad de las distintas configuraciones frente a distintos interferentes (DA, DOPAC, AA, AU). Sin duda alguna, la configuración con PoPD presentó en ambos casos mejores propiedades antiinterferentes. La configuración CFE/PB/NAF presentó baja selectividad frente a la DA. Dicho fenómeno puede entenderse a que la DA a pH fisiológico tiene carga neta positiva, siendo capaz de difundir a través de la matriz polimérica.

Con el fin de demostrar la utilidad del presente dispositivo se construyó el primer prototipo de microbiosensor sensible a glucosa y se realizaron los primeros experimentos *in vivo* de validación. Para la construcción de dicho microbiosensor se partió de un microelectrodo (CFE/PB) al que se le añadió *Gox*, mediante entrecruzamiento con glutaraldehido. Finalmente, se añadió una capa externa de PoPD para mejorar la biocompatibilidad del dispositivo y evitar la respuesta frente a interferentes endógenos. Este microbiosensor se adecuó hasta un rango lineal próximo a 6mM, presentando una sensibilidad de 121 ± 1 pA/mM (R^2= 0.998) y un límite de detección de 54 μM.

6.2.- Microbiosensores sensibles a glucosa, basados en microelectrodos de carbono modificados con PB: Aplicaciones *in vivo* en el sistema nervioso central

Extraído de:

> ***Salazar*** *P, Martín M, Roche R, González Mora JL, O'Neill RD. Microbiosensors for glucose based on Prussian Blue modified carbon fiber electrodes for in vivo monitoring in the central nervous system.* ***Biosensors & Bioelectronics*** *26 (**2010**) 748-753.*
>
> Índice de impacto: 5.637 (5 últimos años)

Si bien, en el primer trabajo se desarrolló y demostró, por primera vez, la idoneidad de un microelectrodo de fibra de carbono modificado con PB y *Gox* para construir un biosensor sensible a glucosa, en el presente artículo, se ha optimizado la deposición de la *Gox,* con el fin de obtener diferentes configuraciones y evaluar su utilidad y viabilidad en aplicaciones *in vivo*. La electrodeposición de PB ha sido realizada mediante CV en un rango de potencial de -0.2 a + 0.4 V frente $Ag/AgCl_{sat}$ (v=

0.1 V/s). Posteriormente, los electrodos modificados con PB (CFE/PB) fueron activados ciclando 50 veces en el medio electrolítico soporte y sometidos a tratamiento térmico (100 ^{o}C, 2 h).

Una vez modificados los microelectrodos (CFE/PB), el siguiente paso consistió en la inmovilización enzimática. La *Gox* se disolvió en PBS a la concentración deseada (300 U/ml) y se emplearon diferentes protocolos para inmovilizar la enzima (*ver detalles en apartado 3.3.1. del presente artículo y resultados en tabla 1*). Uno de los parámetros estudiados fue el número de inmersiones en la configuración básica (CFE/PB/Gox_{α}), siendo α el número de inmersiones aplicadas. Finalmente, con el objetivo de disminuir el tiempo de modificación, fueron seleccionadas 5 inmersiones. Posteriormente, se intentó aumentar la carga enzimática mediante el uso de un polímero catiónico (PEI), mostrando un incremento significativo en la sensibilidad y en la carga enzimática de los dispositivos. En todas las configuraciones la retención definitiva de la enzima se hizo mediante entrecruzamiento con glutaraldehido.

El protocolo definitivo seleccionado fue: (1) inmersión rápida en 5% de PEI y secado durante 1 h; (2) una inmersión durante 5 minutos en *Gox* (300 U / ml) y secado otros 5 minutos. Posteriormente, se procedió a realizar otras 30 inmersiones rápidas en la solución de *Gox* y dejar secar otros 5 minutos. Finalmente, se realizaron 15 inmersiones rápidas en una disolución de glutaraldehido y se dejó secar durante 1 hora a 37 ^{o}C. Con esta configuración se mejoró la sensibilidad y se redujo el límite de detección (ambos en 2 órdenes de magnitud) con respecto a la configuración básica.

En base a la publicación anterior, se electrodepositó una capa de PoPD sobre el biosensor y se hizo un estudio con varios interferentes (AA, AU). El primer resultado significativo, comentado anteriormente fue la pérdida de casi el 50% de sensibilidad debido a una menor difusión de glucosa hacia la superficie del biosensor. No obstante,

el límite de detección se modificó ligeramente. El rango de linealidad encontrado para dicha configuración fue de 0.08-2 mM de glucosa, rango suficiente para realizar medidas en el SNC, cuya concentración se encuentra en torno a 0.5-1 mM.

El estudio de interferencias estuvo en la misma línea que la publicación anterior, no observándose cambios apreciables en la respuesta del microbiosensor en presencia de AA y AU, validando así la presente configuración.

Dado que el pH juega un papel importante en la respuesta del microbiosensor, ya que tanto la bioactividad de *Gox* como la estabilidad de la película PB son pH-dependientes, se procedió al estudio de la respuesta del microbiosensor a distintos pH. De esta forma, se procedió a estudiar la respuesta del biosensor optimizado (CFE/PB/$PEI_{5\%}$/Gox_{opt}/PoPD) en un rango de pH de 6.5 a 8.5. Finalmente, los resultados no mostraron cambios significativos en la respuesta frente a glucosa, confirmando así la excelente estabilidad del dispositivo y que la *Gox* y el PB están bien estabilizados en la superficie del microelectrodo de carbono. Las ventajas del presente diseño son: (1) el PEI y el glutaraldehido, son capaces de reducir los posibles cambios conformacionales de la enzima, puesto que la estructura terciaria y cuaternaria de la enzima no se pueden modificar; (2) la película P_OPD puede, y ha sido demostrado por el grupo de Karyakin, aumentar la estabilidad del PB.

A fin de demostrar la utilidad de este diseño, se evaluó su respuesta *in vivo* frente a cambios en los niveles de glucosa extracelular. Para ello, se examinó el efecto que producía en su respuesta la inyección local de glucosa (2mM en PBS, 100 mM de NaCl) y la despolarización con KCl (150 mM en PBS, 100 mM de NaCl). La inyección localizada se realizó mediante el uso de una microcánula colocada en las cercanías del microbiosensor (50-100 μm) liberando un pequeño volumen de glucosa o KCl (0.1-5 μL).

La inyección de glucosa confirmó la respuesta del microbiosensor en el SNC, observándose un incremento de la señal durante la inyección de glucosa, que posteriormente disminuye y alcanza la línea base inicial al cabo de unos segundos. Esta disminución posterior puede ser atribuida tanto a un fenómeno de dilución como a captación celular de la misma. Por otro lado, la inyección de KCl produjo un incremento de los niveles de glucosa. Dicho comportamiento podría ser explicado por una activación neuronal y su inmediata respuesta: liberación de glucosa hacia el intersticio desde los vasos sanguíneos circundantes que suplirían los costes energéticos de dicha activación. A su vez, la inyección de 5 µL de KCl mostró el comportamiento típico del *spreading depresion* (SD), donde se observa un proceso de máximo consumo, 1 minuto después de finalizar la inyección, que poco a poco recupera los niveles basales iniciales, estableciéndose nuevamente un balance entre el suministro y consumo.

6.3.- Aplicaciones fisiológicas de microbiosensores sensibles a glucosa basados en microelectrodos de carbonos modificados con PB

Extraído de:

> ***Salazar*** *P, O'Neill RD, Martín M, Roche R, González Mora JL. Amperometric glucose microbiosensor based on a Prussian Blue modified carbon fiber electrode for physiological applications.* ***Sensors and Actuators B-Chemical*** *152 (**2011**) 137-143.*

Índice de impacto: 3.751 (5 últimos años)

En este tercer trabajo los principales pasos de construcción del microbiosensor sensible a glucosa han sido examinados en detalle mediante CV y EIS. A su vez, se ha hecho un estudio detallado de la selectividad del microbiosensor optimizado frente a un gran número de posibles interferentes fisiológicos. Finalmente, la respuesta del microbiosensor fue analizada durante modificación farmacológica, inyección intraperitoneal y local, así como mediante estimulación eléctrica local, demostrándose la utilidad del presente diseño en experimentos fisiológicos.

En esta ocasión el proceso de modificación se cambió ligeramente con respecto a las publicaciones anteriores. La disolución electrolítica empleada durante la electrodeposición del PB fue más ácida (0.1 M KCl y HCl 0.1 M) con el fin de mejorar la estabilidad del PB. A su vez, el protocolo de deposición enzimática también fue modificado con el objeto de optimizar la configuración anterior. El protocolo seguido ha sido: (1) 15 inmersiones rápidas en una disolución Nafion y un período de secado de 30 minutos; (2) 15 inmersiones rápidas en una disolución de PEI y un período de secado (30 min); (3) inmersión en *Gox* (300 U/ml) durante 5 minutos y un período de secado (5 min); (4) 30 inmersiones rápidas en la solución de *Gox* y secado durante 5 minutos; (5) 15 inmersiones rápidas en la solución entrecruzamiento (BSA/GLUT). Posteriormente, todos los biosensores se curaron durante 1 hora a 37 ^{o}C y finalmente se electrodepositó una capa de PoPD/BSA sobre cada biosensor.

Mediante el empleo de la CV se ha estudiado como cambia la respuesta del CFE durante las diferentes etapas de construcción, confirmándose así las modificaciones que va sufriendo la superficie del microelectrodo. Para ello se ha usado un barrido de potencial desde -0.2 a +0.4 V (0.1 V/s). Congruentemente, el barrido del CFE sin modificar presentó una respuesta mínima, puesto que la disolución de trabajo no contenía ningún par redox. Sin embargo, después de la electrodeposición de PB sí que aparece la curva característica para el par redox PW/PB, confirmándose así la existencia de dicho compuesto sobre la superficie del electrodo. Posteriormente, los cambios en el CV de los electrodos se pueden explicar debido a dos procesos claramente diferenciados: electrostáticos y difusivos, dado que durante la inter-conversión PW/PB es necesario el transporte de K^+ o cualquier otro catión a través de su estructura. Es por ello que, los polímeros con carga neta negativa facilitan la reversibilidad de dicha conversión (Nafion), mientras que, los polímeros catiónicos (PEI) ofrecen cierta resistencia al transporte de estos cationes a través de su estructura.

Por último, la electrodeposición de PoPD sobre la superficie del microbiosensor mostró una reducción importante del CV, que justifica la disminución de sensibilidad encontrada en las anteriores publicaciones tras la electrodeposición de la misma.

Por otro lado, la EIS es un método eficaz para estudiar las propiedades interfaciales durante la modificación de superficies conductoras. En este caso, se usó el par redox ferro/ferricianuro (ambos cargados negativamente). El espectro de impedancia para el CFE mostró un proceso limitado por transferencia de carga en el rango de frecuencias estudiado. Sin embargo, la configuración CFE/PB mostró también la componente difusiva (tramo lineal) y redujo considerablemente la resistencia eléctrica de la superficie sensora (disminución del diámetro del tramo circular) del proceso de oxido/reducción del par redox empleado. Estos datos indican que el PB mejora las propiedades conductoras favoreciendo los procesos de transferencia de electrones. Así mismo, las sucesivas modificaciones presentaron pequeños cambios en el tamaño de la región semicircular, que pueden ser atribuidas a la facilidad o dificultad con la que ocurren los procesos de transferencia de carga entre la superficie del electrodo y el par ferro/ferricianuro. Por último, la electrodeposición de PoPD produjo un incremento significativo de la resistencia (gran incremento del diámetro de la región semicircular), que puede deberse a su naturaleza no conductora en las condiciones de síntesis.

Para verificar las propiedades antiinterferentes del presente diseño, se evaluó la respuesta del microbiosensor frente a un gran número de potenciales interferentes (15 en total). Los valores de selectividad obtenidos para todas las interferencias fueron < 0,15% excepto para AA (1,6%) que está presente en el cerebro extracelular líquido a una concentración superior (0.4 mM).

Finalmente, se procedió a la evaluación *in vivo* del diseño propuesto. Para ello se recurrió nuevamente a la inyección local de KCl y glucosa, mostrando un comportamiento similar al descrito en las publicaciones anteriores. Adicionalmente, se realizó la administración farmacológica de insulina (administración intraperitoneal). Previamente al experimento, a los animales de experimentación se les retiró la comida (ayuno de 12 h) para disminuir sus niveles de glucógeno. Una vez que el microbiosensor fue insertado se esperó aproximadamente 1 h para alcanzar los niveles basales y posteriormente se procedió a la administración de insulina (20 U/kg). Entre 15-20 minutos después de la inyección se observó un descenso de los niveles de glucosa extracelular que redujo aproximadamente un 70-80% los niveles basales. Posteriormente, los niveles de glucosa fueron incrementados mediante la inyección de glucosa intraperitonealmente (1 g/Kg). La respuesta del biosensor luego de la inyección de glucosa aumentó rápidamente 10 minutos después de la inyección, alcanzando casi el 80% del nivel basal a los 30 minutos siguientes. Sin embargo, no se alcanzaron los niveles basales preinsulina, probablemente debido a la influencia duradera de esta hormona en el organismo.

Adicionalmente, se realizó estimulación eléctrica local, mediante un estimulador bipolar que se posicionó en las proximidades del microbiosensor. La estimulación consistió en una secuencia de pulsos cuadrados que se aplicaron tanto al microbiosensor de glucosa como a un electrodo centinela (sin *Gox*). Bajo las condiciones de estudio se observó que la estimulación producía inmediatamente una señal típica SD (*comentado anteriormente*). No obstante, posterior a la estimulación eléctrica, se observó, una rápida caída de los niveles de glucosa (que se podría atribuir a un consumo por las neuronas excitadas) y luego, se observó, un incremento de la

glucosa extracelular (probablemente debido a un aporte vascular). Por otro lado, la estimulación con los microelectrodos empleados como centinela no presentaron dicha respuesta, hecho que confirma que la respuesta observada anteriormente es debida exclusivamente a cambios de glucosa en el intersticio.

6.4.- Electrodeposición de PB sobre electrodos de carbono mediada por surfactantes: mejoras en la estabilidad, en las propiedades electroquímicas y aplicación en microbiosensores sensibles a lactato

Extraído de:

> ***Salazar*** *P, Martín M, O'Neill RD, Roche R, González Mora JL. Surfactant-promoted Prussian Blue-modified carbon electrodes: Enhancement of electro-deposition step, stabilization, electrochemical properties and application to lactate microbiosensors for the neurosciences.* ***Colloids and Surfaces B*** *92 (**2012**) 180-189.*

Índice de impacto: 3.354 (5 últimos años)

En las últimas décadas el PB, el compuesto más representativo de la familia de los hexacianometalatos, ha recibido mucha atención, debido principalmente, a las propiedades electrocatalíticas de su forma reducida (PW) en la reducción de H_2O_2. Generalmente, su electrodeposición se ha realizado mediante CV en condiciones ácidas. Sin embargo, la adición de surfactantes como el bromuro de cetiltrimetilamonio

(CTAB), ha producido una mejora considerable en el crecimiento del depósito, en su estabilidad y en la eficiencia de transferencia de carga.

En la presente publicación se compara el efecto de diferentes tensioactivos catiónicos como: CTAB, cloruro de bencetonio (BZTC) y cloruro de cetilpiridinio (CPC). En la primera etapa del estudio se han empleado electrodos serigrafiados (SPCE) debido a su alta reproducibilidad, bajo costo y configuración conveniente en comparación con los electrodos de fibra de carbono (CFE) que se necesitan para la implantación in vivo.

La electrodeposición de PB sobre SPCEs se realizó colocando una gota de disolución precursora modificada previamente con surfactante (1 mM) y se procedió al ciclado entre -0.2 y +1 V (0.1 V/s). Análogamente, se prepararon electrodos modificados con PB en ausencia de surfactante para comparar el efecto de los mismos. Una vez preparados, las propiedades electroquímicas de los distintos diseños fueron investigadas, prestando especial atención a parámetros tales como: cantidad de PB depositado, espesor de la película, transferencia de carga, permeabilidad, reversibilidad, estabilidad y sensibilidad a la detección de H_2O_2.

Todos los electrodos modificados en presencia de surfactantes presentaron una mejora significativa en sus propiedades electroquímicas en comparación con los SPCE modificados en ausencia de ellos. Así, la cantidad depositada de PB en presencia de surfactantes alcanzó un valor de ~ 2.05×10^{-8} moles cm^{-2}, mientras que en su ausencia tuvo un valor de 7.25×10^{-9} mol cm^{-2}. En consecuencia, las películas modificadas en presencia de surfactantes alcanzaron un espesor de ~ 33 nm, mientras que en su ausencia fue tan solo de ~ 12 nm. Dichos resultados indicaron que la electrodeposición de PB es más eficiente en presencia de surfactantes catiónicos.

Estudios análogos realizados mediante SEM mostraron una electrodeposición más eficiente en presencia de surfactante. Para ello, se electrodepositó el PB sobre platino, con el fin de tener una mejor superficie de partida. En este caso, se aplicaron aproximadamente 100 ciclos de deposición, con el fin de obtener una buena imagen en SEM, ya que se comprobó que con pocos ciclos la película de PB era demasiado fina para ser observada en detalle. Mientras que en ausencia de surfactantes, se observaron huecos (*pin-holes*) sobre el platino, mostrando zonas donde no se había producido la electrodeposición del PB, el depósito, en presencia de surfactantes, mostró un espectacular crecimiento cristalino, presentando un crecimiento columnar de estructuras cúbicas. Finalmente, dichas imágenes corroboraron los datos anteriores, donde se observaba una mayor electrodeposición de PB en presencia de surfactante.

La permeabilidad del depósito de PB para el K^+, fue 8.24×10^{-12} cm^2 s^{-1}, mientras que para el PB depositado en presencia de surfactantes fue casi un orden de magnitud, mayor, mostrando la configuración PB-CTAB las mejores propiedades difusivas $8{,}53 \times 10^{-11}$ cm^2 s^{-1}. Por otra parte, el coeficiente de difusión para iones más voluminosos como el Na^+ fue mejorado significativamente, comprobándose una mejor reversibilidad para dicho ion y atenuándose la inserción irreversible que se produce al ciclar los electrodos en presencia de Na^+. De esta forma, los sensores de PB modificados con surfactantes recuperaron ~ 86% de la corriente inicial después de haber sido ciclados en presencia de iones Na^+, mientras que la configuración básica logro alcanzar únicamente un valor de 40%.

El depósito obtenido en ausencia de surfactante presentó una constante de transmisión electrónica (k_s) de 1.2 s^{-1}, estando en concordancia con los datos encontrados en la bibliografía. Por otro lado, el valor del coeficiente de transferencia (α) presentó un valor de 0.59, indicando que el proceso de transferencia electrónica no es

del todo simétrica. Curiosamente, los depósitos obtenidos en presencia de surfactante presentaron menores valores para el parámetro k_s y mayores para el parámetro α, mostrando que los fenómenos de transferencia electrónica son más lentos y con un grado mayor de irreversibilidad, pudiendo estar relacionada esta observación con el grosor de la película.

Consecuentemente, se ha hecho un estudio de la sensibilidad hacia el H_2O_2 de las distintas configuraciones, siendo este uno de los parámetros más importantes a tener en cuenta para evaluar la optimización del diseño. Los resultados obtenidos estuvieron en consonancia con otros resultados encontrados. Los sensores modificados en presencia de surfactantes presentaron una mayor sensibilidad frente al H_2O_2 (0.63 A M^{-1} cm^{-2}), así como un mayor rango lineal de trabajo. Dichos resultados pueden atribuirse tanto a la mejora en la difusión iónica a través de su estructura tridimensional, como al incremento de la cantidad del depósito, lo que aumentaría el número de centros redox disponibles para reducir al H_2O_2.

Finalmente, se procedió a la construcción de un microbiosensor sensible a lactato. Para ello, se depositó PB aplicando 3 ciclos de deposición en presencia de BZT (1 mM) La inmovilización enzimática se realizó de acuerdo al siguiente protocolo: 15 y 30 inmersiones rápidas en PEI y *Lox*, respectivamente, con un período de secado de 10 minutos entre ellas; por último se sumergieron 15 veces en glutaraldehido y se curaron durante 4 horas a 37 ^{o}C. Posteriormente, se procedió a la electrodeposición vía CPA de PoPD. Finalmente, los microbiosensores se limpiaron con agua bidestilada y se almacenaron en la nevera.

La respuesta del microbiosensor fue evaluada *in vitro*. De estos resultados se desprende, al igual que en los microbiosensores sensibles a glucosa previamente

diseñados, la idoneidad y las excelentes propiedades del diseño, si bien, el proceso de inmovilización debe ser adecuado para obtener un mayor rango lineal de trabajo. El diseño actual no mostró respuesta alguna frente a la adición de AA a distintas concentraciones, corroborando la buena elección del PoPD como capa antiinterferente. Finalmente, la sensibilidad de los microelectrodos fue estudiada durante un período corto (5h de medidas continuas en PBS) y en un período largo (15 días). Ambos estudios no mostraron pérdida significativa de sensibilidad, demostrando la excelente retención enzimática y la estabilidad de PB a pH fisiológico.

6.5.- Optimización y caracterización de electrodos serigrafiados de carbono modificados con PB en presencia de surfactantes: detección de H_2O_2 a bajos potenciales

Extraído de:

> ***Salazar*** *P, Martín M, O'Neill RD, Roche R, González Mora JL. Improvement and characterization of surfactant-modified Prussian Blue screen-printed carbon electrodes for selective H_2O_2 detection at low applied potentials.* ***Journal of Electroanalytical Chemistry (2012)*** *674 48-56*

Índice de impacto: 2.739 (5 últimos años)

El PB ha resultado ser un compuesto muy útil en la fabricación de biosensores, amperométricos, ya que actúa como una "*peroxidasa artificial*". Sin embargo, su estabilidad operativa en medios básicos y neutros, óptimos para la mayoría de las enzimas empleadas en la construcción de biosensores, sigue siendo un problema. La razón de este comportamiento se atribuye a la fuerte interacción entre los iones férricos

e iones hidróxido para formar $Fe(OH)_3$ a pH superior a 6.4. Para resolver este problema, se han empleado distintas aproximaciones: (1) modificación química del depósito, (2) protección con polímeros, (3) uso de surfactantes en la disolución de electrodeposición.

Este último enfoque representa un método rápido y sencillo que permite mejorar: (1) la cantidad de PB electrodepositado, (2) sus propiedades electrocatalíticas, (3) su sensibilidad frente al H_2O_2, (4) su estabilidad en medios neutros y básicos.

En la presente publicación se ha optimizado la electrodeposición de PB en presencia de BZTC. Para ello, se ha optimizado la concentración de surfactante empleado, así como sus condiciones de electrodeposición. Los principales parámetros estudiados en dicha optimización han sido: (1) reversibilidad, (2) cantidad de depósito generado, (3) coeficiente de difusión para el K^+, (4) estabilidad, (5) sensibilidad frente al H_2O_2.

La electrodeposición de PB sobre SPCEs se realizó colocando una gota de disolución precursora con diferentes concentraciones de surfactante (0-5 mM), procediendo posteriormente al ciclado (CV) entre -0.2 y +1 V (0.1 V/s). Del análisis de estos resultados se desprende que la concentración de surfactante óptima es 2mM, probablemente, siendo esta su concentración miscelar crítica en las condiciones de trabajo. En estas condiciones, la cantidad depositada de PB alcanzó un valor de ~ 6.3×10^{-8} moles cm^{-2}, mientras que en su ausencia tuvo un valor de 9.71×10^{-9} mol cm^{-2}. En consecuencia, las películas obtenidas en condiciones óptimas alcanzaron un espesor de ~ 122 nm, mientras que en su ausencia fue tan solo de ~ 16 nm.

El análisis estructural (SEM) reveló una clara diferencia morfológica en los depósitos, dependiendo ésta de la concentración de surfactante empleada. Mientras

que el depósito de PB sintetizado en ausencia de BZTC mostró un espesor muy fino (apreciable sólo a mayores aumentos), en condiciones óptimas el depósito de PB mostró un excelente recubrimiento. En contraste, a una concentración elevada de surfactante (6 mM) la electrodeposición de PB fue prácticamente inhibida, posiblemente debido a la formación de micelas en estas condiciones.

Los datos obtenidos mediante EIS mostraron nuevamente que en presencia de surfactante la resistencia de transferencia de carga es menor. De estos resultados se desprende que las propiedades conductoras del depósito mejoran considerablemente, siendo nuevamente la concentración de 2 mM la que mejor resultados presenta.

Con el fin de comparar la actividad electrocatalítica de distintas configuraciones (0 y 2 mM de BZTC) se analizó su respuesta frente al H_2O_2. El análisis de la dependencia del pico catódica frente a la velocidad de barrido y la raíz cuadrada de velocidad de barrido sugiere un comportamiento puramente difusivo. Por otro lado, mediante cronoamperometría, se obtuvo el coeficiente de difusión para el H_2O_2, presentando ambas configuraciones un valor ~ 5.5×10^{-6} cm^2 s^{-1}, valores consistentes con los encontrados en la bibliografía. Mediante cronoamperometría también se determinó la constante catalítica (K_{cat}) para dichas configuraciones, encontrándose nuevamente que la configuración obtenida en presencia de BZTC (2mM) es la que presenta mejores resultados.

Se volvió a estudiar la estabilidad de los sensores en presencia de iones Na^+, obteniendo resultados similares a los anteriormente publicados. Estos datos revelan que, el daño causado por la inserción irreversible de iones Na^+, una característica indeseable para los sensores diseñados para aplicaciones biológicas, es atenuado en las condiciones óptimas de electrodeposición encontradas.

Con el fin de estudiar la estabilidad de PB frente al pH, se han examinado distintas configuraciones mediante CV. Los sensores fueron ciclados 100 veces en disoluciones ajustadas en un amplio rango de pH. La actividad residual se calculó utilizando la intensidad del pico anódico antes y después del ciclado. Los resultados mostraron una baja estabilidad del depósito de PB en ausencia de surfactante, incluso en medios ácidos, con un descenso significativo de la señal (~ 70%) a pH 7,4. Por el contrario, la configuración optimizada, BZTC(2mM)/PB, mostró una mejor estabilidad, conservando el 100% de la señal por debajo de pH 6, y perdiendo sólo el 10% de la señal inicial al final de los 100 ciclos a pH 7.4.

La etapa de calibración mostró que la configuración optimizada presenta una mayor sensibilidad (1.07 ± 0.03 A M^{-1} cm^{-2}, n = 5), mejorando significativamente los valores encontrados en la literatura para electrodos serigrafiados. El estudio de interferencias se realizó empleando el AA como prototipo de interferente endógeno. A su vez, se optimizó el potencial aplicado para minimizar dicha contribución. Del análisis de resultados se concluyó que el rango óptimo de potencial se encuentra entre - 0.05 y - 0.15 V, donde la relación de selectividad es menor del 1%.

Finalmente, la estabilidad a largo plazo de los sensores modificados con PB fue estudiada. Para ello, se comprobó la sensibilidad frente al H_2O_2 de distintos sensores almacenados en seco, en la oscuridad y a temperatura ambiente. Del presente estudio se concluyó que: al menos durante el periodo estudiado (4 meses) los sensores retuvieron aproximadamente el 90% de su sensibilidad inicial.

6.6.- Desarrollo de un microbiosensor basado en fibras de carbono modificado con PB para medir lactato en el espacio extracelular del tejido cerebral

Extraído de:

> ***Salazar*** *P, Martín M, O'Neill RD, Roche R, González Mora JL. Biosensors based on Prussian Blue modified carbon fibers electrodes for monitoring lactate in the extracellular space of brain tissue.* ***International Journal of Electrochemical*** *Sciences 7 (****2012****)* 5910-5926.

Índice de impacto: 3.729 (2011)

En esta última publicación se ha presentado un microbiosensor sensible a lactato, análogo a los microbiosensores de glucosa ya presentados en trabajos anteriores. Nuevamente se ha optimizado el procedimiento de fabricación y se ha validado su respuesta frente a algunos de los interferentes más comunes en el SNC. Finalmente, se presentaron algunos resultados *in vivo*, incluyendo: estimulación farmacológica,

fisiológica y electrofisiológicas, que demostraron que el presente diseño es adecuado para explorar el papel del lactato en el SNC.

La electrodeposición del PB se ha realizado de forma análoga a las anteriores publicaciones. La caracterización electrocrómica de PB (CV, EIS, FTIR y Vis-UV) ha coincidido con los datos presentados anteriormente. Adicionalmente, en esta publicación, se ha estudiado cómo afecta la estabilización térmica en dichas propiedades. Los datos obtenidos mediante CV muestran una progresiva disminución de los picos de oxidación/reducción y una importante pérdida de actividad electroquímica a 200 ^{o}C. Los espectros FTIR y absorbancia (Vis-UV) reproducen la característica banda a 2067 cm^{-1} (vibración del enlace Fe-CN) y la banda de absorción a 672 nm (transferencia de carga entre Fe^{3+} a Fe^{2+}), respectivamente. Por otro lado, en el espectro FTIR se observó una banda ancha en las altas frecuencias (~ 3000 cm^{-1}) debida a las tensiones del enlace OH del agua. Esta última banda fue reducida mediante el tratamiento térmico, si bien la banda a 2067 cm^{-1} también disminuyó y desapareció a 200 ^{o}C. El espectro Vis-UV mostró un comportamiento similar al discutido anteriormente, aunque a 200 ^{o}C mostró una banda entre 300 y 400 nm, que corresponde a la región de longitud de onda de Fe_2O_3, indicando que el tratamiento térmico a altas temperaturas produce la oxidación del PB a óxidos de hierro. En vista de estos resultados, la temperatura de 100 ° C fue seleccionada como temperatura óptima.

Siguiendo los protocolos ya descritos anteriormente se procedió a la construcción del microbiosensor sensible a lactato, fijando por defecto el número de inmersiones rápidas en la disolución enzimática en 30. El primer parámetro investigado fue la concentración enzimática, construyéndose varios microbiosensores con diferentes concentraciones de *Lox* (25, 50 y 100 U ml^{-1}). Las curvas de calibración de estos biosensores muestran que la concentración de 100 U ml^{-1} presenta los mejores

resultados con una V_{max} 15 veces mayor que la concentración más baja, siendo dicha concentración, el valor seleccionado para el resto de la investigación.

El siguiente paso en la optimización fue estudiar cómo afecta el PEI (polielectrolito catiónico) en la carga de enzimática. En este contexto, se determinó la concentración óptima de PEI y en cómo afectaba el contenido de agua en la carga enzimática. En respuesta a la primera pregunta, se construyeron varias configuraciones usando distintas disoluciones de PEI en agua (1, 2.5 y 5% w/v). Los resultados mostraron que tanto la concentración de 2.5 como la de 5 % w/v duplicaban la carga enzimática respecto a la obtenida con la concentración de 1% w/v. Finalmente la concentración de 2.5% w/v PEI fue seleccionada para posteriores estudios. Hasta este momento, se había trabajado con un período de secado de 5 minutos entre las disoluciones de PEI y las de *Lox*. Con el fin de estudiar como afectaba este parámetro en la carga enzimática, se elaboraron diferentes electrodos, empleando distintos tiempos de secado. Los resultados sugieren que al aumentar el tiempo de secado se consigue una mayor carga enzimática, presentando la configuración con 15 minutos de secado una carga enzimática aproximadamente 3 veces mayor que para la configuración en donde se ha sumergido el microelectrodo seguidamente en la disolución enzimática (t= 0). En base a estos resultados, el tiempo de secado se aumentó a 15 minutos en los estudios posteriores.

El último paso en la construcción del microbiosensor fue la electrodeposición de una PoPD en su superficie para mejorar la selectividad y la compatibilidad biológica del dispositivo. Los primeros resultados mostraron una pérdida significativa de sensibilidad (~ 60%) que se puede atribuir a varios factores tales como: la desactivación enzimática, la formación de una barrera difusiva en superficie, etc. Dicha configuración presentó una sensibilidad de ~ 42 nA mM^{-1} cm^{-2}, un rango lineal próximo a 0,6 mM, y

un límite de detección de ~ 6 μM (S/N = 3). Teniendo en cuenta que la concentración en el SNC de lactato es de ~ 0,4 mM y que, durante la activación neuronal, los cambios registrados pueden alcanzar ~ 200% de su concentración basal (~ 0,7 mM), esta configuración presenta una excelente sensibilidad, pero el rango lineal está bastante ajustado para su uso en aplicaciones fisiológicas.

Finalmente, se aumentó el rango lineal de la configuración anterior mediante la adición de una capa externa de Nafion. El protocolo consistió en realizar tres inmersiones en una disolución alcohólica de Nafion (5%). Un número mayor de inmersiones produjo la pérdida total de sensibilidad del microelectrodo, principalmente, debido a las repulsiones electrostáticas entre los aniones lactato y los grupos sulfonatos del dicho polímero. En esta configuración la sensibilidad fue inferior ~ 12 nA mM^{-1} cm^{-2}, sin embargo, se logró obtener un límite de detección (~20 μM) aceptable y un rango lineal más apropiado para los estudios fisiológicos (~ 1.2 mM).

Otros dos parámetros importantes a tener en cuenta en el diseño de sensores electroquímicos para aplicaciones *in vivo* son: estabilidad frente a la floculación de proteínas en su superficie y respuesta frente a distintos interferentes endógenos. Para responder a la primera cuestión, se sumergieron diferentes biosensores con y sin PoPD durante 18 horas en una disolución de BSA y se comprobó su sensibilidad frente al lactato antes y después. En vista de los resultados se concluyó que ambas configuraciones eran óptimas para su uso en el SNC. Por otro lado, en el estudio con distintos interferentes, la configuración sin PoPD, no mostró respuesta para la mayoría de interferentes (resultado del bajo potencial aplicado para detectar H_2O_2). Sin embargo, la adición de AA a la concentración basal (0.2 mM) si produjo una respuesta clara, lo que puso de manifiesto la necesidad de añadir PoPD a la configuración definitiva. Finalmente, el microbiosensor de lactato optimizado, con un capa externa

POPD/Naf, superó el test de interferencias, concluyendo así el proceso de optimización y fabricación del microbiosensor.

Una vez finalizada la etapa de optimización, el siguiente paso fue estudiar la respuesta del microbiosensor en experimentos *in vivo* en el SNC. Para ello, se trabajó con ratas Sprague Dawley macho anestesiadas. Bajo estas condiciones, y con los microelectrodos de lactato previamente calibrados, se obtuvo una concentración basal de 0.36 ± 0.02 mM (media ± DE, n = 5), valor acorde al encontrado en la bibliografía. Los estudios farmacológicos y la estimulación eléctrica local mostraron cambios evidentes en la concentración de lactato en el intersticio, coincidiendo con otros datos publicados en la literatura. Finalmente, se procedió al estudio simultáneo de los niveles de lactato y O_2 bajo estimulación electrofisiológica. Los resultados muestran un consumo de lactato inicial y un aporte posterior a la estimulación, mientras que el O_2 descendió ligeramente después de la estimulación. Teniendo en cuenta estos resultados, todo parece indicar que el lactato podría ser sintetizado y/o exportado al compartimento extracelular no solo en condiciones anóxicas severas, sino también, podría ser usado como sustrato energético durante los procesos de activación neuronal en condiciones fisiológicas normales.

CONCLUSIONES

7.-Conclusiones

En la presente memoria de tesis doctoral se han desarrollado microbiosensores orientados a cuantificar las concentraciones de glucosa y lactato en el espacio extracelular del sistema nervioso central de animales de experimentación. A su vez, durante el desarrollo de dichos microbiosensores, se ha realizado un estudio metodológico de las modificaciones previas con Azul de Prusia y de los protocolos de inmovilización enzimática.

A modo de resumen podemos citar las siguientes conclusiones:

1) Se ha desarrollado y demostrado la idoneidad de microelectrodos de fibra de carbono de pequeñas dimensiones ($\Phi \sim 10$ μm) modificados previamente con Azul de Prusia para detectar H_2O_2 a bajo potencial, lo cual permite disminuir los artefactos y la excitación neuronal derivada de aplicar elevados potenciales de trabajo.

2) Se ha estudiado y optimizado las condiciones de electrodeposición del Azul de Prusia. Los resultados mostraron que el potencial óptimo para detectar H_2O_2 se encuentran en el rango de +0.1 a -0.2 V frente SCE, obteniéndose una sensibilidad y un límite de detección de 1.00 ± 0.04 A M^{-1} cm^{-2} y 1 10 nM respectivamente. También se han utilizado distintos polímeros para mejorar la estabilidad y selectividad del microsensor para H_2O_2, encontrando idóneo para tales fines el empleo de la poli-*o*-fenilendiamina.

3) Se ha demostrado el efecto beneficioso del empleo de distintos surfactantes como el bromuro de cetiltrimetilamonio (CTAB), el cloruro de bencetonio (BZTC) y el cloruro de cetilpiridinio (CPC) durante la electrodeposición de Azul de Prusia sobre tarjetas serigrafiadas. Produciendo una mejora considerable en el crecimiento del depósito, así como en la estabilidad, permeabilidad y eficiencia de transferencia de carga. Finalmente, la sensibilidad frente al H_2O_2 ha mejorado significativamente los valores encontrados en la literatura para configuraciones análogas.

4) Se han desarrollado protocolos de modificación y optimización para la construcción de microbiosensores amperométricos enzimáticos de primera generación para medir glucosa y lactato. El estudio concienzudo de cada una de las variables de construcción (materiales de partida, protocolos de modificación, etc.) ha permitido desarrollar microbiosensores con la sensibilidad, selectividad, tiempo de respuesta, rango lineal y límite de detección adecuados para trabajar en el SNC.

5) Se ha demostrado la utilidad de los microbiosensores de glucosa y lactato elaborados mediante evaluación de la respuesta *in vivo* en animales de

experimentación. Obteniéndose concentraciones basales para glucosa y lactato de 1.2 y 0.4 mM respectivamente, valores ampliamente recogidos en la bibliografía. Además, se comprobó la respuesta de dichos microbioensores frente a cambios en los niveles basales de glucosa y lactato mediante estimulación eléctrica local, inyección farmacológica local e intraperitoneal, administración de gases, etc.

6) Se ha resuelto el problema de la limitación estequiométrica derivada de las bajas concentraciones de oxígeno en el SNC (*déficit de oxígeno)* mediante el empleo de polímeros fluorocarbonados (Nafion, H700). De esta forma, se han obtenido microbiosensores de glucosa con mayor sensibilidad y un rango de trabajo óptimo para estudios fisiológicos (*ver anexo II: otras publicaciones*).

7) Se han realizado medidas simultáneas de la respuesta hemodinámica (*flujo local sanguíneo*) y de los niveles de glucosa extracelular frente a estimulación eléctrica local. El presente diseño permitió optimizar el espacio de trabajo en la ventana craneal y el estudio simultáneo de ambas variables. Los resultados mostraron una correlación positiva (R^2 ~ 0.94) entre el flujo y la concentración extracelular de glucosa en el intersticio, pese a que se registró un ligero desacoplamiento entre ambas variables (*ver anexo II: otras publicaciones*).

8) En base a los resultados obtenidos concluimos que los microbiosensores de glucosa y lactato desarrollados y descritos en la presente memoria son adecuados para su uso en estudios neurometabólicos en el SNC de animales de experimentación.

TRABAJOS FUTUROS

8.- Trabajos futuros

Durante el desarrollo de la presente tesis, y especialmente durante esta última etapa he podido ampliar mis conocimientos en el área de los biosensores trabajando con nuevas enzimas (*glutamato oxidasa, peroxidasas*) y materiales (*nanotubos de carbono, nanopartículas*, nano*partículas magnéticas, anticuerpos*). A su vez, he podido interactuar con otros grupos de investigación nacionales e internacionales. En el panorama actual

tenemos que promover la conexión con otros grupos de biosensores, especialmente cuando en Canarias no existen grupos de investigación importantes en dicha área.

El ámbito de la Biotecnología y la Biomédica ofrecen una gran diversidad de aplicaciones en el ámbito de los biosensores como herramienta de diagnóstico, de control de procesos y calidad, así como en estudios de modelos animales. Una vez terminada esta etapa, solo espero poder continuar en la investigación, desarrollo y aplicación de biosensores, ya sea en el sector público o en el privado, entendiendo necesaria la estrecha colaboración entre ambos sectores para hacer sostenible la investigación y el desarrollo tecnológico en Canarias.

ANEXOS

9.-Anexo I: Publicaciones

Electrochimica Acta 55 (2010) 6476–6484

Contents lists available at ScienceDirect

Electrochimica Acta

journal homepage: www.elsevier.com/locate/electacta

Prussian Blue-modified microelectrodes for selective transduction in enzyme-based amperometric microbiosensors for *in vivo* neurochemical monitoring

P. Salazar[a,*], M. Martín[a], R. Roche[a], R.D. O'Neill[b], J.L. González-Mora[a]

[a] Neurochemistry and Neuroimaging Group, Faculty of Medicine, University of La Laguna, La Laguna, Tenerife, Spain
[b] UCD School of Chemistry and Chemical Biology, University College Dublin, Belfield, Dublin 4, Ireland

ARTICLE INFO

Article history:
Received 12 March 2010
Received in revised form 8 June 2010
Accepted 12 June 2010
Available online 19 June 2010

Keywords:
Carbon fiber electrodes
Hydrogen peroxide
Prussian Blue
Poly(o-phenylenediamine)
Biosensor

ABSTRACT

Prussian Blue-modified carbon fiber microelectrodes (CFE/PBs) are proposed as an alternative to the more conventional metal transducers used for H_2O_2-detecting biosensors in brain extracellular fluid (ECF). The main advantages of this approach are the very small dimensions (~10 μm diameter) and the low applied potentials needed (0.0 V versus SCE). Electrocatalytic and physiochemical properties of PB deposits were studied using cyclic voltammetric (CV), amperometric and spectroscopic methods (FTIR and VIS). Optimized CFE/PB microsensors displayed a H_2O_2 current density of 1.00 ± 0.04 A M^{-1} cm^{-2} with a detection limit of 10^{-8} M. Furthermore, to improve stability and selectivity properties, several polymeric films were investigated: Nafion, poly(o-phenylenediamine) (PoPD), and a hybrid configuration of these two polymers. Finally, the PoPD film was selected due to its excellent anti-interference properties. The use of this permselective film also enhanced the stability of PB against solubilization at high pH, albeit at the expense of slightly lower H_2O_2 sensitivity (0.48 ± 0.02 A M^{-1} cm^{-2}) and higher detection limit (~10^{-7} M). However, the use of the PoPD film significantly enhanced the selectivity against the main endogenous brain interference species (ascorbic acid, uric acid, dopamine and 3,4-dihydroxyphenylacetic acid), expressed as the ratio of the sensitivity slopes ($S_{H_2O_2}/S_{interference}$), which was close to 600 for all interference molecules studied. A prototype of a CFE/PB-based glucose microbiosensor design is presented, together with preliminary studies of its characteristics *in vitro* and its functionality in brain ECF *in vivo*.

1. Introduction

1.1. Prussian Blue

Prussian Blue (PB), $Fe_4[Fe(CN)_6]_3$, belongs to a transition metal hexacyanometallate family [1] and is the oldest coordination compound known and used [2]. Electrochemical properties of PB films are known since 1978 when Neff [3] reported the successful deposition of a thin layer on a platinum foil. A large number of studies followed, and different methods for the preparation of PB-modified electrodes have been described [4–7]. In 1984, Itaya et al. [8] showed that the reduced form of PB (Prussian White, PW) displayed catalytic activity for the reduction of O_2 and H_2O_2. The zeolite structure of PB, with a cubic unit cell of 1.02 nm and channel diameters of about 0.32 nm [9], allows the diffusion of low molecular weight molecules (such as O_2 and H_2O_2) through the crystal structure. Nowadays its electrochemical behavior is well-understood with cyclic voltammograms of PB-modified electrode showing two pairs of almost reversible and symmetrical peaks [10]. The first peak pair corresponds to the interconversion of PW and PB forms, and the second pair from PB to Prussian Green (PG) and its reversal. The electron transfer reactions in the presence of potassium chloride as supporting electrolyte may be formulated as follows:

$$(PB)\,Fe(III)_4[Fe(II)(CN)_6]_3 + 4e^- + 4K^+ \rightarrow (PW)\,K_4Fe(II)_4[Fe(II)(CN)_6]_3 \quad (1)$$

$$(PB)\,Fe(III)_4[Fe(II)(CN)_6]_3 + 3Cl^- \rightarrow (PG)\,Fe(III)_4[Fe(III)(CN)_6]_3Cl_3 + 3e^- \quad (2)$$

corresponding to peaks at 0.1 V and 0.9 V versus SCE, respectively [11–13].

Electrochemical properties such as formal electrode potential, sensitivity, stability and electron transfer rate constants of the PB/PW and PB/PG conversions depend on deposition method, pH, nature and concentration of the supporting electrolyte, etc. [14,15].

* Corresponding author at: School of Medicine, University of La Laguna, Department of Physiology, Campus Ciencias de La Salud, 38071 La Laguna, Tenerife, Spain. Tel.: +34 922 319363.
E-mail address: psalazar@ull.es (P. Salazar).

0013-4686/$ – see front matter © 2010 Elsevier Ltd. All rights reserved.
doi:10.1016/j.electacta.2010.06.036

As can be seen in Eqs. (1) and (2), these reduction and oxidation reactions are supported by free diffusion of cationic and anionic species, respectively. In the present work we focus on the first peak (conversion from PB to PW). Due to this mechanism, only cations with small hydrated radii, such as K^+, NH_4^+, Rb^+ and Cs^+, can support this electrochemical activity by diffusing across the PB structure during iron center oxidation/reduction. On the other hand, Na^+, Li^+, Mg^{2+}, Ca^{2+} can be described as blocking cations of the PB film, due to their larger hydrated radii inhibiting the free diffusion referred to above [1,16,17].

The principal handicap of PB is related to its high solubility at neutral and basic pH, although in acid conditions it shows good sensitivity and stability [18,19]. Different pH stability studies indicate that PB films can be made more stable in basic media by changing the deposition procedure, thus modifying slightly PB three-dimensional structure and avoiding OH^- diffusion across the crystal [20,21]. However, a more practical approach has been the use of protective polymer films deposited over PB to enhance both its operational stability and selectivity against electroactive species. Several polymers have been used, such as Nafion, polypyrrole, polyaniline and poly(o-phenylenediamine) [10,17,22]. These films partially block access of interference through different mechanisms (e.g., size and/or charge exclusion). Recently, Lukachova et al. have described a PoPD-coated, PB-modified macrodisk electrode with moderate hydrogen peroxide sensitivity of 0.3 A M^{-1} cm^{-2}, high selectivity ratio (~600) against ascorbic acid (main endogenous interference in physiological media), and high stability under continuous flow of 0.1 mM H_2O_2 (almost total retained sensitivity after 20 h) [22].

1.2. Prussian Blue-modified biosensors

Although the birth of biosensors occurred in the early 1960s [23], when Clark and Lyons coupled an enzyme (glucose oxidase, Gox) to an amperometric electrode for detecting O_2, and PB electrochemical properties have been known since the late 1970s, the first work on biosensors involving the use of a PB-modified electrode was not reported until 1994 [24–26]. In these first reports, the authors proposed the use of PB-modified electrodes as an alternative to the traditional Pt transducer used to detect H_2O_2. During the last decade, a great number of studies involving PB have appeared using different biosensor configurations (carbon paste, screen-printing, glassy carbon, etc. substrates) and different oxidase enzymes (glucose oxidase, lactate oxidase, glutamate oxidase, etc.) [27–29].

On the other hand, in the neuroscience field traditional first-generation biosensors based on noble metal transducers [30], and second-generation biosensors based on artificial redox mediators, have been generally used [31]. Thus, the main purpose of the present work is to present CFE/PBs as an alternative for implantable microbiosensor designs.CFE/PBs were characterized, optimized, coated with permselective polymers, and a range of endogenous interferences in brain ECF (ascorbic acid, uric acid, dopamine, and 3,4-dihydroxyphenylacetic acid) tested. In addition, a prototype of a CFE/PB-based glucose microbiosensor is presented, together with preliminary studies of its characteristics *in vitro* and its responsiveness in brain ECF *in vivo*.

2. Experimental

2.1. Reagents and solutions

The enzyme glucose oxidase (Gox) from *Aspergillus niger* (EC 1.1.3.4, type VII–S, lyophilized powder), glutaraldehyde (Glut, 25% solution) were obtained from Sigma Chemical Co., and stored at −21 °C until used. All chemicals, including o-phenylenediamine (o-PD), polyethyleneimine (PEI), NaCl, KCl, $CaCl_2$, $MgCl_2$, $FeCl_3$, $K_3[Fe(CN)_6]$, HCl (35%, w/w), H_2O_2 (30%, w/v), Nafion (5 wt.% in a mixture of lower aliphatic alcohols and water), bovine serum albumin (BSA, fraction V), glucose and phosphate buffer saline (PBS, pH 7.4 containing 0.1 M NaCl) were obtained from Sigma and used as supplied. Endogenous interference species were obtained from Aldrich (ascorbic acid, AA, and 3,4-dihydroxyphenylacetic acid, DOPAC) and Sigma (dopamine, DA, and uric acid, UA). All solutions were prepared in doubly distilled water (18.2 MΩ cm, Millipore-Q). The stock calibration solution of H_2O_2 (10 mM) was prepared in water just before its use. Stock solutions of glucose (1 and 0.25 M) were prepared in water, left for 24 h at room temperature to allow equilibration of the anomers, and then stored at 4 °C. 300 mM of o-PD monomer solution was prepared using 48.6 mg of o-PD and 7.5 mg of BSA in 1.5 ml of N_2-saturated PBS, and sonicated for 15 min. Carbon fibers (7 μm diameter) were obtained from Goodfellow, glass capillaries from Word Precision Instruments Inc., 250 μm internal diameter Teflon-coated copper wire from RS, and silver epoxy paint was supplied by Sigma. An in-house microinjection cannula was constructed using fused silica capillary (75 μm inner diameter) supplied by Composite Metal Service, Hallow, UK.

2.2. Instrumentation and software

Experiments were computer controlled, using data acquisition software EChem™ for cyclic voltammetry and Chart™ for constant potential amperometry. The data acquisition system used was e-Corder 401 (EDAQ) and a low-noise and high-sensitivity potentiostat, Picostat (EDAQ). To electro-deposit and activate PB film, an in-house Ag/AgCl/saturated KCl reference and platinum wire auxiliary electrode were used. Transmittance spectra of PB films were recorded in the range 300–1000 nm with respect to air in a Transpec® photodiode array spectrophotometer. FTIR spectra were recorded with respect to air, using a Varian 670-IR spectrophotometer in the range 4000–400 cm^{-1}.

The electrochemical characterization experiments, H_2O_2 and glucose calibrations were done in a 25 mL glass cell at 21 °C, using a standard three-electrode setup with a commercial saturated calomel electrode, SCE (CRISON Instrument S.A.), as the reference and platinum wire as the auxiliary electrode. The applied potential for amperometric studies was 0.0 V versus SCE, unless stated otherwise. H_2O_2 and glucose calibrations were performed in quiescent air-saturated PBS (following stabilization of the background current for 20–30 min) by adding aliquots of H_2O_2 or glucose stock solution. After each addition, the solutions were stirred for 10 s and then left to reach the quiescent steady-state current.

2.3. Preparation of the working electrodes

2.3.1. Fabrication of carbon fiber electrodes

CFEs were constructed using the following steps. Carbon fibers (diameter 7 μm, 20–50 mm in length) were attached to Teflon-coated copper wire (diameter 250 μm), using high purity silver paint, and dried for 1 h at 80 °C. The borosilicate glass capillary was pulled to a tip using a vertical microelectrode puller (Needle/Pipette puller, Model 750, David Kopf Instruments). After drying, the carbon fiber was carefully inserted into the pulled glass capillary tube under a microscope, leaving 2–4 mm of the carbon fiber protruding at the pulled end. Subsequently, the carbon fiber was cut to the desired length (approximately 250 or 500 μm), using a microsurgical scalpel. At the stem end of the capillary tube, the copper wire was fixed by casting with non-conducting epoxy glue; the carbon fiber was also sealed into the capillary mouth, using the non-conductive epoxy glue. Finally, CFEs were dried again for 1 h, and were optically and electrochemically inspected before use.

2.3.2. PB deposition onto carbon fiber electrodes

CFEs were modified by means of electro-deposition and activation of a PB film. The PB layer was electro-deposited using cyclic voltammetric (CV) methodology, applying 3 cyclic scans within the limits of −0.2 to 0.4 V at scan rate of 0.1 V/s in a fresh de-aerated solution containing 1.5 mM $K_3[Fe(CN)_6]$ and 1.5 mM $FeCl_3$ in 0.1 M KCl and 3 mM HCl. These CFE/PBs were cleaned in doubly distilled water and activated by applying another 50 cycles in de-aerated electrolyte solution (0.1 M KCl and 3 mM HCl), using the same protocol. Before being used, the CFE/PBs were cleaned again in doubly distilled water for several seconds. Finally, the PB film was tempered at 100 °C for 2 h.

2.3.3. PoPD deposition onto carbon fiber electrodes

To enhance PB stability at neutral pH and selectivity against principal endogenous brain interference species, several permselective polymer coatings were employed: PoPD–BSA electrodeposited; cast Nafion coatings; and a mixed method with Nafion modification before the electro-deposition of the PoPD–BSA film (discussed below). Electrosynthesis of PoPD was carried out with a standard three-electrode setup; an in-house Ag/AgCl/saturated KCl was used as the reference electrode and platinum wire as the auxiliary electrode. The electropolymerization was performed in PBS containing 300 mM o-PD, using two approaches: by CV (scan rate: 0.05 V/s, limits: 0–0.8 V) and by applying a constant potential (+0.75 V) for 20–25 min. BSA was included in the monomer solution because globular proteins trapped in the PoPD polymer matrix can improve its permselectivity under some conditions, as well as acting as a model for trapped enzyme molecules in biosensor applications [32–34]. For clarity in the nomenclature, however, the term BSA will be omitted in all sensor configurations.

2.3.4. In vivo experiments

Experiments were carried out with male rats of ∼300 g (Sprague–Dawley) in accordance with the European Communities Council Directive of November 24, 1986 (86/609/EEC) regarding the care and use of animals for experimental procedures, and adequate measures were taken to minimize pain and discomfort. The rats were anesthetized with urethane (1.5 g/kg), immobilized in a stereotaxic frame, and body temperature maintained at 37 °C with a heating blanket. The skull was surgically exposed and a small hole drilled for microbiosensor implantations. The biosensor, Ag/AgCl reference electrode and platinum auxiliary electrode were placed in the cortex, and the skull kept wet with saline-soaked pads. The reference potential provided by the Ag/AgCl wire in brain tissue was very similar to that of the SCE. Local microinjection was performed using a microcannula based on a fused silica capillary tube with 75 μm inner diameter located 400 μm from the recording electrode tip.

3. Results and discussion

3.1. Prussian Blue electro-deposition

A PB layer was electro-deposited onto CFEs, by applying three cyclic scans (CV) within the limits of −0.2 to 0.4 V versus SCE at scan rate of 0.1 V/s, in a fresh de-aerated solution containing 1.5 mM $K_3[Fe(CN)_6]$ and 1.5 mM $FeCl_3$ in 0.1 M KCl and 3 mM HCl. With these parameters a thin film of 3–4 μm thickness was measured using the Leica microscope (New York Microscope Company Inc.) and the Andor iXon^{EM} DU-897 back-illuminated EMCCD camera (ANDOR^{TM} technology). Fig. 1a shows CV electro-deposition with four scans. A clear increase in the peak currents occurred due to the deposition of PB onto the CFE. The formal electrode potential was centered at about 0.1 V and $\Delta E_p \sim 52$ mV showing a monoelectronic process per unit of Fe, which is in good agreement with data reported previously [11–13]. Such voltammograms reflect the regular structure of PB with homogeneous distribution of electron- and ion-transfer rates throughout the film [13].

During the activation step, conversion between insoluble (free of potassium) and soluble forms of PB ($KFe[Fe(CN)_6]$) occurs, as discussed previously [35] During this conversion a disruption of the structure occurs and one quarter of the high-spin Fe^{3+} is lost; instead a potassium ion occupies interstitial sites in the structure of soluble PB film [16]. Here, the term solubility refers to the ease with which Fe^{3+} is exchanged by potassium, and is not related with the solubility in water. Fig. 1b shows conversion between soluble and insoluble forms [21]. During conversion, the two peaks become slightly narrower and sharper, and after ∼20 cycles the voltammogram is stabilized, while the formal potential does not change appreciably during activation cycles.

Once PB had been electrosynthesized, it was characterized by means of CV, FTIR and VIS techniques. Fig. 2a shows CV of $KFe[Fe(CN)_6]$; two characteristic peaks due to conversion of PW/PB and PB/PG appear well defined with formal potentials of ∼0.10 V and ∼0.85 V, close to values reported previously [11–13]. ΔE_p of the first peak pair (PW/PB) was close to 59 mV, showing a clear monoelectronic and reversible behavior, and can be attributed to the reversible redox interconversion between the two forms, reduced and oxidized species of PB; see Eq. (1).

Absorbance spectrum (Fig. 2b) of an as-deposited PB film showed the characteristic broad absorption peak at 672 nm due to charge transfer between Fe^{3+} and Fe^{2+} ions; this value is in good accord with data reported by other authors [36–38]. FTIR spectrum (Fig. 2c) was measured in the range of 4000–400 cm^{-1}. The transmittance spectrum in the high frequency region is characterized by a very broad band which can be attributed to stretching modes of bonded (2973 cm^{-1}) and free (3435 cm^{-1}) OH^- groups of water [7,38]. This band shows that water molecules can be found in PB

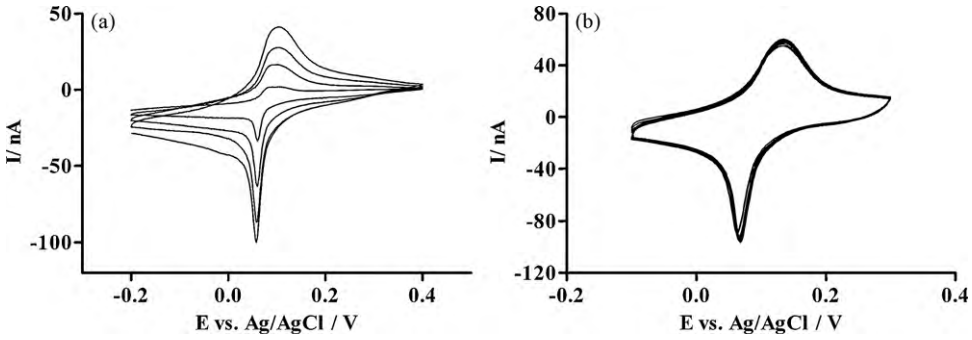

Fig. 1. (a) Electro-deposition of PB film onto a carbon fiber electrode (CFE): four scans of increasing amplitude; scan range, −0.2 to 0.4 V versus Ag/AgCl/saturated KCl; scan rate, 0.1 V s^{-1} in a fresh de-aerated solution containing 1.5 mM $K_3[Fe(CN)_6]$ and 1.5 mM $FeCl_3$ in 0.1 M KCl and 3 mM HCl. (b) Activation of the PB film by applying another 50 cycles in de-aerated electrolyte solution (0.1 M KCl and 3 mM HCl) under the same conditions.

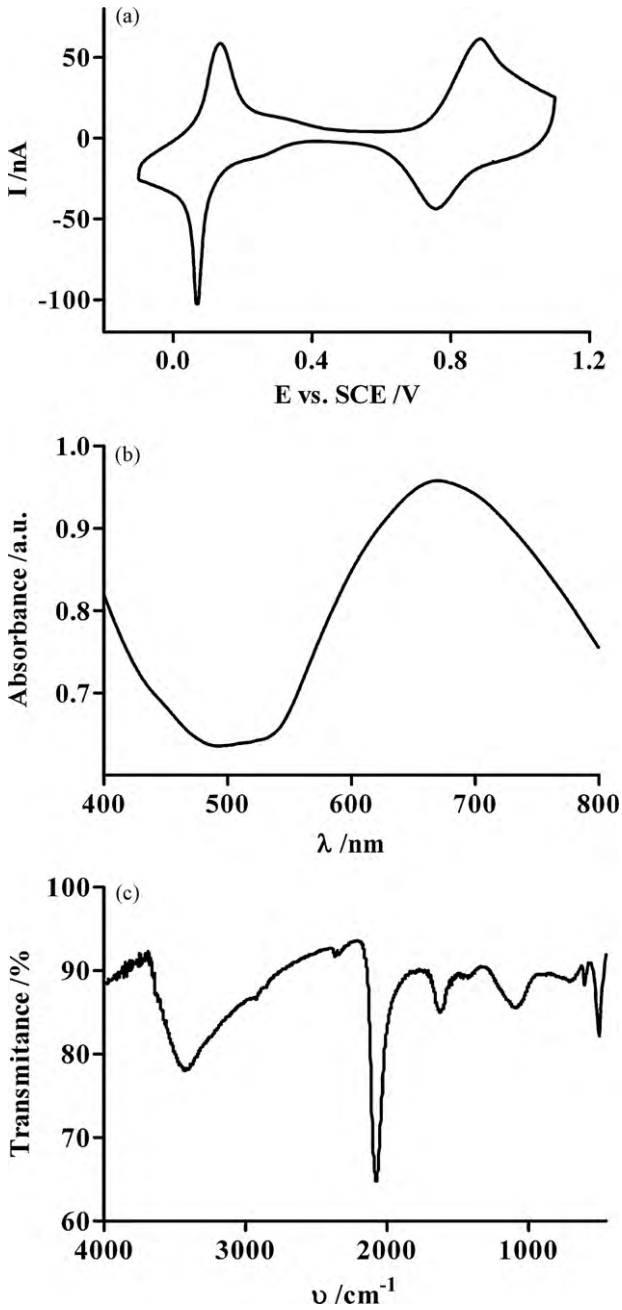

Fig. 2. (a) Cyclic voltammogram in de-aerated electrolyte solution of a PB-modified CFE showing the reduction and oxidation peaks of Prussian Blue at 0.1 and 0.85 V versus SCE, respectively. (b) Absorbance spectrum of electrosynthesized as-deposited PB film (c) FTIR spectra of PB electrosynthesized as-deposited.

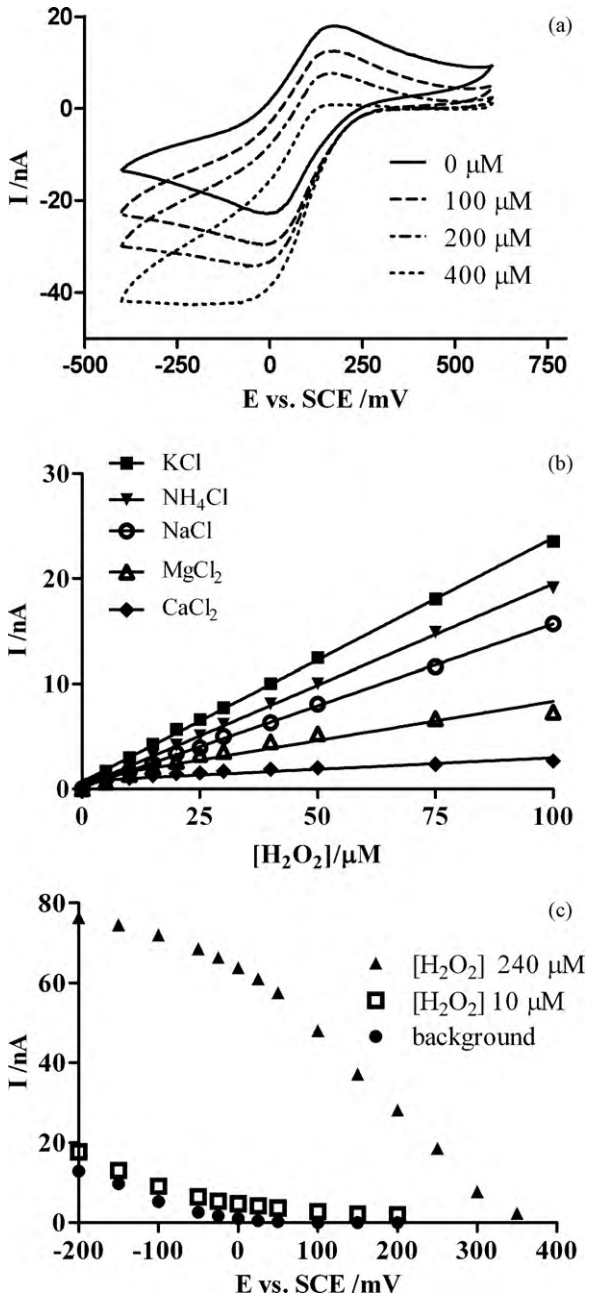

Fig. 3. (a) Cyclic voltammograms in de-aerated electrolyte solution of modified CFE/PB in absence and in the presence of several concentrations of H_2O_2 (0–400 μM). (b) Effect of hydrated radii of monovalent and divalent cations on the H_2O_2 sensitivity of a PB film. (c) Currents for CFE/PB in background in air-saturated solution, [O_2] ~240 μM (dot), background in air-saturated solution with 10 μM of H_2O_2 (square) and with 240 μM of H_2O_2 (triangle).

coordinated in the shell of high spin iron or occupying interstitial positions as uncoordinated water. The characteristic Fe–CN band, observed as a very sharp peak at 2067 cm^{-1}, is related to the stretching vibration of Fe–CN, where the CN groups are bonded to an Fe^{2+} ion. This peak has been used by several authors as a fingerprint of PB film formation [39].

3.2. Optimization of PB film: sensitivity

The most important applications of PB have involved modification of surface transducers (Pt, Pt/Ir, ITO, etc.) to detect H_2O_2 at low potential (~0.0 V versus SCE). Its immediate application in the biosensor field allows the detection of H_2O_2 as the intermediate of enzymatic reactions of oxidase enzymes (e.g., glucose oxidase, lactate oxidase, glutamate oxidase). Because of this low applied potential, artifacts due to endogenous interferences and bio-polymerization reactions can be avoided. Fig. 3a shows the cyclic voltammograms of a modified CFE/PBs microelectrode in the absence and presence of several concentrations of H_2O_2 (0–400 μM). Voltammograms in the absence of H_2O_2 display a well defined cathodic and anodic peak centered about 0.1 V versus SCE, with an I_{ox}/I_{red} ratio of ~1. Increasing the concentration of H_2O_2 systematically enhanced the cathodic current, whereas the anodic current displayed a parallel decrease. This observation indicates a catalytic reduction reaction, which can be ascribed to the reduction of H_2O_2 to water as previously reported [3,8].

During the oxidation/reduction reaction (PB ↔ PW; see Eq. (1)), the transfer of electrons must be compensated for by the entrapment in the film or liberation to the bulk solution of cationic species. Due to this mechanism and specially due to structural conditions of the PB film, only monovalent cations with low hydrated radii, such us, K^+ and NH_4^+ (both with hydrated radii equal to 0.125 nm) can support this electrochemical activity and can diffuse across the zeolite PB structure (cubit cell of 1.02 nm and channel radius of 0.16 nm). On the other hand, monovalent and divalent cations with higher hydrated radii, such as Na^+, $Ca^{2+}$and Mg^{2+} (with hydrated radii of 0.135, 0.156 and 0.161 nm, respectively), have difficulty penetrating the film [6,8]. Therefore, electrolyte support plays an important role and affects sensitivity and conductivity properties of PB films. Fig. 3b shows how PB films in the presence of monovalent cations with lower hydrated radii display better H_2O_2 sensitivity than monovalent and divalent cations with higher hydrated radii. Nevertheless, K^+ and NH_4^+ with similar radii exhibit different H_2O_2 sensitivities. This observation can be explained by taking hydration enthalpies into account. García-Jarreño et al., showed that cations enter and leave the PB film without water of hydration, so that energy is needed to dehydrate cations at the film/solution interface which can act as an energy barrier to the cation insertion or expulsion [17]. This factor is consistent with PB displaying better electrocatalytic properties in the presence of K^+ ($\Delta H_{hyd} = -336\ kJ\ mol^{-1}$) as supporting electrolyte than NH_4^+ ($\Delta H_{hyd} = -365\ kJ\ mol^{-1}$).

In the early 1980s, Itaya claimed that the reduced form of PB showed catalytic effects for the reduction of O_2 and H_2O_2 [8,11,12]. It can be seen in Fig. 3c that PB, electro-deposited and conditioned under the present conditions, is highly selective toward H_2O_2 reduction in the presence of O_2. Here we present current–potential curves of H_2O_2 reduction at CFE/PBs at 10 and 240 μM H_2O_2 against background electrolyte in air-saturated solution ($[O_2] \sim 240\ \mu M$). At potentials between 0.00 and 0.05 V against SCE the current reduction of H_2O_2 was at least two orders of magnitude higher (67:0.6 nA) than the O_2 reduction current generated in air-saturated solution.

3.3. Optimization of PB film with poly(o-phenylenediamine): stability and selectivity

Since the discovery of the electrocatalytic properties of PB to reduce H_2O_2, the principal inconvenience has been its instability in neutral and basic medium [5,13]. While in acid media PB films display high stability, in neutral and basic pH PB is disrupted after few seconds or minutes. The source of this instability has been attributed to hydroxyl ion interactions forming $Fe(OH)_3$ at pH higher than 6.4, and hence solubilizing PB. On the other hand, even at optimum pH, another source of OH^-must be taken into account, *viz* H_2O_2 electro-reduction [40].

Different strategies have been used to increase PB stability in neutral and basic medium: (1) varying the deposition procedure [22,41]; and (2) coating PB with permselective membranes such as Nafion, polyaniline, or poly(o-phenylenediamine) (PoPD) [22,42]. Here we employed a thin film of PoPD on the top surface of CFE/PBs to prevent its solubilization. Two main methods (CV and amperometry) have been proposed to electro-deposit PoPD [43–46]. Both of these approaches have been shown to be effective in generating permselective PoPD films. However, PoPD electrosynthesized amperometrically exhibits better reproducibility and permselective properties [47]. In our case PoPD films were electro-deposited in a PBS solution of monomer (300 mM, pH 7.4). Fig. 4a and b shows the two methods employed for PoPD electrodeposition; both techniques show typical self-sealing behavior (during growth of the PoPD film, the electrode surface is sealed and the oxidation of new monomer on the surface is inhibited). The CV method (Fig. 4a) reveals the irreversible nature of o-PD electro-oxidation, with a dramatic decrease in current after first scan which continued to diminish in subsequent scans. Electropolymerization for 15–20 min at a fixed high potential (+0.75 V versus. Ag/AgCl/saturated KCl) and neutral pH has been proposed as optimal conditions to obtain better interference rejecting films in the amperometric methodology [33,46]. Due to the self-sealing nature of PoPD electro-deposition, longer amperometric polymerization times are not necessary and do not improve selectivity [34]. Fig. 4b shows PoPD electro-deposition at constant potential, where a rapid decrease in current was observed, consistent with self-sealing behavior. Data have been fitted using a one- and two-phase exponential decay equation with a high coefficient of determination ($R^2 \sim 0.956$ and ~0.996, respectively). Nevertheless, the two-phase exponential decay model was significantly better ($p < 0.001$) in fitting the electropolymerization phenomena, with fast and slow half-life values of 0.3 and 2.6 min, respectively.

Fig. 5a shows CV scans for CFE/PBs in PBS (pH 7.4) with 0.1 M of NaCl. Two clear effects are evident associated with the supporting electrolyte solution employed: an increase in ΔE_p (~200 mV), showing a decrease in its reversibility and a shift in formal potential of about−150 mV. Nevertheless, the I_{Ox}/I_{Red} ratio was ~1, similar to behavior described by other authors previously [48]. The solid line represents the first CV scan at 0.1 V s^{-1} between−0.4 and +0.4 V versus SCE, and the dotted line is the 250th scan. A clear decrease of ~80% in I_{Ox} and I_{Red} was observed, presumably due to OH^- groups present at pH 7.4. After PoPD electro-deposition, CFE/PB/PoPDs showed a clear decrease in I_{Ox} and I_{Red} for scan 1 (Fig. 5b). This effect can be ascribed due to additional diffusion resistance across the PoPD film. Nevertheless, this covering provided a significant improvement in stability, and no significant changes in peak currents were observed during the 250 scan cycles.

The dependence of the peak currents on scan rate was also studied for CFE/PB/PoPD. Fig. 5c and d show the results obtained when the scan rate was changed from 0.05 to 0.50 V s^{-1} in PBS (pH 7.4) containing 0.1 M NaCl. Both I_{Ox} and I_{Red} were linearly proportional ($R^2 = 0.996$) to the square root of scan rate, suggesting that the diffusion of ions through the electrode coatings is rate determining, as commented above.

Electrosynthesized PoPD has been widely employed in biosensor configurations due to its excellent permselective properties [49,50]. PoPD blocks and/or minimizes the access of interference species by different mechanisms (size and/or charge exclusion) [51]. This film also excludes surface-active macromolecules, hence protecting the surface and giving higher stability *in vivo* [52–54]. In addition, the self-controlling mechanism of non-conducting polymer formation, reproducibly provides a thin and uniform film thickness (~10–30 nm) for PoPD [55–57].

To investigate CFE/PB/PoPD permselective properties, several endogenous electroactive species found in brain ECF (such as AA, UA, DA and DOPAC) were tested. To understand better the intrinsic mechanism and the advantages of the use of this permselective film, in preference to other more conventional membranes like Nafion, the behavior of several sensor configurations was also studied. Three different anti-interference films were fabricated and characterized: CFE/PB/PoPD (the main design), CFE/PB/Naf (5%) and CFE/Naf (0.5%)/PB/PoPD.

The first configuration involved coating the PB surface with PoPD (15 min at +0.75 V) and in the second configuration Nafion at 5 wt.% (15 fast immersions and then left to dry for 1 h at room temperature) was applied over the PB layer. Last method consisted of applying 15 fast immersions in Nafion (0.5 wt.%) to the CFE surface, and then the Nafion was annealed for 10 min at 200 °C. After that, the PB and PoPD films were deposited in the same way as described for the first configuration. Electrode sensitivity was determined by calculating the slope of the calibration curve using linear regres-

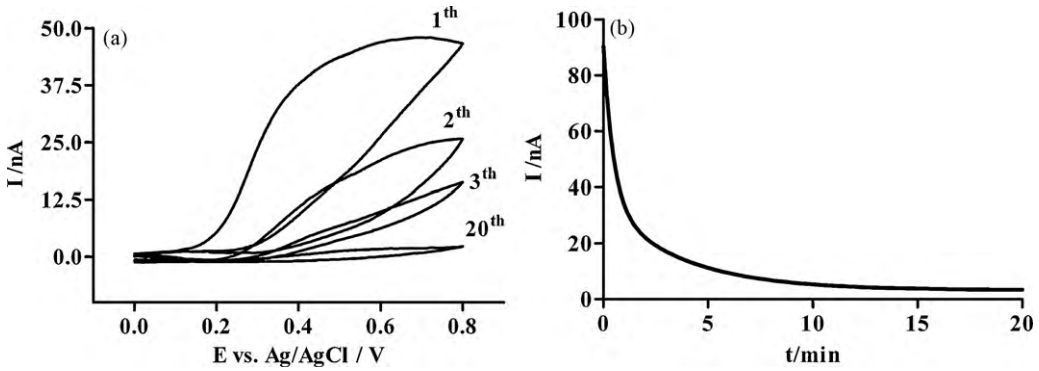

Fig. 4. (a) Cyclic voltammograms obtained during electropolymerization of 300 mM o-phenylenediamine at a CFE in phosphate buffer (pH: 7.4, NaCl 0.1 M scan rate: 0.05 V/s). (b) Current–time change during fixed-potential electropolymerization of 300 mM o-phenylenediamine at a CFE in PBS (time: 20 min, potential: +0.75 V versus Ag/AgCl/saturated KCl.

sion analysis of the different species in a range concentration of 0–40 μM (DA and DOPAC), 0–400 μM (AA and UA) and 0–100 μM for H_2O_2. These data were then normalized with respect to the electrode surface area. Results obtained using these different configurations are shown in Fig. 6, where sensitivity (S) is expressed as current density, and Fig. 7 where selectivity (sensitivity ratios) to H_2O_2 (expressed as: $S_{H_2O_2}/S_{interference}$) are plotted using different protective configurations (a: CFE/PB/PoPD, b: CFE/PB/Naf (5%), and c: CFE/Naf (0.5%)/PB/PoPD.

A clear decrease of 50% in H_2O_2 sensitivity occurred when PoPD was electropolymerized onto the PB surface, presenting the final configuration H_2O_2 sensitivity of 0.48 ± 0.02 A M^{-1} cm^{-2} ($n = 4$). This effect appears to be due to a new diffusive film on the PB layer, i.e., the free diffusion of analyte across PoPD film was impeded. Greater decreases in H_2O_2 sensitivity were found for the other two approaches: ~75% CFE/Naf (0.5%)/PB/PoPD and ~85% for CFE/PB/Naf (5%). H_2O_2 sensitivity ratios between CFE/PB/PoPD (sensitivity 480 nA μM^{-1} cm^{-2}) and to the other two configurations, CFE/Naf (0.5%)/PB/PoPD (sensitivity 256 nA μM^{-1} cm^{-2}) and CFE/PB/Naf (5%) (sensitivity 167 nA μM^{-1} cm^{-2}) were ~2 and ~3 respectively; this last value is in good agreement with values reported previously by Hamdi et al. [58].

Evolution of selectivities (H_2O_2 against AA) was also studied, and all films improved the selectivity properties of the sensor, although CFE/PB/PoPD gave the best results with a selectivity ratio ~536 compared to 7, 237 and 72 for CFE/PB, CFE/Naf (0.5%)/PB/PoPD

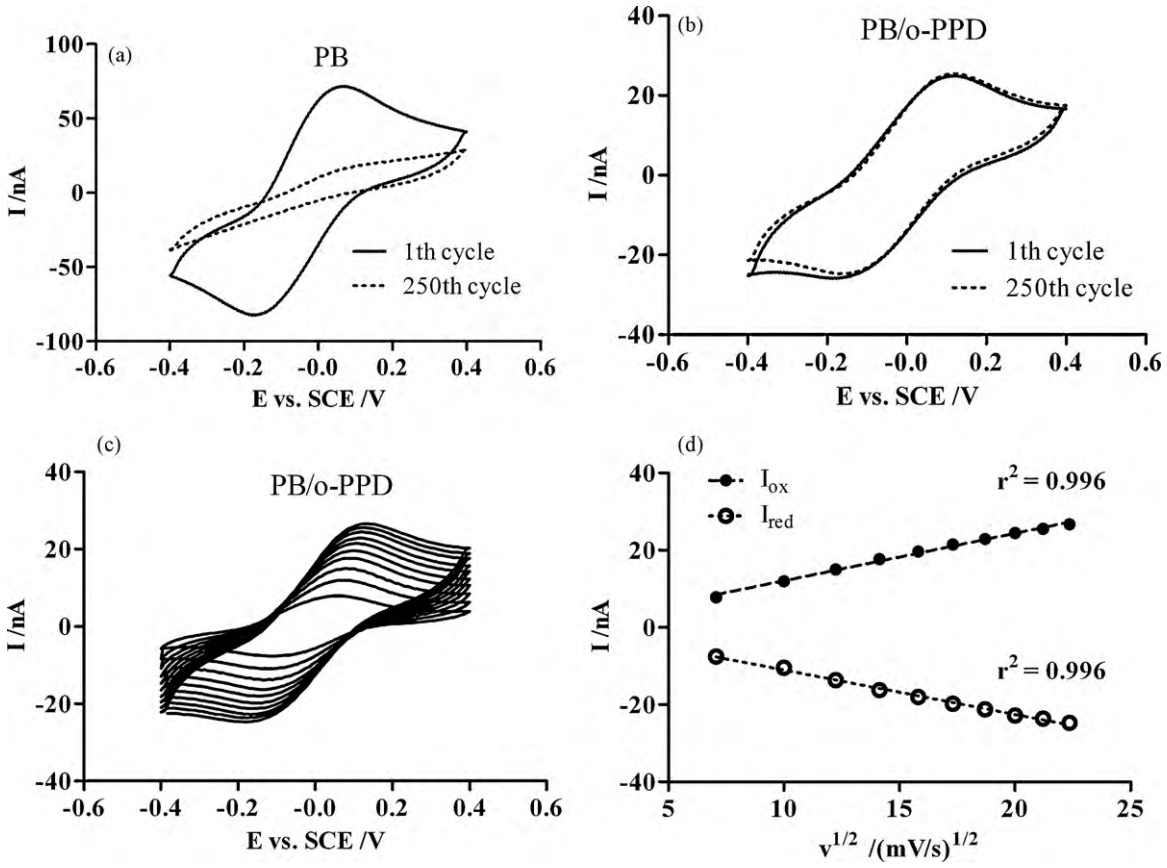

Fig. 5. 1st and 250th scans in cyclic voltammograms of an uncovered (a) and covered with PoPD (b) PB-modified microelectrode in phosphate buffer (pH: 7.4, NaCl 0.1 M). (c) Cyclic voltammograms of PB microelectrode covered with PoPD at different scan rates in phosphate buffer (pH 7.4, NaCl 0.1 M). From inner to outer curve: 0.05–0.50 V s^{-1}. (d) Linear dependence of anodic and cathodic peak currents on the square root of the potential scan rate.

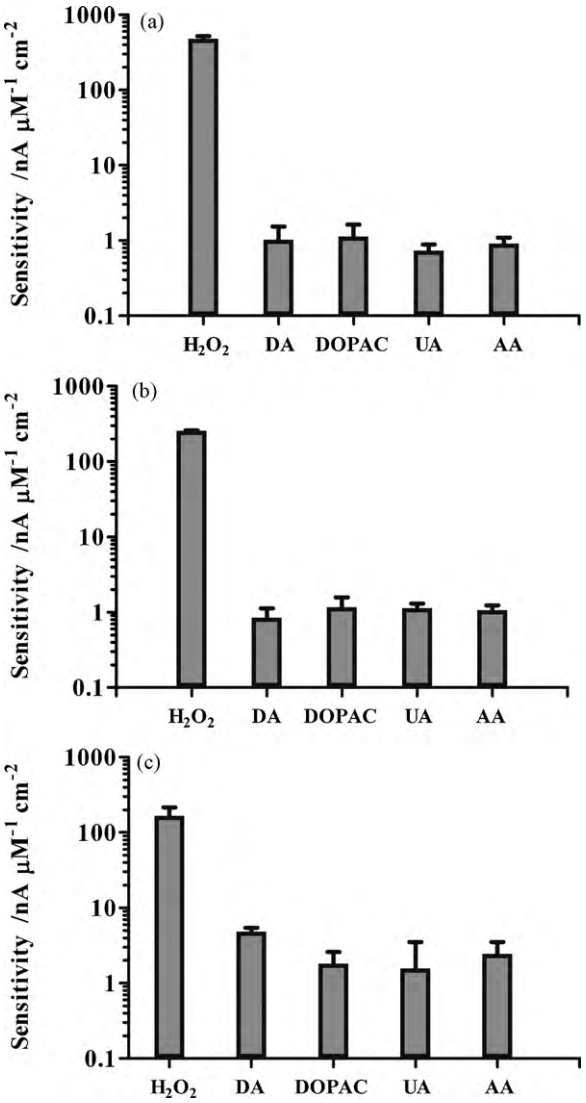

Fig. 6. Sensitivities of different PB microsensor configurations to H_2O_2 and some of the main endogenous brain interference species (DA, DOPAC, UA, AA). Working potential: 0.0 V versus SCE in phosphate buffer solution (pH 7.4, 0.1 M NaCl). (a) CFE/PB/PoPD, (b) CFE/Naf (0.5%)/PB/PoPD, (c) CFE/PB/Naf (5%). Error bars are expressed as the standard deviation, $n = 4$.

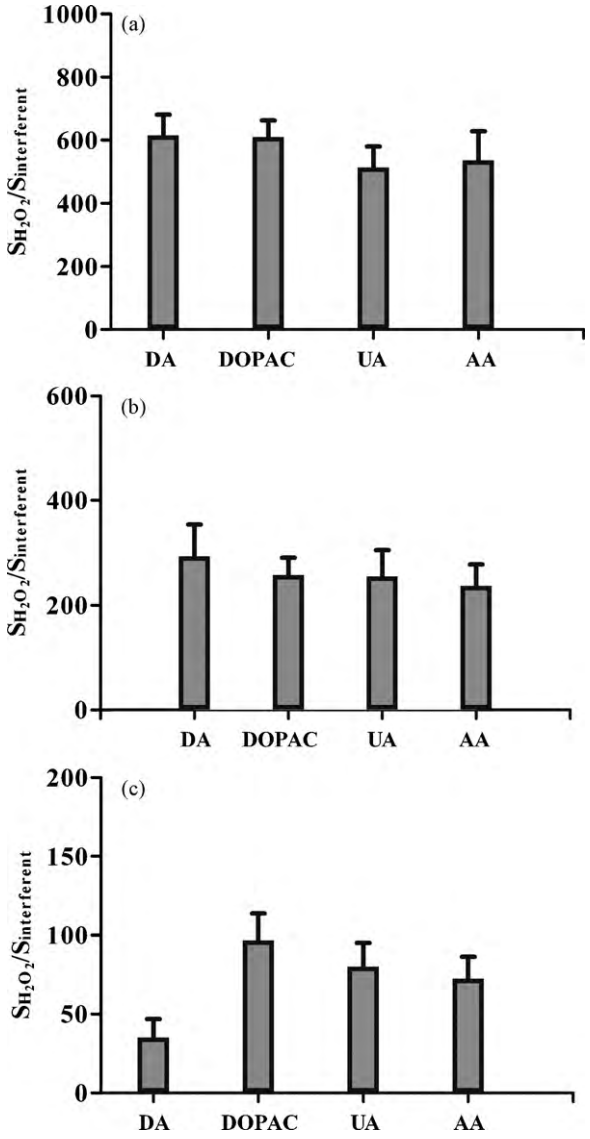

Fig. 7. Selectivities ratios of different PB microsensor configurations expressed as $S_{H_2O_2}/S_{interference}$ for some of the main endogenous interference species (DA, DOPAC, UA, AA). Working potential: 0.0 V versus SCE in phosphate buffer solution (pH 7.4, 0.1 M NaCl); (a) CFE/PB/PoPD, (b) CFE/Naf (0.5%)/PB/PoPD, (c) CFE/PB/Naf (5%). Error bars are expressed as the standard deviation, $n = 4$.

and CFE/PB/Naf (5%) respectively. A similar selectivity ratio against AA has been reported by Lukachova et al. for non-implantable PB/PoPD-modified glassy carbon macro-disk electrodes [22], showing not only its anti-interference properties, but also the long-term stability obtained using this approach. On the other hand, the selectivity ratio (against AA), between PoPD and Naf configurations (536:72), is close to the value reported by Hamdi et al. [58].

Sensitivities for H_2O_2 and endogenous interference molecules (AA, AU, DA, and DOPAC) of the three different configurations are represented in Fig. 6a–c. In all cases sensitivity for H_2O_2 was several orders of magnitude higher than for interference species. Nevertheless, CFE/PB/Naf (5%) showed higher sensitivities for electroactive species than for both PoPD configurations, as commented above, and its sensitivity for H_2O_2 was slightly lower.

Selectivity ratios were expressed as the ratio between sensitivity for H_2O_2 and sensitivity for interference compounds. For the configuration CFE/PB/PoPD, all selectivity ratios are close to 600 (Fig. 7a), while for the configuration using hybrid permselective layers, CFE/Naf (0.5%)/PB/PoPD, the selectivity ratios are close to 300 (Fig. 7b) because the sensitivities for the endogenous interference analytes studied were not very different for these two approaches. The difference in the selectivity ratios can be partly attributed to the sensitivity for H_2O_2 being lower in this last configuration compared to the PoPD layer only. The configuration with Nafion as the external permselective film, CFE/PB/Naf (5%), displayed selectivities significantly lower than those of the others configurations, with selectivity ratios close to 80 (Fig. 7c).

Another important insight into the anti-interference mechanism of the different protective films can be obtained from Fig. 7. Here we can see that selectivity against anionic interferences (AA, UA and DOPAC) was higher than for the cationic interference (DA) in CFE/PB/Naf (5%) configuration. As expected, and in good agreement with previous literature [58], Nafion-coated surfaces showed good rejection properties of anionic compounds, yet had poor permselectivity against cationic species like dopamine and other catecholamines such as serotonin, epinephrine, and norepinephrine. This is due to the fact that Nafion is a negatively charged polymer, which repels anionic compounds while attracting the positively charged DA. In addition, this negatively charged poly-

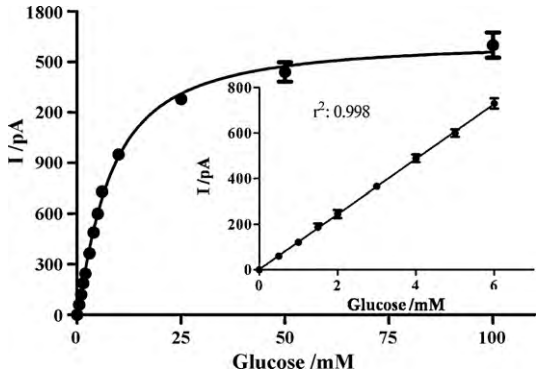

Fig. 8. Calibration curve for glucose microbiosensor based on Prussian Blue-modified carbon fiber electrode (diameter: 7 μm and length: 250 μm) working at 0 mV versus SCE. Apparent Michaelis–Menten constant $K' = 12 \pm 1$ mM, maximum response $V_m = 1629 \pm 36$ pA and sensitivity in the linear range, $S = 121 \pm 1$ pA/mM. Data are represented as mean ± SEM ($n = 3$ biosensors).

mer suffers other drawbacks, such as non-uniform thickness and poor reproducibility. The PoPD layer displayed lower permeability to both interference species types (cations and anions) thanks to different mechanisms (size and/or charge exclusion).

Another important parameter, the H_2O_2 detection limit, was evaluated for all configurations. Detection limits were calculated on the basis of a signal to noise ratio of 3 in a background solution. While CFE/PB presented a detection limit in the range of 10^{-8} M, configurations covered with PoPD (CFE/PB/PoPD and CFE/Naf (0.5%)/PB/PoPD) layers presented a higher detection limit of approximately $(1–4) \times 10^{-7}$ M, which is more than adequate for most biosensor applications.

3.4. *In vitro and in vivo response of glucose microbiosensor based on PB-modified CFE*

In order to check that the proposed method can be used to develop microbiosensors with low dimensions (~10 μm diameter, and 250 μm length), glucose oxidase (Gox), an archetype of oxidase enzymes, was immobilized on the surface of the sensor. CFE/PBs were immersed for several seconds in PEI (5% (w/v) in water) and, after a drying period of 30 min, they were dip coated for 5 min in an enzyme solution (300 U/mL in PBS, pH 7.4) to adsorb the Gox, and finally cross-linked with glutaraldehyde (0.1%, w/v) and BSA (1%, w/v) (one fast immersion). After a 5 min curing period, additional rapid immersions in enzyme and cross-linking solutions were done. This last step was repeated another 4 times, waiting 5 min between each cycle. Finally, microbiosensors were cured at 37 °C for 1 h and stored at 4 °C for use the next day.

Calibration plots (see Fig. 8) for glucose ($n = 3$ microbiosensors) were generated by plotting averaged steady-state currents against substrate concentration and fitting the data, using non-linear regression to obtain the apparent Michaelis–Menten constant, $K' = 12 \pm 1$ mM, maximum response, $V_m = 1629 \pm 36$ pA, and the Hill parameter, $h = 1.21 \pm 0.06$, the latter parameter showing a reasonable hyperbolic behavior in the microbiosensor response. Linear regression was used in the linear range to determine biosensor sensitivity, $S = 121 \pm 1$ pA/mM with a coefficient of determination, $R^2 = 0.998$. Detection limit was 54 μM (calculated as 3× SD of the background current) and linear range up to 6 mM glucose.

During the present work, preliminary *in vivo* response studies of glucose microbiosensors based on PB-modified CFE were also carried out. For *in vivo* experiments, PoPD film was electro-deposited on the top of the microbiosensor to avoid interference response to electroactive compounds, as commented above, observing a significant loss of sensitivity of ~50% due to diffusional phenomena across the polymeric film. To measure the glucose response in ECF, the microbiosensor was implanted in prefrontal cortex according to Paxinos and Watson, coordinates: $A/P + 2.7$ mm from Bregma, $M/L + 1.2$ mm and $D/V - 0.5$ mm from the Dura [60]. Glucose responses were evaluated by quantifying the microbiosensor current following depolarization of the surrounding tissue with 150 mM KCl in PBS (pH 7.4 and 0.1 M NaCl) administered in the extracellular medium with a microcannula located ~400 μm from the microbiosensor tip. Previous work [61] has shown that, under these conditions, an increment of extracellular glucose concentration occurs due to a response of neural activation.

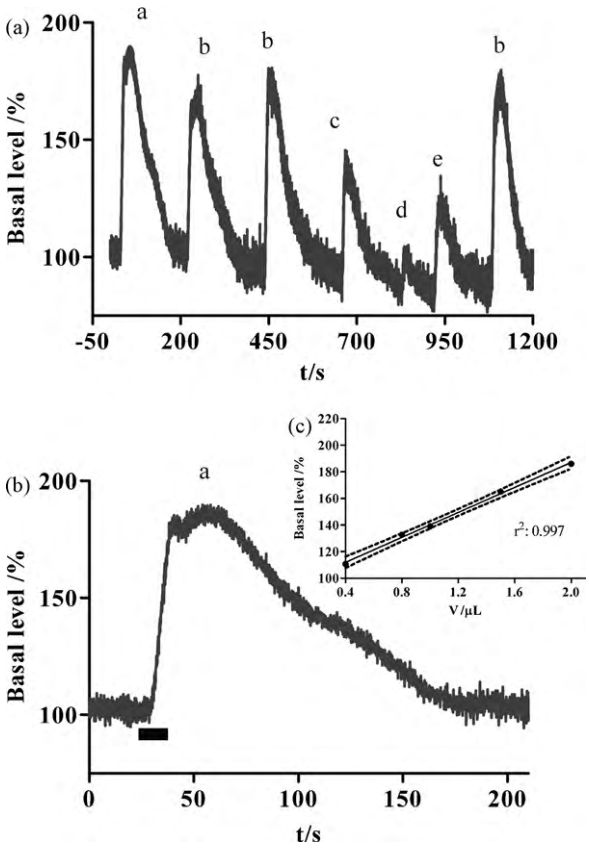

Fig. 9. (a) Variations of glucose microbiosensor response (expressed as basal level of glucose (%) after subtracting the background current) in prefrontal cortex due to different volume injections (a: 2 μL, b: 1.5 μL, c: 1 μL, d: 0.4 μL, e: 0.8 μL) of 150 mM KCl in PBS (pH 7.4 100 mM NaCl) at 10 μL min^{-1}. (b) Current variations of glucose microbiosensor in prefrontal cortex due an injection of 2 μL of the KCl solution, with a $t_{90\%} \sim 5.5$ s. (c) Linear correlation between glucose current change and injected volume, the dotted line representing the 95% confidence interval.

Fig. 9a shows the current variations (expressed as basal level of glucose (%) after subtracting the background current) of a glucose microbiosensor due to different volume injections (a: 2 μL, b: 1.5 μL, c: 1 μL, d: 0.4 μL, e: 0.8 μL) of 150 mM KCl. A calibration curve determined before implantation allowed us to estimate the glucose basal level at ~0.5 mM, which is in good agreement with previous data reported in literature for rat striatum [50]. Reproducibility of the *in vivo* response was studied by injecting an aliquot of 1.5 μL three times (Fig. 9a and b). The increase (normalized respect to basal level) was calculated, and represented a value of 164% ± 2% (mean ± SEM) and a coefficient of variation (CV) of ~2%. Microbiosensor responses after each injection were analyzed; Fig. 9b shows the increase of glucose in ECF after an injection of 150 mM KCl. A delay of ~5 s between injection and a clear current change was observed, which can be attributed to diffusion phenomena of the KCl in the ECF from microcannula located at ~400 μm. The total response registered was ~186% which corresponds to a

glucose concentration of ~0.95 mM. Microbiosensor time response based on *in vivo* experiments was estimated as the 90% of current change after each injection and it presented a value of $t_{90\%} \sim 5$–6 s, showing in this way the fast response of microbiosensor and validating it use in physiological measurements; on the other hand, after KCl depolarization, extracellular glucose returned to its basal levels after 2–3 min. The relationship between injected volume and total change is shown in Fig. 9c, where a clear linear correlation, with $r^2 = 0.997$ observed.

4. Conclusions

We have demonstrated that PB-modified CFEs can be used as a selective transducer to detect H_2O_2. Due to its electrocatalytic behavior, H_2O_2 can be detected at a very low potential (0.0 V versus SCE) avoiding principal problems of biofouling and interference reactions. To implement such electrocatalytic films and solve solubility problems, a PoPD film was employed which improved stability and selectivity properties. Sensitivity, selectivity and detection limits obtained in this work are in good agreement with values reported by other groups with significantly higher electrode dimensions. Finally, preliminary biosensor calibrations and glucose changes in brain ECF during local microinjection showed good results and validated the methodology presented in this work to develop implantable microbiosensors. Nevertheless, in future studies, PB electro-deposition, selectivity against a wide range of endogenous interferences, and enzyme immobilization will be systematically examined in order to optimize a microbiosensor configuration for use in physiological studies *in vivo*.

Acknowledgements

The funds for the development of this device had been promoted by the following national public projects: ULLAPD-08/01 granted by the Agencia Canaria de Investigación, Innovación y Sociedad de la Información, Ministerio de Industria, Turismo y Comercio (Proyecto AVANZA) TSI-020100-2008-337 and Ministerio de Ciencia e Innovación (Proyecto CICYT) TIN2008-06867-C02-01/TIN.

References

[1] A. Abbaspour, M.A. Kamyabi, J. Electroanal. Chem. 584 (2005) 117.
[2] J. Brown, J. Philos. Trans. 33 (1724) 17.
[3] V.D. Neff, J. Electrochem. Soc. 125 (1978) 886.
[4] A.A. Karyakin, O.V. Gitelmacher, E.E. Karyakina, Anal. Chem. 67 (1995) 2419.
[5] S.A. Jaffari, A.P.F. Turner, Biosens. Bioelectron. 12 (1997) 1.
[6] F. Ricci, A. Amine, G. Palleschi, D. Moscone, Biosens. Bioelectron. 18 (2003) 165.
[7] J.D. Qiu, H.Z. Peng, R.P. Liang, J. Li, X.H. Xia, Langmuir 23 (2007) 2133.
[8] K. Itaya, N. Shoji, I. Uchida, J. Am. Chem. Soc. 106 (1984) 3423.
[9] F. Herren, P. Fischer, A. Ludi, W. Halg, Inorg. Chem. 19 (1980) 956.
[10] Ricci, G. Palleschi, Biosens. Bioelectron. 21 (2005) 389.
[11] K. Itaya, T. Ataka, S. Toshima, J. Am. Chem. Soc. 104 (1982) 4767.
[12] K. Itaya, T. Ataka, S. Toshima, T. Shinohara, J. Phys. Chem. 86 (1982) 2415.
[13] A.A. Karyakin, Electroanalysis 13 (2001) 813.
[14] J. Kawiak, T. Jendral, Z. Galus, J. Electroanal. Chem. 145 (1983) 163.
[15] H. Gomathi, G. Prabhakara Rao, J. Appl. Electrochem. 20 (1990) 454.
[16] K. Itaya, K. Shibayama, H. Akahoshi, S. Toshima, J. Appl. Phys. 53 (1982) 804.
[17] J.J. García-Jareño, D.F.V. Giménez-Romero, F. Vicente, C. Gabrielli, M. Keddam, H. Perrot, J. Phys. Chem. B 107 (2003) 11321.
[18] D. Stilwell, K.H. Park, M.H. Miles, J. Appl. Electrochem. 22 (1992) 325.
[19] B.J. Feldman, R.W. Murray, Inorg. Chem. 26 (1987) 1702.
[20] D. Moscone, D. D'Ottavi, D. Compagnone, G. Palleschi, A. Amine, Anal. Chem. 73 (2001) 2529.
[21] B. Haghighi, S. Varma, F.M.Sh. Alizadeh, Y. Yigzaw, L. Gorton, Talanta 64 (2004) 3.
[22] L.V. Lukachova, E.A. Kotel'nikova, D. D'Ottavi, E.A. Shkerin, E.E. Karyakina, D. Moscone, G. Palleschi, A. Curulli, A.A. Karyakin, IEEE Sens. J. 3 (2003) 326.
[23] L.C. Clark, C. Lyons, Ann. NY. Acad. Sci. 102 (1962) 29.
[24] A.A. Karyakin, O. Gitelmacher, E.E. Karyakina, Anal. Lett. 27 (1994) 2861.
[25] A.A. Karyakin, M. Chaplin, J. Electroanal. Chem. 56 (1994) 85.
[26] A.A. Karyakin, E.E. Karyakina, Sens. Actuators B 57 (1999) 268.
[27] B. Haghighi, S. Varma, F.M. Alizadeh, Y. Yigzaw, L. Gorton, Talanta 64 (2004) 3.
[28] H. Shi, Y. Yang, J. Huang, Z. Zhao, X. Xu, J. Anzai, T. Osa, Q. Chen, Talanta 70 (2006) 852.
[29] X. Wang, H. Gu, F. Yin, Y. Tu, Biosens. Bioelectron. 24 (2009) 1527.
[30] J.P. Lowry, R.D. O'Neill, Electroanalysis 6 (1994) 369.
[31] W.H. Oldenziel, G. Dijkstra, T.I.F.H. Cremers, B.H.C. Westerink, Brain Res. 1118 (2006) 34.
[32] K. McAteer, R.D. O'Neill, Analyst 121 (1996) 773.
[33] B.M. Dixon, J.P. Lowry, R.D. O'Neill, J. Neurosci. Methods 119 (2002) 135.
[34] M.R. Ryan, J.P. Lowry, R.D. O'Neill, Analyst 122 (1997) 1419.
[35] R.J. Lin, N. Toshima, Bull. Chem. Soc. Jpn. 64 (1991) 136.
[36] Y.L. Hu, J.H. Yuan, W. Chen, K. Wang, X.H. Xia, Electrochem. Commun. 7 (2005) 1252.
[37] S.A. Agnihotry, P. Singh, A.G. Joshi, D.P. Singh, K.N. Sood, S.M. Shivaprasad, Electrochim. Acta 51 (2006) 4291.
[38] P.J. Kulesza, S. Zamponi, M.A. Malik, K. Miecznikowski, M. Berrettoni, R. Marassi, J. Solid State Electrochem. 1 (1997) 88.
[39] K. Itaya, I. Uchida, V.D. Neff, Acc. Chem. Res. 19 (1986) 162.
[40] R. Araminaité, R. Garjonyté, A. Malinauskas, Cent. Eur. J. Chem. 6 (2008) 175.
[41] I.L. Mattos, L. Gorton, T. Ruzgas, A.A. Karyakin, Anal. Sci. 16 (2000) 795.
[42] J. García-Jareño, J. Navarro-Laboulais, F. Vicente, Electrochim. Acta 41 (1996) 2675.
[43] I. Losito, F. Palmisano, P.G. Zambonin, Anal. Chem. 75 (2003) 4988.
[44] S.A. Rothwell, S.J. Killoran, E.M. Neville, A.M. Crotty, R.D. O'Neill, Electrochem. Commun. 10 (2008) 1078.
[45] Y.Q. Dai, D.M. Zhou, K.K. Shiu, Electrochim. Acta 52 (2006) 297.
[46] C.P. McMahon, S.J. Killoran, R.D. O'Neill, J. Electroanal. Chem. 580 (2005) 193.
[47] S.A. Rothwell, C.P. McMahon, R.D. O'Neill, Electrochim. Acta 55 (2010) 1051.
[48] M.P. O'Halloran, M. Pravda, G.G. Guilbault, Talanta 55 (2001) 605.
[49] F. Palmisano, P.G. Zambonin, D. Centonze, Fresen. J. Anal. Chem. 366 (2000) 586.
[50] R.D. O'Neill, J.P. Lowry, G. Rocchitta, C.P. McMahon, P.A. Serra, Trends Anal. Chem. 27 (2008) 78.
[51] D. Centonze, C. Malitesta, F. Palmisano, P.G. Zambonin, Electroanalysis 6 (1994) 423.
[52] S. Myler, S. Eaton, S.P.J. Higson, Anal. Chim. Acta 357 (1997) 55.
[53] M. Yuqing, C. Jianrong, W. Xiaohua, Trends Biotechnol. 22 (2004) 227.
[54] S.M. Kirwan, G. Rocchitta, C.P. McMahon, J.D. Craig, S.J. Killoran, K.B. O'Brien, P.A. Serra, J.P. Lowry, R.D. O'Neill, Sensors 7 (2007) 420.
[55] Y. Ohnuki, H. Matsuda, T. Ohsaka, N. Oyama, J. Electroanal. Chem. 158 (1983) 55.
[56] J.D. Craig, R.D. O'Neill, Analyst 128 (2003) 905.
[57] S.J. Killoran, R.D. O'Neill, Electrochim. Acta 53 (2008) 7303.
[58] N. Hamdi, J. Wang, H.G. Monbouquette, J. Electroanal. Chem. 581 (2005) 258.
[60] G. Paxinos, C. Watson, Academic Press, Sydney (1986).
[61] Y. Hu, G.S. Wilson, J. Neurochem. 68 (1997) 1745.

Biosensors and Bioelectronics 26 (2010) 748–753

Contents lists available at ScienceDirect

Biosensors and Bioelectronics

journal homepage: www.elsevier.com/locate/bios

Microbiosensors for glucose based on Prussian Blue modified carbon fiber electrodes for *in vivo* monitoring in the central nervous system

P. Salazar[a,*], M. Martín[a], R. Roche[a], J.L. González–Mora[a], R.D. O'Neill[b]

[a] Neurochemistry and Neuroimaging Group, Faculty of Medicine, University of La Laguna, Tenerife, Spain
[b] UCD School of Chemistry and Chemical Biology, University College Dublin, Belfield, Dublin 4, Ireland

ARTICLE INFO

Article history:
Received 9 April 2010
Received in revised form 4 June 2010
Accepted 25 June 2010
Available online 24 July 2010

Keywords:
Biosensor
Carbon fiber electrode
Glucose oxidase
Prussian Blue
Hydrogen peroxide
Poly(o-phenylenediamine)

ABSTRACT

Carbon fiber electrodes (CFEs) were used to develop microbiosensors for glucose as an alternative to the classical Pt and Pt–Ir transducers. Their low dimensions (~250 μm CFE length and ~10 μm diameter) are important factors for measurements in physiological environments. An electrocatalytic Prussian Blue (PB) film facilitated detection of enzyme-generated hydrogen peroxide at a low applied potential (~0.0 V against SCE), contrasting the high potential used in many previous designs (~0.7 V). The electrosynthesized polymer, poly-o-phenylenediamine (PoPD), was used to improve biosensor stability and selectivity against endogenous interference species, such as ascorbic and uric acids. Optimization of the fabrication procedure is described, including activation of CFE/PB, enzyme immobilization and stabilization, anti-interference films, optimizing applied potential, and pH effects. Analytical properties were also characterized such as sensitivity, LOD, linear range, and enzyme loading. Finally, an optimized biosensor displaying a linear sensitivity of 9.3 ± 0.1 μA mM^{-1} cm^{-2} ($n = 3$), a 2% RSD and free of interference, is proposed as a suitable candidate for *in vivo* glucose monitoring in the CNS.

1. Introduction

First generation biosensors are based on the detection of any electroactive metabolite that is generated (e.g., H_2O_2) or consumed (e.g., O_2) during the enzyme reaction. The principal problem of these approaches for oxidase-based biosensors is the high overpotential needed to detect either O_2 or H_2O_2 on Pt (Clark and Lyons, 1962; Clark, 1979) and other native electrode materials (Schuvailo et al., 2005). At high potentials, interference and polymerization reactions can occur at the biosensor surface. Biosensors in biological media are subject to interference by endogenous electroactive reducing agents, especially ascorbic acid (AA) and uric acid (UA) (D'Orazio, 2003; Osborne and Hashimoto, 2004; Garjonyte and Malinaus, 1999). These problems have been solved by several approaches: (a) the use of polymer films with anti-interference properties, such as poly-o-phenylenediamine (PoPD) (Lowry and O'Neill, 1994; Dai et al., 2006); (b) the use of artificial redox mediators (Castillo et al., 2003; Gregg and Heller, 1990; Habermüller et al., 2000; Mitala and Michael, 2006); (c) the use of electrocatalytic films to detect H_2O_2 at lower applied potentials (see Fig. 1) (Karyakin et al., 1995; Karyakin and Karyakina, 1999).

The neurophysiological motivation for this work is based on glucose being the principal source of energy in the brain. Fellows and Boutelle (1993) showed that physiological stimulation of neural activity is associated with an increase in glucose concentration in the extracellular compartment, which has a much longer duration than the associated change in regional cerebral blood flow (rCBF). On the other hand, recent studies suggest that increased energy requirements of activated neurons are met by neuronal utilization of lactate (Pellerin et al., 2007). Thanks to the development and use of microbiosensors to determine principal energy metabolites and neurotransmitters (Dale et al., 2005; Lowry et al., 1998), we can now further explore the relationship between neural activation, rCBF and brain metabolites.

Biosensors offer a variety of advantages over classical techniques for neurochemical monitoring: high spatial and temporal resolution; good selectivity; ease of implementation; amenable to miniaturization; rapid response time; etc. Recently, O'Neill et al. (2008) reviewed the development of wire-based amperometric polymer–enzyme composite biosensors, focusing on the relationship between key design features and analytical parameters. Using a carbon fiber substrate, we now propose a novel glucose biosensor, developed following this systematic approach, with significantly

* Corresponding author.
E-mail address: psalazar@ull.es (P. Salazar).

0956-5663/$ – see front matter © 2010 Elsevier B.V. All rights reserved.
doi:10.1016/j.bios.2010.06.045

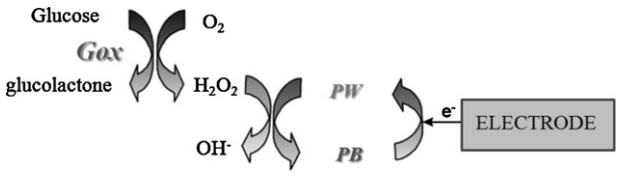

Fig. 1. Detection scheme for glucose biosensor based on a Prussian Blue (PB) modified electrode. Glucose is converted to gluconolactone, catalyzed by glucose oxidase (Gox) immobilized on the electrode surface. Secondary to this reaction is the production of hydrogen peroxide that can be reduced amperometrically at low applied overpotentials, electrocatalyzed by the PB.

smaller dimensions and a low working potential, which provide significant advantages for *in vivo* monitoring.

2. Materials and methods

2.1. Reagents and solutions

The enzyme glucose oxidase (Gox) from *Aspergillus niger* (EC 1.1.3.4, Type VII–S, lyophilized powder), glutaraldehyde (Glut, 25% solution) were obtained from Sigma Chemical Co., and stored at −21 °C until used. Other chemicals, including o-phenylenediamine (oPD), glucose, ascorbic acid (AA), uric acid (UA), polyethyleneimine (PEI), KCl, $FeCl_3$, $K_3[Fe(CN)_6]$, HCl (35%, w/w), H_2O_2 (30%, w/v), Nafion (5%, w/w, in a mixture of lower aliphatic alcohols and water), bovine serum albumin (BSA, fraction V) and phosphate buffer saline solution containing 0.1 M NaCl (PBS), were obtained from Sigma and used as supplied. PBS stock solutions (pH 7.4) were prepared in doubly distilled water (18.2 MΩ cm, Millipore–Q), and stored at 4 °C. Enzyme solutions were prepared in PBS, which also served as the background electrolyte for all *in vitro* experiments. Stock 1 M and 250 mM solutions of glucose were prepared in water, left for 24 h at room temperature to allow equilibration of the anomers, and stored at 4 °C. The PEI solutions used were prepared by dissolving PEI at 1% (w/v) and 5% (w/v) ratios in H_2O. The cross-linking solution was prepared in PBS with 1% (w/v) BSA and 0.1% (w/v) glutaraldehyde. Monomer solution of 300 mM oPD was prepared using 48.6 mg oPD and 7.5 mg BSA in 1.5 mL of N_2-saturated PBS and sonicating for 15 min. A 300 U/mL solution of Gox was prepared by dissolving 3.7 mg in 2 mL of PBS. Carbon fibers (8 μm diameter) were obtained from Goodfellow, glass capillaries from Word Precision Instruments Inc., 250 μm internal diameter Teflon-coated copper wire from RS, and silver epoxy paint was supplied by Sigma.

2.2. Instrumentation and software

Experiments were computer controlled with data acquisition software EChem™ for cyclic voltammetry and Chart™ for constant potential amperometry (ADInstruments Pty Ltd., Australia). The data acquisition system used was e–Corder 401 and a low-noise and high-sensitivity potentiostat, Picostat (eDAQ Pty Ltd., Australia). The linear and non-linear regression analyses were performed using the graphical software package Prism (ver. 5.00 GraphPad Software, San Diego, CA, USA). To electro-deposit and activate the PB (see Section 2.5), an in-house Ag/AgCl/saturated KCl reference electrode and platinum wire auxiliary electrode were used.

2.3. Amperometric experiments

All experiments were done in a 25 mL glass cell at 21 °C, using a standard three-electrode set-up with a commercial saturated calomel electrode (SCE) (CRISON Instrument S.A. Barcelona, Spain) as the reference and platinum wire as the auxiliary electrode. The applied potential chosen for most amperometric studies was 0.0 V against SCE. Glucose calibrations were performed in quiescent air-saturated PBS (following stabilization of the background current for 30 min) by adding aliquots of glucose stock solution (1 or 0.25 M) to the electrochemical cell. After the addition of glucose aliquots, the solutions were stirred for 10 s and then left to reach the quiescent steady-state current.

2.4. Data analysis

Calibration plots for glucose were generated by plotting averaged steady-state currents against substrate concentration and fitting the data, using non-linear regression to obtain the apparent Michaelis–Menten constants, K' (mM), maximum biosensor response, V_m (pA), and the Hill parameter, h. Linear regression was used in the linear range to determine biosensor sensitivity, signal to noise ratio and coefficient of determination (r^2). In all cases, the currents recorded in background electrolyte were subtracted from the calibration responses. Data are reported as mean ± SEM, n being the number of biosensors or number of measurements (as specified).

2.5. Preparation of the working electrodes

2.5.1. Fabrication of carbon fiber electrodes

Carbon fiber electrodes (CFEs) were constructed using the following steps. A carbon fiber (diameter 8 μm, 20–50 mm in length) was attached to Teflon-coated copper wire (diameter 250 μm)

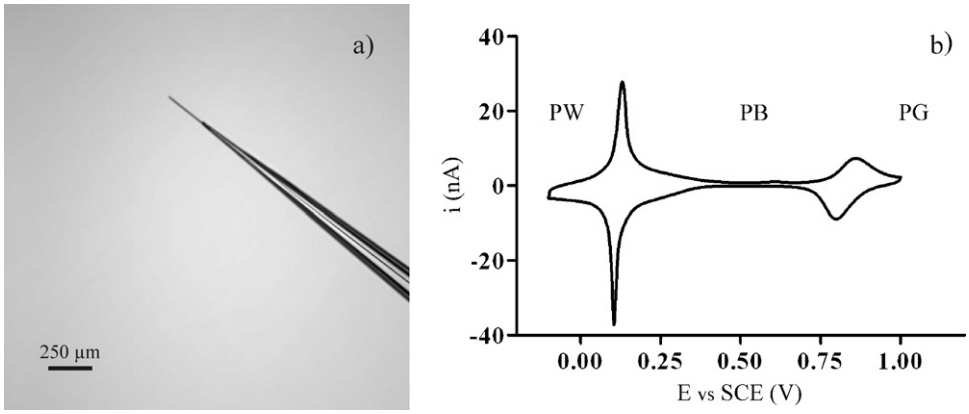

Fig. 2. a) Carbon fiber electrodes (CFEs) with a diameter of 8 μm and length of 250 μm. b) Cyclic voltammogram of the PB-modified CFE in de-aerated electrolyte solution (0.1 M KCl and 3 mM HCl) at a scan rate of 10 mV/s. PW is Prussian White, and PG is Prussian Green.

using high purity silver paint, and dried for 1 h at 80 °C. A borosilicate glass capillary was pulled to a tip using a vertical microelectrode puller (Needle/Pipette puller, Model 750, David Kopf Instruments, California, USA). After drying, the carbon fiber was carefully inserted into the pulled glass capillary tube under a microscope, leaving 2–4 mm of the carbon fiber protruding at the pulled end. Subsequently, the carbon fiber was cut to the desired length (approximately 250 μm), using a microsurgical scalpel. At the stem end of the capillary tube, the copper wire was fixed by casting with non-conducting epoxy glue; the carbon fiber was also sealed into the capillary mouth, using the same epoxy glue (Fig. 2a). Subsequently, CFEs were dried again for 1 h and were optically and electrochemically inspected before use.

2.5.2. PB electro-deposition onto carbon fiber electrodes

CFEs were modified by electro-deposition and activation of a Prussian Blue (PB) film. The PB layer was electro-deposited by a cyclic voltammetric (CV) method, applying *n* cyclic scans within the limits of −0.2 to 0.4 V, at a scan rate of 50 mV/s, to the CFEs in a fresh de-aerated solution containing 1.5 mM $K_3[Fe(CN)_6]$ and 1.5 mM $FeCl_3$ in 0.1 M KCl and 3 mM HCl. The electrode was then cleaned in doubly distilled water, and the CFE/PB activated by applying another *m* scans within the limits of −0.2 to 0.4 V at a scan rate of 100 mV/s in de-aerated electrolyte solution (0.1 M KCl and 3 mM HCl). Before being used, the CFE/PB was cleaned again in doubly distilled water for several seconds. Finally, the PB film was tempered at 100 °C for 2 h.

2.5.3. Microbiosensor construction based on CFE/PB

When modified Prussian Blue CFEs (CFE/PB) were ready to use, the next step was to immobilize the enzyme glucose oxidase (Gox). Gox was dissolved in PBS to the desired concentration (300 U/mL). Different methodologies to immobilize the enzyme were investigated to improve the analytical response (described in Section 3). After the immobilization step, all biosensors were cured for 1 h at 37 °C.

2.5.4. PoPD deposition onto the microbiosensors

Finally, an interference-rejection film of PoPD–BSA was electropolymerized onto the CFE/PB/Gox surface. Electrosynthesis of PoPD was carried out with a standard three-electrode set-up in PBS containing 300 mM oPD and 5 mg/mL of BSA, by applying a constant potential (+0.75 V) for 20–25 min. BSA was included in the monomer solution because globular proteins trapped in the PoPD polymer matrix can improve its permselectivity under some conditions (McAteer and O'Neill, 1996; Kirwan et al., 2007). For clarity in the nomenclature, however, the term BSA will be omitted in all sensor configurations, e.g., CFE/PB/Gox/PoPD.

After the biosensor fabrication procedure was completed, they were cleaned in doubly distilled water and stored overnight at 4 °C in a refrigerator, and used the next day. When not in use, biosensors were stored again at 4 °C in a refrigerator.

3. Results and discussion

3.1. Prussian Blue film

Prussian Blue (PB) has been widely used in biosensor construction to suppress or attenuate interference contributions (Li and Gu, 2006). Due to the peculiar structure of PB, its reduced form (Prussian White, PW) has a catalytic activity for H_2O_2 reduction in neutral media [*ec.1*], indirectly allowing H_2O_2 detection at potentials close to 0.0 V against SCE, and exhibiting better properties than other H_2O_2-detecting devices, such as Pt or horseradish peroxidase (Karyakin and Karyakina, 1999).

$$(PW)\,Fe_4K_4[Fe(CN)_6]_3 + 2H_2O_2 \rightarrow (PB)\,Fe_4[Fe(CN)_6]_3 + 4OH^- + 4K^+ \quad (1)$$

The zeolitic structure of PB with a cubic unit cell of 10.2 Å and with channel diameters of about 3.2 Å allows the diffusion of low molecular weight molecules (such as O_2 and H_2O_2) through the crystal structure (Ricci and Palleschi, 2005). A voltammogram of a PB-modified CFE is shown in Fig. 2b; two pairs of almost symmetrical peaks appear with formal potential values of ∼0.15 and ∼0.9 V, coinciding with formal potentials reported previously by others authors (Karyakin, 2001). The first peak pair corresponds to the interconversion of PW and PB, and the second pair from PB to Prussian Green (PG). Nevertheless, only the first peak pair will be studied; the response of this first peak pair points to a mono-electron, quasi-reversible process corresponding to a surface-adsorbed redox couple (Karyakin, 2001).

Due to this high activity and selectivity towards H_2O_2 reduction, some authors have named Prussian Blue an "artificial enzyme peroxidase" (Karyakin et al., 2000). Further improvements in the stability and selectivity of PB-based H_2O_2 transducers can be obtained by electropolymerizing a non-conducting PoPD permselective coating. Such improvements can increase 600-fold the selectivity of the PB/PoPD-based transducer relative to ascorbate, which is much better compared to the other reported systems (Lukachova et al., 2003; Salazar et al., in press).

3.2. Applied potential selection

To study the best operating potential, the effect of applied potential on the PB-modified electrode was studied in the range from −0.2 V to +0.2 V in PBS. The current generated by addition of 2.5 μM H_2O_2, was registered and represented as sensitivity in pA/μM. As can be seen in Fig. 3a the maximum response was obtained at 0.0 V, but no significant differences were found compared with other negative potentials; on the other hand, it was observed that sensitivity decreased rapidly at positive potential, giving significant differences between 0.0 V and +0.05 V ($p < 0.007$, $n = 3$), and complete loss of sensitivity at potentials close to +0.2 V. This observation can be justified on the basis that only the reduced form of PB (PW) possesses these electrocatalytic properties, so only at potentials where this form is present the electro-reduction of H_2O_2 can occur. This range of potentials is in agreement with the CV of the PB-modified CFE showed in Fig. 2b. Finally, 0.0 V was selected as the applied potential for glucose sensing.

3.3. Enzyme immobilization

3.3.1. Study of immobilization techniques

Glucose oxidase was immobilized on the transducer surface via dip-coating procedures. The principal problem of this method is the continuous loss of enzyme during the measurement process, due to the low strength of the non-specific interactions. To avoid this, enzyme can be attached to the surface by means of glutaraldehyde. The addition of another non-catalytic protein, with high numbers of lysine residues such us BSA, can help to diminish deactivation during the cross-linking phase and increase Gox stability (Gouda et al., 2001). The use of pre-casting with a polyelectrolyte, such as polyethyleneimine (PEI), has also been shown to stabilize and increase enzyme loading (Breccia et al., 2002; Qian et al., 2004).

To study how different methodologies of immobilization can improve the analytical properties of CFE/PB-based biosensors, several biosensor groups were developed. As a starting point, we used the following parameters in the electro-deposition of PB film: $n = 2$ and $m = 10$ to produce ∼10-μm diameter CFE/PB electrodes.

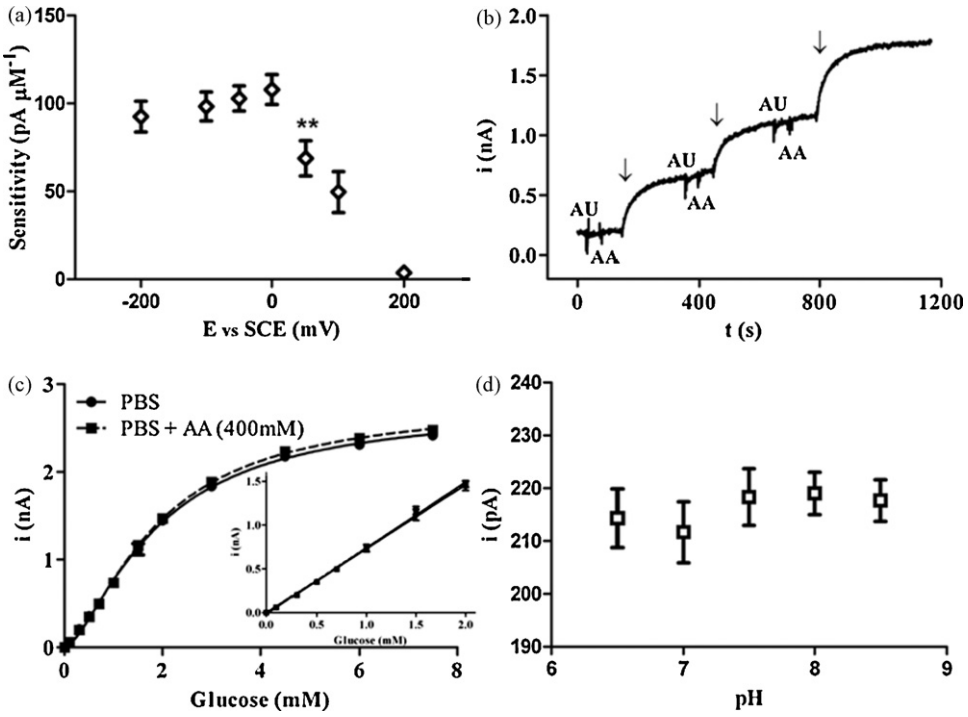

Fig. 3. a) Effect of the applied potential in the sensitivity of H_2O_2 in a PB-modified electrode in the studied range from −0.2 V to +0.2 V in PBS. b) Calibration raw data in PBS for optimized glucose biosensor with a PoPD film (CFE/PB/$PEI_{5\%}$/Gox_{opt}/PoPD): glucose additions of 1, 1 and 2 mM (arrows); and interference additions of 100 μM UA and 400 μM AA (current artifacts). c) Calibration curves of the optimized glucose biosensor in presence and absence of 400 μM of AA. d) Optimized glucose biosensor response to 0.5 mM addition of glucose in artificial extracellular fluid ECF adjusted at different pH values. Data are represented as mean ± SEM ($n = 3$).

Enzyme loading was modified by applying different immobilization protocols: (1) changing numbers of immersions (α) in Gox solution, and (2) the presence or absence of PEI in solutions before and during Gox immobilization.

The first group of CFE/PB microelectrodes were dip coated for 5 min to adsorb the enzyme (Gox) from the enzyme solution and finally cross-linked with glutaraldehyde (0.1%, w/v) and BSA (1%, w/v) (one fast immersion). This group was denoted by CFE/PB/Gox_0. The second and third groups were constructed in the similar way to the basic CFE/PB/Gox_0 design, but with additional α rapid immersions in enzyme and cross-linking solutions, waiting 5 min between each dip-evaporation cycle. Accordingly, this fabrication procedure, for which $\alpha = 5$ or 10, provided biosensors of the form: CFE/PB/Gox_5 and CFE/PB/Gox_{10}.

A fourth group of biosensors were constructed using the same protocol of CFE/PB/Gox_5, but adding an additional solution (1% PEI). The biosensors were dipped briefly in this PEI solution after the enzyme solution and before cross-linking solution. According to this fabrication procedure, the biosensors produced were: CFE/PB/$(Gox–PEI_{1\%})_5$. A fifth group of biosensors were constructed using the same protocol as CFE/PB/$(Gox–PEI_{1\%})_5$, but after stabilizing the PB film and before enzyme immobilization, biosensors were dipped in a 5% PEI solution and dried for 1 h. In this case the nomenclature was: CFE/PB/$PEI_{5\%}$/$(Gox–PEI_{1\%})_5$. The last group of biosensors were constructed using the same protocol as for CFE/PB/$PEI_{5\%}$/$(Gox–PEI_{1\%})_5$, but using 5% PEI for all PEI applications. In this case the nomenclature selected was: CFE/PB/$PEI_{5\%}$/$(Gox–PEI_{5\%})_5$.

Table 1 shows the enzyme kinetic and analytical parameters obtained from calibration curves for different ~10-μm diameter glucose biosensors fabricated with and without PEI and different deposition procedures. These results show that increased numbers of dip-coatings increased the relative active enzyme loading (increasing V_m) and linear range sensitivity. Increasing the amount of PEI also increased sensitivity significantly. The value of apparent Michaelis constant (K') for the basic configuration (CFE/PB/Gox_0, 20–30 mM) was close to the value reported for free enzyme (Swoboda and Massay, 1965), indicating that immobilization on PB had no detrimental effect on enzyme affinity. The incorporation of PEI increased enzyme affinity, which was the main mechanism for enhanced linear sensitivity ($\sim V_m/K'$ (O'Neill et al., 2008)), leading to lower LOD values. Almost all biosensors showed hyperbolic behavior (Hill parameter, $h \approx 1$), except the last 'basic' design, where $h \approx 2$ (sigmoidal behavior) making it unsuitable for straightforward glucose monitoring applications.

When the number of deep-coatings is increased, the biosensor manufacturing time suffers a considerable increase. So the final fabrication process (*developed below*) was optimized with respect to time. Several configurations of PB deposition, activation steps and enzyme immobilization were studied (data not shown) to optimize the balance of glucose sensitivity and fabrication time. The most important fabrication parameters selected, following systematic optimization, are summarized as follows:

(1) *PB deposition*: $n = 3$, PB activation: $m = 50$ and stabilization for 2 h at 100 °C.
(2) *Enzyme immobilization*: one fast immersion in 5% PEI and dried for 1 h; one immersion in Gox (300 U/mL) and drying period (5 min for each step); 30 fast immersions in Gox solution, and finally, 15 fast immersions in cross-linking solution (BSA/Glut).

This microbiosensor design will be referred to as: CFE/PB/$PEI_{5\%}$/Gox_{opt} (see enzyme and analytical parameters in Table 1)

3.3.2. Study of poly-o-phenylenediamine anti-interference film

At the low applied potential used in the present work, the influence of physiological interferences on the response of the biosensor should be very low. One useful way in diminishing this electroactive interference further, and also improve the stability

Table 1
Enzyme kinetic and analytical parameters of different glucose biosensor designs.

Biosensors	Sensitivity (pA/mM)	r^2 in L.R.	Detection Limit (μM)	K' (mM)	V_m (pA)	h
CFE/PB/Gox_0	10.0 ± 0.3	0.999	564	27 ± 3	339 ± 33	0.9 ± 0.1
CFE/PB/Gox_5	20.3 ± 1.3	0.984	270	19 ± 3	643 ± 68	0.9 ± 0.1
CFE/PB/Gox_{10}	38.5 ± 1.3	0.996	103	19 ± 2	1240 ± 128	0.8 ± 0.1
CFE/PB/$(Gox–PEI_{1\%})_5$	74.8 ± 2.7	0.997	57	13 ± 2	1306 ± 42	1.1 ± 0.1
CFE/PB/$PEI_{5\%}/(Gox–PEI_{1\%})_5$	111 ± 7	0.991	47	10.3 ± 1.5	1661 ± 55	1.2 ± 0.1
CFE/PB/$PEI_{5\%}/(Gox–PEI_{5\%})_5$	523 ± 5	0.999	10	3.2 ± 0.6	1967 ± 41	2.0 ± 0.2
CFE/PB/$PEI_{5\%}/Gox_{opt}$	1814 ± 29	0.999	3	1.7 ± 0.2	5300 ± 57	1.6 ± 0.1
CFE/PB/$PEI_{5\%}/Gox_{opt}$/PoPD	747 ± 7	0.999	8	2.6 ± 0.1	2790 ± 20	1.4 ± 0.1

Mean ± SEM (n = 3 biosensors) for: linear sensitivity, coefficient of determination; and apparent Michaelis constant (K') and calibration plateau (V_m; see Fig. 3). Detection limit was calculated as 3 × SD of the background current. The Hill parameter is included to highlight possible deviations from straightforward Michaelis–Menten kinetics, for which h = 1. Calibration curves were obtained by applying 0.0 V against SCE in air-saturated PBS (pH 7.4).

of the PB film, is to employ permselective films (Salazar et al., in press). These films minimize access of interference species and exclude surface-active macromolecules (Lyne and O'Neill, 1990). Among these electropolymerized films are PoPD and analogues, polyphenol, and overoxidized polypyrrole (Basudam Adhikari and Majumdar, 2004; Yuqing et al., 2004). The self-controlling film thickness of PoPD during electropolymerization, reproducibly provides a thin and uniform film thickness (3–15 nm) (Killoran and O'Neill, 2008; Rothwell et al., 2008). The use of BSA can increase the interference rejecting properties of the PoPD (McAteer and O'Neill, 1996; Ryan et al., 1997; Dixon et al., 2002; Kirwan et al., 2007).

PoPD films were grown potentiostatically on the CFE/PB/$PEI_{5\%}/Gox_{opt}$ surface at +0.75 V against Ag/AgCl. After electropolymerization, biosensors were rinsed with distilled water and allowed to dry for approximately 1 h before being used. The PoPD film reduced the biosensor sensitivity to glucose by ~40–50% compared with the PoPD-free CFE/PB/$PEI_{5\%}/Gox_{opt}$ design (see Table 1). Nevertheless, the sensitivity of CFE/PB/$PEI_{5\%}/Gox_{opt}$/PoPD was 0.75 nA/mM corresponding to a current density of $9.3 \pm 0.1\ \mu A\ mM^{-1}\ cm^{-2}$ (n = 3). This was due to a combination of significantly higher V_m and lower K' values compared with the non-optimized designs; see Table 1. Biosensor responses to glucose (1 mM), with and without 400 μM AA (principal physiological interference), were recorded and normalized as a percentage with respect to current observed without AA. No significant differences were found in the absence (100 ± 2%) and presence of 400 μM AA (99 ± 3%, n = 5, p > 0.66).

Fig. 3b and c show calibration data for glucose and the effect of two principal endogenous brain interference species, using CFE/PB/$PEI_{5\%}/Gox_{opt}$/PoPD. In Fig. 3b several additions of AA (400 μM) and UA (100 μM) had no effect on either the background current or on the sensitivity of biosensor when glucose concentration was increased by 1, 1 and 2 mM, respectively. No significant difference was found in the entire glucose calibration plot (Fig. 3c), and specifically the linear sensitivity of the optimized biosensor design (Fig. 3c, *inset*) in the absence (737 ± 7 pA/mM) and presence (756 ± 14 pA/mM) of AA (400 μM), p > 0.23, n = 8. These results indicate that the effects of electroactive interference, at low applied potentials and using PoPD as permselective films, are negligible and suggest that these devices might be suitable for monitoring a complex matrix like CNS tissue.

3.3.3. pH dependence

pH plays an important role in affecting the sensitivity of glucose biosensors, because both the bioactivity of Gox and the stability of the PB film are pH dependent. It is clearly reported that PB is unstable and dissolves at pH values above 7 (Feldman and Murray, 1987), suggesting an important problem when working in physiological media. One way to solve these problems is by using a polyelectrolyte, such as PEI, to reduce possible changes in enzyme conformation by the formation of cationic–anionic complexes, and an external polymer film (PoPD) to increase the stability of the PB layer. The effect of pH of the detection solution on the response of optimized glucose biosensor (CFE/PB/$PEI_{5\%}/Gox_{opt}$/PoPD) was investigated using artificial extracellular fluid ECF (135 mM NaCl, 3 mM KCl, 1 mM $MgCl_2$, 1.2 mM $CaCl_2$) in a pH range from 6.5 to 8.5. Fig. 3d shows no significant changes in the glucose response at different pH values, confirm the excellent stability of the devices, and shows that Gox and PB are well stabilized on the CFE surface.

3.4. In vivo recording

In order to demonstrate that glucose biosensors based on CFE/PB respond to changes in glucose levels in brain extracellular fluid (ECF), we examined the effect of local injection of glucose and depolarization with 150 mM KCl on responses recorded with (CFE/PB/$PEI_{5\%}/Gox_{opt}$/PoPD) in the ECF; all experiments were done after reaching the baseline (~30 min). Fig. 4 shows changes of glucose registered in prefrontal cortex after local injections of 2 mM glucose via a micro-pipette on the surface exposed of the cortex in the proximity of the biosensor: (a) 1 μL; (b) 0.5 μL and (c) 0.1 μL at an injection flux of 3 $\mu L\ min^{-1}$. Clear biosensor response changes during infusion are evident and, after the first injection, the glucose levels remained augmented (upper inset). Linear correlation appears between glucose change and volume injected (r^2 = 0.97), i.e., no saturation effect was observed.

Spreading depression (SD) is a striking and highly reproducible response of the gray matter of the CNS. Normoxic SD can be triggered by high-frequency electrical pulses and a variety of chemicals. Among the chemical agents noteworthy are potassium ions

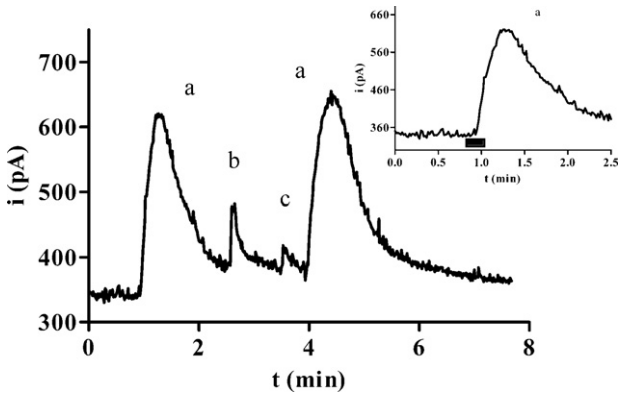

Fig. 4. Raw current changes of glucose microbiosensor recorded with the optimized configuration (CFE/PB/$PEI_{5\%}/Gox_{opt}$/PoPD) in brain extracellular fluid after local injections of 2 mM glucose (PBS, pH 7.4 100 mM NaCl) in an anesthetized Sprague Dawley rat: (a) 1 μL; (b) 0.5 μL and (c) 0.1 μL at injection flux of 3 $\mu L\ min^{-1}$. Upper inset represents the first peak where the injection period is denoted with a black bar.

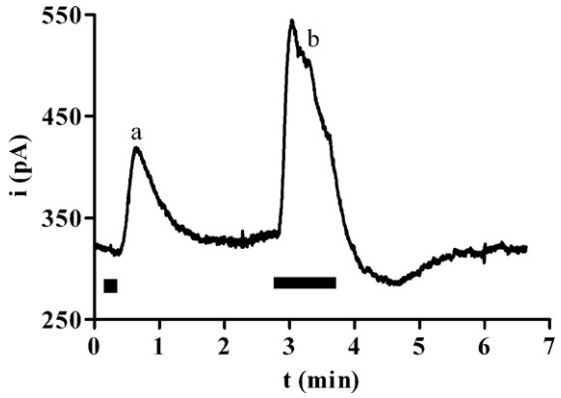

Fig. 5. Raw current changes of glucose microbiosensor recorded with the optimized configuration (CFE/PB/$PEI_{5\%}$/Gox_{opt}/PoPD): response in brain extracellular fluid after several transient of spreading depression generated by injection of 150 mM KCl in PBS in anesthetized Sprague Dawley rat. Injection flux 5 μL min^{-1}: a) volume injected 1 μL; b) volume injected 5 μL.

and glutamate. In our case a single SD episode was elicited by applying an aliquot of 150 mM KCl in PBS to the surface of the cortex beside the implanted biosensor. Biosensor responses associated with different volume injections of KCl are shown in Fig. 5, where a clear increase in current (dose dependent) was observed after different KCl injections. This was followed by a slower restoration of the basal levels, especially for the last injection where the volume injected was 5 μL and the time to reach basal levels, after terminating local injection, was estimated to be ~2 min. After each experiment, the sensitivity of the biosensors did not show significant changes, demonstrating its good anti-biofouling properties.

4. Conclusions

Microbiosensors of glucose based on PB-modified CFEs have been developed. Several advantages of this approach were: small dimensions, low applied potentials (associated with electrocatalysis by the PB deposit) and anti-interference properties (due to low applied potential and a PoPD permselectivity film), and these have been contrasted to conventional Pt–Ir-based biosensors (higher dimensions and potentials) for work in physiological media. Principal steps of fabrication have also been discussed: electrodeposition and activation of CFE with PB, enzyme immobilization, etc. By exploring enzyme immobilization steps, biosensors with different analytical properties have been developed. Optimal applied potential studies for H_2O_2 detection, and pH effects on biosensor response have also been investigated and discussed. Finally, an optimized biosensor configuration, CFE/PB/$PEI_{5\%}$/Gox_{opt}/PoPD, is proposed as an effective candidate to be used for *in vivo* studies with a sensitivity of 9.3 ± 0.1 μA mM^{-1} cm^{-2} ($n = 3$), RSD of 2% and free of electroactive interference.

Acknowledgements

The funds for the development of this device have been provided by the following national public projects: ULLAPD-08/01 granted by the Agencia Canaria de Investigación, Innovación y Sociedad de la Información, Ministerio de Industria, Turismo y Comercio (Proyecto AVANZA) TSI-020100-2008-337 and Ministerio de Ciencia e Innovación (Proyecto CICYT) TIN2008-06867-C02-01/TIN.

References

Basudam Adhikari, B., Majumdar, S., 2004. Prog. Polym. Sci. 29 (7), 699–766.
Breccia, J.D., Andersson, M.M., Hatti–Kaul, R., 2002. Biochim. et Biophys. Acta 1570 (3), 165–173.
Castillo, J., Gáspár, S., Sakharov, I., Csöregi, E., 2003. Biosens. Bioelectron. 18 (5–6), 705–714.
Clark Jr., L.C., 1979. Methods in Enzymology, vol. 56. Academic Press, New York.
Clark Jr., L.C., Lyons, C., 1962. Ann. N. Y. Acad. Sci. 102, 29–45.
Dai, Y.Q., Zhou, D.M., Shiu, K.K., 2006. Electrochim. Acta 52 (1), 297–303.
Dale, D., Hatz, S., Tian, F., Llaudet, E., 2005. Trends Biotechnol. 23 (8), 420–428.
Dixon, B.M., Lowry, J.P., O'Neill, R.D., 2002. J. Neurosci. Methods 119, 135–142.
D'Orazio, P., 2003. Clin. Chim. Acta 334 (1–2), 41–69.
Feldman, B.J., Murray, R.W., 1987. Inorg. Chem. 26 (11), 1702–1708.
Fellows, L.K., Boutelle, M.G., 1993. Brain Res. 604 (1–2), 225–231.
Garjonyte, R., Malinaus, A., 1999. Sens. Actuators B 56 (1–2), 85–92.
Gouda, M.D., Thakur, Karanth, N.G., 2001. Electroanalysis 13 (10), 849–855.
Gregg, B.A., Heller, A., 1990. Anal. Chem. 62 (3), 258–263.
Habermüller, K., Mosbach, M., Schuhmann, W., 2000. Fresenius J. Anal. Chem 366 (6–7), 560–568.
Karyakin, A.A., 2001. Electroanalysis 13 (10), 813–819.
Karyakin, A.A., Gitelmacher, O.V., Karyakina, E.E., 1995. Anal. Chem. 67 (14), 2419–2423.
Karyakin, A.A., Karyakina, E.E., 1999. Sens. Actuators B 57 (1–3), 268–273.
Karyakin, A.A., Karyakina, E.E., Gordon, L., 2000. Anal. Chem. 72 (7), 1720–1723.
Killoran, S.J., O'Neill, R.D., 2008. Electrochim. Acta 53 (24), 7303–7312.
Kirwan, S.M., Rocchitta, G., McMahon, C.P., Craig, J.D., Killoran, S.J., O'Brien, K.B., Serra, P.A., Lowry, J.P., O'Neill, R.D., 2007. Sensors 7 (4), 420–437.
Li, J.P., Gu, H.N., 2006. J. Chin. Chem. Soc. 53 (3), 575–582.
Lowry, J.P., Miele, M., O'Neill, R.D., Boutelle, M.G., Fillenz, M., 1998. J. Neurosci. Methods 79 (1), 65–74.
Lowry, J.P., O'Neill, R.D., 1994. Electroanalysis 6 (5–6), 369–379.
Lukachova, L.V., Kotel'nikova, E.A., D'Ottavi, D., Shkerin, E.A., Karyakina, E.E., Moscone, D., Palleschi, G., Curulli, A., Karyakin, A.A., 2003. IEEE Sens. J. 03 (3), 326–332.
Lyne, P.D., O'Neill, R.D., 1990. Anal. Chem. 62 (21), 2347–2351.
McAteer, K., O'Neill, R.D., 1996. Analyst 121 (6), 773–777.
Mitala, J.J., Michael, A.C., 2006. Anal. Chim. Acta 556 (2), 326–332.
O'Neill, R.D., Lowry, J.P., Rocchitta, G., McMahon, C.P., Serra, P.A., 2008. Trends Anal. Chem. 27 (1), 78–88.
Osborne, P., Hashimoto, M., 2004. Analyst 129, 759–765.
Pellerin, L., Bouzier–Sore, A.K., Aubert, A., Serres, S., Merle, M., Costalat, R., Magistretti, P.J., 2007. Glia 55 (12), 1251–1262.
Qian, J.M., Suo, A.L., Yao, Y., Jina, Z.H., 2004. Clin. Biochem. 37 (2), 155–161.
Ryan, M.R., Lowry, J.P., O'Neill, R.D., 1997. Analyst 122 (11), 1419–1424.
Ricci, F., Palleschi, G., 2005. Biosens. Bioelectron. 21 (3), 389–407.
Rothwell, S.A., Killoran, S.J., Neville, E.M., Crotty, A.M., O'Neill, R.D., 2008. Electrochem. Commun. 10 (7), 1078–1081.
Salazar P., Martín M., Roche R., O'Neill R.D., González-Mora J.L., Electrochim. Acta, in press, doi:10.1016/j.electacta.2010.06.036.
Schuvailo, O.N., Dzyadevych, S.V., El'skaya, A., Gautier-Sauvigne, S., Csoregi, E., Cespuglio, R., Soldatkin, A.P., 2005. Biosens. Bioelectron. 21 (1), 87–94.
Swoboda, B.E.P., Massay, V., 1965. J. Biol. Chem. 240 (5), 2209–2215.
Yuqing, M., Jianrong, C., Xiaohua, W., 2004. Trends Biotechnol. 22 (5), 227–231.

Sensors and Actuators B 152 (2011) 137–143

Contents lists available at ScienceDirect

Sensors and Actuators B: Chemical

journal homepage: www.elsevier.com/locate/snb

Amperometric glucose microbiosensor based on a Prussian Blue modified carbon fiber electrode for physiological applications

P. Salazar[a,*], R.D. O'Neill[b], M. Martín[a], R. Roche[a], J.L. González-Mora[a]

[a] Neurochemistry and Neuroimaging Group, Faculty of Medicine, University of La Laguna, Tenerife, Spain
[b] UCD School of Chemistry and Chemical Biology, University College Dublin, Belfield, Dublin 4, Ireland

ARTICLE INFO

Article history:
Received 30 September 2010
Received in revised form
16 November 2010
Accepted 25 November 2010
Available online 3 December 2010

Keywords:
Biosensor
Carbon fiber electrode
Brain glucose
Prussian blue
Polyphenylenediamine

ABSTRACT

Results of experiments *in vitro* and *in vivo*, using an amperometric glucose microbiosensor based on a Prussian Blue (PB) modified carbon fiber electrode with very low dimensions (~10 μm diameter), are presented. The electrocatalytic properties of the PB film enable detection of an enzymatic by-product (H_2O_2) at a very low applied potential: 0.0 V against SCE. The main steps during glucose microbiosensor construction were examined by cyclic voltammetry and electrochemical impedance spectroscopy. Excellent selectivity of the glucose microbiosensors against a large number of physiological interference compounds is demonstrated. Finally, microbiosensor responses during intraperitoneal injection, local infusion and local electrical stimulation showed sufficient sensitivity and stability to monitor multiphasic and reversible changes in brain ECF glucose levels during physiological experiments, illustrating the excellent properties and utility of this biosensor design in the neurosciences.

1. Introduction

First generation devices have been used preferentially in amperometric biosensor design over recent decades. They are based on the measurement of one product (H_2O_2) or one co-factor (O_2) involved in the enzymatic reaction [1,2]. The principal problems of this approach are: the high overpotential that needs to be applied to the working electrode to detect either O_2 or H_2O_2 (in the region of −0.6 and +0.7 V against SCE, respectively) [3–5]; and possible fluctuations in O_2 concentration that are not related to the enzymatic reaction, especially in biological tissues [6–9]. Also, electroactive interference [10–15] and bio-polymerization reactions [16–18] can occur on the biosensor surface held at high working potentials. To solve these problems Karyakin proposed to modify the transduction element with a thin film of Prussian Blue (PB), $Fe_4[Fe(CN)_6]_3$, the most representative compound of the transition metal hexacyanometallate family [19–21]. This deposit has electrocatalytic effects on the reduction of H_2O_2 [22], allowing its detection at a potential close to 0.0 V against SCE. By detecting H_2O_2 at this low potential, artifacts due to interference and fluctuations of O_2 concentration are attenuated.

After the introduction of PB in the biosensor field by Karyakin et al. [19] in the 1990s, different material supports and deposition methodologies have been reported in order to enhance its electrocatalytic properties and stability [23–27]. Furthermore, an ultra-small glucose biosensor based on a PB-modified transducer has been reported [28], although its application for *in vivo* studies, and especially in neuroscience, has been poorly developed. In contrast, first generation microbiosensors based on noble metal transducers with high dimensions (~100 μm diameter) have been employed successfully during last decades for neurochemical monitoring of glucose [15,29]. Consequently, our group has been working in recent years to implement microbiosensors based on PB-modified carbon fiber electrodes (CFEs) with low dimensions (~10 μm diameter) for use in physiological studies [30,31].

Based on these previous studies, now we present a more detailed investigation of an optimized glucose microbiosensor configuration (described below), paying special attention to: the evolution of surface physicochemical properties at different stages of microbiosensor construction (by using electrochemical impedance and voltammetric studies); biosensor response and linear range in order to obtain higher sensitivity (~5 times greater than our previous design [30]); selectivity against a large number of potential interference species (our previous work focused on ascorbic and uric acids) [30,31]; and the response of the novel biosensor under previous [30,31] and new *in vivo* experimental conditions to demonstrate the excellent properties of this microbiosensor design

* Corresponding author at: University of La Laguna, School of Medicine, Dept. of Fisiology, Facultad Ciencias de La Salud, La Laguna, Tenerife, Spain.
E-mail address: psalazar@ull.es (P. Salazar).

0925-4005/$ – see front matter © 2010 Elsevier B.V. All rights reserved.
doi:10.1016/j.snb.2010.11.056

and its potential utility for electrophysiological and pharmacological studies in the neurosciences.

2. Materials and methods

2.1. Reagents and solutions

The enzyme glucose oxidase (Gox) from *Aspergillus niger* (EC 1.1.3.4, Type VII-S), purchased as a lyophilized powder, and glutaraldehyde 25% (Glut) were obtained from Sigma Chemical Co., and stored at −21 °C until use. Bovine serum albumin (BSA, fraction V) was also obtained from Sigma. All chemicals, including o-phenylenediamine (o-PD), glucose, polyethyleneimine (PEI), KCl, $FeCl_3$, $K_3[Fe(CN)_6]$, HCl (35% w/w), H_2O_2 (30% w/v), Nafion (5 wt% in a mixture of lower aliphatic alcohols and water), phosphate buffer saline (PBS, pH 7.4 containing 0.1 M NaCl) were obtained from Sigma and used as supplied. All interference compounds: ascorbic acid (AA), uric acid (UA), dopamine (DA), 3,4-dihydroxyphenylacetic acid (DOPAC), serotonin (5-HT), glycine (Gly), L-tryptophan (L-Tryp), aspartate (Asp), L-cysteine (L-cys), norepinephrine (Nep), epinephrine (Ep), L-tyrosine (L-tyr), γ-aminobutyric acid (GABA), homovanillic acid (HVA), and 5-hydroxyindoleacetic acid (5-HIAA) were obtained for Aldrich–Sigma and used as supplied. PBS stock solutions were prepared in doubly distilled water (18.2 MΩ cm, Millipore-Q), and stored at 4 °C when not in use. Stock 250 mM solutions of glucose were prepared in water, left for 24 h at room temperature to allow equilibration of the anomers, and then stored at 4 °C. The PEI solution used was prepared by dissolving PEI at 5% w/v in H_2O. The cross-linking solution was prepared in PBS with 1% w/v of BSA and 0.1% w/v of Glut. Monomer solution (300 mM o-PD) was prepared using 48.6 mg of o-PD and 7.5 mg of BSA in 1.5 mL of N_2-saturated PBS and sonicated for 15 min [32]. A 300 U/mL solution of Gox was prepared by dissolving 3.7 mg in 2 mL of PBS. Interference solutions were prepared in water just before use and, if necessary, pH was adjusted to 7.4. Carbon fibers (8 μm diameter), glass capillaries, and 250 μm internal diameter Teflon-coated copper wire were obtained from Word Precision Instruments Inc., and silver epoxy paint was supplied by Sigma. N_2 (high grade, $O_2 \leq 2$ ppm) was supplied by Air Liquide.

2.2. Instrumentation and software

Experiments were computer controlled with data-acquisition software EChem™ for CV and Chart™ for CPA. The data-acquisition system used was e-Corder 401 (EDAQ) and a low-noise and high-sensitivity potentiostat, Picostat (EDAQ). CV and EIS experiments for microbiosensor characterization were conducted with an Autolab PGSTAT 20 potentiostat and a FRA module from EcoChemie, computer controlled by their general purpose electrochemical system (GPES) and FRA software, respectively. The linear and non-linear regression analyses were performed using the graphical software package Prism (ver. 5.00 GraphPad Software). To electrodeposit and activate the PB, a custom-made Ag/AgCl/saturated KCl reference electrode and platinum wire auxiliary electrode were used.

2.3. Amperometric experiments

2.3.1. In vitro

All *in vitro* experiments were done in a 25 mL glass cell at 21 °C, using a standard three-electrode set-up with a commercial saturated calomel electrode (SCE) (CRISON Instrument S.A.) as the reference and platinum wire as the auxiliary electrode. The optimized applied potential for amperometric studies was 0.0 V against SCE [30,31]. Glucose calibrations were performed in quiescent air-saturated PBS (following stabilization of the background current for 30 min) by adding aliquots of glucose stock solution (0.25 M) to the electrochemical cell. After the addition of glucose aliquots, the solution was stirred for 10 s and then left to reach the steady-state current. CV experiments were carried out in electrolyte support solution (0.1 M KCl and 3 mM HCl). EIS measurements were performed in the presence of a 2.5 mM $K_3[Fe(CN)_6]/K_4[Fe(CN)_6]$ (1:1) mixture as a redox probe in PBS. The stabilization potential was set to 0.1 V against SCE, the signal amplitude was 5 mV and the frequency range was 40 kHz−0.5 Hz.

2.3.2. In vivo

These experiments were carried out with male rats of ∼300 g (Sprague Dawley) in accordance with the European Communities Council Directive of 1986 (86/609/EEC) regarding the care and use of animals for experimental procedures, and adequate measures were taken to minimize pain and discomfort. After being anesthetized with urethane (1.5 g/kg), the animal's head was immobilized in a stereotaxic frame and its body temperature maintained at 37 °C with a heating blanket. The skull was then surgically exposed and a small hole drilled for microbiosensor implantations. To measure prefrontal cortex glucose, the microbiosensors were implanted according to Paxinos and Watson coordinates: A/P +2.7 from bregma, M/L +1.2 and D/V −0.5 from dura [33]. The Ag/AgCl reference electrode and platinum auxiliary electrode were placed over the skull near the prefrontal cortex, and the skull kept wet with saline-soaked pads. Local infusion was performed using a polymicro tube based on a fused silica capillary tube with 75 μm inner diameter located 400 μm from the recording electrode tip. Electrical stimulation was provided by an S-8800 Grass model and a bipolar electrode made with two tungsten rods (100 μm diameter; A-M Systems Inc.) etched with an oxyacetylene torch flame, insulated with glass fused silica capillary (Composite Metal Service). The two active tips were separated by 25 μm, and the exposed active surface of each tip was approximately 0.5 mm long. Stimuli were given from 0.02 to 0.15 mA at 100 Hz for 400 ms, using 0.9 ms square biphasic pulses.

2.4. Microbiosensor construction based on CFE/PB

Carbon fiber electrodes (CFEs: 8 μm diameter, 250–500 μm length) where constructed and modified as described previously [30,31]; however, the electrolyte solution employed during PB modification was 0.1 M KCl and 0.1 M HCl, according to Karyakina et al. [22], in order to improve PB film stability. When the PB/CFEs were ready to use, the next step was to immobilize the permselective films and the Gox using the following protocol: 15 fast immersions in Nafion solution and a drying period of 30 min; 15 fast immersions in PEI solution and a drying period (30 min); one immersion in Gox (300 U/mL) for 5 min and a drying period (5 min); 30 fast immersions in the Gox solution; and 15 fast immersions in the cross-linking solution (BSA/Glut). After the immobilization steps, all biosensors were cured for 1 h at 37 °C, and finally an interference-rejection film of PoPD/BSA was electropolymerized over the biosensor [31]. After the fabrication procedure of the biosensors was completed, they were cleaned in doubly distilled water, stored overnight at 4 °C in a refrigerator, and used the next day. When not in use, biosensors were stored again at 4 °C in a refrigerator in dry conditions.

3. Results and discussion

3.1. CV analysis of the PB film

Once the PB film was electro-deposited, activated and stabilized [30,31], it was characterized using CV and EIS. Fig. 1a shows a CV

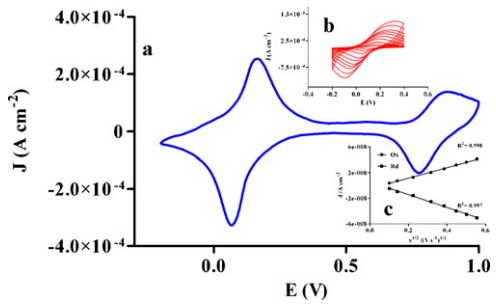

Fig. 1. a) CV of CFE/PB in electrolyte solution (0.1 M KCl, 0.1 M HCl) at a scan rate of 0.1 V s^{-1}. b) CV of CFE/PB in electrolyte solution changing the scan rate from 0.01 to 0.3 V s^{-1}. c) Linear dependence of I_{ox} and I_{rd} against the square root of scan rate.

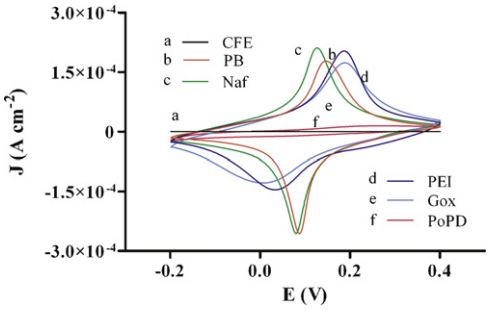

Fig. 2. CV of PW/PB conversion during each step of biosensor construction in electrolyte solution (0.1 M KCl, 0.1 M HCl) at a scan rate of 0.1 V s^{-1} against SCE.

of PB, where two characteristic peak couples due to conversion of high and low spin ions appear well defined with formal potentials of 0.15 V and 0.85 V, close to values reported previously [11–13]. As shown in Fig. 1a, the reduction peak is sharper than the oxidation one, similar to that previously reported, and indicating a regular inorganic polycrystalline structure [34]. The effect of potential scan rate on the oxidation and reduction peak currents (I_{ox} and I_{rd} respectively) was also studied for the couple centered at 0.15 V. Fig. 1b shows an increase in I_{ox}, I_{rd} and ΔE_p when scan rate was augmented. These higher values of ΔE_p reveal a more irreversible inter-conversion between PB and Prussian White (PW) forms. Plotting I_{ox} and I_{rd} against the square root of scan rate (Fig. 1c) a linear relationship is observed, indicating that diffusion of electrolyte across the film limits the reaction rate rather than a surface-bound process.

3.2. CV analysis during biosensor construction method

The electrochemical behavior of different stages of the modified microelectrode fabrication procedure was studied by CV in electrolyte solution (0.1 M KCl and 0.1 M HCl) at 0.1 V/s in the potential range corresponding to the first peak pair in Fig. 1 (−0.2 to 0.4 V); these results are shown in Fig. 2. No obvious redox peaks were observed at native, unmodified CFEs. After PB electro-deposition, however, a well-defined pair of redox peaks centered at 0.15 V corresponding to the inter-conversion between PW and PB forms was seen. In order to attenuate possible oxygen deficits in biosensor applications, Nafion was added to the modified surface. This, and other fluorocarbon-derived polymers, have been shown to act as internal O_2 reservoirs at low solution oxygen concentration due to their extraordinary capacity to dissolve O_2 [35]. A slight increase in I_{ox} and decrease in ΔE_p appeared due to a displacement of the anodic peak, indicating more reversible behavior after Nafion addition; both effects can be attributed to the negatively charged Nafion backbone.

The next step involved addition of polycationic PEI to exploit its ability to inhibit enzyme inactivation and to improve its stability by formation of cationic–anionic complexes, thus increasing the loading of active enzyme [36]. During this step a significant decrease in I_{rd} and reduction potential were observed, accompanied by a broader anodic peak. These observations can be explained by considering PEI as a positively charged poly-electrolyte and this can affect the entrapment of the counter-ion (K^+) in the PB film during the reduction step, producing a more irreversible CV (significant increase in ΔE_p). Following Gox immobilization, a small decrease of the peak currents and increase in ΔE_p were observed reflecting some inhibition of charge transfer associated with the adsorbed enzyme.

In order to avoid unwanted interference reactions during biosensor applications, a poly-o-phenylenediamine (PoPD) film was used as a permselective layer. Such films have been used in our previous studies and showed excellent anti-interference properties [30,31]. After electropolymerization of PoPD, voltammograms showed a large decrease in the peak currents and significantly broader ΔE_p characteristic of electrodes with greatly increased resistance to charge flow.

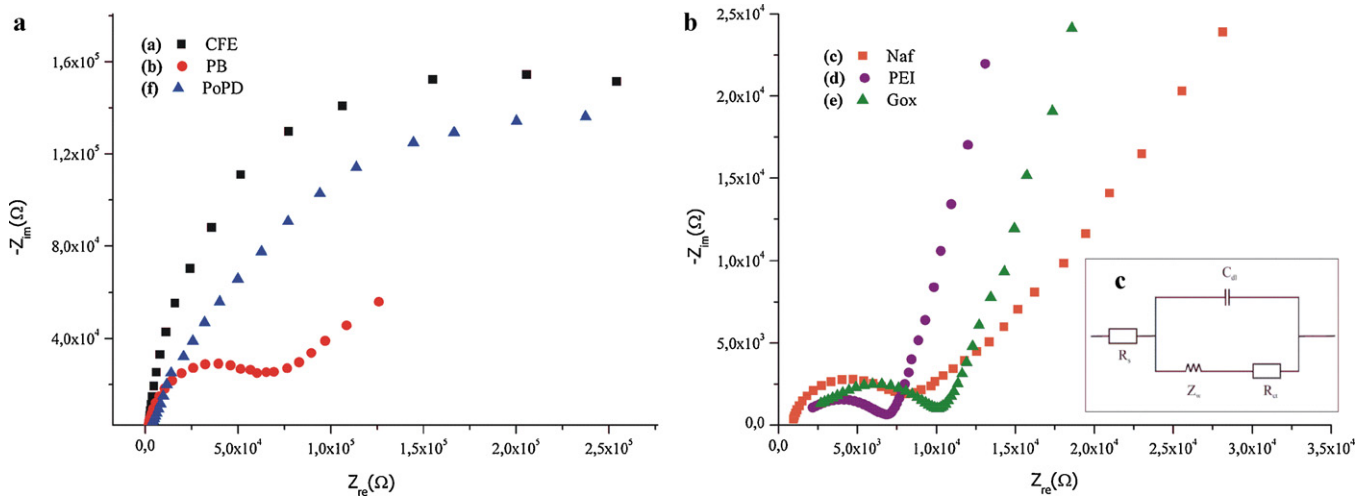

Fig. 3. (a and b) EIS of modified CFE during each step of biosensor construction in PBS with 2.5 mM $Fe(CN)_6^{4-/3-}$, 0.1 V against SCE, signal amplitude 5 mV and the frequency range 40 kHz–0.5 Hz. c) Randles electronic equivalent circuit employed to model impedance data.

Table 1
Selectivity coefficients for glucose against a large number of physiological interferences found in the ECF. Selectivity coefficients have been calculated according Eq. (1). Glucose biosensor design (CFE/PB/Nafion/PEI/Gox/PoPD) used in this study showed a sensitivity of 751 ± 3 pA/mM (mean ± SEM) $n = 5$.

Interference	Basal concentration (μM)	Calibration range (μM)	$i_x \pm$ SEM (pA)	$S \pm$ SEM (%)	n
AA	200	0–500	5.88 ± 0.42	1.57 ± 0.12	4
L-Tryp	30	0–50	0.37 ± 0.07	0.10 ± 0.02	5
L-cys	30	0–50	0.29 ± 0.05	0.08 ± 0.01	5
L-tyr	30	0–50	0.48 ± 0.06	0.13 ± 0.02	5
Gly	10	0–50	0.308 ± 0.04	0.08 ± 0.01	5
5-HLAA	10	0–50	0.44 ± 0.04	0.12 ± 0.01	5
UA	10	0–50	0.213 ± 0.02	0.06 ± 0.01	4
HVA	10	0–50	0.06 ± 0.02	0.02 ± 0.01	5
DOPAC	10	0–50	0.29 ± 0.08	0.08 ± 0.02	4
GABA	5	0–50	0.30 ± 0.02	0.08 ± 0.01	5
Asp	5	0–50	<0.01	<0.001	4
DA	0.01	0–1	<0.01	<0.001	4
5-HT	0.01	0–1	<0.01	<0.001	4
Nep	0.005	0–1	<0.01	<0.001	4
Ep	0.005	0–1	<0.01	<0.001	5

3.3. Electrochemical impedance spectroscopy analysis during construction procedure

Electrochemical impedance spectroscopy (EIS) is an effective method to probe the interfacial properties of surface-modified electrodes. A typical shape of a Faradic impedance spectrum includes a semicircle region (at higher frequencies) and a straight line portion (at lower frequencies). The semicircle portion corresponds to the charge-transfer limited process, and the linear portion represents the diffusion-limited process. The semicircle diameter in the impedance spectrum equates to the charge-transfer resistance, R_{ct}, at the electrode surface [37]

The experimental Faradaic impedance spectra were fitted using a general Randles electronic equivalent circuit (Fig. 3c), which is very often used to model interfacial phenomena [38], including the ohmic resistance of the electrolyte solution, R_s, the Warburg impedance, Z_w, the double layer capacitance, C_{dl} and the charge-transfer resistance, R_{ct}. The two components, R_s and Z_w, represent bulk properties of the electrolyte solution and diffusion feature of the redox probe in solution, respectively; therefore, these parameters are not affected by the electrochemical reaction occurring at the electrode surface. On the other hand, C_{dl} and R_{ct} depend on the dielectric and insulating features at the electrode/electrolyte interface, respectively.

At an unmodified CFE, the redox process of the $[Fe(CN)_6^{3-/4-}]$ probe showed an electron transfer resistance (R_{ct}) of about 339 kΩ (Fig. 3a, curve a); the CFE modified with a PB film showed a much lower resistance (157 kΩ) for the same redox probe (Fig. 3a, curve b), indicating that the PB improved the electric conducting properties and facilitated electron transfer. The succeeding modifications for biosensor construction were: addition of Nafion and coating with PEI (Fig. 3b, curves c and d, respectively); these two modifications gave R_{ct} values of 37 and 5 kΩ, respectively. This can be attributed to the fact that both are charged polymers and so improve charge transfer at the electrode/electrolyte interface. Nevertheless, Nafion showed a higher value of R_{ct}, presumably due to repulsion between the negatively charged SO_3^- groups of the Nafion polymer backbone and the negatively charged $Fe(CN)_6^{3-/4-}$ ions. When Gox was immobilized with BSA/Glut onto the CFE/PB/Nafion/PEI-modified electrode surface, the charge transfer resistance increased, reaching a value of 15 kΩ (Fig. 3b, curve e), which is consistent with the immobilization of the globular protein (Gox) on the electrode. The last step, electropolymerization of PoPD/BSA, increased again the resistance value to 374 kΩ (Fig. 3a, curve f), and indicates a significant blocking of charge exchange between the redox probe and the electrode surface, in good agreement with conclusions reached from CV analysis (Fig. 2).

3.4. Anti-interference properties

To quantify the anti-interference properties of these glucose micro-biosensors, a large number of potential interference compounds were checked by means of *in vitro* calibrations of glucose and interference in their physiological range (see Table 1). The selectivity coefficient for glucose against interference, S (%), was calculated using Eq. (1)

$$S\ (\%) = \frac{i_x}{i_{gluc}} \times 100 \quad (1)$$

where i_x refers to the current measured for estimated basal concentration of interference species and i_{gluc} is the current measured for 0.5 mM of glucose (Table 1). For ideally selective polymer-modified electrodes that block interferences efficiently and yet allow glucose access to the biosensor surface, S (%) approaches 0%. Selectivity coefficient values obtained for all interferences were lower than 0.15% except for AA (1.6%) which is present in brain extracellular fluid at significantly higher concentration. These results indicate that the effects of electroactive interference, at low applied potentials and using PoPD as a permselective film, are negligible and suggest that these devices might be suitable for a complex matrix like CNS tissue. Reproducibility expressed as the CV between different biosensors (intra and inter-group) was 2.7% ($n = 6$) and 5.1% ($n = 3$) respectively, and stability (loss of ~10% of the initial response after 2 weeks) showed that these biosensors are adequate for short- and medium-term applications.

3.5. In vivo glucose microbiosensor response

During all *in vivo* experiments glucose levels were in the range of 0.2–2 mM, the value depending on the experimental conditions, especially electrical and pharmacological stimulation. Taking account of biosensor calibrations before and after implantation, baseline extracellular fluid glucose concentration in prefrontal cortex was 1.2 ± 0.2 mM (mean ± SD, $n = 5$) for the state of anesthesia used here. This value is about twice that reported for the more commonly studied striatal brain region [15,30], but closer to that estimated for another subcortical region, the hippocampus [39].

3.5.1. Effects of glucose local infusion (LI) and glucose and insulin intraperitoneal injections (IP)

In order to demonstrate that CFE/PB/Nafion/PEI/Gox/PoPD biosensors respond to glucose changes in brain extracellular fluid we began *in vivo* characterization by examining the effect of glucose 2 mM LI. Fig. 4 inset shows different injections, where the injected volume was increased from 0.1 to 2 μL. As expected, a clear saturation effect and asymptotic behavior was observed, with

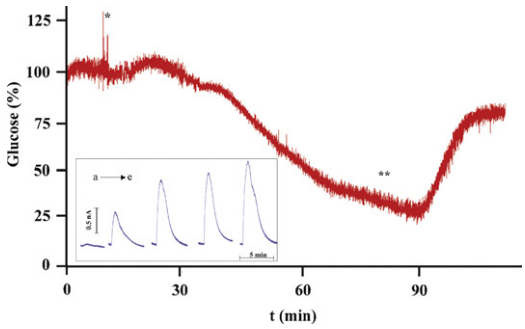

Fig. 4. Effect of intraperitoneal injections of insulin (*) (20 U/kg) and glucose (**) (1 g/kg) on the response of a glucose microbiosensor (CFE/PB/Nafion/PEI/Gox/PoPD) placed in the prefrontal cortex of anesthetized rat. Data are normalized with respect to basal levels before the injection taken as 100%. Inset: current changes in glucose microbiosensor after local infusion of different volumes (a: 0.1 μL; b: 0.2 μL; c: 0.5 μL; d: 0.8 μL; e: 2 μL) of 2 mM glucose at 10 μL min^{-1}.

the maximum current registered (comparing with previous *in vitro* calibration) corresponding to a value of 2 mM glucose, the concentration of the infused stock solution.

The effects of insulin and glucose IP were also studied. The experimental rats ($n = 3$) were isolated and access to food restricted for 12 h prior to recording. Glucose biosensors were inserted in the right prefrontal cortex and after a stabilization period (1 h) the effect of insulin (20 U/kg, IP) was studied. Fig. 4 shows the mean baseline glucose current, normalized as a percentage of basal values. At 40 ± 10 min after the injection, the measured current of glucose started to decrease and reached 20 ± 10% of basal values. The maximum hormone effect was observed approximately 1 h after injection. Fig. 4 also shows the increase in biosensor response after glucose (1 g/kg, IP), reaching almost 80% of the pre-insulin glucose basal level. Similar results have been obtained in the striatum of unanesthetized freely moving rats, using 125-μm diameter biosensors [29]. The biosensor response following glucose injection increased rapidly by 10 ± 5 min after injection but did not reach the full basal levels, probably because of the lasting influence of the injected insulin.

3.5.2. *Spreading depression produced by local infusion of 150 mM KCl and local electrical stimulation*

Spreading depression (*SD*) is a striking and highly reproducible response of the gray matter of the central nervous system. At the core of *SD* is a rapid and nearly complete depolarization of a sizable population of brain cells [40]. Normoxic *SD* can be triggered by high-frequency electrical pulses, mechanical stimuli and a variety of chemicals, such as potassium ions and glutamate. In our case a single *SD* episode was elicited by applying an aliquot (from 1 to 3 μL) of 150 mM of KCl at 10 μL min^{-1}.

The effect on the biosensor response caused by depolarization by different volume injections of KCl is shown in Fig. 5, where a clear increase in glucose level was observed after different KCl infusion (~2.5 s), followed by a rapid decreased of glucose concentration and a not-so-rapid restoration of the basal levels (~5 min). The increase in glucose response was dose dependent. The rapid depolarization of neurons and astrocytes can explain the glucose kinetics after the K^+ injection: the increased signal during injection could be due a rapid global depolarization, especially glutamatergic neurons, and the subsequent decrease could be explained by the inhibition of the synaptic activity [41] which recovers in a few minutes; similar results were found in all animals employed ($n = 3$).

SD episodes were also elicited by applying high-frequency (100 Hz) electrical pulses of 0.15 mA for 400 ms. Both the glucose biosensor and a blank sensor (without Gox) were stereotaxically positioned close to each other in the prefrontal cortex of rat brain ~200 μm from a bipolar stimulating electrode described above.

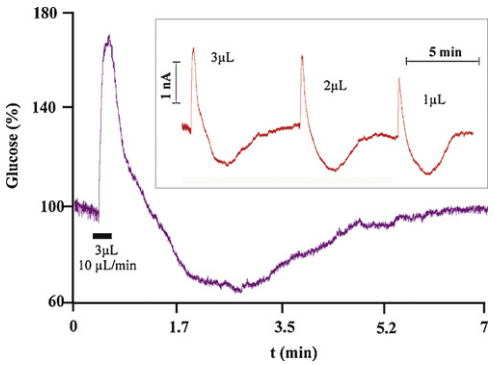

Fig. 5. Changes in CFE/PB/Nafion/PEI/Gox/PoPD biosensor response after several transients of spreading depression generated by local infusion of different volumes (from 1 to 3 μL) of 150 mM KCl at 10 μL min^{-1}.

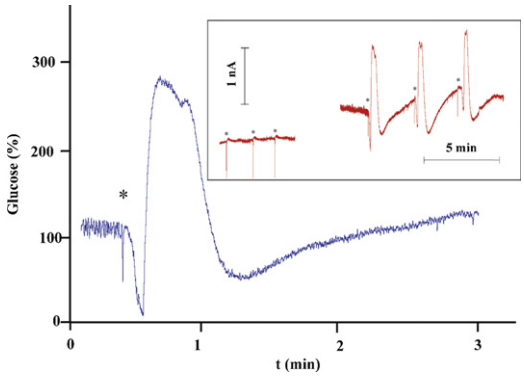

Fig. 6. Typical recordings showing the physiological responses registered with a glucose microbiosensor (CFE/PB/Nafion/PEI/Gox/PoPD) after electrical stimulation at 100 Hz for 400 ms (*): left inset, three consecutive responses with blank sensor; right inset, glucose microbiosensor response. Similar results were found in all corresponding *in vivo* experiments ($n = 4$).

While blank sensors only displayed a brief artifact during electrical stimulus (Fig. 6, left inset), glucose microbiosensors (Fig. 6, right inset) showed the same artifact and a typical *SD* response after a rapid and short decrease of glucose current (~8 s), due to the physiological consumption of glucose caused by electrical stimulation.

4. Conclusions

A new implantable glucose biosensor based on PB-modified CFE with a very small cross-sectional area (10 μm diameter) and a low working potential (0.0 V against SCE) has been designed and characterized. Incorporating an electrocatalytic layer (PB), as well as Nafion to attenuate oxygen dependence, PEI to stabilize the enzyme, and PoPD as a permselective layer, these microbiosensors displayed good glucose sensitivity (~12 nA μM^{-1} cm^{-2}) and excellent anti-interference properties. During microbiosensor construction each step was studied in detail to provide insight into how surface properties changed following each modification. Moreover, exploratory pharmacological and electrical stimulations reported here demonstrate that these devices have sufficient sensitivity and stability to monitor multi-phasic and reversible changes in brain ECF glucose levels *in vivo*.

Acknowledgement

The funds for the development of this device have been provided by the following national public grants: ULLAPD-08/01 granted by the Agencia Canaria de Investigación, Innovación y Sociedad de la Información, Ministerio de Industria, Turismo y Comercio (AVANZA) TSI-020100-2008-337 and Ministerio de Ciencia e

Innovación (CICYT) TIN2008-06867-C02-01/TIN. We thank Dr JL Rodriguez Marrero and J Florez Montaño for help in EIS measurements.

References

[1] L.C. Clark Jr., C. Lyons, Electrode system for continuous monitoring in cardiovascular surgery, Ann. N. Y. Acad. Sci. 102 (1962) 29–46.
[2] S.J. Updike, G.P. Hicks, The enzyme electrode, Nature 214 (1967) 986–988.
[3] J. Liu, J. Wang, Improved design for the glucose biosensor, Food Technol. Biotechnol. 39 (2001) 55–58.
[4] J. Wang, Glucose biosensors: 40 years of advances and challenges, Electroanalysis 13 (2001) 983–988.
[5] M. Stoytcheva, R. Zlatev, Z. Velkova, B. Valdez, M. Ovalle, Analytical characteristics of electrochemical biosensors, Portugaliae Electrochim. Acta 27 (2009) 353–362.
[6] C.P. McMahon, S.J. Killoran, R.D. O'Neill, Design variations of a polymer–enzyme composite biosensor for glucose: enhanced analyte sensitivity without increased oxygen dependence, J. Electroanal. Chem. 580 (2005) 193–202.
[7] C.P. McMahon, R.D. O'Neill, Polymer–enzyme composite biosensor with high glutamate sensitivity and low oxygen dependence, Anal. Chem. 77 (2005) 1196–1199.
[8] C.P. McMahon, G. Rocchitta, P.A. Serra, S.M. Kirwan, J.P. Lowry, R.D. O'Neill, Control of the oxygen dependence of an implantable polymer/enzyme composite biosensor for glutamate, Anal. Chem. 78 (2006) 2352–2359.
[9] B.M. Dixon, J.P. Lowry, R.D. O'Neill, Characterization in vitro and in vivo of the oxygen dependence of an enzyme/polymer biosensor for monitoring brain glucose, J. Neurosci. Methods 119 (2002) 135–142.
[10] F. Palmisano, P.G. Zambonin, Ascorbic acid interferences in hydrogen peroxide detecting biosensors based on electrochemically immobilized enzymes, Anal. Chem. 65 (1993) 2690–2692.
[11] D. Carelli, D. Centonze, A. De Giglio, M. Quinto, P.G. Zambonin, An interference-free first generation alcohol biosensor based on a gold electrode modified by an overoxidised non-conducting polypyrrole film, Anal. Chim. Acta 565 (2006) 27–35.
[12] S.M. Kirwan, G. Rocchitta, C.P. McMahon, J.D. Craig, S.J. Killoran, K.B. O'Brien, P.A. Serra, J.P. Lowry, R.D. O'Neill, Modifications of poly(o-phenylenediamine) permselective layer on Pt–Ir for biosensor application in neurochemical monitoring, Sensors 7 (2007) 420–437.
[13] M.C. Rodríguez, G.A. Rivas, Highly selective first generation glucose biosensor based on carbon paste containing copper and glucose oxidase, Electroanalysis 13 (2001) 1179–1184.
[14] J. Wang, L. Chen, J. Liu, F. Lu, Enhanced selectivity and sensitivity of first-generation enzyme electrodes based on the coupling of rhodinized carbon paste transducers and permselective poly(o-phenylenediamine) coatings, Electroanalysis 8 (2005) 1127–1130.
[15] R.D. O'Neill, J.P. Lowry, G. Rocchitta, C.P. McMahon, P.A. Serra, Designing sensitive and selective polymer/enzyme composite biosensors for brain monitoring in vivo, Trends Anal. Chem. 27 (2008) 78–88.
[16] M. Gerritsena, A. Krosb, V. Sprakelb, J.A. Luttermanc, R.J.M. Nolteb, J.A. Jansen, Biocompatibility evaluation of sol–gel coatings for subcutaneously implantable glucose sensors, Biomaterials 21 (2000) 71–78.
[17] M. Yuqing, C. Jianrong, W. Xiaohua, Using electropolymerized non-conducting polymers to develop enzyme amperometric biosensors, Trends Biotechnol. 22 (2004) 227–231.
[18] N. Wisniewski, F. Moussy, W.M. Reichert, Characterization of implantable biosensor membrane biofouling, Fresenius J. Anal. Chem. 366 (2000) 611–621.
[19] A.A. Karyakin, O.V. Gitelmacher, E.E. Karyakina, A high sensitive glucose amperometric biosensor based on Prussian Blue modified electrodes, Anal. Lett. 27 (1994) 2861–2869.
[20] A.A. Karyakin, O.V. Gitelmacher, E.E. Karyakina, Prussian Blue based first generation biosensors A high sensitive amperometric electrode for glucose, Anal. Chem. 67 (1995) 2419–2423.
[21] A.A. Karyakin, E.E. Karyakina, L. Gorton, Prussian Blue based amperometric biosensors in flow-injection analysis, Talanta 43 (1996) 1597–1606.
[22] A.A. Karyakina, E.E. Karyakina, L. Gorton, On the mechanism of H_2O_2 reduction at Prussian Blue modified electrodes, Electrochem. Commun. 1 (1999) 78–82.
[23] I.L. Mattors, L. Gorton, T. Ruzgas, A.A. Karyakin, Sensor for hydrogen peroxide based on Prussian Blue modified electrode: improvement of the operational stability, Anal. Sci. 16 (2000) 795–798.
[24] F. Ricci, G. Palleschi, Sensor and biosensor preparation, optimisation and applications of Prussian Blue modified electrodes, Biosens. Bioelectron. 21 (2005) 389–407.
[25] D. Lowinsohn, M. Bertotti, Flow injection analysis of blood L-lactate by using a Prussian Blue-based biosensor as amperometric detector, Anal. Biochem. 265 (2007) 260–265.
[26] A.K.M. Kafi, F. Yin, H.K. Shin, Y.S. Kwon, Amperometric thiol sensor based on Prussian blue-modified glassy carbon electrode, Curr. Appl. Phys. 7 (2007) 496–499.
[27] Y. Liua, Z. Chua, W. Jin, A sensitivity-controlled hydrogen peroxide sensor based on self-assembled Prussian Blue modified electrode, Electrochem. Commun. 11 (2009) 484–487.
[28] X. Zhang, J. Wang, B. Ogorevc, U.E. Spichiger, Glucose nanosensor based on Prussian-Blue modified carbon-fiber cone nanoelectrode and an integrated reference electrode, Electroanalysis 11 (1999) 945–949.
[29] J.P. Lowry, M. Miele, R.D. O'Neill, M.G. Boutelle, M. Fillenz, An amperometric glucose-oxidase/poly(o-phenylenediamine) biosensor for monitoring brain extracellular glucose: in vivo characterisation in the striatum of freely-moving rats, J. Neurosci. Methods 79 (1998) 65–74.
[30] P. Salazar, M. Martín, R. Roche, R.D. O'Neill, J.L. González-Mora, Prussian Blue-modified microelectrodes for selective transduction in enzyme-based amperometric microbiosensors for in vivo neurochemical monitoring, Electrochim. Acta 55 (2010) 6476–6484.
[31] P. Salazar, M. Martín, R. Roche, J.L. González-Mora, R.D. O'Neill, Microbiosensors for glucose based on Prussian Blue modified carbon fiber electrodes for *in-vivo* monitoring in the central nervous system, Biosens. Bioelectron. 26 (2010) 748–753.
[32] K. McAteer, R.D. O'Neill, Strategies for decreasing ascorbate interference at glucose oxidase-modified poly(o-phenylenediamine)-coated electrodes, Analyst 121 (1996) 773–777.
[33] G. Paxinos, C. Watson, The Rat Brain in Stereotaxic Coordinates, Academic Press, Sydney, 1986.
[34] A.A. Karyakin, Prussian blue and its analogues: electrochemistry and analytical applications, Electroanalysis 13 (2001) 813–819.
[35] J. Wang, L. Chen, M.P. Chatrathi, Evaluation of different fluorocarbon oils for their internal oxygen supply in glucose microsensors operated under oxygen-deficit conditions, Anal. Chim. Acta 411 (2000) 187–192.
[36] J.D. Breccia, M.M. Andersson, R. Hatti-Kaul, The role of poly(ethyleneimine) in stabilization against metal-catalyzed oxidation of proteins: a case study with lactate dehydrogenase, Biochim. Biophys. Acta 1570 (2002) 165–173.
[37] M. Zhou, L. Shang, B. Li, L. Huang, S.J. Dong, Highly ordered mesoporous carbons as electrode material for the construction of electrochemical dehydrogenase- and oxidase-based biosensors, Biosens. Bioelectron. 24 (2008) 442–447.
[38] Y. Liu, X. Qu, H. Guo, H. Chen, B. Liu, S. Dong, Facile preparation of amperometric laccase biosensor with multifunction based on the matrix of carbon nanotubes–chitosan composite, Biosens. Bioelectron. 21 (2006) 2195–2201.
[39] E.C. McNay, R.C. McCarty, P.E. Gold, Fluctuations in brain glucose concentration during behavioral testing: dissociations between brain areas and between brain and blood, Neurobiol. Learn. Mem. 75 (2001) 325–337.
[40] G.G. Somjen, Mechanisms of spreading depression and hypoxic spreading depression-like depolarization, Physiol. Rev. 81 (2001) 1065–1096.
[41] V.I. Koroleva, V.I. Davydov, G.Y. Roshchina, Properties of spreading depression identified by EEG spectral analysis in conscious rabbits, Neurosci. Behav. Physiol. 39 (2009) 87–97.

Biographies

Pedro Salazar Carballo received his degree in Chemical Sciences (2003) and his DEA (Advanced Studies Diploma) (2005) from the University of La Laguna (ULL). Since 2006 he has been a researcher at the Neurochemical and Neuroimaging headed by J.L. González-Mora. In 2010 he received his Master in Chemistry from ULL: nowadays, he is working in different areas: (1) development and implementation of enzymatic amperometric biosensors focused on the connection between the neurovascular system and the central nervous system, (2) surface nanostructuration with electroactive compounds and (3) development of label-free immunosensors based on Prussian Blue films.

Robert D. O'Neill BSc (Chemistry, University College Dublin, 1976); Ryan Gold Medal (Chemistry, 1976); PhD (Electrochemistry, supervised by Prof. David Feakins, UCD, 1980). Postdoctoral research (1980–1983) with John Albery, FRS (Chemistry, Imperial College London) and Marianne Fillenz, MD, PhD (Physiology, Oxford University). Research Fellowships (1983–1985) in Physiology (Worcester College, Oxford) and Neurochemistry (Beit Memorial Fellowship in Medical Research) at Oxford University. Appointed to UCD in 1985 and is now UCD Professor of Electrochemistry. Core research interests include design and characterization of amperometric sensors and biosensors; neurotransmitter glutamate and dopamine monitoring; and brain vitamin-C/glutamate interactions.

Miriam Martín Hernández received her degree in Chemical Sciences from the University of La Laguna (ULL, 2005). Since 2006 she has worked as researcher at the Neurochemical and Neuroimaging laboratory headed by J.L. González-Mora. In 2007 and 2010 she received her DEA (Advanced Studies Diploma) and her Master in Chemistry respectively from the ULL. Nowadays, she is working in two different areas: (1) development and implementation of enzymatic amperometric biosensors and (2) development and implementation of ISE microelectrodes, both of which are focused on the connection between the neurovascular system and the central nervous system.

Rossany Roche received her Chemical Engineer degree in 2000 and her Doctorate degree in 2006, both from Universidad Simón Bolívar, in Caracas, Venezuela. She worked at Processes and Systems Department of the Simón Bolívar University in the Automatic Control Systems area until 2006. She joined the Neurochemistry and Neuroimaging group of the Physiology Department at La Laguna University in 2007. Her research interests have been focused on modelling and identification of dynamical systems and specially the mathematical modelling of bio-medical systems.

J.L. González-Mora received his MD and PhD degrees in 1982 and 1987, respectively. Since 1992, he has been senior professor in the Department of Physiology (School of Medicine, University of La Laguna, ULL), and is the head of the Neurochemical and Neuroimaging laboratory. His group has worked on "*in vivo*" voltammetry from 1988 using this methodology for continuous on-line monitoring of monoamine neurotransmitter release in living animals and humans. His group has also been a pioneer in the application of this technique in the study of neurochemical release, associated with complex behavior such as social and sexual interaction.

Colloids and Surfaces B: Biointerfaces 92 (2012) 180–189

Contents lists available at SciVerse ScienceDirect

Colloids and Surfaces B: Biointerfaces

journal homepage: www.elsevier.com/locate/colsurfb

Surfactant-promoted Prussian Blue-modified carbon electrodes: Enhancement of electro-deposition step, stabilization, electrochemical properties and application to lactate microbiosensors for the neurosciences

P. Salazar[a,*], M. Martín[a], R.D. O'Neill[b], R. Roche[a], J.L. González-Mora[a]

[a] Neurochemistry and Neuroimaging Group, Faculty of Medicine, University of La Laguna, Tenerife, Spain
[b] UCD School of Chemistry and Chemical Biology, University College Dublin, Belfield, Dublin 4, Ireland

ARTICLE INFO

Article history:
Received 8 August 2011
Received in revised form
22 November 2011
Accepted 22 November 2011
Available online 8 December 2011

Keywords:
Prussian Blue
Surfactant
BZT
H_2O_2 sensor
Lactate biosensor

ABSTRACT

We report here for the first time a comparison of the beneficial effects of different cationic surfactants – cetyl trimethyl ammonium bromide (CTAB), benzethonium chloride (BZT) and cetylpyridinium chloride (CPC) – for the electrochemical synthesis of Prussian Blue (PB) films, using cyclic voltammetry (CV), on screen-printed carbon electrodes (SPCEs). Their electrochemical properties were investigated, paying special attention to parameters such as the amount of PB deposited, film thickness, charge transfer rate, permeability, reversibility, stability and sensitivity to hydrogen peroxide detection. All surfactant-enhanced PB-modified SPCEs displayed a significant improvement in their electrochemical properties compared with PB-modified SPCEs formed in the absence of surfactants. Surfactant-modified electrodes displayed a consistently higher PB surface concentration value of $2.1 \pm 0.4 \times 10^{-8}$ mol cm^{-2} (mean ± SD, $n = 3$) indicating that PB deposition efficiency was improved 2–3 fold. K^+ and Na^+ permeability properties of the films were also studied, as were kinetic parameters, such as the surface electron transfer rate constant (k_s) and the transfer coefficient (α). The hydrogen peroxide sensitivity of surfactant-modified PB films generated by 10 electro-deposition CV cycles gave values of 0.63 A M^{-1} cm^{-2}, which is higher than those reported previously for SPCEs by other authors. Finally, the first lactate microbiosensor described in the literature based on BZT-modified PB-coated carbon fiber electrodes is presented. Its very small cross-section (~10 μm diameter) makes it particularly suitable for neuroscience studies in vivo.

1. Introduction

Over recent decades, Prussian Blue (PB), $Fe_4[Fe(CN)_6]_3$, the most representative compound of the transition metal hexacyanometallate family [1,2], has received much attention in a variety of fields. Although its magnetic and electrochromic properties have proved very attractive [3,4], the electrocatalytic effect of its reduced form (Prussian White, PW) on the reduction of H_2O_2 at low applied potentials is the most important application to date [5]. Together with the facile modification of the electrode substrate and the low cost of production, this has led to an on-going replacement of the common enzymatic detection method – horseradish peroxidase (HRP) – which is more expensive and complicated than PB-modified substrates [6–13].

Screen printing technology has been employed with great success in the manufacture of electrodes in the last decade, allowing the mass production of electrodes with extremely low cost and therefore suitable for production of disposable electrodes [14]. Relatively few papers appear in the literature combining screen-printed carbon electrodes (SPCEs) and PB. These reports were based on the chemical synthesis of PB and subsequent bulk modification of the carbon ink by PB microparticles [15] or the in situ modification of glassy carbon or graphite powder with PB [16], both methods giving similar hydrogen peroxide sensitivity of ~0.14 A M^{-1} cm^{-2}. Another method, proposed by Ricci et al. [17], involved the direct chemical synthesis of PB onto SPCEs, placing a drop of precursor solution onto the working electrode area. With this approach a H_2O_2 sensitivity of ~0.23 A M^{-1} cm^{-2} has been achieved.

An important advance in the context of the electro-deposition of PB (and other hexacyanoferrates) was the addition of cetyl trimethyl ammonium bromide (CTAB), a cationic surfactant [18–21]. With this approach, a significantly enhanced film growth, efficient and rapid charge transfer, and extremely high stability have been reported [18–23]. However, many of these studies to date have focused mainly on the use of CTAB as a stabilizing agent for PB deposited on classical electrodes, usually GCEs.

In the present paper we compare the effect of different cationic surfactants (CTAB, benzethonium chloride (BZT) and

* Corresponding author. Tel.: +34 922319363; fax: +34 922319397.
E-mail address: psalazar@ull.es (P. Salazar).

0927-7765/$ – see front matter © 2011 Elsevier B.V. All rights reserved.
doi:10.1016/j.colsurfb.2011.11.047

cetylpyridinium chloride (CPC)) on the electrochemical properties of PB films electro-deposited on SPCEs, paying special attention to parameters such as the amount of PB deposited, film thickness, charge transfer rate, permeability, reversibility, stability and sensitivity to hydrogen peroxide detection. At the first stage of the study SPCEs were selected due to their high reproducibility, low-cost and convenient configuration compared with carbon fiber electrodes (CFEs) which are needed for in vivo implantation. Building on this experience with SPCEs, a novel lactate microbiosensor based on BZT-modified PB-coated CFEs (~10 μm diameter) is then presented with a view to future applications in the neurosciences.

2. Experimental

2.1. Reagents and solutions

The enzyme lactate oxidase (Lox) from *Pediococcus* sp. (50 units, L0638), purchased as a lyophilized powder, and glutaraldehyde 25% (Glut) were obtained from Sigma Chemical Co., and stored at −21 °C until use. Bovine serum albumin (BSA, fraction V) was also obtained from Sigma. All other chemicals, including o-phenylenediamine (o-PD), sodium L-lactate, polyethyleneimine (PEI), KCl, NaCl, $FeCl_3$, $K_3[Fe(CN)_6]$, HCl (35%, w/w), H_2O_2 (30%, w/v), Nafion (5 wt% in a mixture of lower aliphatic alcohols and water), phosphate buffer saline (PBS, pH 7.4 containing 0.1 M NaCl), ascorbic acid (AA), CTAB, BZT and CPC were obtained from Sigma and used as supplied. The background electrolyte for electro-deposition and electrochemical characterization consisted of a solution of 0.02 M HCl and 0.1 M KCl (pH 1.7). PBS stock solutions were prepared in doubly distilled water (18.2 MΩ cm, Millipore-Q), and stored at 4 °C when not in use. The PEI solution used was prepared by dissolving PEI at 5% (w/v) in H_2O. The cross-linking solution was prepared in PBS with 1% (w/v) of BSA and 0.1% (w/v) of Glut. Monomer solution (300 mM o-PD) was prepared using 48.6 mg of o-PD and 7.5 mg of BSA in 1.5 mL of N_2-saturated PBS, and sonicated for 15 min. A 100 U/mL solution of Lox was prepared by dissolving 50 units of Lox in 0.5 mL of PBS, stock 50 mM solutions of lactate were prepared in PBS and stored at 4 °C when not in use. The stock calibration solution of H_2O_2 (10 mM) was prepared in H_2O just before use. Carbon fibers (8 μm diameter), glass capillaries, and 250 μm internal diameter Teflon-coated copper wire were obtained from Word Precision Instruments Inc., and silver epoxy paint was supplied by Sigma. High grade N_2 ($O_2 \leq 2$ ppm) was supplied by Air Liquide.

2.2. Instrumentation

Experiments were computer controlled with data-acquisition software EChem™ for CV and Chart™ for CPA. The data-acquisition system used was e-Corder 401 (EDAQ) and a low-noise and high-sensitivity potentiostat, Quadstat (EDAQ). Screen-printed carbon electrodes (SPCEs) were purchased from DropSens. These electrodes incorporate a conventional three-electrode configuration, printed on ceramic substrates (3.4 cm × 1.0 cm). Both working (disk-shaped 4 mm diameter) and counter electrodes were made of carbon inks, whereas the pseudoreference electrode and electric contacts were made of silver. Scanning electron micrographs (SEMs) were obtained using a JEOL JSM-6300 microscope.

2.3. PB electro-deposition

The deposition of the PB-surfactant composite film onto SPCEs was accomplished by placing a drop of precursor solution (background electrolyte solution (see above) containing 1.5 mM $FeCl_3$ + 1.5 mM $K_3[Fe(CN)_6]$ + 1 mM surfactant) onto the working, pseudoreference and counter electrodes, and cycling between −0.2 and 1 V at a scan rate of 0.1 V s^{-1} (default 10 cycles). The unmodified PB film was prepared under the same conditions except that the solution was free of surfactant. All electro-deposition and characterization were done using this internal silver pseudoreference (~0.026 V against SCE in background electrolyte solution (0.02 M HCl and 0.1 M KCl)) at 25 °C. PB-surfactant-modified CFEs were obtained by introducing CFEs into the precursor solution in the similar way as SPCEs and cycled three times using an Ag wire as pseudoreference and a platinum wire as counter electrode.

2.4. PB characterization

Electrochemical characterizations of PB deposits were done in background electrolyte solution (0.02 M HCl and 0.1 M KCl). However, to study the PB permeability of Na^+, the background electrolyte solution consisted of 0.02 M HCl and 0.1 M NaCl.

2.5. H_2O_2 sensor calibrations

In order to determine the hydrogen peroxide sensitivity of the different PB films prepared in the present work, the modified SPCEs were placed in 25 mL of a stirred background electrolyte solution at an applied potential of −0.05 V versus the pseudoreference electrode. When a stable current background was reached (60–80 s), H_2O_2 aliquots were added and their response measured after 30 s.

2.6. Lactate microbiosensor construction

Carbon fiber electrodes (CFEs: 8 μm diameter, 250 μm length) where constructed as described previously [12,13], and modified in precursor solution containing 1 mM BZT by applying three deposition cycles (CFE/PB-BZTs). Enzymatic immobilization was done according next protocol: 15 and 30 fast immersions in PEI and Lox solutions respectively with a drying period of 10 min each time; lastly they were immersed 15 times in the cross-linking solution (BSA/Glut) and cured for 4 h at 37 °C. To include an interference-rejection film, PoPD/BSA was electropolymerized over the biosensors [12,13]. After the biosensor fabrication procedure was completed, they were rinsed in doubly distilled water, stored overnight at 4 °C in a refrigerator under dry conditions, and used the next day.

2.7. Lactate microbiosensor calibration

Lactate calibrations were done in a 25 mL glass cell at 21 °C, using a standard three-electrode setup with a commercial saturated calomel electrode, SCE (CRISON Instrument S.A.), as the reference and platinum wire as the auxiliary electrode. The applied potential for amperometric studies was 0.0 V versus SCE. Lactate calibrations were performed in quiescent air-saturated PBS (following stabilization of the background current for 20–30 min) by adding aliquots lactate stock solution. After each addition, the solutions were stirred for 5 s and then left to reach the quiescent steady-state current.

3. Results and discussion

3.1. Enhancement of electro-deposition and film thickness

Fig. 1(A) and (B) shows the CVs recorded during film formation for 10 cycles for unmodified (PB) and modified (PB-BZT) films, respectively. Right from the first cycle the CV response was greater during the formation of the BZT-modified PB than for the unmodified film. Similar results were found for PB-CPC and PB-CTAB films. Taking into consideration that the charge under the

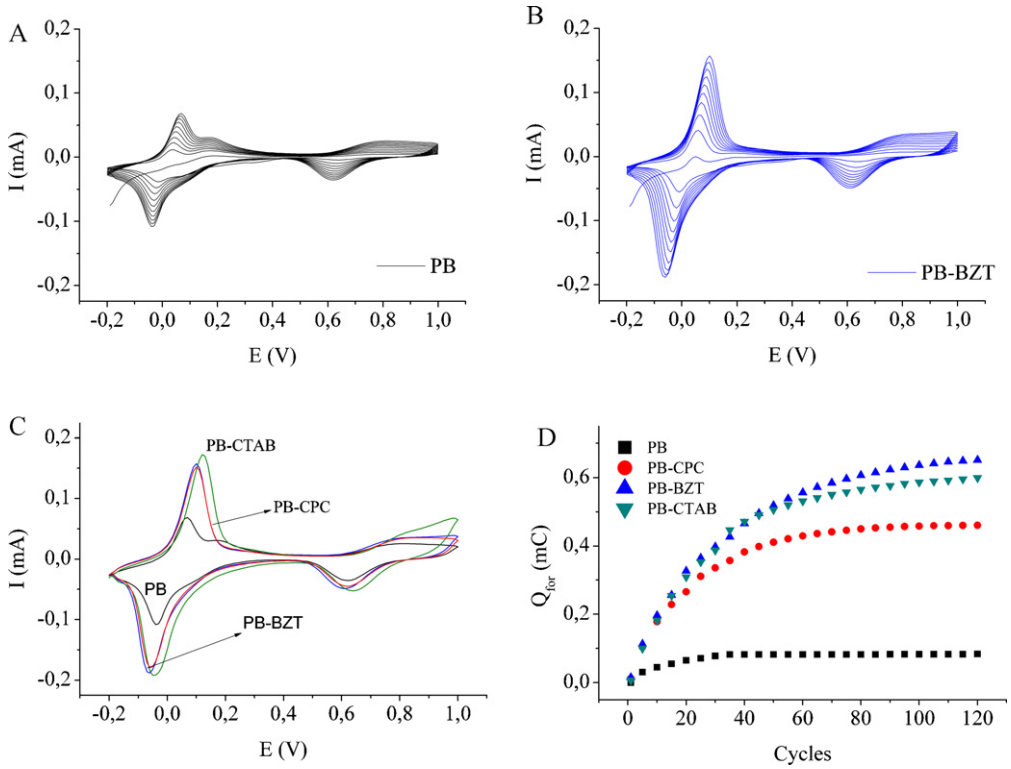

Fig. 1. (A) CV of PB electrodeposition onto SPCE without surfactant cycling at a scan rate of 0.1 V s^{-1} (10 cycles). (B) CV of PB electrodeposition onto SPCE adding BZT 1 mM (10 clycles). (C) CV of unmodified and surfactant modified PB SPCE between −0.2 and 1 V at a scan rate of 0.1 V s^{-1}. (D) Comparison of the charge storage capacity of different PB films studied by cycling SPCEs over 120 successive cycles between −0.2 and 1 V at a scan rate of 0.1 V s^{-1}. Q_{for} represents the accumulate charge under the anodic peak for each scan.

CV trace is a measure of the amount of PB deposited, these results indicate that the presence of these cationic surfactants promote the deposition of larger quantities of PB onto the SPCE surface. Table 1 shows the deposition rate, expressed as charge accumulated per cycle under the anodic (forward) peak (Q_{for}). The beneficial effect of cationic surfactants is evident from the deposition rate of the modified PB film which was 2–3 times faster than the unmodified case. The film electrodes prepared by 10 cycles are shown in Fig. 1(C); all films showed the characteristic CV peaks at ~0.05 V (PB ↔ PW transition) and at ~0.7 V (Berlin green, BG ↔ PB transition) [24–27]. Nevertheless, for the more detailed analysis below, only the first peak pair was studied because of its critical involvement in the electrocatalytic detection of hydrogen peroxide [5].

All CVs for the PB ↔ PW transition showed a broad composite anodic peak and narrower cathodic peak characteristic of PB redox behavior. The unmodified PB film displayed a peak separation (ΔE_p) of 50 mV (Table 1) which is a higher value than that associated for a fully reversible surface-bound reaction (theoretical $\Delta E_p = 0$). The electrochemistry of PB immobilized on an electrode is complicated by the possibility that either electron transfer or diffusion of counterions through the matrix might be rate determining depending on the conditions, including scan rate (see scan-rate dependence studies below). The surfactant-modified films displayed even higher values of ΔE_p which correlated well with the amount of PB deposited (see Table 1). This overpotential may emerge from a combination of the intrinsic activation barrier of transferring electrons from the electrode surface to the iron centers and/or from the counterion diffusion rates, and is not inconsistent with recent indications that the kinetics of charge transfer in PB is controlled by the diffusion of counterions through the film [12], which would be more difficult for thicker PB layers. The formal potential, $E^{0\prime}$, for the unmodified film was 0.025 V (Table 1), whereas $E^{0\prime}$ for modified films increased to ~0.05 V, indicating a small bias in the difficulty of oxidation over reduction. The amount of charge associated with the anodic (Q_{ox}) and cathodic (Q_{rd}) peaks (Table 1) also increased (3–4 times) when cationic surfactants were used. As expected from this observation, similar behavior was found for anodic (I_{ox}) and cathodic (I_{rd}) currents. Q_{ox}/Q_{rd} ratios for modified PB films (~1) indicate a more reversible behavior than for the unmodified film (0.887). On the other hand, the I_{ox}/I_{rd} ratio did not reach unity in any case, which may be attributed to the more diverse factors affecting peak current compared with total peak charge. Finally, the mean charge (Q_m) between Q_{ox} and Q_{rd} was normalized with respect to the PB-CTAB film (Table 1). These results suggest that the three cationic surfactants studied improved PB electro-deposition by 50–70%, with CTAB providing the best results.

Table 1
Voltammetric parameters for PB films obtained in background solution (0.02 M HCl and 0.1 M KCl) at a scan rate of 0.04 V s^{-1}.

	Q_{for} (mC $cycle^{-1}$)	E_{ox} (V)	E_{rd} (V)	$E^{0\prime}$ (V)	ΔE_p (V)	Q_{ox} (mC)	Q_{rd} (mC)	Q_{ox}/Q_{rd}	I_{ox} (mA)	I_{rd} (mA)	I_{ox}/I_{rd}	Q_m (μC)	Q_{mX}/Q_{mCTAB}
PB	6.20E−03	0.090	0.040	0.025	0.050	0.096	−0.108	−0.887	0.037	−0.048	−0.774	0.102	0.363
PB-CPC	1.41E−02	0.110	0.020	0.045	0.090	0.207	−0.208	−0.997	0.087	−0.114	−0.763	0.207	0.740
PB-BZT	1.68E−02	0.120	0.010	0.055	0.110	0.247	−0.249	−0.994	0.099	−0.123	−0.804	0.248	0.884
PB-CTAB	2.16E−02	0.116	0.004	0.056	0.112	0.280	−0280	−1.000	0.126	−0.151	−0.836	0.280	1.000

The surface coverage of the electroactive species generated from the PW → PB transition, $\Gamma^0_{Fe^{3+}}$, was calculated using Eq. (1):

$$\Gamma^0_{Fe^{3+}} = \frac{Q_{ox}}{nfA} \quad (1)$$

where n the number of electrons consumed ($n = 1$), F is the Faraday constant and A the working electrode area, calculated geometrically ($A = 0.126\,cm^2$); these results are summarized in Table 2. The unmodified electrode gave a $\Gamma^0_{Fe^{3+}}$ value of $7.25 \pm 0.18 \times 10^{-9}\,mol\,cm^{-2}$ (mean ± SD, $n = 3$). Surfactant-modified electrodes displayed a consistently higher value: $2.05 \pm 0.35 \times 10^{-8}\,mol\,cm^{-2}$ (mean ± SD, $n = 3$), indicating that PB deposition was improved (2–3 times) when surfactants were used, consistent with data reported previously for other substrates [18–23].

The thickness of the film, d, was estimated taking account of the number of unit cells present on the electrode surface, geometrical parameters of the PB cell, and the working electrode area, according the Eq. (2):

$$d = \left(\frac{Q_{ox}}{nFA}\right)\left(\frac{l^3 N_A}{4}\right) = \Gamma^0_{Fe^{3+}}\left(\frac{l^3 N_A}{4}\right) \quad (2)$$

where N_A is Avogadro's number and l is the length of the unit cell (1.02 nm) [27], although this value must be considered an estimation because the density of the modified film is not available. Modified films showed a thickness of 33 ± 6 nm (mean ± SD, $n = 3$) which is likely to represent a minimum value due to the additional bulk of the surfactant, whereas the PB film electro-deposited without any surfactant was only ~12 nm thick (Table 2). This finding confirms that thicker films are obtained in the presence of cationic surfactants [18–23].

The charge storage capacity of different films was also studied by cycling SPCEs over 120 successive cycles. Fig. 1(D) shows the Q_{for} evolution against number of cycles, starting with the bare SPCE. All films showed an increase in accumulated charge in each successive cycle. Nevertheless, the rate of formation was greater when surfactants were present in the precursor solution (discussed above). For the unmodified PB film after ~20 cycles, Q_{for} reached a plateau value (0.082 mC), after which there was no significant increase. In contrast, Q_{for} for modified PB films continued increasing until 50–80 cycles, showing higher deposition efficiency and higher quantity of PB deposited onto the SPCE surface in the presence of surfactants. According Kumar's mechanism [23], surfactants, close to their miscellar concentration (*cmc*), can assist deposition of PB on the electrode surface by interacting favorably with solution constituents and the SPCE surface, increasing the efficiency of PB formation. In our case 1 mM concentration was used for all surfactants, which is close to the *cmc* of CTAB [23], CPC [28–30] and BZT [31,32]. Finally CTAB and BZT show better deposition efficiency (~0.6 mC) than CPC (~0.45 mC).Fig. 2 shows PB films generated cycling 120 times in the absence of surfactant (Fig. 2(A)) and with 1 mM BZT (Fig. 2(B)), and indicate that the two films have a markedly different morphology. Whereas the unmodified PB film showed a very thin deposit with some areas apparently PB free (revealing the bare Pt), the PB-BZT film displayed the important columnar growing pattern of cubic structures onto a well defined PB film background. These findings demonstrate better deposition efficiency when BZT is present in the precursor solution and is in good concordance with data described above; see Fig. 1(D). The SEM data reveal a clear improvement in the crystal growth during PB electro-deposition when surfactant is used. This is in agreement with independent studies [21], where the authors found, using X-ray diffraction, that the degree of crystallinity is much higher for PB films incorporating surfactant.

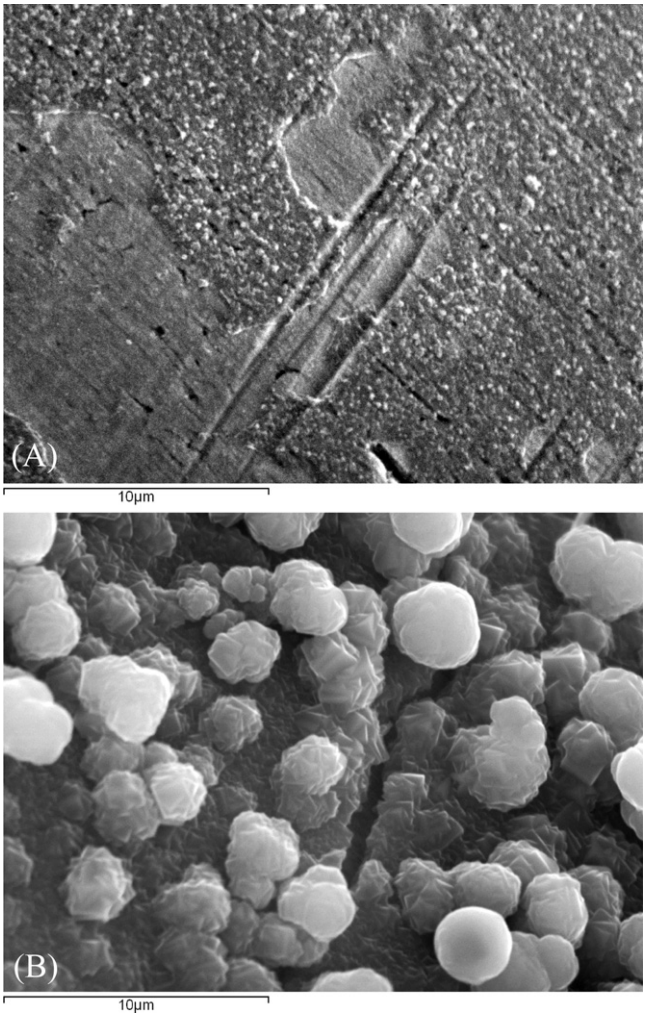

Fig. 2. Scanning electron micrographs (SEM) at a 5000 magnification for: (A) PB and (B) PB-BZT electrodes. Both films were deposited onto Pt over 120 successive cycles between −0.2 and 1 V at a scan rate of $0.1\,V\,s^{-1}$.

3.2. Permeability of PB films

It has been demonstrated that PB films display a specific transport of alkali metal cations due to its zeolite structure [33,34,1], with a cubic cell of 1.02 nm and channel diameter of about 0.32 nm [27,35]. These geometrical conditions affect the transport of cations during PB ↔ PW transition (see Eq. (3) for electron transfer reactions in the presence of potassium chloride as supporting electrolyte), so only cations with lower hydrated diameter such as K^+ (0.25 nm), Rb^+ (0.26 nm), and Cs^+ (0.24 nm) [35] can penetrate into the structure during this conversion.

$$(PB)\,Fe(III)_4[Fe(II)(CN)_6]_3 + 4e^- + 4\,K^+ \leftrightarrow (PW)\,K_4Fe(II)_4[Fe(II)(CN)_6]_3 \quad (3)$$

In order to demonstrate beneficial effects of modified PB films on ionic transport, the permeability for K^+ was investigated. The effect of scan rate (ν) on I_{ox} and I_{rd} for all configurations was studied in background electrolyte (0.02 M HCl and 0.1 M KCl) from 0.14 to $0.26\,V\,s^{-1}$. Plotting I_{ox} and I_{rd} against the square root of scan rate, a linear relationship was observed (data not shown), indicating that diffusion of electrolyte across the films, at this scan rate range, limits the reaction rate rather than surface-bound processes (for further discussion see below). Considering a

Table 2
Surface coverage, film thickness and electrode-kinetic parameters obtained for the PB anodic peak of different electrodes recorded in pH 1.7 (0.02 M HCl + 0.1 M KCl), except for m_{Na^+} and D_{Na^+} that were obtained in the presence of 0.02 M HCl + 0.1 M NaCl.

	Cycles	$\Gamma^0_{Fe^{3+}}$ (mol cm^{-2})	d (nm)	m_{K^+} (mA (V s^{-1})$^{-1/2}$)	D_{K^+} (cm^2 s^{-1})	m_{Na^+} (mA (V s^{-1})$^{-1/2}$)	D_{Na^+} (cm^2 s^{-1})	k_s (s^{-1})	α	S (A M^{-1} cm^{-2})
PB	10	7.25E−09	11.6	0.38	8.24E−12	0.17	2.59E−12	1.20	0.59	0.44
PB-CPC	10	1.71E−08	27.3	0.79	4.42E−11	0.42	2.12E−11	0.57	0.67	0.63
PB-BZT	10	2.04E−08	32.5	0.81	5.33E−11	0.44	2.53E−11	0.42	0.67	0.62
PB-CTAB	10	2.40E−08	38.3	0.89	8.53E−11	0.55	4.58E−11	0.41	0.70	0.63

reversible diffusion-controlled process and using Eq. (4) at 25 °C [36]:

$$I_{ox} = 2.69 \times 10^5 n^{3/2} A C D^{1/2} v^{1/2} \quad (4)$$

where D is the apparent diffusion coefficient of cation and C the concentration of cation in the PB film. C_{K^+}, concentration of potassium in the film, has been calculated for each film according Purnaghi-Azar et al. [37,38], and finally the apparent diffusion coefficient for potassium, D_{K^+}, has been obtained from the slope (m_{K^+}) of I_{ox} against $v^{1/2}$ (Table 2). These data reveal that the permeability of the modified PB film was greater than the unmodified one ($D_{K^+\ unmodified} = 8.24 \times 10^{-12}$ cm^2 s^{-1}), by almost an order of magnitude, and PB-CTAB film showed the highest value ($D_{K^+\ PB\text{-}CTAB} = 8.53 \times 10^{-11}$ cm^2 s^{-1}). Thus modified films, with increased porosity and lower rigidity for facile entry and exit of charge compensating K^+ ions, can facilitate interconversion between PB ↔ PW forms and enhance its electrochemical properties.

Permeability for Na^+, with higher hydrated diameter (0.37 nm), was also obtained for all films, in a similar way to K^+. During these studies background electrolyte consisted of a solution of 0.02 M HCl and 0.1 M NaCl (pH 1.7). These data (m_{Na^+}, D_{Na^+}) are reported in Table 2. Permeability for this larger hydrated cation was lower than the values obtained for K^+. Nevertheless, D_{Na^+} for all modified films are greater than D_{K^+} for the unmodified film, highlighting the beneficial effect of surfactants and the enhancement of PB electrochemical properties. However, a significant current decrease and a negative shift of $E^{0\prime}$ occurred when films were cycled (at 0.1 V s^{-1} in the presence of Na^+), indicating that although crystallinity and lattice defects have been improved, lattice channel size is enough to allow freer diffusion of Na^+. In this context it is interesting to compare CVs (in 0.02 M HCl and 0.1 M KCl) before and after cycling PB films in a medium containing Na^+ ions (50 cycles at 0.1 V s^{-1} in 0.02 M HCl and 0.1 M NaCl) (see Fig. 3). The surfactant-modified PB films recovered by ~86% (I_{after}/I_{before}) of the initial current (I_{ox}), whereas unmodified PB films reached a value of only ~40%, indicating a significant degradation. These data reveal that the irreversible damage due to the insertion of hydrated Na^+ ions is attenuated for surfactant-modified PB films, and is consistent with higher D_{Na^+} values obtained for modified films reported in this work and by others [21].

3.3. Charge transfer rate of PB films

Surfactant-modified PB films displayed higher values of peak separation, ΔE_p, than the unmodified film. Nevertheless all films showed an increase in ΔE_p when the scan rate was increased, characteristic of quasi-reversible electrochemistry. This behavior was accentuated in modified PB films even at low scan rate (0.04 V s^{-1}) where unmodified PB films displayed the lowest ΔE_p value (see Table 1). Fig. 4(A) shows a CV obtained for a PB-CTAB film scanning from 0.03 to 0.9 V s^{-1}. Plotting I_{ox} and I_{rd} against v and $v^{1/2}$ (Fig. 4(B) and (C), respectively) we can observe how peak currents are linearly proportional to the scan rate between a range of 0.03–0.15 V s^{-1}, suggesting that the kinetic limitations are

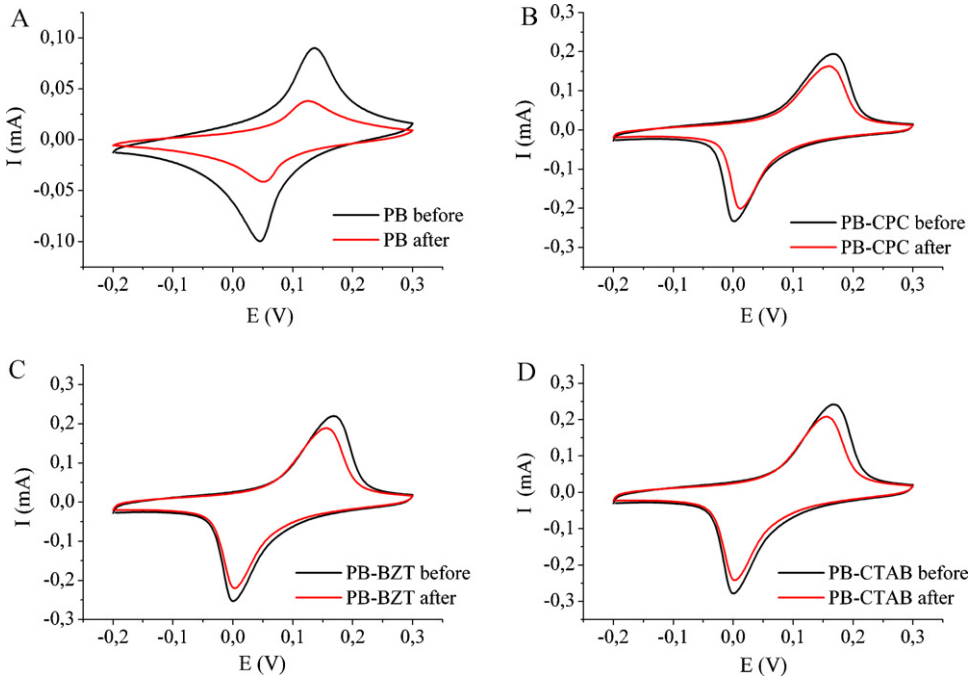

Fig. 3. CVs of PB deposited in the presence of 1 mM CTAB at different scan rates (ranging from 0.005 to 0.9 V s^{-1}) in background electrolyte solution. (B) Non-linear dependence of anodic and cathodic peak currents of PB-CTAB modified SPCE on the potential scan rate (v). (C) Linear dependence of anodic and cathodic peak currents of PB-CTAB modified SPCE on the square root of v. (D) Dependence of anodic and cathodic potential of PB-CTAB modified SPCE on log v.

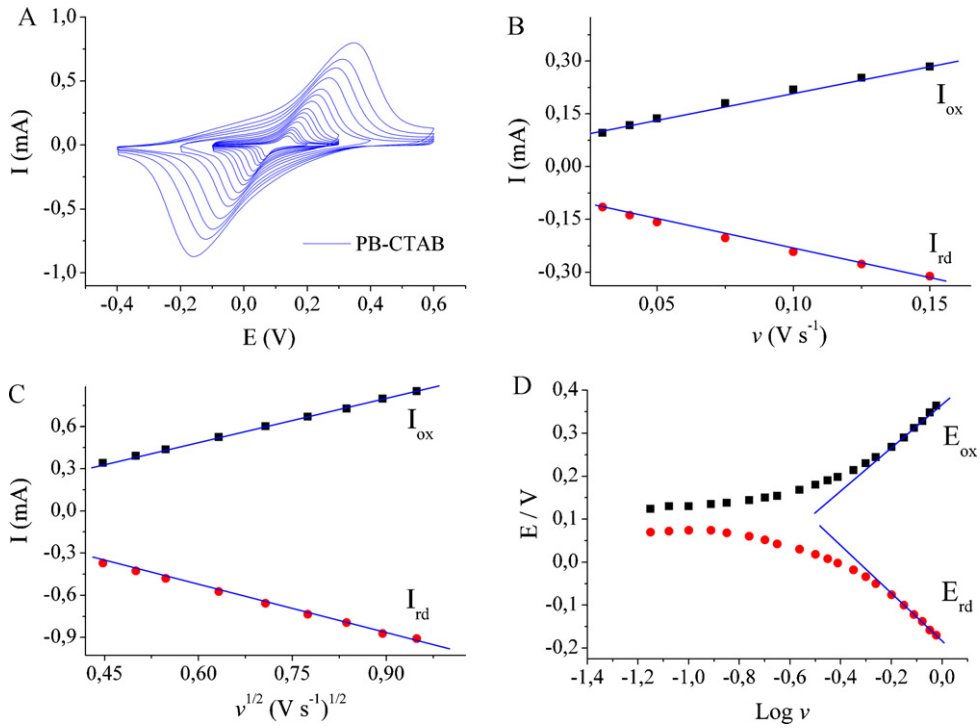

Fig. 4. CVs of different H_2O_2 sensor in background solution (0.02 M HCl and 0.1 M KCl) before and after cycling PB films in presence of Na^+ (0.02 M HCl and 0.1 M NaCl) during 50 cycles at a scan rate of 0.1 V s^{-1}.

associated mainly with charge propagation in the film. Nevertheless at higher scan rates 0.2–0.9 V s^{-1} the anodic and cathodic peaks are linearly proportional to the square root of scan rate, which is expected for a diffusion-controlled process. Similar results were found for the other three configurations (data not shown). These data reveal that electrochemistry of PB immobilized on an electrode is complicated by the possibility that either electron transfer or diffusion of counterions through the matrix might be rate determining depending on the experimental conditions, including scan rate, as showed previously Pournaghi-Azar et al. [38].However, the greater ΔE_p values obtained at higher scan rate may result from limiting charge transfer kinetics. Plotting E_{ox} and E_{rd} against log(v) (Fig. 4(D)) we obtain a linear dependence at high v as indicated by Laviron [39]. Similar results were found for the other films. Finally, kinetic parameters, such as the surface electron transfer rate constant (k_s) and the transfer coefficient (α) were calculated (see Table 2) from the linear E_{ox} versus log(v) plot based on Laviron's equation (Eq. (5)), derived for $\Delta E_p > 200/n$ mV [37]:

$$E_{ox} = E^{0'} + \left[\frac{RT}{(1-\alpha)nF}\right] \ln\left\{\left[\frac{(1-a)nF}{RT}\right]\left[\frac{v}{k_s}\right]\right\} \quad (5)$$

where

$$\text{slope} = \frac{2.303RT}{(1-a)nF} = S \quad (6)$$

$$\text{intercept} = E^{0'} + S\log\left(\frac{2.303}{S}\right) - S\log(k_s) \quad (7)$$

where $E^{0'}$ was obtained for each film experimentally. For the unmodified film, k_s gave a value of 1.2 s^{-1} that is in good agreement with data reported previously for PB and analogues [23,37,38]. The α value ($\alpha = 0.59$) obtained indicates that the redox transition state is not fully symmetrical. Interestingly, for films prepared under similar conditions ΔE_p values for modified films was higher than for the unmodified PB film (see Table 1); this finding together with the k_s and α values (see Table 2) obtained for modified PB films suggest that electron-transfer rate is slower and displays a more irreversible behavior than for the unmodified film.

3.4. Sensitivity of PB films toward H_2O_2

For similar electro-deposition conditions (10 cycles), all surfactant-modified PB films displayed higher sensitivities toward H_2O_2 than for the unmodified PB film (Table 2). Fig. 5 shows a calibration curve for PB and PB-BZT films from 0 to 1.1 mM H_2O_2, showing clearly the higher sensitivity of the modified film. Fig. 5 (inset) denotes the CV response for background electrolyte solution and for this background solution plus 10 mM H_2O_2. In this case the catalytic reduction at PB-BZT film is again clear compared with the unmodified PB film. Even unmodified PB showed a hydrogen peroxide sensitivity of 0.44 A M^{-1} cm^{-2} that is ~3 [15,16] and ~2 [17] times higher than previous values reported in the literature for SPEs; see Table 3. The mean value for surfactant-modified PB gave a sensitivity of 0.63 ± 0.01 A M^{-1} cm^{-2} which is ~5 [15,16] and ~3 [17] times higher than previous, and is close to data reported by Liu et al. [40], using a platinum foil electrode modified with PB as a working electrode, and close to other PB configurations; see Table 3. However, this Pt-based sensor was fabricated by a self-assembly process, including multiple sequential adsorption of ferric and hexacyanoferrate ions, and represents a time-consuming method when compared with the electrochemical method reported in the present work. Notably, Razmi et al. [41] described a highly sensitive (0.76 A M^{-1} cm^{-2}) H_2O_2 electrochemical sensor based on self-assembled PB nanoparticles on a carbon ceramic electrode, which exhibited good mechanical and electrochemical stability compared with other PB based H_2O_2 sensors [see references in 42].

A more detailed study of the two configurations (unmodified PB and modified PB-BZT films) showed similar time response for the two cases ($t_{90\%}$ ~ 4 s). Nevertheless, linearity in the range from 0 to 400 μM H_2O_2 was improved slightly in the modified film ($r^2 = 0.998$) compared with the basic configuration ($r^2 = 0.992$).

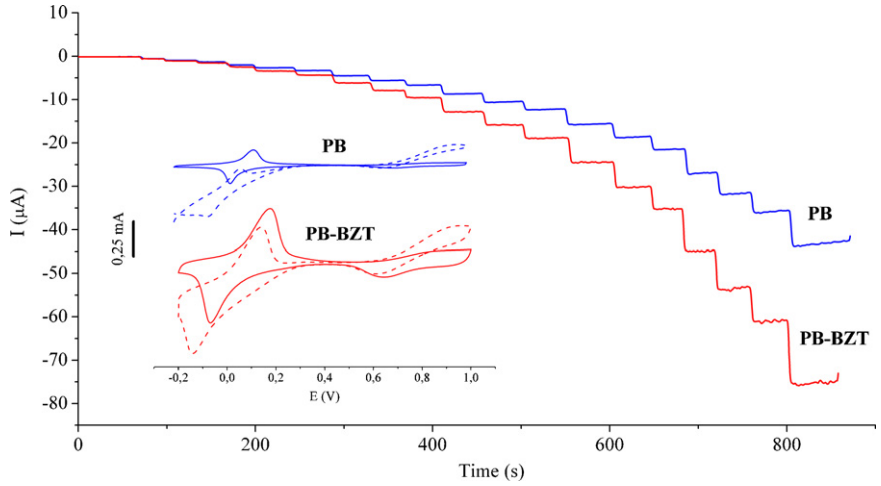

Fig. 5. Calibration curves from 0 to 1.1 mM H_2O_2 for PB and PB-BZT films recorded at −0.05 V in a stirred background electrolyte solution (0.1 M KCl, 0.02 HCl). Inset: cyclic voltammogram recorded at 0.1 V s^{-1} for PB and PB-BZT films in background electrolyte solution (solid) and in background solution plus 10 mM H_2O_2 (dashed).

H_2O_2 detection limits were calculated on the basis of a signal to noise ratio of 3 in a background electrolyte solution. While PB displayed a detection limit of 2.6×10^{-7} M, the value for the PB-CTAB sensor was 1.6×10^{-7} M showing a slight improvement of the detection limit, and both of which were more than adequate for most biosensor applications. Comparing the optimized PB sensor reported in the present work with similar sensitivity devices [41], our configuration exhibited a lower LOD and higher operational range, while allowing a perfect control of the amount of PB deposited, and hence represents a versatile approach for future development of microsensor devices [22].

3.5. Stability of PB films

The stability of modified and unmodified films was analyzed by cycling SPCEs over 250 successive cycles (see Fig. 6) in background solution at 0.1 V s^{-1} from 0.1 to 0.3 V (for ~33 min). The residual activity was calculated using the anodic peak intensity (I_n) for each measurement cycle and normalizing respect to the first one (I_1). Whereas the unmodified PB film showed a significant residual activity decay ($I_{250}/I_1 = 0.65$), typical for soluble PB forms [22], PB-BZT and PB-CTAB presented a slight increase ($I_{250}/I_1 = 1.2$) and PB-CPC remained invariant during all cycles. Kumar et al. [22] found similar behavior for PB-CTAB and suggested that this increase may be related to slow conversion of the insoluble PB to soluble form in modified PB films during continuous cycles. Nevertheless, PB-CPC behavior has not been described previously. Additional stability, especially in neutral media, may be obtained because CPC, BZT and CTAB are quaternary ammonium compounds and acting as an acid can nullify the effect of OH-ions, thereby stabilizing the PB film. Finally, electrostatic stabilization between cationic surfactants bilayers and clay layers may offer an additional stabilization mechanism to prevent its dissolution.

3.6. Lactate microbiosensor

Following design strategies of glucose microbiosensors developed by our group [12,13,42], we assembled a lactate microbiosensors (CFE/PB – BZT/Lox) based on PB – BZT modified CFEs. The main advance of the present configuration over classical biosensors

Table 3
Comparison of some analytical parameters of different PB sensors obtained with stirred batch amperometry.

Type of sensor	Deposition method	Applied potential (mV)	LOD (μM)	LR (μM)	S (mA M^{-1} cm^{-2})	Ref.
Carbon fiber electrode	Cyclic voltammetry	0	0.01	–	1000	[12]
Carbon fiber electrode	Cyclic voltammetry	0	0.1	–	480	[12]
Graphite screen printed electrode	PB microparticles mixed with carbon ink	0	0.25	0.4–100	137	[15]
Graphite screen printed electrode	Chemical deposition on graphite/GC mixed with carbon ink	−50	0.3	0.5–1000	135	[16]
Graphite screen printed electrode	Chemical deposition on graphite screen printed electrode	−50	0.1	0.1–50	234	[17]
Glassy carbon electrode	Cyclic voltammetry	0	0.036	0.079–15.8	153	[22]
Glassy carbon electrode	Cyclic voltammetry in presence of surfactant	0	0.012	0.0038–100	979	[22]
Platinum foil electrodes	Chemical deposition based on self-assembly process	−50	1	1–400	625	[40]
Carbon ceramic electrode	Chemical deposition based on self-assembly process	−100	0.8	1–260	755	[41]
Graphite screen printed electrode	Cyclic voltammetry	−50	0.26	0.26–400	440	This work
Graphite screen printed electrode	Cyclic voltammetry in presence of surfactant	−50	0.16	0.16–400	630	This work

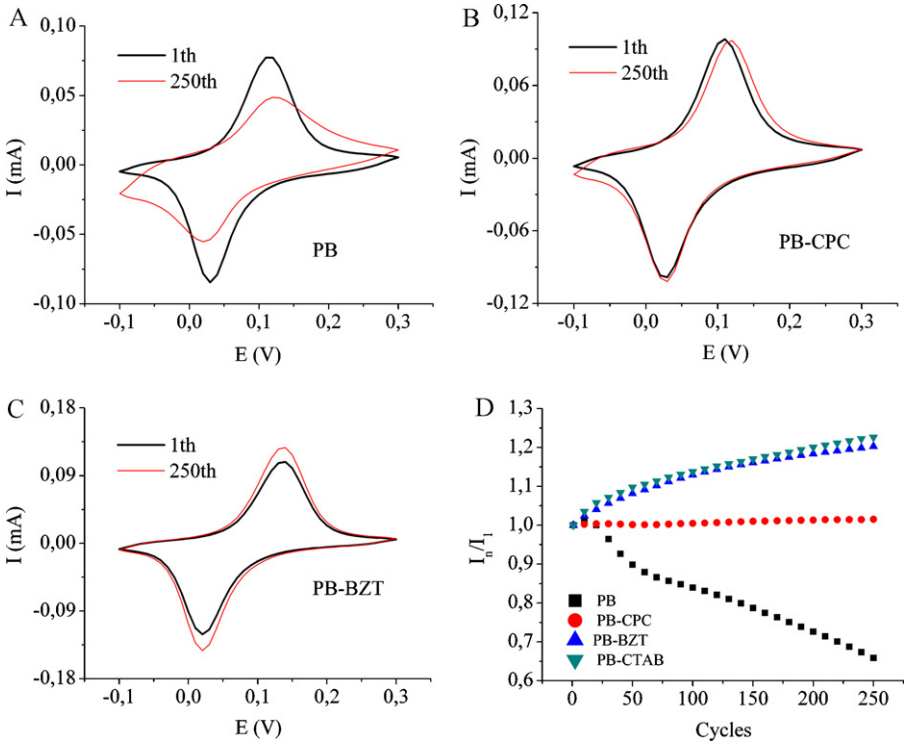

Fig. 6. First and 250th CVs for different H_2O_2 sensors – (A) PB, (B) PB-CPC and (C) PB-BZT – obtained cycling SPCEs over 250 successive cycles in background solution at 0.1 V s^{-1} from 0.1 to 0.3 V (~33 min) in background electrolyte solution (0.02 M HCl and 0.1 M KCl). (D) Evolution of the residual activity over the 250 cycles obtained as peak current ratio between the *n*th cycle and the first (I_n/I_1).

(based on the detection of over Pt, Pt–Ir, etc.) is its low dimensions and low applied working potential of ~0.0 V against SCE. These low dimensions (~10 μm diameter, 250 μm length) will allow its use in neuroscience applications. The modification protocol was described in detail above. Due to the PB stability issues discussed above, acidified K^+-containing media were used for many of the experiments to this point, and so an important question for biosensor applications is the functionality of PB-BZT films in physiological conditions. Biosensors were therefore calibrated in PBS (pH 7.4, 0.1 M NaCl).

Fig. 7(A) shows calibration data for lactate microbiosensors (mean ± SD, $n = 3$). Enzymatic parameters obtained using a Hill-modified Michaelis–Menten equation [43] were (mean ± SEM): the apparent Michaelis constant, $K' = 0.22 \pm 0.03$ mM; maximum response, $I_{max} = 2.76 \pm 0.08$ nA; and the Hill parameter, $h = 1.14 \pm 0.05$. Finally an external permselective film,

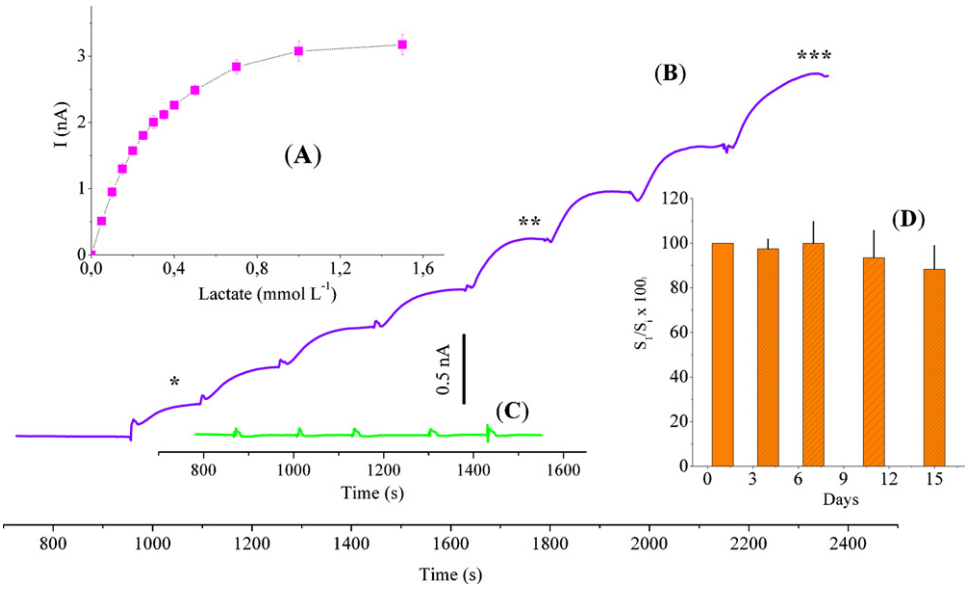

Fig. 7. (A) Calibration curve in PBS for lactate microbiosensors, CFE/PB – BZT/Lox (diameter: ~10 μm and length: 250 μm), working at 0 V vs. SCE (mean ± SD $n = 3$). (B) Calibration raw data for CFE/PB – BZT/Lox/PoPD microbiosensor for 4 successive additions of 0.1 mM lactate (*), 3 successive additions of 0.2 mM (**) and 1 addition of 0.4 mM (***). (C) CFE/PB – BZT/Lox/PoPD response for 5 successive additions of 0.2 mM AA. (D) CFE/PB – BZT/Lox/PoPD stability during a period of 15 days (mean ± SD, $n = 3$).

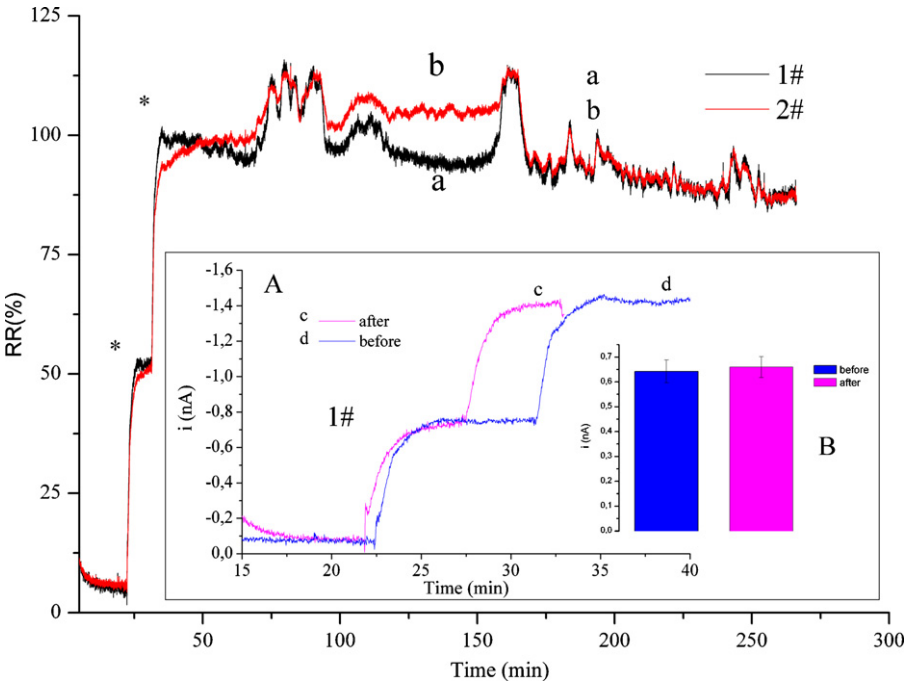

Fig. 8. Temporal evolution of retained response (RR%) for two CFE/PB – BZT/Lox/PoPD biosensors after 2 × 0.2 mM lactate in physiological saline (PBS pH: 7.4, 0.1 M NaCl) at 0 V vs. SCE; (*) denotes 0.2 mM lactate additions. Inset: (A) biosensor response (1#) to 0.2 mM lactate additions in physiological saline before and after being exposed to physiological saline for 5 h. (B) Sensitivity for 0.2 mM lactate additions for previous data (inset A) ($n = 3$).

poly-o-phenylenediamine (PoPD), was added to the microbiosensor. Fig. 7(B) shows raw calibration data for a CFE/PB-BZT/Lox/PoPD microbiosensor. Due to the additional diffusion layer (PoPD), the linear range was slightly increased to ~0.5 mM, and no response was obtained after 5 successive additions of 0.2 mM ascorbic acid, the main biosensor interference species in neuroscience applications [41] (Fig. 7(C)). Nevertheless, for future work the lactate microbiosensor design will be revised in order to increase the operational lineal range for in vivo studies where lactate basal level is close to 0.3 mM, but higher levels may be reached during neuronal activity.

Following on from the PB stability issues discussed above, biosensors were calibrated in PBS and their responses evaluated over several hours (Fig. 8). These lactate microbiosensors showed highly stable response over ~5 h, showing only a ~10% signal decrease. Lactate sensitivity (~3.7 nA mM^{-1}) was compared before and after long time exposure to physiological saline. As is shown in Fig. 8 (insets A and B), no significance difference was found (two-tailed t-test, p value > 0.65, $n = 3$) suggesting that Lox is well immobilized and PB-BZT films are stable in slightly basic media containing NaCl. Finally, the stability over a long period (days) in physiological saline was evaluated and expressed as $S_i/S_1 \times 100$ where S_1 is the sensitivity on the first day and S_i is the sensitivity for successive i-days, was calculated. For the considerable time period studied (15 days), these lactate microbiosensors displayed an excellent stability (~88%, Fig. 7(D)) and no significant difference compared with day 1 (two-tailed unpaired t-test, $p > 0.05$).

4. Conclusions

It is shown here for the first time that all cationic surfactants employed in the present work promote the electro-deposition of PB onto SPCEs, and the enhancement of their electrochemical properties. Surfactant-modified electrodes displayed a consistently higher surface concentration value (~2.05×10^{-8} mol cm^{-2}) relative to the unmodified PB film (7.25×10^{-9} mol cm^{-2}) indicating that PB deposition is more efficient when cationic surfactants are presented in the precursor solution. Consequently, modified films formed from 10 electro-deposition CV cycles showed a thickness of ~33 nm, whereas the PB film electro-deposited without any surfactant was only ~12 nm thick.

The permeability of the modified PB film for K^+ ions, D_{K^+}, was greater than the unmodified one (8.24×10^{-12} cm^2 s^{-1}), by almost an order of magnitude, with the PB-CTAB film showing the highest value (8.53×10^{-11} cm^2 s^{-1}). Modified PB films recovered by ~86% of the initial current after being cycled in solution with Na^+ ions, whereas unmodified PB film reached a value of only ~40%, revealing that irreversible damage due to the insertion of hydrated Na^+ ions was attenuated in surfactant-modified PB films. Hydrogen peroxide sensitivity for surfactant-modified PB films for 10 electro-deposition cycles gave a value of 0.63 A M^{-1} cm^{-2} and represents the highest values ever reported in the literature for SPCEs. Finally, our preliminary results assembling a lactate microbiosensor (CFE/PB – BZT/Lox/PoPD) were presented as the first step to obtain an optimized device that may be used in future neurophysiological studies.

Acknowledgments

The funds for the development of this device have been provided by the following national public grants: ULLAPD-08/01 granted by the Agencia Canaria de Investigación, Innovación y Sociedad de la Información, Ministerio de Industria, Turismo y Comercio (AVANZA) TSI-020100-2008-337 and Ministerio de Ciencia e Innovación (CICYT) TIN2008-06867-C02-01/TIN.

References

[1] A. Abbaspour, M.A. Kamyabi, J. Electroanal. Chem. 584 (2005) 117.
[2] V.D. Neff, J. Electrochem. Soc. 125 (1978) 886.
[3] J. Li, X. Wei, Y. Yuan, Sens. Actuators B 139 (2009) 400.
[4] T. Lenarczuk, S. Gła, R. Koncki, J. Pharmaceut. Biomed. 26 (2001) 163.
[5] K. Itaya, N. Shoji, I. Uchida, J. Am. Chem. Soc. 106 (1984) 3423.
[6] A.A. Karyakin, O. Gitelmacher, E.E. Karyakina, Anal. Lett. 27 (1994) 2861.
[7] A.A. Karyakin, M. Chaplin, J. Electroanal. Chem. 56 (1994) 85.

[8] A.A. Karyakin, E.E. Karyakina, Sens. Actuators B 57 (1999) 268.
[9] B. Haghighi, S. Varma, F.M. Alizadeh, Y. Yigzaw, L. Gorton, Talanta 64 (2004) 3.
[10] H. Shi, Y. Yang, J. Huang, Z. Zhao, X. Xu, J. Anzai, T. Osa, Q. Chen, Talanta 70 (2006) 852.
[11] X. Wang, H. Gu, F. Yin, Y. Tu, Biosens. Bioelectron. 24 (2009) 1527.
[12] P. Salazar, M. Martín, R. Roche, R.D. O'Neill, J.L. González-Mora, Electrochim. Acta 55 (2010) 6476.
[13] P. Salazar, M. Martín, R. Roche, J.L. González-Mora, R.D. O'Neill, Biosens. Bioelectron. 26 (2010) 748.
[14] J. Wang, X. Zhang, Anal. Lett. 32 (1999) 1739.
[15] M.P. O'Halloran, M. Pravda, G.G. Guilbault, Talanta 55 (2001) 605.
[16] F. Ricci, A. Amine, C.S. Tuta, A.A. Ciucu, F. Lucarelli, G. Palleschi, D. Moscone, Anal.Chim. Acta 485 (2003) 111.
[17] F. Ricci, A. Amine, G. Palleschi, D. Moscone, Biosens. Bioelectron. 18 (2003) 165.
[18] R. Vittal, M. Jayalakshmi, H. Gomathi, G. Prabhakara Raoa, J. Electrochem. Soc. 146 (1999) 786.
[19] R. Vittal, H. Gomathi, G. Prabhakara Rao, Electrochim. Acta 45 (2000) 2083.
[20] R. Vittal, H. Gomathi, K.J. Kim, Adv. Colloid Interface 119 (2006) 55.
[21] R. Vittal, K.J. Kim, H. Gomathi, V. Yegnaraman, J. Phys. Chem. B 112 (2008) 1149.
[22] S.M. Senthil Kumar, K. Chandrasekara Pillai, Electrochem. Commun. 8 (2006) 621.
[23] S.M. Senthil Kumar, K. Chandrasekara Pillai, J. Electroanal. Chem. 589 (2006) 167.
[24] K. Itaya, T. Ataka, S. Toshima, J. Am. Chem. Soc. 104 (1982) 4767.
[25] K. Itaya, T. Ataka, S. Toshima, T. Shinohara, J. Phys. Chem. 86 (1982) 2415.
[26] A.A. Karyakin, Electroanalysis 13 (2001) 813.
[27] F. Herren, P. Fischer, A. Ludi, W. Halg, Inorg. Chem. 19 (1980) 956.
[28] E.W. Anacker, J. Phys. Chem. 62 (1958) 41.
[29] A.B. Mandal, B.U. Nair, J. Phys. Chem. 95 (1991) 9008.
[30] T.V. Vladimirova, L.M. Ramenskaya, Russ. J. Phys. Chem. 80 (2006) 836.
[31] H.H. Paradies, U. Hinze, M. Thies, Berich. Bunsen.Gesell. 98 (1994) 938.
[32] F. Kopecký, B. Kopecká, P. Kaclík, Ceska Slov. Farm. 55 (2006) 175.
[33] K. Itaya, K. Shibayama, H. Akahoshi, S. Toshima, J. Appl. Phys. 53 (1982) 804.
[34] J.J. García-Jareño, D. Giménez-Romero, F. Vicente, C. Gabrielli, M. Keddam, H. Perrot, J. Phys. Chem. B 107 (2003) 11321.
[35] F. Ricci, G. Palleschi, Biosens. Bioelectron. 21 (2005) 389.
[36] J. Wang, Analytical Electrochemistry, third ed., John Wiley & Sons Inc., New Jersey, 2006.
[37] M.H. Pournaghi-Azar, H. Razmi-Nerbin, Electroanalysis 12 (1999) 209.
[38] M.H. Pournaghi-Azar, N. Nahalparvari, J. Solid State Electrochem. 8 (2004) 550.
[39] E. Laviron, J. Electroanal. Chem. 101 (1979) 19.
[40] Y. Liu, Z. Chua, W. Jin, Electrochem. Commun. 11 (2009) 484.
[41] H. Razmi, R. Mohammad-Rezaei, H. Heidari, Electroanalysis 21 (2009) 2355.
[42] P. Salazar, R.D. O'Neill, M. Martín, R. Roche, J.L. González-Mora, Sens. Actuators B 152 (2011) 137.
[43] S.S. El Atrash, R.D. O'Neill, Electrochim. Acta 40 (1995) 2791.

Journal of Electroanalytical Chemistry 674 (2012) 48–56

Contents lists available at SciVerse ScienceDirect

Journal of Electroanalytical Chemistry

journal homepage: www.elsevier.com/locate/jelechem

Improvement and characterization of surfactant-modified Prussian blue screen-printed carbon electrodes for selective H_2O_2 detection at low applied potentials

P. Salazar [a,*], M. Martín [a], R.D. O'Neill [b], R. Roche [a], J.L. González-Mora [a]

[a] Neurochemistry and Neuroimaging Group, Faculty of Medicine, University of La Laguna, Tenerife, Spain
[b] UCD School of Chemistry and Chemical Biology, University College Dublin, Belfield, Dublin 4, Ireland

ARTICLE INFO

Article history:
Received 7 February 2012
Received in revised form 30 March 2012
Accepted 9 April 2012
Available online 19 April 2012

Keywords:
Prussian blue
Screen-printed carbon electrodes (SPCEs)
Surfactant
Benzethonium chloride (BZTC)
H_2O_2 sensor

ABSTRACT

The development of a highly selective and sensitive H_2O_2 sensor, based on the electro-deposition of Prussian blue (PB) onto screen-printed carbon electrodes (SPCEs) modified by benzethonium chloride (BZTC), is described. This methodology provides a time-efficient method for producing stable films in the presence of a BZTC concentration which was optimized with respect to electrochemical and electroanalytical properties. Some parameters such as the amount of PB deposited, film thickness, reversibility, permeability, stability, electrocatalytic properties and sensitivity to H_2O_2 were considered in order to select the optimal sensor. Under optimal conditions (2 mM BZTC), the surface coverage and apparent diffusion coefficient for K^+ displayed values of $6.4 \pm 0.2 \times 10^{-8}$ mol cm^{-2} and 5.2×10^{-11} cm^2 s^{-1}, respectively, one order of magnitude higher than without surfactant. The catalytic rate constant for the optimized film was 2.8×10^3 M^{-1} s^{-1} which was in good agreement with data found in the literature. BZTC(2 mM)/PB operating at ~0 V vs. SCE displayed the highest H_2O_2 sensitivity (1.07 ± 0.03 A M^{-1} cm^{-2}, $n = 5$) reported in the literature to date for PB-modified SPCEs, and showed an excellent limit of detection (<10^{-7} M) and linearity range (up to ~1.5 mM). Sensors incorporating BZTC were significantly more stable in media containing Na^+ ions, even at neutral pH, than unmodified devices, critical properties for sensor applications in biological environments. Finally, BZTC(2 mM)/PB-based sensors stored dry at room temperature over 4 months retained the ~90% of their initial response to H_2O_2, a useful property for commercial applications.

1. Introduction

Prussian blue (PB) is a hexacyanoferrate with two different iron valences (+2 and +3) and was initially developed as a blue pigment in the 1700s [1]. Since Neff [2] reported for the first time the successful deposition of a thin layer on a platinum foil and Itaya et al. [3] showed that the reduced form of Prussian blue (also called Prussian white, PW) had a catalytic effect on the reduction of both O_2 and H_2O_2, many publications have appeared exploring its electrocatalytic, electromagnetic and electrochromic properties [4]. Following reports by Karyakin et al. [5] that PB was an excellent material for use in the fabrication of biosensors because it acts as an artificial peroxidase, its applications in the biosensor field have continued to diversify. In addition, other useful properties such as non-toxicity, high electrocatalytic activity and low operating overpotential have contributed to the diversification of its use in enzyme-based biosensors [4–6] and label-free immunosensors [7–10].

However, the stability of PB during operation remains a central problem, especially in basic and neutral media which is an optimal condition for the majority of enzymes employed in biosensor applications. The reason for this behavior is ascribed to the strong interaction between ferric ions and hydroxide ions to form $Fe(OH)_3$ at pH higher than 6.4 [11], leading to the destruction of the Fe–CN–Fe bond, and solubilizing PB [12]. To solve this problem, numerous approaches (more or less complicated and tedious) have been developed, such as: (1) modifying the chemical and/or electrochemical deposition of PB [13–15]; (2) adding external protective polymer films, such as poly(o-phenylenediamine), poly(o-aminophenol), poly(vinylpyrrolidone), and Nafion [16–19]; (3) using additives in the working solution, such as tetrabutylammonium toluene 4-sulfonate [20].

Focusing on the last of these approaches, surfactants have been employed in a great number of applications in chemistry [21], exploiting their tendency to accumulate at a surface or interface between two different bulk phases, such as the electrode-solution interface. This property has been utilized in recent years in the

* Corresponding author. Tel.: +34 922319363.
E-mail address: psalazar@ull.es (P. Salazar).

1572-6657/$ - see front matter © 2012 Elsevier B.V. All rights reserved.
http://dx.doi.org/10.1016/j.jelechem.2012.04.005

surface modification of electrodes with PB and other hexacyananoferrates, where the presence of added surfactant offers enhanced film growth, improved stability and excellent electrochemical reversibility [22–24]. This new approach represents a fast and easy method to improve its electrocatalytic and electrochemical properties, and to increase its stability in neutral and basic media. Although, studies to date have focused mainly on the use of cetyltrimethyl ammonium bromide (CTAB), we have recently shown that other cationic surfactants such as benzethonium chloride (BZTC) may also be used successfully [25].

Here we optimize the electro-deposition method for BZTC, and study the electrochemical and analytical properties of different modified BZTC/PB films. The improved electro-deposition methods, pH stability and permeability of the optimized BZTC/PB film provide a further boost in its sensitivity for H_2O_2 detection, which can be a critical parameter in biosensor design and application.

2. Experimental

2.1. Reagents and solutions

All chemicals were obtained from Sigma and used as supplied. Stock solutions were prepared in doubly distilled water (18.2 MΩ cm, Millipore-Q), and stored at 4 °C when not in use.

2.2. Instrumentation

Screen-printed carbon electrodes (SPCEs) were purchased from DropSens, model DRP-110. Experiments were computer controlled, using data-acquisition software EChem™ for CV and Chart™ for CPA. The data-acquisition system used was e-Corder 401 (EDAQ) and a low-noise and high-sensitivity potentiostat, Quadstat (EDAQ). EIS experiments for sensor characterization were conducted with an Autolab PGSTAT 20 potentiostat and a FRA module from EcoChemie, computer controlled by their general purpose electrochemical system (GPES) and FRA software, respectively. Scanning electron micrographs (SEMs) were obtained using a JEOL JSM-6300 microscope.

2.3. PB electro-deposition

The background electrolyte solution consisted of (0.02 M HCl and 0.1 M KCl; pH, 1.7). Electro-deposition of the BZTC/PB composite film onto SPCEs was accomplished by placing a drop of background solution with 1.5 mM $FeCl_3$, 1.5 mM $K_3[Fe(CN)_6]$ and x mM BZTC onto the combined working electrode, silver pseudoreference and counter electrode. Finally, the SPCE was cycled between −0.2 and 1.0 V at a scan rate of 0.1 V s^{-1} (default 10 cycles). These sensors will be termed BZTC(x mM)/PB. The unmodified PB film was prepared under the same conditions except that the solution was free of surfactant. All electro-deposition and characterization were carried out using the internal silver pseudoreference (∼0.026 V against SCE in background solution at 25 °C).

2.4. PB characterization

Electrochemical characterization was done in background electrolyte at 0.1 V s^{-1}. However, to study the PB stability in Na^+-containing solutions, the background electrolyte solution consisted of 0.02 M HCl and 0.1 M NaCl (solution-*A*). PB stability as a function of pH was investigated in phosphate buffer and in background solution adjusted to different pH values, both in 0.1 M KCl. EIS measurements were performed in background electrolyte solution. The stabilization potential was set to +80 mV against SCE, the signal amplitude was 5 mV and the frequency range was 130 kHz−10 Hz. In order to obtain better SEMs, unmodified and modified PB films were electro-deposited onto Pt electrodes.

2.5. H_2O_2 sensor calibrations

H_2O_2 sensitivities were obtained according to the following protocol. The modified SPCEs were placed in 25 mL of a stirred background solution sample. The stock calibration solution of H_2O_2 (10 mM) was prepared in water just before use. When a stable current was reached in the background electrolyte (∼100 s) H_2O_2 aliquots were added and their response measured after 20 s. The response time ($t_{90\%}$) for the sensors was also determined in this way.

3. Results and discussion

3.1. Electrochemical characterization

Fig. 1A shows the CVs recorded during film formation for 10 cycles for PB and BZTC(2 mM)/PB films (scan rate 0.1 V s^{-1}). Right from the first cycle the CV response was greater during the formation of the BZTC(2 mM)/PB film. Taking into consideration that the charge under the CV trace is a measure of the amount of PB deposited (see Section 3.2), these results indicate that the presence of BZTC promotes the deposition of larger quantities of PB onto the SPCE surface. The BZTC concentration in the precursor solution was optimized in the range 0–5 mM, values straddling its critical micellar concentration ($cmc \sim 2.8$ mM) (Supplementary Material SM_figure 1). BZTC(x mM)/PB showed the characteristic CV peak pair at ∼0.07 V (PB ↔ PW (Prussian White) transition) and at ∼0.8 V (PB ↔ BG (Berlin Green) transition) [3–6]. Nevertheless, only the first peak pair was studied here because of its critical involvement in the electrocatalytic detection of H_2O_2 in first generation biosensor [4,6,16,25–27]. Fig. 1B shows that more PB was deposited when BZTC concentration was increased until 2 mM; at higher concentrations the CV amplitude decreased considerably, suggesting that electro-deposition is inhibited to some extent at higher surfactant concentration.

Peak charge, current and potential were calculated for different configurations and summarized in Table 1 (scan rate 20 mV s^{-1}). Current and charge data displayed similar behavior, showing higher values close to 2 mM BZTC (Q_{ox} = 0.544 mC). The formal potential, $E^{0'}$, also showed a minimum in this concentration region. The finding that Q_{ox}/Q_{rd} and I_{ox}/I_{rd} ratios for this quasi-reversible system were ∼1 under most conditions studied highlights the trapped nature of the electroactive centers on the electrode surface. Peak separation, ΔE (Table 1), which showed a strong correlation (>0.9) with both Q_{ox} and Q_{rd}, displayed a maximum value just below the *cmc* (∼0.1 V), significantly greater than the ideal reversible value of 0 V and indicating an increased energy of activation for this redox process in the thicker layers. The data for all configurations are consistent with the mono-electronic process characteristic of the PB system [3,16]. Furthermore, the more detailed BZTC concentration profiles shown in Table 1 and the Supplementary Material SM_figure 2 indicate its optimal level in the electrodeposition solution was close to 2.0 mM.

The charge under the oxidation (forward) peak during PB electro-deposition was taken as *charge storage capacity* (Q_{for}) and was calculated for different configurations cycling SPCEs over 120 successive cycles SM_figure 2. Again a maximum value (∼1.7 mC) was obtained at 2 mM BZTC. Above this concentration a clear inhibition effect appeared. This finding may be related with the stabilization of the miscelles with $Fe(CN)_6^{3-}$ anions after the *cmc* is reached. The lower *cmc* value in our precursor solution may be explained taking account that Cl^- and $Fe(CN)_6^{3-}$ anions decrease the solvation of the hydrophilic part of the BZT^+ molecules and reduce the electrostatic

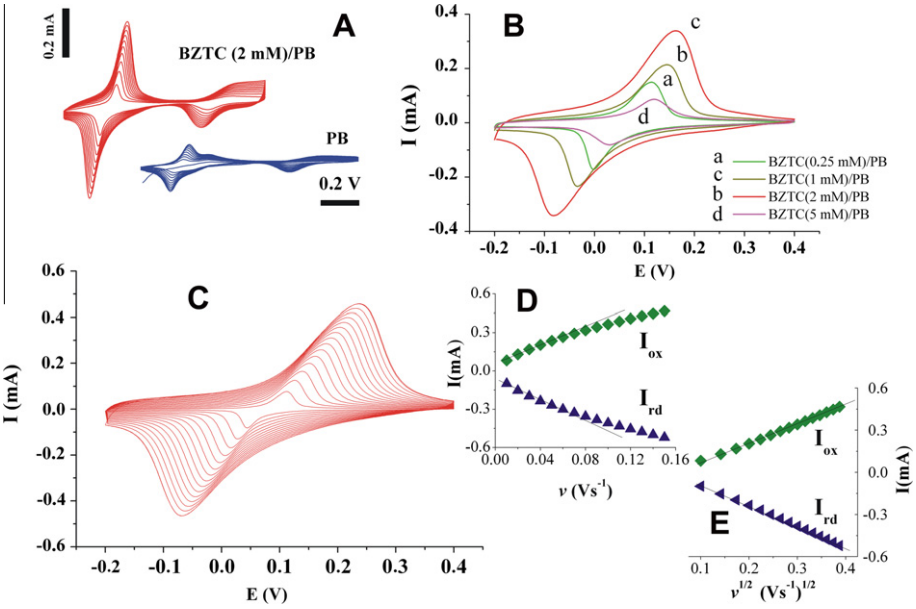

Fig. 1. (A) CV for PB electro-deposition onto SPCE without (PB) and with 2 mM BZTC (BZTC(2 mM)/PB) at 0.1 V s^{-1} against the internal silver pseudoreference. (B) CV of BZTC(*x* mM)/PB (scan rate of 0.1 V s^{-1}). (C) CVs of BZTC(2 mM)/PB at different scan rates (ranging from 10 to 150 mV s^{-1}) in background electrolyte (0.02 M HCl and 0.1 M KCl); (D) dependence of peak currents on the scan rate and the square root of scan rate (E).

Table 1
Cyclic voltammetric parameters, surface coverage and film thickness for different PB sensors obtained in background electrolyte (0.02 M HCl and 0.1 M KCl) at a scan rate of 0.02 V s^{-1}.

BZTC (*x* mM)/PB	I_{rd} (mA)	I_{ox} (mA)	I_{rd}/I_{ox}	E_{rd} (V)	E_{ox} (V)	δE (V)	$E^{o'}$ (V)	Q_{rd} (mC)	Q_{ox} (mC)	Q_{rd}/Q_{ox}	$(Q_{ox})_i/(Q_{ox})$ 2 mM	$\Gamma^0_{Fe^{3+}}$ (mol cm^{-2})	*d* (nm)
0	−0.048	0.037	−1.293	0.040	0.090	0.050	0.065	−0.108	0.096	−1.128	0.191	9.71E−09	16.34
0.25	−0.063	0.044	−1.432	0.052	0.108	0.056	0.080	−0.138	0.131	−1.051	0.262	1.43E−08	28.99
0.5	−0.059	0.048	−1.239	0.060	0.118	0.058	0.089	−0.148	0.140	−1.057	0.279	1.53E−08	32.53
1	−0.084	0.070	−1.203	0.042	O.I24	0.082	0.083	−0.261	0.252	−1.038	0.502	2.75E−08	52.96
1.5	−0.116	0.111	−1.044	0.022	0.120	0.098	0.071	−0.481	0.462	−1.041	0.921	5.27E−08	101.93
2	**−0.140**	**0.133**	**−1.055**	**0.018**	**0.123**	**0.105**	**0.071**	**−0.582**	**0.554**	**−1.051**	**1.104**	**6.30E−08**	**122.60**
2.25	−0.135	0.125	−1.083	0.022	0.119	0.097	0.071	−0.510	0.502	−1.017	1.000	5.53E−08	108.32
3	−0.086	0.086	−1.009	0.034	0.109	0.075	0.072	−0.430	0.399	−1.077	0.796	4.36E−08	79.69
4	−0.050	0.050	−1.008	0.050	0.102	0.052	0.076	−0.260	0.218	−1.194	0.434	2 39E−08	48.64
5	−0.021	0.021	−1.019	0.072	0.104	0.032	0.088	−0.125	0.091	−1.375	0.182	9.97E−09	22.97

repulsion between charged hydrophilic parts. These effects favor the formation of micelles, and tend to decrease the *cmc* compared with that observed in water [21,23].

The beneficial effect of BZTC during electro-deposition may be understood according to Kumar's mechanisms for CTAB [24]. In our case, BZT^+ is absorbed forming a bilayer between the negative electrode surface (unmodified electrode or PB film) and solution. This positive bilayer containing well oriented BZT^+ shows higher reactivity towards $Fe(CN)_6^{3-}$, which is the precursor in forming PB. The process of alternate layer-by-layer deposition of PB and BZT^+ bilayer can continue in each successive potential cycle indefinitely until the reactant materials become exhausted in solution [24]. With this mechanism, it is suggested that, when surfactant concentration exceeds its *cmc*, $Fe(CN)_6^{3-}$-stabilized micelles decrease free $Fe(CN)_6^{3-}$ in the bulk solution and hence inhibits PB electro-deposition.

3.2. Surface coverage and morphological study

The surface coverage of the electroactive species generated from the PW → PB transition, $\Gamma^0_{Fe^{3+}}$, was determined in background electrolyte and calculated using the following equation:

$$\Gamma^0_{Fe^{3+}} = Q_{ox}/nFA \quad (1)$$

where *n* the number of electrons consumed (*n* = 1), *F* is the Faraday constant, and *A* the electrochemical surface area (cm^2) of the bare SPCE calculated using the Randles–Sevcik equation for a reversible electrochemical process under diffusion control (*T* = 25 °C):

$$I_p = 2.69 \times 10^5 n^{3/2} A C D^{1/2} v^{1/2} \quad (2)$$

where *C* is the concentration (mol cm^{-3}) of the electroactive molecule, *D* is its diffusion coefficient, and *v* is the scan rate (V s^{-1}). The area was determined using $Fe(CN)_6^{3-}$ in 0.1 M KCl background electrolyte ($D = 6.3 \times 10^{-6}$ cm^2 s^{-1} for 0.5 mM $Fe(CN)_6^{3-}$ in 0.1 M KCl) [28]. The electrochemical area of the bare SPCE from DropSens thus determined was 0.095 cm^2 (*CV*% = 2.2, *n* = 4) and represents only 75% of the geometrical area (0.126 cm^2). This result indicates that the rough carbon is partially passivated due to surface contaminants or organic binder of the carbon ink, and the value is in good agreement with previous data in the literature [29].

The PB film deposited in the absence of BZTC showed a $\Gamma^0_{Fe^{3+}}$ value of 9.61 ± 0.24 × 10^{-9} mol cm^{-2} (mean ± SD, *n* = 3) and is in good agreement with the amount of PB deposited by other authors using different protocols [30,31]. $\Gamma^0_{Fe^{3+}}$ for the BZTC-modified electrodes studied here displayed a consistently higher value with the highest $\Gamma^0_{Fe^{3+}}$ value (6.43 ± 0.16 × 10^{-8} mol cm^{-2}, *n* = 8) corresponding to the BZTC(2 mM)/PB film, approximately seven times higher than

without surfactant. Based on the value of $\Gamma^0_{Fe^{3+}}$, the electro-deposition method gave an excellent reproducibility (*CV*% = 2.5, *n* = 8), in agreement with values reported by other authors [14,32] and providing a time-efficient method.

Morphological analysis was done by mean of scanning electron micrographs (SEMs). Fig. 2 shows PB films generated by cycling 120 times in the absence of surfactant (Fig. 2A) and with 2 and 6 mM BZT (Fig. 2B and C, respectively). The present analysis reveals a clear morphological difference, depending on the experimental conditions. Whereas the unmodified PB film showed a very thin deposit (appreciable only at higher magnifications), the BZTC(2 mM)/PB film displayed a significant amount of deposit with a columnar growing pattern of cubic structures onto a well-defined PB film background. In contrast, the BZTC(6 mM)/PB film formation appeared inhibited due to the high surfactant concentration, where a very thin and poor deposit was observed at higher magnification. This observation is in good concordance with the mechanism and electrochemical data discussed above. As expected, microanalysis (Fig. 2D and E) revealed a significant amount of Fe atoms in the films, confirming PB deposition onto the Pt electrodes used in the SEM studies. However, the Fe/Pt peak ratio was orders of magnitude greater for BZTC(2 mM)/PB compared with the unmodified PB film, confirming the higher deposition efficiency in the presence of surfactant inferred from the electrochemical data discussed above.

Finally, the thickness of the film, *d* (Table 1), was estimated by taking account of the number of unit cells present on the electrode surface, geometrical parameters of the PB cell, and the electrochemical surface area, according to Eq. (3) [25]:

$$d = (Q_{ox}/nFA)(l^3 N_A/4) = \Gamma^0_{Fe^{3+}}(l^3 N_A/4) \quad (3)$$

where N_A is Avogadro's number and *l* is the length of the unit cell (1.02 nm) [4]. Although this value must be considered an estimation because the density of the modified film is not available, BZTC(2 mM)/PB film showed a thickness of ~122 nm whereas the PB film electro-deposited without any surfactant was only ~16 nm thick, the latter value being in good agreement with previous work [25]. This finding confirms that thicker films are obtained in the presence of BZTC and thickness showed a similar evolution vs. surfactant concentration as discussed above.

3.3. Permeability properties

As can be seen in reaction (4), PB redox behavior depends on the free diffusion of cationic species across the film [4]. Due to this mechanism, only cations with small hydrated radii, such as K^+, NH_4^+, Rb^+ and Cs^+, can support this electrochemical activity by diffusing across the PB structure during iron center oxidation/reduction [4].

$$(PB)Fe_4^{(III)}[Fe^{(II)}(CN)_6]_3 + 4e^- + 4K^+ \leftrightarrow (PW)K_4Fe_4^{(II)}[Fe^{(II)}(CN)_6]_3 \quad (4)$$

In order to demonstrate the beneficial effects of modified BZTC/PB films on ionic transport, the permeability for K^+ was investigated by plotting peak currents (I_{ox} and I_{rd}), Fig. 1C, against the scan rate (v) and the square root of the scan rate ($v^{1/2}$). This analysis (for the BZTC(2 mM)/PB film) demonstrated that peak currents were linearly proportional to scan rate at low scan rates ($v < 50$ mV s^{-1}), Fig. 1D, suggesting that the kinetic limitations were associated mainly with charge propagation in the film. At higher scan rates, however, the anodic and cathodic peaks were linearly proportional to the $v^{1/2}$, Fig. 1E, which is expected for a diffusion-controlled process. These data revealed that the electrochemistry of PB immobilized on an electrode is complicated by the possibility that either electron transfer or diffusion of counterions through the matrix might be rate determining depending on the experimental conditions, including scan rate.

Trends in the apparent diffusion coefficient for potassium in the film, D_{K^+}, for different PB configurations were determined from the

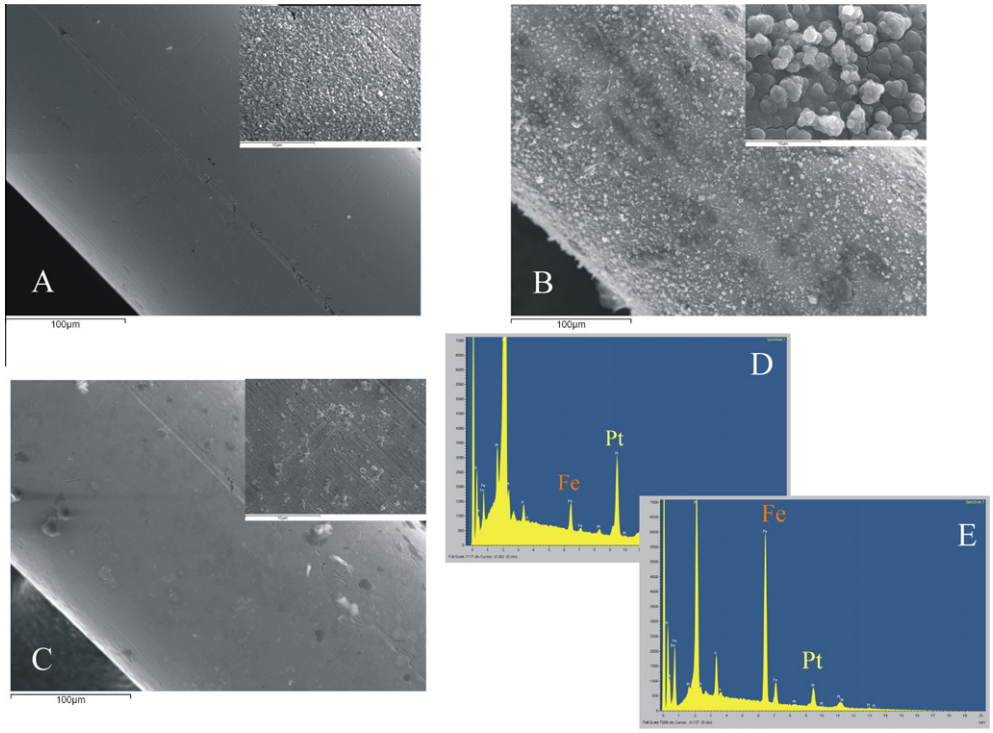

Fig. 2. Scanning electron micrographs (SEMs) at a 350 and 5000 magnification for: (A) PB, (B) BZTC(2 mM)/PB and (C) BZTC(6 mM)/PB electrodes. All films were deposited onto Pt over 120 successive cycles between −0.2 and 1.0 V at a scan rate of 0.1 V s^{-1}. Microanalysis of the of PB (D) and BZTC(2 mM)/PB (E) films.

Table 2
Apparent diffusion coefficient for potassium, D_{K^+}, for different sensor configurations obtained in background electrolyte (0.02 M HCl + 0.1 M KCl).

BZTC (x mM)/PB	A (cm^2)	$\{D_{K^+}\}_{ox}$ ($cm^2\ s^{-1}$)	$\{D_{K^+}\}_{rd}$ ($cm^2\ s^{-1}$)	$\{D_{K^+}\}_{ox}/\{D_{K^+}\}_{rd}$
0	0.121	8.5E−12	1.0E−11	0.84
1	0.235	4.2E−11	4.3E−11	0.92
2	**0.342**	**5.2E−11**	**5.3E−11**	**0.98**
3	0.250	5.1E−11	4.9E−11	1.04
4	0.136	5.2E−11	5.1E−11	1.02
5	0.103	4.7E−11	4.7E−11	1.00

slope of I against $v^{1/2}$ (Fig. 1E), using Eq. (2) as an approximation, where C_{K^+}, the concentration of potassium in the film, was calculated for each film according previous reports [25,33]. In these estimations, A has been replaced by the modified electrochemical active area (A^*) of each PB-modified sensor, calculated according to literature methods [29]. This approach differs from previous publications where the bare electrode area was employed [22,25,34]. From data in Table 2 we observe that A^* shows a similar behavior described above, displaying its highest value at 2 mM BZTC. The apparent K^+ permeability of all modified PB films ($\{D_{K^+}\}_{ox} \sim 5.2\times 10^{-11}\ cm^2\ s^{-1}$) was greater than for the unmodified case ($\{D_{K^+}\}_{ox} = 8.5\times 10^{-12}\ cm^2\ s^{-1}$). In order to study the global diffusion process, the ratio ($\{D_{K^+}\}_{ox}/\{D_{K^+}\}_{rd}$) has been calculated for different configurations (see Table 2 for details). In the absence of BZTC, this ratio was 0.84 revealing a more facile diffusion process during the reduction step compared with oxidation, in good concordance with previous data [22,34]. In contrast, in the presence of surfactant this ratio was close to unity, indicating a significant improvement in ion diffusion during the oxidation step.

A possible explanation for this finding is that the electrochemical behavior of PB films not only depends on the real rate of transport of cations through the film but also on the ease of insertion-expulsion of cations during the electrochemical processes [35]. In this sense, the slightly modified zeolite channels dimensions, or more probably the increased porosity and lower rigidity of the surfactant-modified PB film, may improve potassium expulsion during the oxidation step and hence facilitate the interconversion between PW → PB forms, enhancing its electrochemical reversibility.

3.4. Electrochemical impedance spectroscopy analysis

Electrochemical impedance spectroscopy (EIS) was used to determine the interfacial properties of surface-modified electrodes for PB, BZTC(1 mM)/PB and BZTC(2 mM)/PB films in background electrolyte. A typical shape of a Faradic impedance spectrum includes a semicircle region (at higher frequencies, corresponding to a charge-transfer limited process) and a straight line portion (at lower frequencies, representing a diffusion-limited process). The semicircle diameter in the impedance spectrum equates to the charge-transfer resistance, R_{ct}, at the electrode surface. The experimental Faradaic impedance spectra were fitted using a general Randles electronic equivalent circuit, which is very often used to model interfacial phenomena (for details see [26]). Fig. 3 shows EIS data for the three configurations, where it is clear that, depending on the concentration of BZTC employed, the PB film displayed different charge-transfer resistance properties. Fitting these data with the equivalent circuit (see above), the R_{ct} values obtained were 12.7, 6.8 and 3.2 Ω for PB, BZTC(1 mM)/PB and BZTC(2 mM)/PB, respectively. These data reveal that, in the presence of surfactant, electron-transfer properties of the PB film are enhanced. The lower R_{ct} value for BZTC(2 mM)/PB shows that this configuration improves the electric conducting properties of the film and facilitates the charge-transfer process, in good agreement with the CV data discussed above.

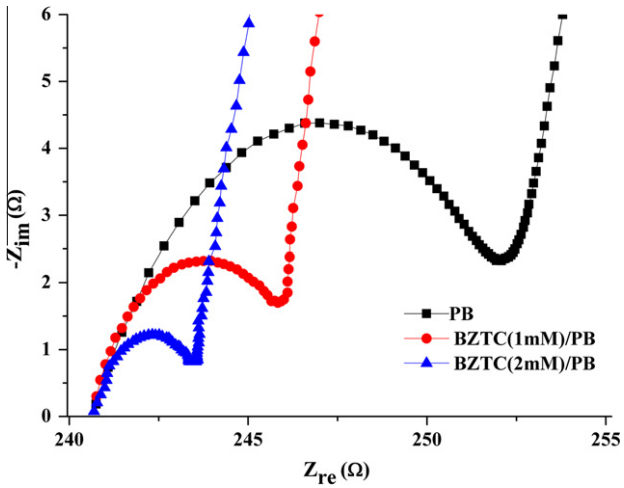

Fig. 3. EIS of PB, BZTC(1 mM)/PB and BZTC(2 mM)/PB configurations in background electrolyte (0.02 M HCl and 0.1 M KCl), stabilization potential: +0.08 mV, signal amplitude: 5 mV and frequency range: 130 kHz–10 Hz.

3.5. Electrocatalytic reduction of H_2O_2 on PB-modified electrodes

In order to compare the electrocatalytic activity of BZTC(2 mM)/PB and PB modified electrodes, their response to H_2O_2 was measured. In acid media, H_2O_2 detection can be described by the following reaction [36]:

$$H_2O_2 + 2e^- + 2H^+ \rightarrow 2H_2O \quad (5)$$

CV analysis revealed that, with the addition of 10 mM H_2O_2, the cathodic peak current increased and the anodic peak current decreased, indicating an electrocatalytic reduction of H_2O_2 for both configurations (data not shown). In order to get more information about the catalytic reaction mechanism, CVs of the modified electrodes were recorded in the presence of 1 mM H_2O_2 at various scan rates; data for the BZTC(2 mM)/PB configuration are shown in Fig. 4A. Plots of cathodic peak current against scan rate (Fig. 4B) and square root of scan rate (Fig. 4C) suggest a mass-transfer controlled process for H_2O_2; furthermore the current function, $I_{rd}/v^{1/2}$ vs. v plot (Fig. 4D) indicates that exchange process between H_2O_2 and the redox site of the BZTC(2 mM)/PB modified electrode is controlled by an EC′ mechanism [37]; qualitatively similar results were obtained for the unmodified PB electrode.

More information about the electrocatalytic reaction of the two configurations (PB and BZTC(2 mM)/PB) was obtained from chronoamperometric data. Fig. 5A shows the current-time plots for the PB sensor recorded following stepping the applied potential from open circuit conditions to −0.05 V in the absence and presence of H_2O_2 in the concentration range 0–6 mM. The time evolution of the semi-infinite linear diffusion-controlled current is described by the Cottrell equation [38]:

$$I = nFA^*C(D/\pi t)^{1/2} \quad (6)$$

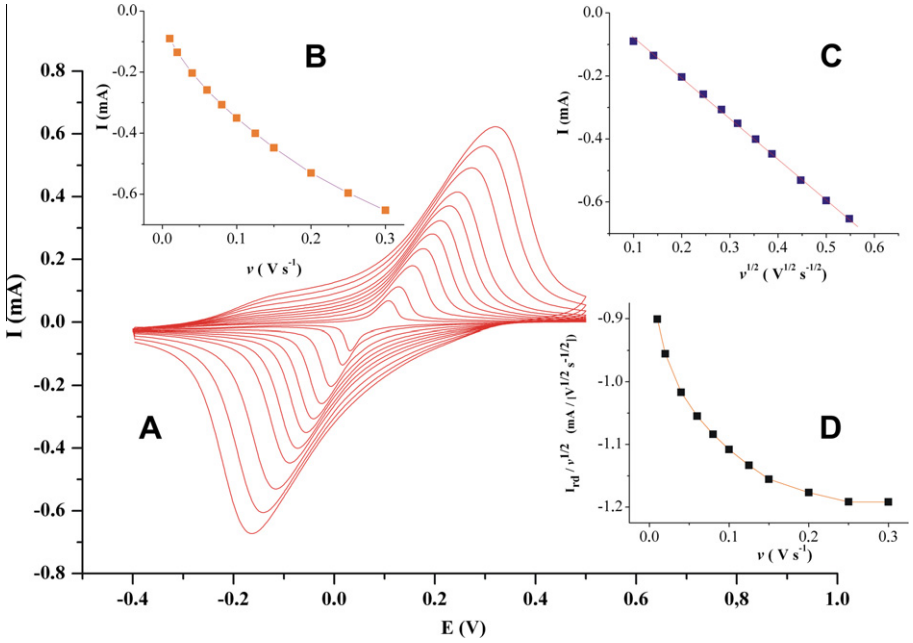

Fig. 4. (A) CV for BZTC(2 mM)/PB in the presence of 1 mM H_2O_2 at different potential scan rates, from 10 to 300 mV s^{-1}. Insets (B) and (C) represent the variations of the cathodic peak current against scan rate (v) and the square root of scan rate ($v^{1/2}$), respectively; (D) variation of the cathodic current function, $I/v^{1/2}$ vs. v. Supporting electrolyte was as in Fig. 1.

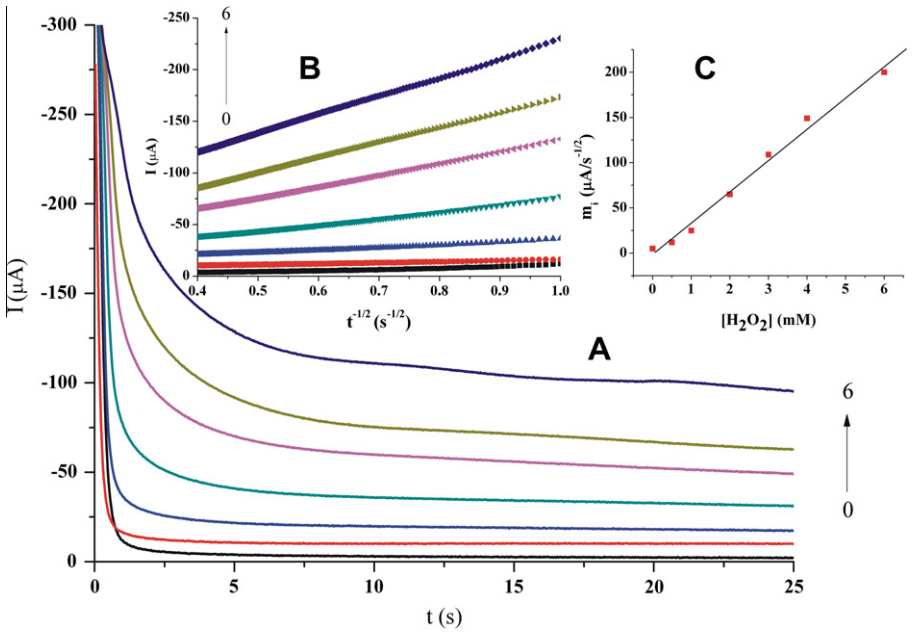

Fig. 5. (A) Chronoamperograms for a PB sensor in different concentration of H_2O_2: 0, 0.5, 1, 2, 3, 4, 6 mM; (B) plots of I vs. $t^{-1/2}$ obtained from the data of (A); (C) plot of the absolute value of the slopes (m_i) obtained from (B) vs. the concentration of H_2O_2. The step potential was −0.05 V against the internal silver pseudoreference.

where the modified electrochemical active area (A^*) of each PB-modified sensor was used, as in Eq. (2). The plot of I vs. $t^{-1/2}$ at each concentration of H_2O_2 was linear (Fig. 5B), and the slopes of the resulting straight lines were plotted vs. H_2O_2 concentration. The slope of the resulting straight line was then used to estimate the diffusion coefficient for H_2O_2 (Fig. 5C). The average values of D were 5.4×10^{-6} and 5.6×10^{-6} cm^2 s^{-1} for unmodified PB and BZTC(2 mM)/PB sensors, respectively. These values are fairly consistent with the range 2.3×10^{-6} to 1.6×10^{-5} cm^2 s^{-1} reported elsewhere [37,39–42], and are in good agreement with the value obtained for other PB and hexacyanoferrate sensors found in the literature [36,37,42].

Chronoamperometry was also used for the evaluation of the catalytic rate constant, k_{cat}. At intermediate times, when the current is dominated by the rate of the electrocatalyzed reduction of H_2O_2, the catalytic current (I_{cat}) can be written as follows [43]:

$$I_{cat}/I_L = (k_{cat}\pi Ct)^{1/2} \quad (7)$$

where I_L is the current of the BZTC(2 mM)/PB or PB in the absence of H_2O_2 and I_{cat} is the catalytic current due to the addition of 1 mM H_2O_2. Over a limited time frame, the values of I_{cat}/I_L were linearly dependent on $t^{1/2}$, and from its slope k_{cat} was calculated. The values obtained were 1.1×10^3 and 2.8×10^3 M^{-1} s^{-1} for PB and

BZTC(2 mM)/PB, respectively, and are in good agreement with data found in the literature [44]. The higher value for BZTC(2 mM)/PB is consistent with the finding that k_{cat} has been found to be dependent on the amount of Prussian blue deposited, indicating that H_2O_2 penetrates the films, and the inner layers of the polycrystalline matrix take part in the catalysis [44].

3.6. Stability of PB films

Due to geometrical restriction in the lattice, PB is sensitive to the insertion of the more highly hydrated Na^+ ions [14,16,25]. PB and BZTC(2 mM)/PB sensors were cycled three times in the standard background electrolyte, 250 times in solution-*A* (containing Na^+), and finally a further three times in background electrolyte. The peak current ratio after and before being exposed to Na^+ ions showed a recovery of 86% for BZTC(2 mM)/PB, whereas the surfactant-free PB sensor recovered only 47%, showing a significant lost of redox activity (for details, see SM_figure 4). These data reveal that the irreversible damage caused by Na^+, an undesirable property for sensors designed for biological applications, is attenuated for the BTZC(2 mM)/PB configuration, and is consistent with higher D_{Na^+} values obtained for surfactant-modified films reported in our previous work [25].

In order to study the pH stability here, sensors were cycled 100 times (at 0.1 V s^{-1} from 0.1 to 0.3 V) in different solutions adjusted in a large pH range. The residual activity was calculated using the anodic peak intensity for the 100th cycle (I_{100}) for each configuration and normalizing it with respect to the first one (I_1) (Fig. 6A). Unmodified PB films were highly unstable, even in acid media, and displayed a significant signal decrease (by 70%) at pH 7.4. In contrast, the optimized BZTC(2 mM)/PB sensors, with and without thermal treatment (100 °C during 1 h) [14], showed highly stable response, conserving ~100% of the signal below pH 6, and losing only ~10% of the initial signal at the end of the 100 cycles at pH 7.4. This excellent stability, especially in neutral media, may be obtained because BZTC is a quaternary ammonium compound, and acting as an acid to nullify the effect of OH^- ions, thereby stabilizing the PB film. Finally, electrostatic interactions between cationic surfactants bilayers and clay layers may offer an additional stabilization mechanism to prevent its dissolution [24].

3.7. Sensitivity and selectivity toward H_2O_2

In previous work [16,25–27], we demonstrated that ascorbic acid (AA) is the main endogenous interference in physiological applications due to its low redox potential and high concentration in many biological media. Thus AA is the prototypical electroactive interference species in a great number of analytical applications. The choice of applied potential at the working electrode is therefore fundamental to achieve the lowest detection limit and to avoid the possibility of interference in biosensor applications. The response to 0.1 mM H_2O_2 and 1 mM AA (one order of magnitude higher) was therefore evaluated here. These data (Fig. 6B) reveal that PB at negative applied potentials, where it is in the PW form, showed higher sensitivity to H_2O_2, whereas at positive potentials the PB form did not respond significantly to H_2O_2. In contrast, the AA response (oxidation) displayed a higher response when the applied potential was more positive, reaching a maximum value at +0.2 V, close to the optimal range found by other authors for the electro-catalytic detection of AA based on PB-modified electrodes [45]. On the other hand, a small cathodic increment in the interference signal appeared at −0.2 V, which may be attributed to the electrocatalytic reduction of O_2 reported by our group [16] and by other authors at this potential [3,4]. From these results (Fig. 6B), it is evident that the optimal potential range was observed between −0.05 and −0.15 V, where the selectivity ratio

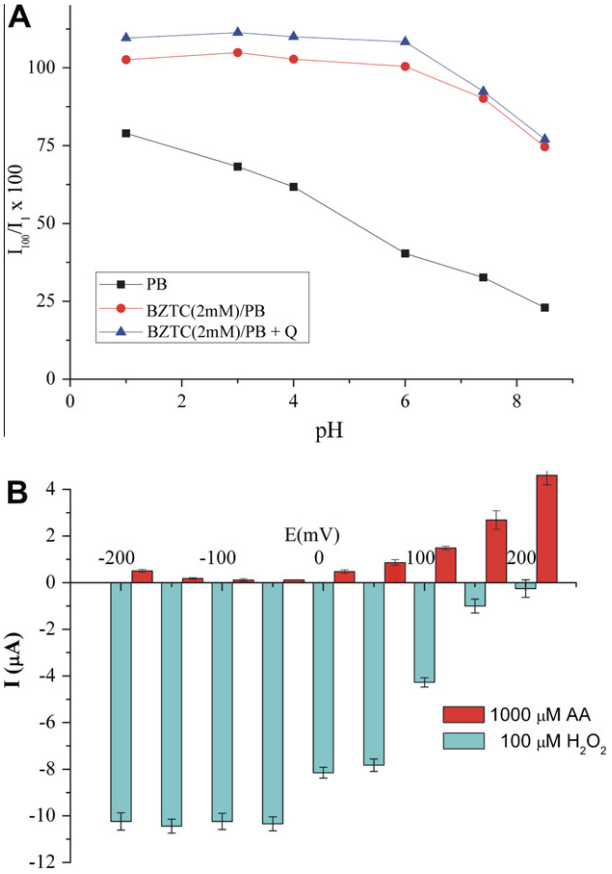

Fig. 6. (A) pH stability for different sensor configurations: without (PB) and with 2 mM BZTC (BZTC(2 mM)/PB) present during the electro-deposition step, and with and without additional thermal treatment (*Q*) at 100 °C for 1 h. Experiments were done in phosphate buffer and in background electrolyte adjusted to different pH values, both in 0.1 M KCl. (B) Sensitivity (H_2O_2) and selectivity (ascorbic acid, AA) responses plotted against applied potential, background solution being employed as supporting electrolyte.

(100 × AA/H_2O_2) was ⩽1%. An applied potential value of −0.05 V was therefore selected for further sensor characterization to avoid possible interference by reduction of molecular oxygen at more cathodic potentials.

Calibration curves for different H_2O_2 sensors configurations (from 0 to 1.1 mM H_2O_2) were obtained (Fig. 7A). A visual inspection (Fig. 7B) revealed that BZTC(2 mM)/PB showed the highest sensitivity and linearity. Analytical parameters, summarized in Table 3, showed that BZTC(2 mM)/PB displayed the best sensitivity (1.07 ± 0.03 A M^{-1} cm^{-2}, $n = 5$), limit of detection (LOD = 9.3×10^{-8} M) and linearity ($r^2 = 0.9998$). Sensitivity, coefficient of determination, and LOD (see Table 3 and SM_figure 5) for the different configurations showed similar behavior described above for other electrochemical parameters, displaying analytically better values when BZTC concentration was increased up to the optimal concentration (2 mM), and then a clear deterioration occurred at higher surfactant concentrations.

This H_2O_2 sensitivity value represents an improvement on our previous work [25] and is higher than previous PB-modified SCPEs values found in the literature (for details see SM_Table 1 and references in [25]). The time response for all configurations was measured in batch conditions after H_2O_2 additions; in this case all sensors studied showed fast response times ($t_{90\%} \sim 4$ s), Fig. 7C.

The last important parameter investigated in the present study was the effect of storage time on H_2O_2 sensitivity. In order to examine this effect, different sensor configurations were prepared and stored in dark and dry conditions at room temperature for

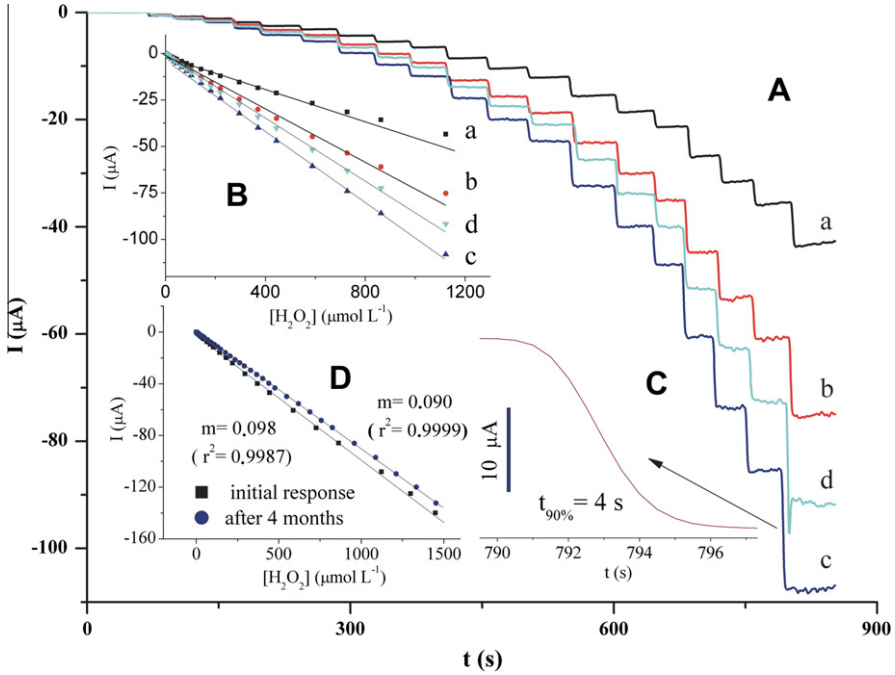

Fig. 7. (A) Successive amperometric response for BZTC(*x* mM)/PB films from 0 to 1.1 mM H_2O_2 recorded at −0.05 V in stirred background electrolyte: (a) 0, (b) 1, (c) 2 and (d) 3 mM BZTC; (B) Calibration curves for the sensors in (A); (C) Time response of BZTC(2 mM)/PB. (D) Calibration curves for BZTC(2 mM)/PB sensor, both fresh and after 4 months of dry storage in the dark, from 0 to 1.5 mM H_2O_2. Calibration conditions were as in (A).

Table 3
Comparison of some analytical parameters of different PB sensors obtained with batch amperometry at −0.05 V in a stirred background electrolyte. Sensitivity data normalized respect to the electrochemical area of the bare SPCE.

BZTC (mM)	S (A M^{-1})	r^2	S (A M^{-1} cm^{-2})	LOD (μM)
0	0.0399	0.9876	0.420	0.340
1	0.0692	0.9936	0.728	0.202
2	**0.102**	**0.9998**	**1.074**	**0.093**
3	0.0832	0.9976	0.876	0.119
4	0.0405	0.9981	0.426	0.205
5	0.0213	0.9852	0.224	0.451

4 months. Fig. 7D shows calibration curves in a range from 0 to 1.5 mM H_2O_2 for a freshly prepared BZTC(2 mM)/PB and for a stored BZTC(2 mM)/PB sensor. As can be seen, sensitivity after this long storage time was well retained, preserving 92% of the initial response. Other BZTC(2 mM)/PB sensors showed similar results (between 86 and 90% of the initial response). Other configurations such as BZTC(1 mM)/PB also showed similar stability. These data reveal the excellent stability of the BZTC-modified PB deposited onto SPCEs that may be stored during long time periods, which may be useful for future commercial applications.

4. Conclusions

We have optimized the electro-deposition method for PB in the presence of BZTC, and studied the electrochemical and analytical properties for different PB film configurations. The BZTC(2 mM)/PB configuration showed the best electrochemical behavior with improved surface coverage and diffusion parameters. The electro-deposition method displayed an excellent reproducibility, *CV*% 2.5. Under optimal conditions we were able to develop a highly sensitive H_2O_2 sensor (1.07 A M^{-1} cm^{-2}) with a detection limit of $\sim 10^{-7}$ M. At the selected applied potential, the defined selectivity ratio against AA was better than 1%. This design showed better H_2O_2 sensitivity than previous configurations based on modified SPCEs, and represents a less time-consuming method when compared with other highly sensitive sensors. PB-modified electrodes showed good stability in neutral and weakly alkali solutions, without further treatment. The stability of PB-modified SCPEs was satisfactory, at least for 4 months stored dry in the dark at room temperature.

Acknowledgments

The funds for the development of this device have been provided by the Ministerio de Industria, Turismo y Comercio (TSI-020100-2011-189 and TSI-020100-2010-346) and Ministerio de Ciencia e Innovación (TIN2011-28146 and TIN2008-06867-C02-01/TIN). We thank Dr. J.L. Rodriguez Marrero and J. Florez Montaño for help in EIS measurements.

Appendix A. Supplementary material

Supplementary data associated with this article can be found, in the online version, at http://dx.doi.org/10.1016/j.jelechem.2012.04.005.

References

[1] J. Brown, J. Philos. Trans. 33 (1724) 17–24.
[2] V.D. Neff, J. Electrochem. Soc. 125 (1978) 886–887.
[3] K. Itaya, T. Ataka, S.J. Toshima, J. Am. Chem. Soc. 104 (1982) 4767–4772.
[4] F. Ricci, G. Palleschi, Biosens. Bioelectron. 21 (2005) 389–407.
[5] A.A. Karyakin, O. Gitelmacher, E.E. Karyakina, Anal. Lett. 27 (1994) 2861–2869.
[6] P. Salazar, M. Martín, R. Roche, J.L. González-Mora, R.D. O'Neill, Biosens. Bioelectron. 26 (2010) 748–753.
[7] Z. Song, R. Yuan, Y. Chai, J. Wang, X. Che, Sens. Actuators B 145 (2010) 817–825.
[8] Z. Zhong, J. Shan, Z. Zhang, Yi Qing, D. Wang, Electroanalysis 22 (2010) 2569–2575.
[9] S. Chen, R. Yuan, Y. Chai, Y. Xu, Ligen Min, N. Li, Sens. Actuators B 135 (2008) 236–244.
[10] W. Shi, Z. Ma, Biosens. Bioelectron. 26 (2011) 3068–3071.
[11] B.J. Feldman, R.W. Murray, Inorg. Chem. 26 (1987) 1702–1708.
[12] A.A. Karyakin, E.E. Karyakina, Sens. Actuators B 57 (1999) 268–273.

[13] D. Moscone, D. D'Ottavi, D. Compagnone, G. Palleschi, A. Amine, Anal. Chem. 73 (2001) 2529–2535.
[14] F. Ricci, A. Amine, G. Palleschi, D. Moscone, Biosens. Bioelectron. 18 (2003) 165–174.
[15] I.L. de Mattos, L. Gorton, T. Ruzgas, Biosens. Bioelectron. 18 (2003) 193–200.
[16] P. Salazar, M. Martín, R. Roche, R.D. O'Neill, J.L. González-Mora, Electrochim. Acta 55 (2010) 6476–6484.
[17] L.V. Lukachova, E.A. Kotel'nikova, D. D'Ottavi, E.A. Shkerin, E.E. Karyakina, D. Moscone, G. Palleschi, A. Curulli, A.A. Karyakin, Bioelectrochemistry 55 (2002) 145–148.
[18] T. Uemura, S. Kitagawa, J. Am. Chem. Soc. 125 (2003) 7814–7815.
[19] D. Pan, J. Chen, L. Nie, W. Tao, S. Yao, Electrochim. Acta 49 (2004) 795–801.
[20] M.S. Lin, W.C. Shih, Anal. Chim. Acta 381 (1999) 183–189.
[21] S. Paria, K.C. Khilar, Adv. Colloid Interface 110 (2004) 75–95.
[22] R. Vittal, H. Gomathi, G. Prabhakara Rao, Electrochim. Acta 45 (2000) 2083–2093.
[23] R. Vittal, K.J. Kim, H. Gomathi, V. Yegnaraman, J. Phys. Chem. B 112 (2008) 1149–1156.
[24] S.M. Senthil Kumar, K. Chandrasekara Pillai, J. Electroanal. Chem. 589 (2006) 167–175.
[25] P. Salazar, M. Martín, R.D. O'Neill, R. Roche, J.L. González-Mora, Colloid Surface B 92 (2012) 180–189.
[26] P. Salazar, R.D. O'Neill, M. Martín, R. Roche, J.L. González-Mora, Sens. Actuators B 152 (2011) 137–143.
[27] R. Roche, P. Salazar, M. Martín, F. Marcano, J.L. González-Mora, J. Neurosci. Method 202 (2011) 192–198.
[28] A.J. Bard, L.R. Faulkner, Electrochemical Methods: Fundamentals and Applications, second ed., John Wiley & Sons, Inc., New York, 2001.
[29] P. Fanjul-Bolado, P. Queipo, P.J. Lamas-Ardisana, A. Costa-García, Talanta 74 (2007) 427–433.
[30] B. Haghighi, N. Shams, L. Gorton, Electroanalysis 19 (2007) 1921–1932.
[31] A.A. Karyakin, E.A. Puganova, I.A. Budashov, I.N. Kurochkin, E.E. Karyakina, V.A. Levchenko, V.N. Matveyenko, S.D. Varfolomeyev, Anal. Chem. 76 (2004) 474–478.
[32] B. Haghighi, H. Hamidi, L. Gorton, Sens. Actuators B 147 (2010) 270–276.
[33] M.H. Pournaghi-Azar, N. Nahalparvari, J. Solid State Electrochem. 8 (2004) 550–557.
[34] R. Vittal, M. Jayalakshmi, H. Gomathi, G. Prabhakara Rao, J. Electrochem. Soc. 146 (1999) 786–793.
[35] J.J. García-Jareño, D. Giménez-Romero, F.V.C. Gabrielli, M. Keddam, H. Perrot, J. Phys. Chem. B 107 (2003) 11321–11330.
[36] L. Mureşan, G.L. Turdean, I.C. Popescu, J. Appl. Electrochem. 38 (2008) 349–355.
[37] H. Razmi, R. Mohammad-Rezaei, H. Heidari, Electroanalysis 21 (2009) 2355–2362.
[38] A.J. Bard, L.R. Faulkner, Electrochemical Methods: Fundamentals and Applications, Wiley, New York, 1980.
[39] B. Csoka, G. Nagy, J. Biochem. Biophys. Method 61 (2004) 57–67.
[40] P.A. Forshey, T. Kuwana, Inorg. Chem. 22 (1983) 699–707.
[41] J. Huang, C. Zhang, W. Zhang, X. Zhou, J. Electroanal. Chem. 433 (1997) 33–39.
[42] H. Yu, Q.L. Sheng, J.B. Zheng, Electrochim. Acta 52 (2007) 4403–4410.
[43] H. Razmi, A. Taghvimi, Int. J. Electrochem. Sci. 5 (2010) 751–762.
[44] A.A. Karyakin, E.E. Karyakina, L. Gorton, J. Electroanal. Chem. 456 (1998) 97–104.
[45] S.S.L. Castro, V.R. Balbo, P.J.S. Barbeira, N.R. Stradiotto, Talanta 55 (2001) 249–254.

Supplementary Materials

Figure and Table Captions

SM_figure 1.- Conductometric determination of the critical micellar concentration (cmc) for BZTC in water as the change in the slope when the specific conductance vs. surfactant concentration in H_2O was plotted.

SM_figure 2.- (***Top***) Comparison of the charge storage capacity of different BZTC(*x* mM)/PB films studied by cycling SPCEs over 120 successive cycles between –0.2 and 1.0 V at a scan rate of 0.1 V s^{-1}. Q_{for} represents the accumulated charge under the anodic peak for each scan. (***Bottom***) Plot of the maximum charge stored vs. the concentration of BZTC in the solution.

SM_figure 3.- CVs for PB and BZTC(*2* mM)/PB films in background electrolyte before and after being cycled 250 times in *solution-A* (0.02 M HCl and 0.1 M NaCl) at a scan rate of 0.1 V s^{-1}.

SM_figure 4.- Analytical parameter evolution for different BZTC(*x* mM)/PB configurations, *x* = 0, 1, 2, 3, 4 and 5.

SM_table 1.- Comparison of some analytical parameters of different PB sensors obtained with stirred batch amperometry.

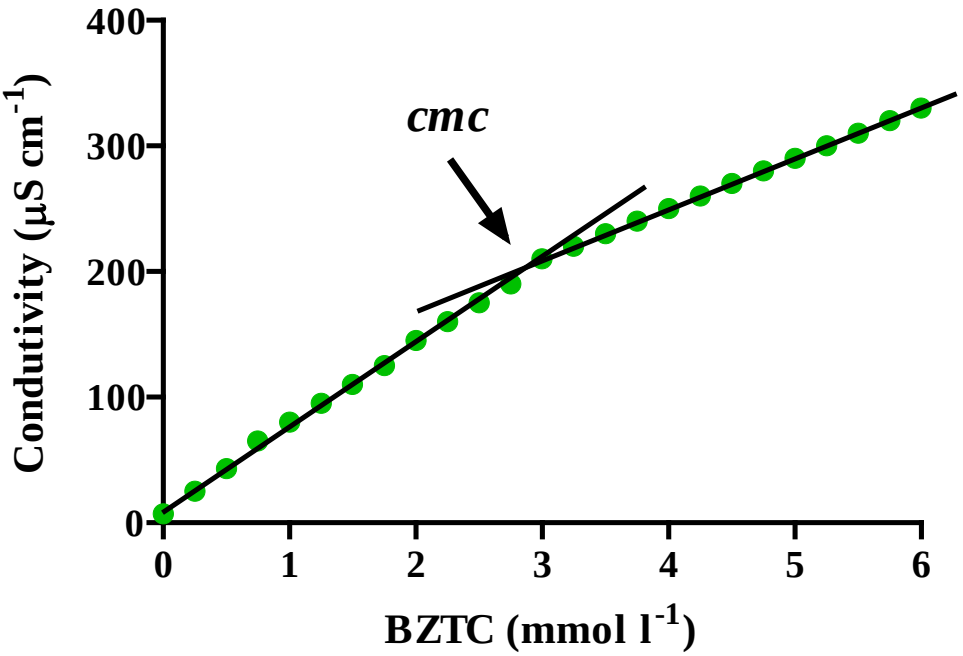

SM_figure 1.- Conductometric determination of the critical micellar concentration (cmc) for BZTC in water as the change in the slope when the specific conductance vs. surfactant concentration in H_2O was plotted.

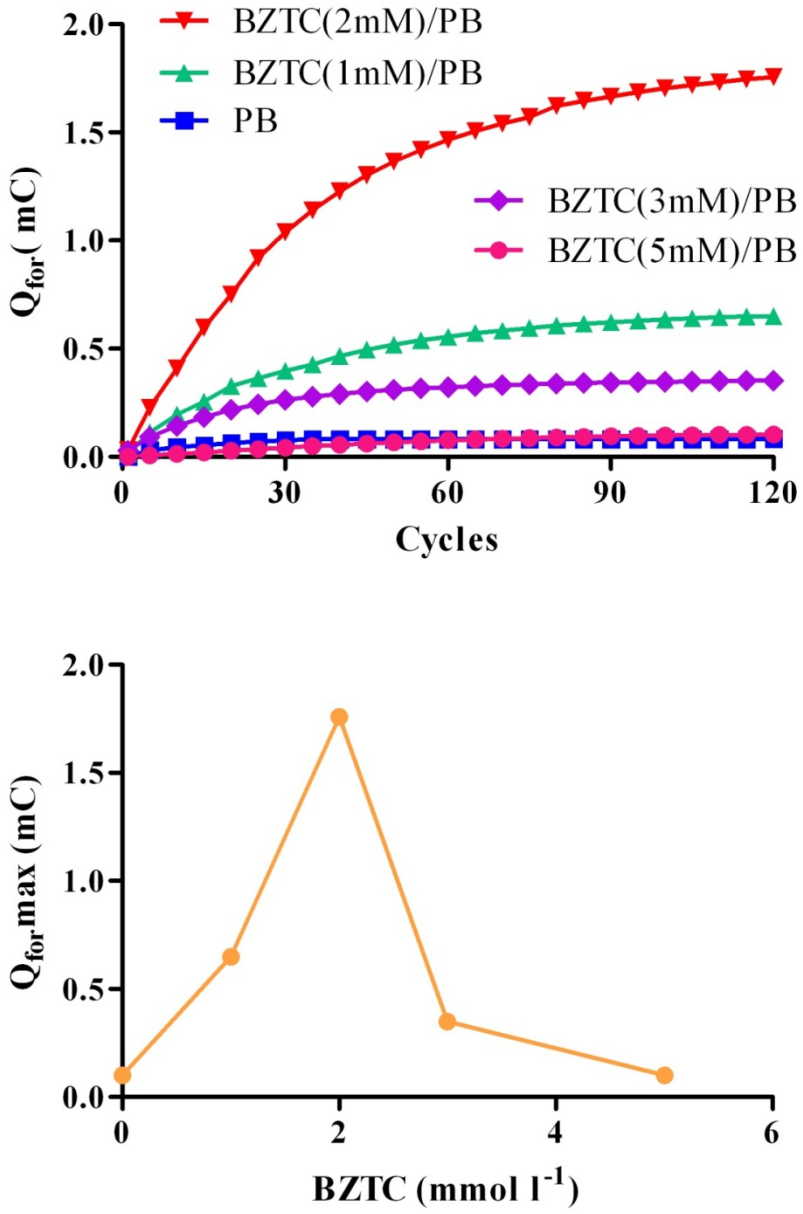

SM_figure 2.- (***Top***) Comparison of the charge storage capacity of different BZTC(*x* mM)/PB films studied by cycling SPCEs over 120 successive cycles between –0.2 and 1.0 V at a scan rate of 0.1 V s^{-1}. Q_{for} represents the accumulated charge under the anodic peak for each scan. (***Bottom***) Plot of the maximum charge stored vs. the concentration of BZTC in the solution.

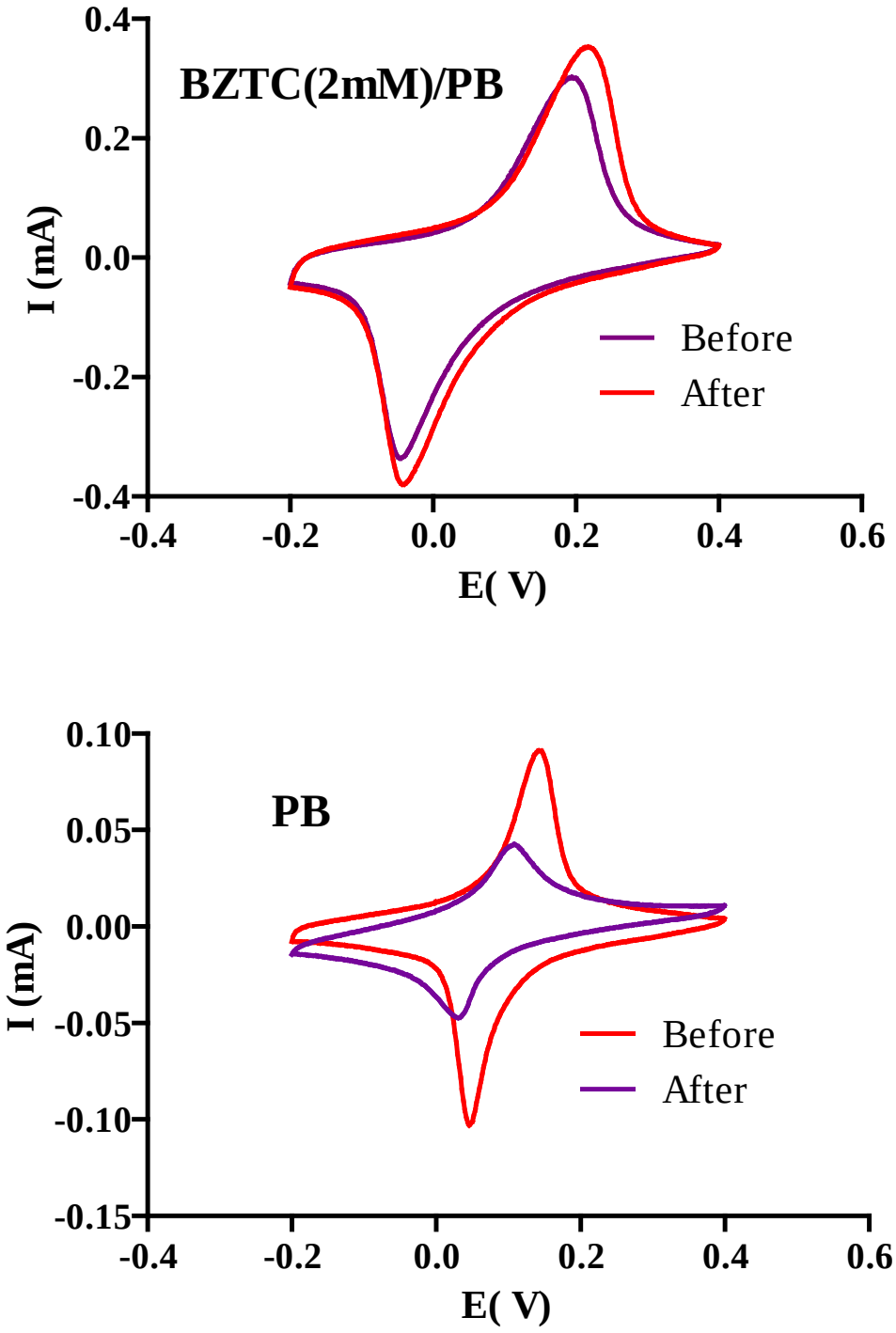

SM_figure 3.- CVs for PB and BZTC(*2* mM)/PB films in background electrolyte before and after being cycled 250 times in *solution-A* (0.02 M HCl and 0.1 M NaCl) at a scan rate of 0.1 V s^{-1}.

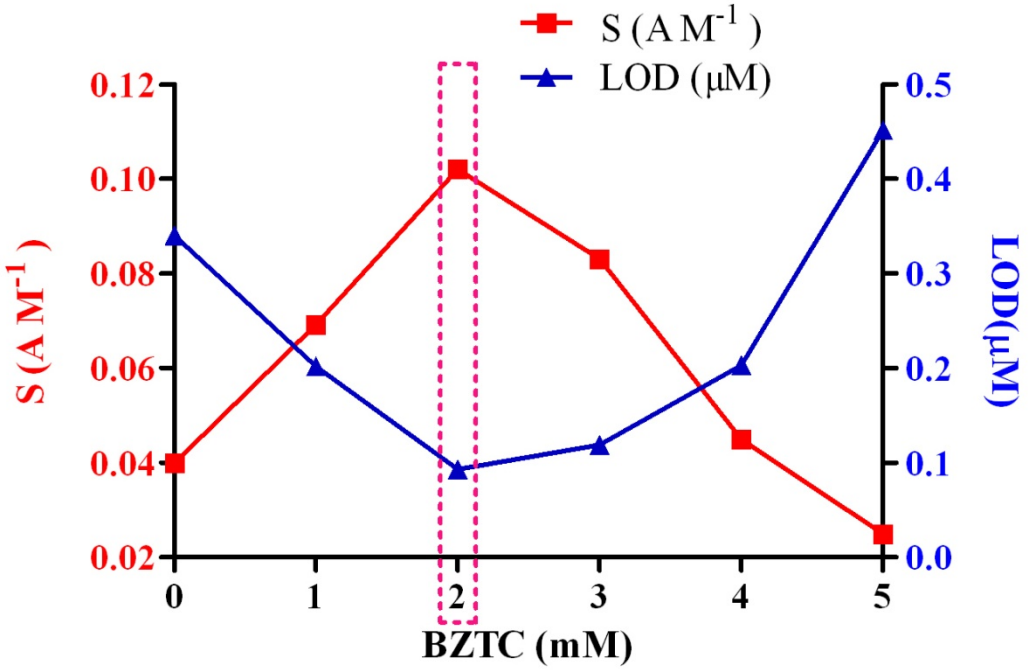

SM_figure 4.- Analytical parameter evolution for different BZTC(*x* mM)/PB configurations, *x* = 0, 1, 2, 3, 4 and 5.

SM_table 1.- Comparison of some analytical parameters of different PB sensors obtained with stirred batch amperometry.

Type of sensor	Deposition method	Applied potential (mV)	LOD (µM)	LR (µM)	S (mA M^{-1} cm^{-2})	Ref.
Carbon fiber electrode	Cyclic voltammetry	0	0.01	-	1000	[12]*
Carbon fiber electrode	Cyclic voltammetry	0	0.1	-	480	[12]*
Graphite screen printed electrode	PB microparticles mixed with carbon ink	0	0.25	0.4 - 100	*137*	[15]*
Graphite screen printed electrode	Chemical deposition on graphite/GC mixed with carbon ink	-50	0.3	0.5 - 1000	*135*	[16]*
Graphite screen printed electrode	Chemical deposition on graphite screen printed electrode	-50	0.1	0.1 - 50	*234*	[17]*
Glassy carbon electrode	Cyclic voltammetry	0	0.036	0.079 - 15.8	153	[22]*
Glassy carbon electrode	Cyclic voltammetry in presence of surfactant	0	0.012	0.0038 - 100	979	[22]*
Platinum foil electrodes	Chemical deposition based on self-assembly process	-50	1	1 - 400	625	[41]*
Carbon ceramic electrode	Chemical deposition based on self-assembly process	-100	0.8	1 - 260	755	[42]*
Graphite screen printed electrode	Cyclic voltammetry	-50	0.26	0.26 - 400	*440*	[25]
Graphite screen printed electrode	Cyclic voltammetry in presence of surfactant	-50	0.16	0.16 - 400	*630*	[25]
Graphite screen printed electrode	**Cyclic voltammetry in presence of surfactant**	**-50**	**0.093**	**0.093 - 1500**	**1074**	**This work**

**References in previous group's publications* [25].

Int. J. Electrochem. Sci., 7 **(2012)** 5910 - 5926

International Journal of
ELECTROCHEMICAL
SCIENCE
www.electrochemsci.org

Biosensors Based On Prussian Blue Modified Carbon Fibers Electrodes for Monitoring Lactate in The Extracellular Space of Brain Tissue

P. Salazar[1*], *M. Martín*[1], *R.D. O'Neill*[2], *R. Roche*[1] *and J.L. González-Mora*[1]

[1] Neurochemistry and Neuroimaging group, Faculty of Medicine, University of La Laguna, Tenerife, Spain.
[2] UCD School of Chemistry and Chemical Biology, University College Dublin, Belfield, Dublin 4, Ireland.
[*]E-mail: psalazar@ull.edu.es

Received: 10 May 2012 / *Accepted:* 4 June 2012 / *Published:* 1 July 2012

During recent decades, a new paradigm has emerged in neuroscience from growing evidence that lactate, and not glucose, has the more important role as an energy substrate during neural activation. Based on these findings, the astrocyte–neuron–lactate shuttle hypothesis (ANLSH) has been proposed. Over the same period, biosensors have become an important tool for in-vivo studies, providing higher time and spatial resolution over microdialysis and other neuroanalytical techniques. In this work we present a new lactate microbiosensor based on Prussian Blue (PB)-modified carbon fiber electrodes (CFEs) that allows the detection of enzyme-generated hydrogen peroxide at a low applied potential (~0 V against SCE), contrasting the high overpotential used in many previous designs based on platinum transducers (~0.7 V). Here, optimization of the fabrication procedure is described, including activation of CFE/PB, enzyme immobilization, anti-biofouling and anti-interference properties. Finally, to illustrate the potential use of this approach, some in-vivo results are presented, including pharmacological, physiological and electrophysiological stimulation, showing that this microbiosensor design is well suited to exploring the role of lactate in brain extracellular fluid.

Keywords: Biosensor, Carbon fiber electrode, Brain lactate, Prussian Blue, Oxygen sensor.

1. INTRODUCTION

During the last decade an important debate has been generated about the regulation of brain metabolic responses to neuronal activity [1-6]. Brain cells are dependent on a continuous supply of energy, glucose being its main fuel under normal physiological conditions. Because the brain has very little energy reserve, a continuous vascular supply of glucose and oxygen is mandatory to sustain

neuronal activity. Historically, lactate was considered a dead-end metabolite of glycolysis or a sign of hypoxia and anaerobic energy metabolism [7, 8]. However, a body of evidence has been accumulated to indicate that large amounts of lactate can be produced in many tissues under fully aerobic conditions [8-13]. Therefore, some authors point out that lactate could be used as a supplementary fuel [2, 14, 15], and has even been suggested to be the predominant oxidative substrate over glucose during neural activation [6, 16, 17]. Due to these findings, the astrocyte–neuron–lactate shuttle hypothesis (ANLSH) has been suggested [14, 15, 18]. According to this model, during neural activation the uptake of glutamate leads to glucose uptake into the astrocytes, and its glycolysis generates lactate which is exported into the extracellular compartment where it is taken up by neurons for its ultimate phosphorylation. This idea has divided the neuroscience community into two schools, and has generated an intense discussion [1-6, 14-22]. Most of the evidence for ANLSH are based on in-vitro experiments and on the presence of some enzymes and transporters required in the proposed hypothesis [3, 11-13]. ANLSH argues a causal sequence of events that can only be tested under in-vivo conditions. Traditionally, microdialysis has been employed for monitoring extracellular metabolites in vivo [23-25]; unfortunately, this technique often displays poor time resolution (10–30 min). More recently, biosensors have been shown to be an excellent analytical tool, providing high spatial and temporal resolution, and enough sensitivity and selectivity for in-vivo experiments [26]. In this way, microdialysis technique has been coupled with biosensor technology [27, 28], presenting as its main advance over conventional sample collection better time resolution (as low as 30 s) [29]. Nevertheless, implantable biosensors based on carbon fiber electrodes (CFEs) have smaller dimensions (~10 μm diameter) than microdialysis probes (200–500 μm), which attenuates traumatic brain injury during insertion [30], and provides yet higher time resolution, allowing real-time correlation with animal behavior [31-35].

In recent years our group has been working on Prussian Blue modified microelectrodes to detect enzyme-generated H_2O_2 at low applied potentials (0 V vs. SCE) as an alternative to conventional noble metal based transducers often employed in first-generation biosensors for physiological applications. Thanks to this approach glucose biosensors reached very low dimensions (~10 μm diameter) and displayed excellent in-vitro and in-vivo responses [32-35]. Now we present a new lactate biosensor adapting our previous glucose biosensor design, exploring and optimizing the main fabrication steps in order to improve sensitivity, stability, selectivity and anti-biofouling properties. Finally, in order to show its potential use in physiological studies we present some in-vivo experiments with this optimized lactate biosensor.

2. EXPERIMENTAL

2.1 Reagents and Solutions

The enzyme lactate oxidase (Lox) from *Pediococcus sp.*, purchased as a lyophilized powder, and glutaraldehyde (Glut, 25%) were obtained from Sigma Chemical Co., and stored at –21 ºC until use. Bovine serum albumin (BSA, fraction V) and all other chemicals, including *o*-phenylenediamine

(o-PD), lactate, polyethyleneimine (PEI), KCl, NaCl, $CaCl_2$, $FeCl_3$, $K_3[Fe(CN)_6]$, HCl (35% w/w), H_2O_2 (30% w/v), Nafion (5% w/w in a mixture of lower aliphatic alcohols and water) and phosphate buffer saline (PBS, pH 7.4 containing 0.1 M NaCl) were also obtained from Sigma, and used as supplied. The interference compounds: glucose, ascorbic acid (AA), uric acid (UA), dopamine (DA), 3,4-dihydroxyphenylacetic acid (DOPAC), serotonin (5-HT), glutamate (Glu) and glutamine (Gln) were obtained for Aldrich-Sigma, and used as supplied. PBS stock solutions were prepared in doubly distilled water (18.2 MΩ cm, Millipore-Q), and stored at 4 °C when not in use. A stock 50 mM solution of lactate was prepared in water, and stored at 4 ºC when is not in use. The PEI solutions were prepared by dissolving PEI at *x*% w/v in H_2O. The cross-linking solution was prepared in PBS with 1% w/v of BSA and 0.1% w/v of Glut. Monomer solution of 300 mM o-PD was prepared using 48.6 mg of o-PD and 7.5 mg of BSA in 1.5 mL of N_2 saturated PBS and sonicating for 15 min. A 100 units/mL solution of Lox was prepared by dissolving 50 units in 0.5 mL of PBS. Interference solutions were prepared in water just before use and, if necessary, the pH was adjusted to 7.4. Carbon fibers (8 μm diameter), Platinum/Iridium wire (25 μm diameter), glass capillaries, and 250 μm internal diameter Teflon-coated copper wire were obtained from Word Precision Instruments Inc. and silver epoxy paint was supplied by Sigma.

2.2 Instrumentation and Software

Experiments were computer controlled with data-acquisition software EChem™ for CV and Chart™ for constant potential amperometry (CPA). The data-acquisition system used was e-Corder 401 (EDAQ) and a low-noise and high-sensitivity potentiostat, Quadstat (EDAQ). CV and electrochemical impedance spectroscopy (EIS) experiments for micro-biosensor characterization were conducted with an Autolab PGSTAT 20 potentiostat and a FRA module from EcoChemie, computer controlled by their General Purpose Electrochemical System (GPES) and FRA software, respectively. The linear and non-linear regression analyses were performed using the graphical software package Prism (GraphPad Software, ver. 5.00). To electro-deposit and activate the PB, a custom-made Ag/AgCl/saturated KCl reference electrode and platinum wire auxiliary electrode were used.

2.3 Amperometric experiments

2.3.1 In vitro

CV and EIS experiments for PB characterization were measured in electrolyte support solution (0.1 M XCl and 0.1 M HCl (X being either Na or K)) or (0.1 M $CaCl_2$ and 0.1 M HCl). Experimental conditions for EIS measurements were: applied potential +0.1 V against SCE, signal amplitude 5 mV and frequency range 40 kHz–0.5 Hz. All in-vitro experiments were done in a 25 mL glass cell at 21 °C, using a standard three-electrode set-up with a commercial saturated calomel electrode (SCE, CRISON Instrument S.A.) as the reference and platinum wire as the auxiliary electrode. The previously determined optimum applied potential for amperometric studies on CFE/PB-based biosensors was 0 V against SCE [32-35]. Lactate calibrations were performed in quiescent air-

saturated PBS (following stabilization of the background current for 20 min) by adding aliquots of lactate stock solution to the electrochemical cell. After each addition, the solutions were stirred for 5 s and then left to reach the steady-state current.

2.3.2 In vivo

These experiments were carried out with male rats of ~300 g (Sprague Dawley) in accordance with the European Communities Council Directive of 1986 (86/609/EEC) regarding the care and use of animals for experimental procedures, and adequate measures were taken to minimize pain and discomfort. After being anesthetized with urethane (1.5 g/kg), the animal's head was immobilized in a stereotaxic frame and its body temperature maintained at 37 ºC with a heating blanket. The skull was then surgically exposed and small hole drilled for microbiosensor implantations. To measure prefrontal cortex lactate, the microbiosensor was implanted according to Paxinos and Watson coordinates: A/P +2.7 from bregma, M/L +1.2 and D/V –0.5 from dura [36]. The Ag/AgCl reference electrode and platinum auxiliary electrode were placed in the cortex, and the skull kept wet with saline-soaked pads. The reference potential provided by the Ag/AgCl wire in brain tissue is very similar to that of the SCE. For in-vivo oxygen measurement a CFE/PoPD was polarized at –0.65 V. Electrical stimulation was provided by an S-8800 Grass model and a bipolar electrode made with two unmodified CFE mounted in a two-barrel glass capillary. The exposed surface of the tip was approximately 500 μm long. Electrical stimuli parameters were: 0.15 mA of 1-ms square biphasic pulses for 3–5 seconds at 20–30 Hz. During oxygen-manipulation studies, the appropriate gas was pumped close to the rat's nose to ensure optimal exposure, and alternatively pure O_2 and N_2 were administered during ~1 min, after which the air flux was restored. Intraperitoneal injection (*i.p.*) was selected for pharmacological administration.

2.4 Preparation of the Working Electrodes

2.4.1 Fabrication of Carbon Fiber Electrodes

Carbon fibers (diameter 8 μm, 20–50 mm in length) were attached to Teflon-coated copper wire (diameter 250 μm), using high purity silver paint, and dried for 1 h at 80 ºC. The borosilicate glass capillary was pulled to a tip using a vertical microelectrode puller (Needle/Pipette puller, Model 750, David Kopf Instruments). After drying, the carbon fiber was carefully inserted into the pulled glass capillary tube under a microscope, leaving 2–4 mm of the carbon fiber protruding at the pulled end. Subsequently, the carbon fiber was cut to the desired length (approximately 250 μm) using a microsurgical scalpel. At the stem end of the capillary tube, the copper wire was fixed by casting with non-conducting epoxy glue; the carbon fiber was also sealed into the capillary mouth, using the same epoxy glue.

2.4.2 PB electro-deposition onto Carbon Fiber Electrodes

CFEs were modified by means of electro-deposition and activation of a PB film. Briefly, the PB layer was electro-deposited using CV and applying 1, 3, 6, 9 or 12 cyclic scans within the limits of –0.2 to 0.4 V at scan rate of 0.05 or 0.1 V/s in a solution containing 1.5 mM $K_3[Fe(CN)_6]$ and 1.5 mM $FeCl_3$ in 0.1 M KCl and 0.1 M HCl. These CFE/PBs were cleaned in doubly-distilled water and activated by applying another 50 cycles in electrolyte solution (0.1 M KCl and 0.1 M HCl), using the same protocol. Before being used, the CFE/PBs were cleaned again in doubly-distilled water for several seconds. Finally, the PB film was tempered for 1 h at 100 – 200 ^{o}C.

2.4.3 Micro-biosensor construction based on CFE/PB

When CFE/PBs were ready to use, the next step was to immobilize the Lox using the following protocol: 15 fast immersions in the PEI (2.5% w/v; default configuration) solution and a drying period (default 5 min at room temperature); 30 fast immersions in the Lox solution; and 15 fast immersions in the cross-linking solution (BSA/Glut). After the immobilization step, all biosensors were cured for 2 h at 37 ºC and stored overnight at 4 ºC in a refrigerator. Finally, an interference-rejection film of PoPD/BSA (PoPD for clarity, below) was electropolymerized over the biosensor. Electropolymerization of PoPD was carried out with a standard three-electrode setup; a custom-made Ag/AgCl /saturated KCl reference was used as the reference electrode and platinum wire as the auxiliary electrode. The electropolymerization was driven at a constant potential (+0.75 V) for 20–25 min. After the fabrication procedure of the biosensors was completed, they were cleaned in doubly-distilled water. When not in use, biosensors were stored in dry condition at 4 ºC.

3. RESULTS AND DISCUSSION

3.1 Prussian Blue film: characterization and optimization

PB-modified microsensors were characterized using CV. Two well-defined characteristic peaks appeared with formal potentials of 0.1 V and 0.9 V, in good agreement with previous data [32-34, 37]. The PB ↔ PW (Prussian White) transition (Figure 1a) showed a broad composite anodic peak and narrower cathodic peak characteristic of PB redox behavior displaying a mono-electronic quasi-reversible inter-conversion (ΔE ~ 65 mV and I_{rd}/I_{ox} ~ 0.8 at a scan rate 25 mV s^{-1}).

A clear change in the CV of PB (Figure 1a) was observed in the presence of H_2O_2: an enhancement of the cathodic current and a concomitant decrease in the anodic current. This observation reflects the catalytic reduction reaction, which can be ascribed to the reduction of H_2O_2 to water by PW, as previously reported [32, 38].

The thickness of the film, *d*, was estimated taking account of the number of unit cells present on the electrode surface, geometrical parameters of the PB cell, and the working electrode area [39], according to equation 1:

$$d = (Q_{ox}/nFA)\ (l^3 N_A/4) \qquad (1)$$

where Q_{ox} is the electrical charge associated to the anodic peak, n the number of electrons in the redox process (l), F the Faraday constant, A the electrode area (6.33×10^{-5} cm^2), l is the length of the unit cell (1.02 nm) [37] and N_A is Avogadro's number. The value 4 appears in the equation since there are four effective iron atoms in the unit cell.

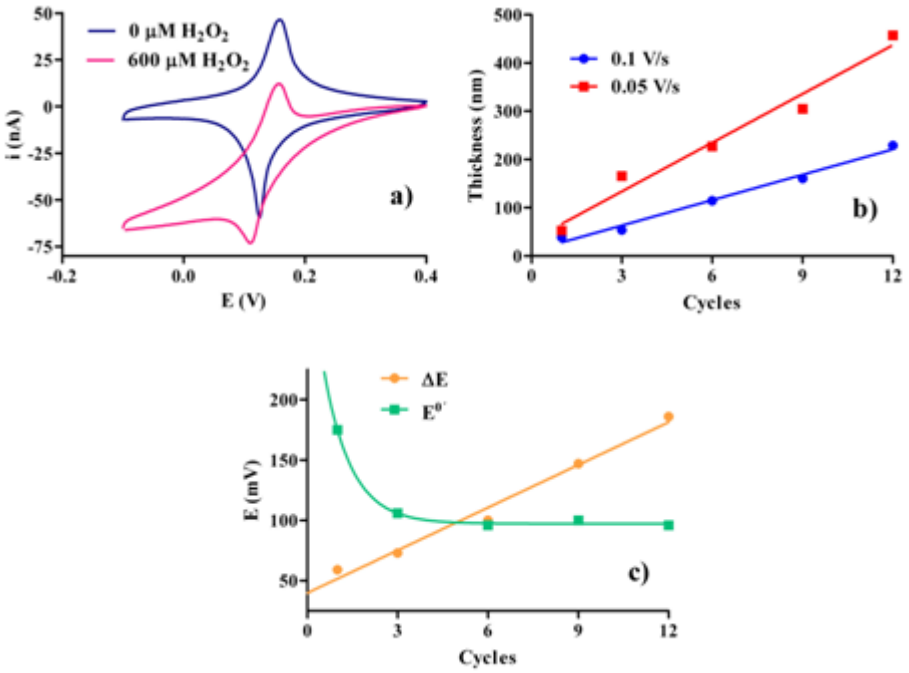

Figure 1. (a) CV for PB-modified carbon fiber electrodes (CFE/PB) without and with 600 µM H_2O_2. (b) Thickness evolution of PB deposit against the number of cycles employed during electro-deposition at two different scan rates. (**c**) Evolution of the peak separation (ΔE) and the formal potential (E°′) against the number of cycles applied during the electro-deposition at 0.01 V s^{-1}.

Our results indicate a linear relationship between film thickness (Figure 1b) and the number of cycles, as well as faster growth when the potential scan rate was decreased (*i.e.*, 17 and 35 nm/cycle at 0.1 and 0.05 V s^{-1}, respectively), in agreement with previous reports [40]. The PB film deposited at 0.1 V s^{-1} showed a positive correlation between peak separation, ΔE, and the number of cycles (Figure 1c). In contrast, the formal potential, $E^{0\prime}$, remained constant after 3 cycles (Figure 1c). From these results, 0.1 V s^{-1} and three cycles were selected to deposit a thin film onto CFEs for biosensor fabrication (*Section 3.2*), which gave a thickness of 51 ± 5 nm (mean ± SD, n = 6).

The CV shape of deposited PB films showed a clear dependence on the ionic composition of the background electrolyte solution (Figure 2, inset). Previously, it has been demonstrated that PB films display a specific transport of alkali metal cations due to its zeolite structure [32, 37]. These geometrical conditions affect the transport of cations during PB ↔ PW transitions, determining its electrochemical properties. In order to explore the ionic transport across the film, electrochemical

impedance spectroscopy (EIS) was used. EIS is an effective method to probe the interfacial properties of surface-modified electrodes [39, 41, 42]. The experimental Faradaic impedance spectra were fitted using a general Randles electronic equivalent circuit (for details see reference [34]), which is very often used to model interfacial phenomena [42]. The semicircle diameter in the impedance spectrum (Figure 2), equates to the charge-transfer resistance, R_{ct}, and displays a clear dependence on cation diffusion.

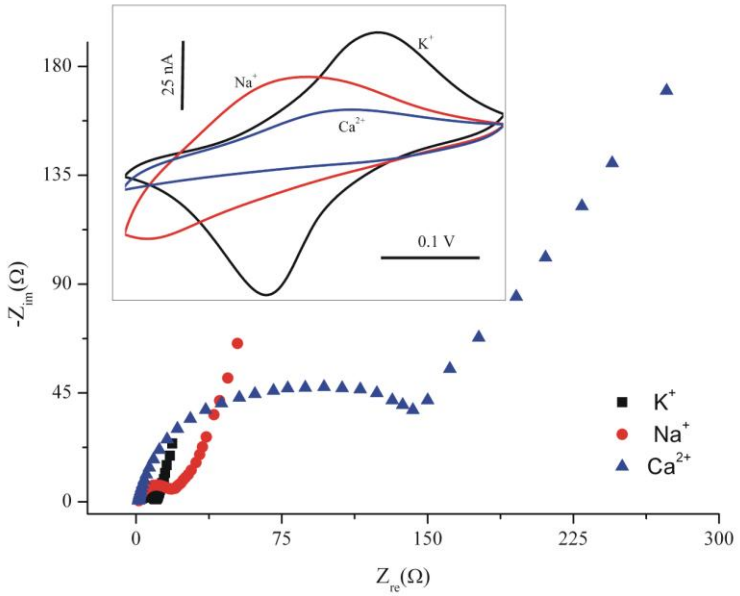

Figure 2. EIS of PB-modified carbon fiber electrodes (CFE/PB) in different background electrolytes: 0.1 M KCl, NaCl or $CaCl_2$, with 0.02 M HCl. Stabilization potential: +0.1 V vs. SCE, signal amplitude: 5 mV and frequency range: 40 kHz−0.5 Hz. Inset: CV of PB-modified carbon fiber electrodes (CFE/PB) in different background electrolytes: 0.1 M KCl, NaCl or $CaCl_2$, with 0.02 M HCl, scan rate 0.1 V s^{-1} vs. SCE.

Our results showed that more highly hydrated cations (Ca^{2+}) display higher R_{ct}, whereas lesser hydrated cations, with lower resistance values ($K^+ < Na^+$), exhibits facilitated transport across the film, consistent with the CV shapes shown in Figure 2 (inset).

Freshly deposited PB films have been shown to be highly hydrated and unstable; accordingly, some authors have suggested activation and heat-treatment steps before their use [43, 44]. In our case activation was carried out in electrolyte solution (0.1 M HCl, 0.1 M KCl), using the same parameters as in the deposition step until the CV was stable (~50 cycles). Heat treatment was then investigated at different temperatures for 1 hour, and its effect on PB electro-chromic properties studied. The CVs for PB (Figure 3a) after heat treatment showed a progressive peak-current decrease and a significant lost of electrochemical activity at 200 ºC. The FTIR and UV-Vis absorbance spectra of the as-deposited PB film showed the characteristic Fe–CN band (2067 cm^{-1}) related to the stretching vibration of Fe–CN and the broad absorption peak at 672 nm due to charge transfer between Fe^{3+} to Fe^{2+} ions, respectively [32]. The FTIR spectrum (Figure 3b) in the high frequency region was characterized by a very broad band which can be attributed to stretching modes of bonded (2973 cm^{-1}) and free (3435 cm^{-1}) OH

groups of water [45, 46]. This band shows that water molecules can be found in PB, either coordinated in the shell of high spin iron or occupying interstitial positions as uncoordinated water. With heat treatment these bands gradually decrease in intensity. On the other hand, the Fe–CN band suffers only a slight decrease up to 150 ^{o}C, but almost disappeared at 200 ºC, showing a clear thermal decomposition of PB. The UV-Vis spectrum (Figure 3c) showed a similar behavior discussed for the FTIR, although at 200 ºC it displayed a typical rust color and a clear band between 300 and 400 nm that corresponds to the wavelength region of Fe_2O_3 [47]. In view of these results, 100 ºC was selected for further investigation.

The effect of pH during electro-deposition was studied by using different electrolyte solutions: 0.02 (Figure 3d_i) and 0.1 M HCl (Figure 3d_j and 3d_k), and then cycling CFE/PB at 0.1 V s^{-1} (~33 min) in PBS (pH 6). Our results indicate that PB films deposited in the more acid medium (Figure 3d_j) showed better stability, whereas PB electro-deposited with 0.02 M HCl (Figure 3d_i) showed a significant peak reduction when the first and the last (150th) cycles were compared. Nevertheless, only with an additional thermal treatment (Figure 3d_k), does PB display enough stability for useful application in electro-analytical devices.

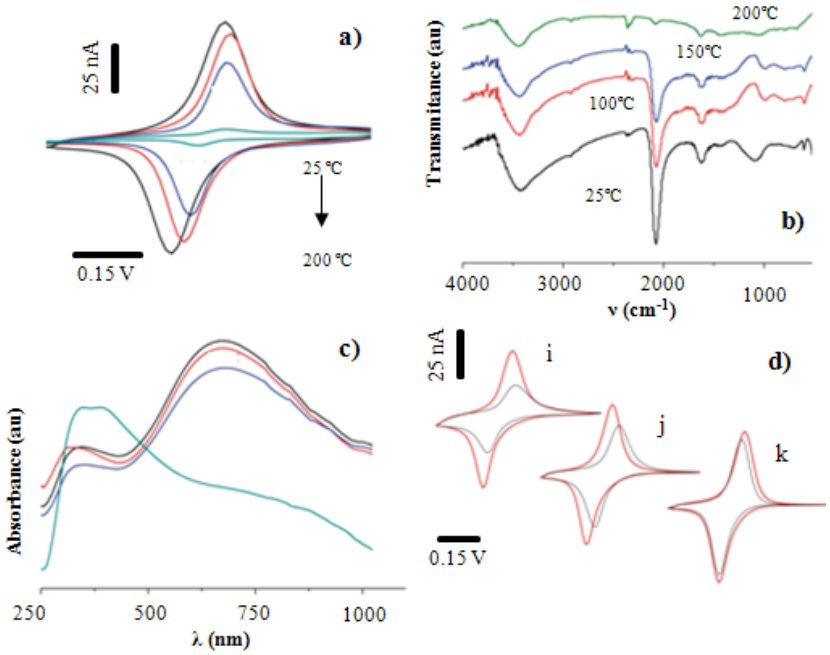

Figure 3.– Effect of annealing PB films at different temperatures, illustrated by CV (a), FTIR (b) and UV–Vis (c) spectra. (d) Stability for PB-modified electrodes (CFE/PB) electrodeposited at different pH conditions (scan-1 in *red*; scan-150 in *blue*: 0.02 M HCl (*i*) and 0.1 M HCl (*j*) and (*k*), without (*j*) and with (*k*) thermal treatment.

3.2 Lactate biosensor optimization

Following the design of glucose microbiosensors developed by our group [32-35], we assembled new lactate microbiosensors. Previously we showed that enzyme loading depends on the

number of dip-immersions employed during the manufacturing process [33]. Consequently, in the present work this number was fixed at 30 fast immersions. The first parameter investigated was the enzyme concentration. In order to optimize this concentration several biosensors were assembled using different Lox concentrations (25, 50 and 100 U mL^{-1}). Calibration curves for these biosensors (Figure 4a) showed that 100 U mL^{-1} displayed the best result with V_{max} [26] 15 times higher than the lowest concentration; for further studies this concentration was selected.

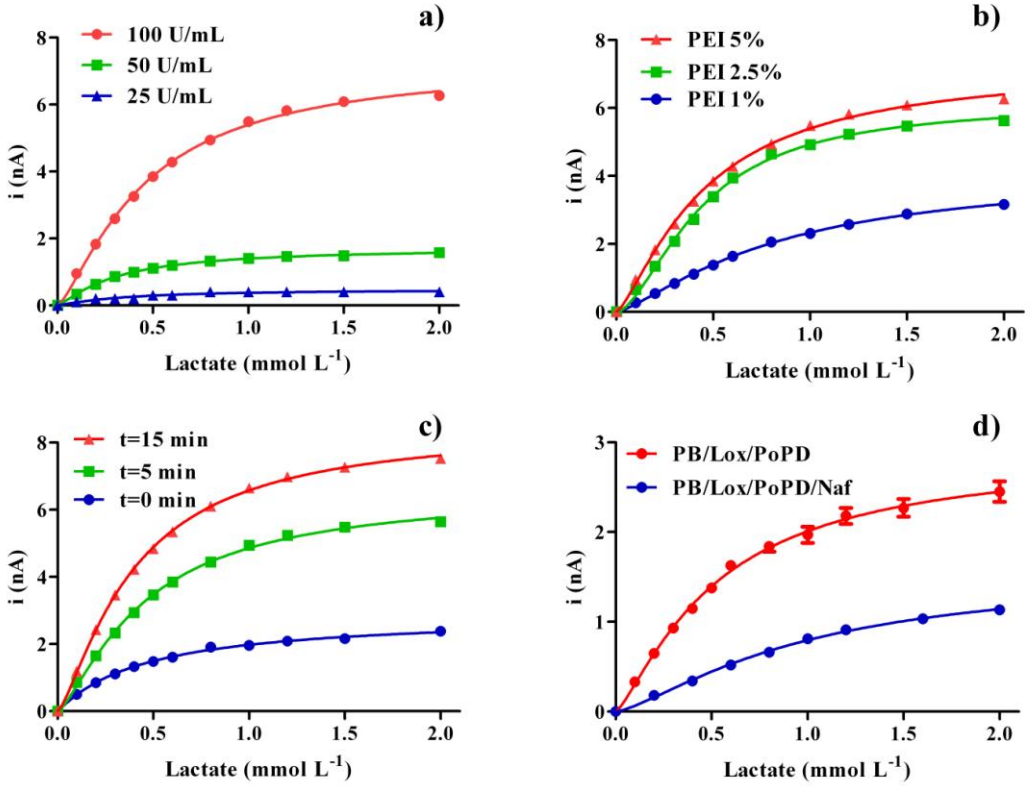

Figure 4.– Calibration curves for different lactate biosensors during optimization by changing different assembly parameters: (a) enzyme concentration, (b) polyethyleneimine (PEI) concentration, and (c) drying time between PEI immersion and enzyme loading. (d) Calibration curves for both types of lactate biosensors proposed in the present work (mean ± SEM, n = 4). The background electrolyte solution was PBS (0.1 M NaCl) pH 7.4; the applied potential was 0 V against SCE.

The next step was to study the effect on the enzyme loading of a polyelectrolyte such as PEI [33-34]. In recent years its ability to inhibit enzyme inactivation, and to improve its stability by the formation of cationic–anionic complexes, has been exploited [48]. In this context we studied the optimal concentration of PEI and how water content affects the enzyme loading during biosensor assembly. Responding to the first question, several PEI solutions were prepared (1, 2.5 and 5 % w/v) in water and used during biosensor construction. Figure 4b shows that both 2.5 and 5 % w/v almost doubled the enzyme loading (higher V_{max} values) compared with 1% w/v. So 2.5 % w/v PEI was maintained for further studies. Until now a drying period of 5 min was employed between immersion

in PEI and Lox solutions. In order to explore if water content affects the enzyme loading, several drying times were selected (0, 5 and 15 min). Our results (Figure 4c) suggest that longer drying times provide higher enzyme loading (V_{max} ~ 3 times with respect to the wet configuration), and that the hydration conditions of PEI are an important parameter in order to improve the enzyme loading. On the basis of these data, drying times were increased to 15 min in the following development studies.

The final step during microbiosensor construction was the addition of an external permselective film, (Lox/PoPD), which improves anti-biofouling properties and selectivity against potential endogenous interferences such as AA, UA, DA, *etc*. [32-34, 49]. First results showed a significant loss of sensitivity (~60%) that may be attributed to several factors such as: enzyme deactivation, the new diffusion barrier [32-34] and electrostatic repulsion between BSA and lactate anions. Figure 4d shows calibration data for lactate microbiosensors incorporating PoPD. Enzyme parameters, obtained using a Hill-modified Michaelis–Menten equation [50], and analytical parameters are summarized in Table 1. Lox/PoPD showed a linear range up to 0.6 mM with a sensitivity (S) of 2.68 $\pm$ 0.12 nA mM^{-1} (~42 nA μM^{-1} cm^{-2}); meanwhile the detection limit (S/N = 3) and reproducibility (CV%) were ~6 µM and 4 %, respectively.

Taking into account that extracellular fluid (ECF) concentration of lactate is ~0.4 mM [51, 52] and that changes registered during neuronal activation may reach ~200% of its basal concentration (~0.7 mM) [10, 51, 52], the present configuration possessed excellent sensitivity, but the operational linear range is pretty tight for use in physiological applications. However, we were able to increase the linear range up to 1.2 mM by means of an external Nafion film (Lox/PoPD/Naf). Three dip immersions in 5% Nafion proved enough for our purpose, whereas a higher number of dips (eight) resulted in the complete loss of sensitivity. This new diffusion film provides a barrier to lactate, decreasing sensitivity to 0.77 nA mM^{-1} (~12 nA μM^{-1} cm^{-2}) by both decreasing V_{max} and increasing K´ [26] (see Table 1). Meanwhile free diffusion of O_2 to the enzyme was maintained where it is needed to regenerate its active center. Thus we present two possible configurations that may be used depending on the in-vivo requirements.

Table 1. Enzyme kinetic (apparent Michaelis constant (K'), calibration plateau (V_{max}), and Hill coefficient (*h*)), and analytical parameters (sensitivity (S), coefficient of determination (R^2), detection limit (D.L.), linear range (L.R.) and coefficient of variation (CV%)) of different *optimized* lactate biosensor designs, Mean $\pm$ SEM, n = 4. D.L. was calculated as 3 × SD of the background current. The Hill parameter is included to highlight possible deviations from straightforward Michaelis–Menten kinetics, for which *h* = 1. Calibration curves were obtained by applying 0 V against SCE in air-saturated PBS 0.1 M NaCl (pH 7.4).

Configuration	K' (mM)	Vmax (nA)	h	S (nA mM-1)	S (nA µM-1 cm-2)	R2	D.L. (M)	L.R. (mM)	CV (%)
PB/Lox/PoPD (n =4)	0.44 ± 0.05	2.88 ± 0.09	1.3 ± 0.1	2.68 ±0.09	42.3 ± 1.5	0.994	5.6 · 10-6	D.L - 0.6	7.1
PB/Lox/PoPD/Naf (n =4)	0.97 ± 0.14	1.57 ± 0.1	1.4 ± 0.1	0.77 ±0.03	12.2 ±0.4	0.994	16.8 · 10-6	D.L - 1.2	6.7

Another two important questions, when designing sensors for an electrochemically hostile environment such as brain [53], are protein biofouling and interference response. In order to study the anti-biofouling properties of our biosensors, they (with and without PoPD/Naf) were immersed for 18 h in a solution of BSA (10% w/v), and lactate sensitivity before and after BSA exposure determined in its linear range (n = 3). Surprisingly, both configurations showed no significant difference (two-tailed paired t-test, p-value: 0.11 and 0.07, respectively) before and after being dipped in the protein solution, demonstrating the excellent anti-biofouling properties of the present configurations (Figure 5a). In this sense, PoPD films have been shown to be stable during long periods (~15 days) in in-vivo experiments, displaying excellent biocompatibility and anti-interference properties [26, 52].

Non-optimized lactate biosensors free of PoPD film (Figure 5b) showed good anti-interference properties (as a result of the low applied potential used to detect H_2O_2 at the PB-modified surface) for a considerable number of interference species and metabolites at their basal concentration [34], and responded well to lactate additions (c: 0.4 and g: 0.2 mM). Only AA (0.2 mM), one of the major endogenous interferences in the CNS, produced a clear change in the biosensor current, indicating that although we were working at a low potential, we needed an additional permselective film to avoid AA effects on biosensor responses [49]. Finally, the optimized lactate biosensor (with an external PoPD/Naf film) didn't response to the main interferences and metabolites (including AA; see Figure 5c).

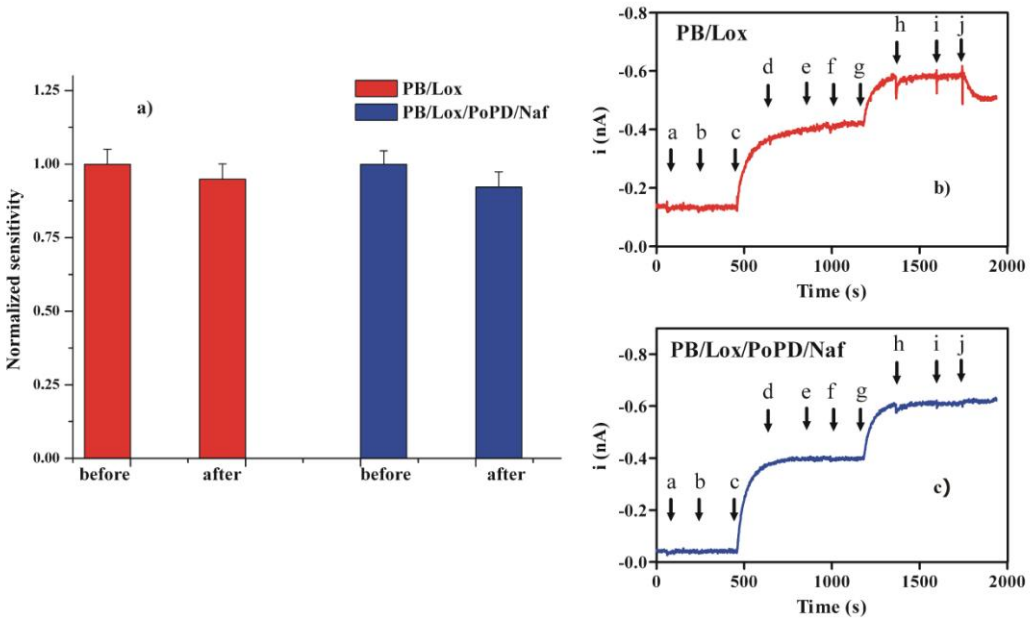

Figure 5. (a) Normalized sensitivity (mean ± SEM, n = 4) for PB/Lox and PB/Lox/PoPD/Naf configurations before and after being immersed in a BSA solution (10% w/v) for 18 h. Amperometric response for *non–optimized* PB/Lox (b) and *optimized* PB/Lox/PoPD/Naf (c) configurations with successive additions of: (a) 10 nM dopamine (DA), (b) 10 µM 3,4-dihydroxyphenylacetic acid (DOPAC), (c) 0.4 mM lactate, (d) 10 nM serotonin (5-HT), (e) 20 µM glutamate (Glu), (f) 0.4 mM glutamine (Gln), (g) 0.2 mM lactate, (h) 1 mM glucose, (i) 10 µM uric acid (UA) and (j) 0.2 mM ascorbic acid (AA). Calibration conditions as in Figure 4.

3.3 Lactate biosensor measurements in in-vivo experiments

Although there is an extensive bibliography about lactate biosensors [54-60], there are few papers published regarding lactate microbiosensors measuring directly in the CNS [10, 51, 52, 61, 62]. Much of these reports were based on either modified Pt transducers [10, 51], ceramic-based multisite microelectrodes [62] or CFEs [52, 61], working at a high applied potential (~0.7 V) [10, 51, 62] or using differential normal pulse voltammetry (DNPV) [52, 61] to detect the H_2O_2 generated during the enzymatic reaction. Here we present, for the first time, a lactate microbiosensor based on PB-modified CFE that is able to detect physiological changes in lactate levels at a low applied potential in the CNS.

For all in-vivo experiments, a time of 30 min after biosensor insertion was used to stabilize the baseline current. This was used to estimate the basal lactate concentration, comparing this current with previous calibration data. The basal lactate concentration (0.36 $\pm$ 0.02 mM, mean $\pm$ SD, n = 5) was in good agreement with previous data reported by other authors [51, 52], although factors such as the state of anesthesia will influence such comparisons [63].

It is known that extracellular fluid lactate concentration can be increased by the stimulation of neuronal activity [2, 14, 15, 52] and studies concerning such a stimulation by glutamate and *N*-methyl-D-aspartate (NMDA) have been reported [52]. In the present work, we also used NMDA, an ionotropic glutamate receptor agonist. After obtaining a stable baseline for the biosensors (normalized basal response: 100 $\pm$ 12 %; mean $\pm$ SD, n = 3), NMDA (5 mg in 2 mL PBS) was administered (*i.p.*). After 5–10 min a clear increase in lactate level was observed reaching a value of 205 $\pm$ 13 % which remained at this level for ~1 h. These results are in good concordance with previous data [52] and with ANLSH [2, 6, 14-18].

The lactate biosensor response was also evaluated during electrophysiological stimulation. In this context, local electrical stimulation was applied (30 Hz for 3 s) at intervals of 3 min approximately, allowing enough time to reach the basal resting level again. Data showed (Figure 6a) a slight decrease (~25 %) in lactate level during local electrical stimulation, suggesting that lactate is consumed during neural activity. After that, an increase in extracellular lactate concentrations (~90 % of the basal concentration) appears to be a response of the tissue to the demand for additional energy [10, 14-18]. Similar results were obtained with a lactate biosensor employing a 25-µm diameter Pt wire transducer and detecting H_2O_2 at +0.7 V (Figure 6b), the configuration commonly employed in biosensors for in-vivo applications, validating the kinetic and physiological lactate response. Finally, theses data are in good agreement with previous publications where extracellular lactate concentration fluctuations and its relationships with neural activity were explored in the dentate gyrus of the hippocampus of the rat brain after electrical stimulation of the perforant pathway [10].

The last sets of experiments were conducted to study changes of lactate and O_2 in the extracellular compartment. An O_2 sensor was constructed by coating an unmodified CFE with PoPD (CFE/PoPD) to reject interferences and to improve biocompatibility properties of the sensor [51]. This sensor was polarized at –0.65 V to detect O_2 [64]. Firstly, the in-vivo oxygen response was checked by changing extracellular oxygen concentration *via* gas administration (pure O_2 or N_2). Under these conditions, the O_2 sensor showed a clear current increase during mild hyperoxia (O_2 supply; Figure 7a), whereas the same period of mild hypoxia (N_2 supply) showed the opposite effect (Figure 7b).

Under these conditions, the O_2 signal suffered a change of 40–50% with respect to its basal level, in good agreement with previous work [65]. Changes in both cases were immediate and, on cessation of gas administration, the signals quickly returned to baseline levels indicating a rapid return to normoxic conditions. These results confirmed that CFE/PoPDs implanted in anesthetized animals respond rapidly to changes in cerebral tissue O_2 concentrations.

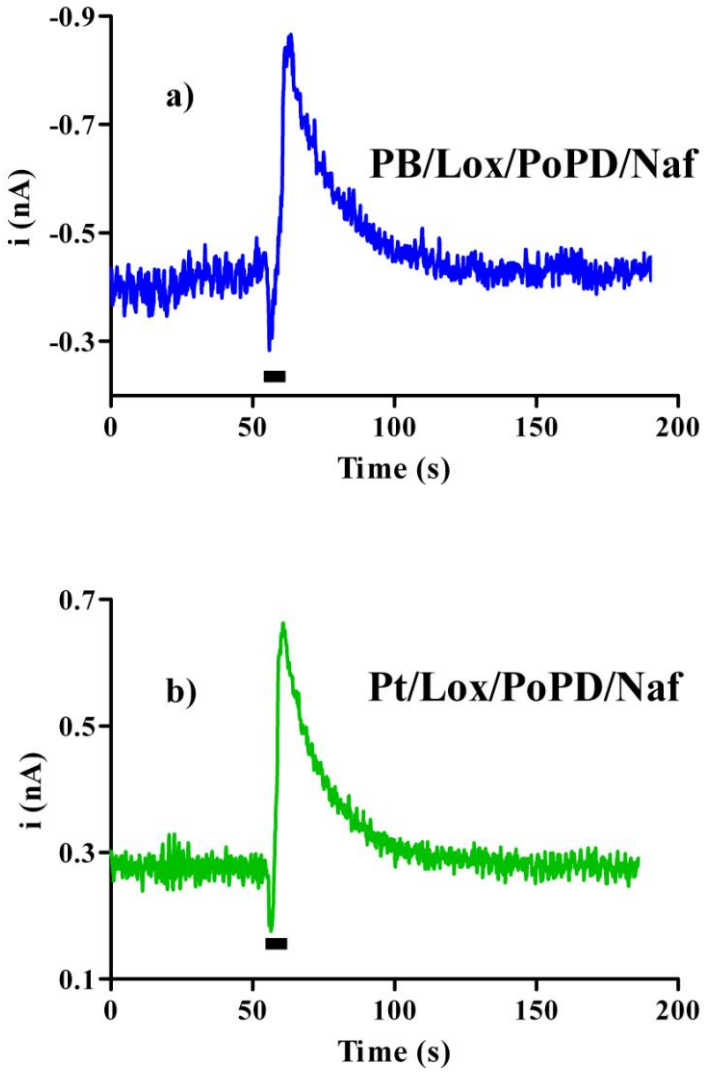

Figure 6. Extracellular lactate changes during electrical stimulation (30 Hz, 3 s) registered in the prefrontal cortex of an anesthetized rat. Data were obtained with (a) a PB/Lox/PoPD/Naf biosensor and with (b) a Pt/Lox/PoPD/Naf biosensor proposed in the present work

In order to study simultaneous changes in lactate and O_2 levels, both sensors were inserted in the prefrontal cortex close to the stimulation electrodes (50–100 μm). Electrical stimulation (20 Hz during 5 s) generated a lactate change consisting of a short period of lactate consumption followed by an increase of almost 90 % of the basal lactate concentration, similar to that seen in Figure 6 (see Figure 7c). In contrast, the O_2 sensor response showed an immediate decrease in extracellular O_2 levels (~20% of the basal value) during the stimulation, and this level was held for ~30 s after the stimulus. A

similar time was needed to reach the lactate basal level after stimulation. Taking into account that extracellular analyte concentrations are determined by a balance between consumption and supply from different compartments, these data reveal that O_2 may be consumed during oxidative processes (TCA cycles) in active neurons [1-6], and lactate could serve as an additional non-oxidative fuel during activation events [2, 14, 15] or may be the predominant oxidative substrate [6, 16, 17]. Nevertheless to obtain more robust arguments, additional experiments will be needed. At this point, these experiments have been presented to illustrate the potential use of our lactate biosensors in physiological applications. Future work will be done in order to explore lactate changes during neural activation and its relationship with hemodynamic responses, and with other metabolic substrates such as glucose, pyruvate and O_2.

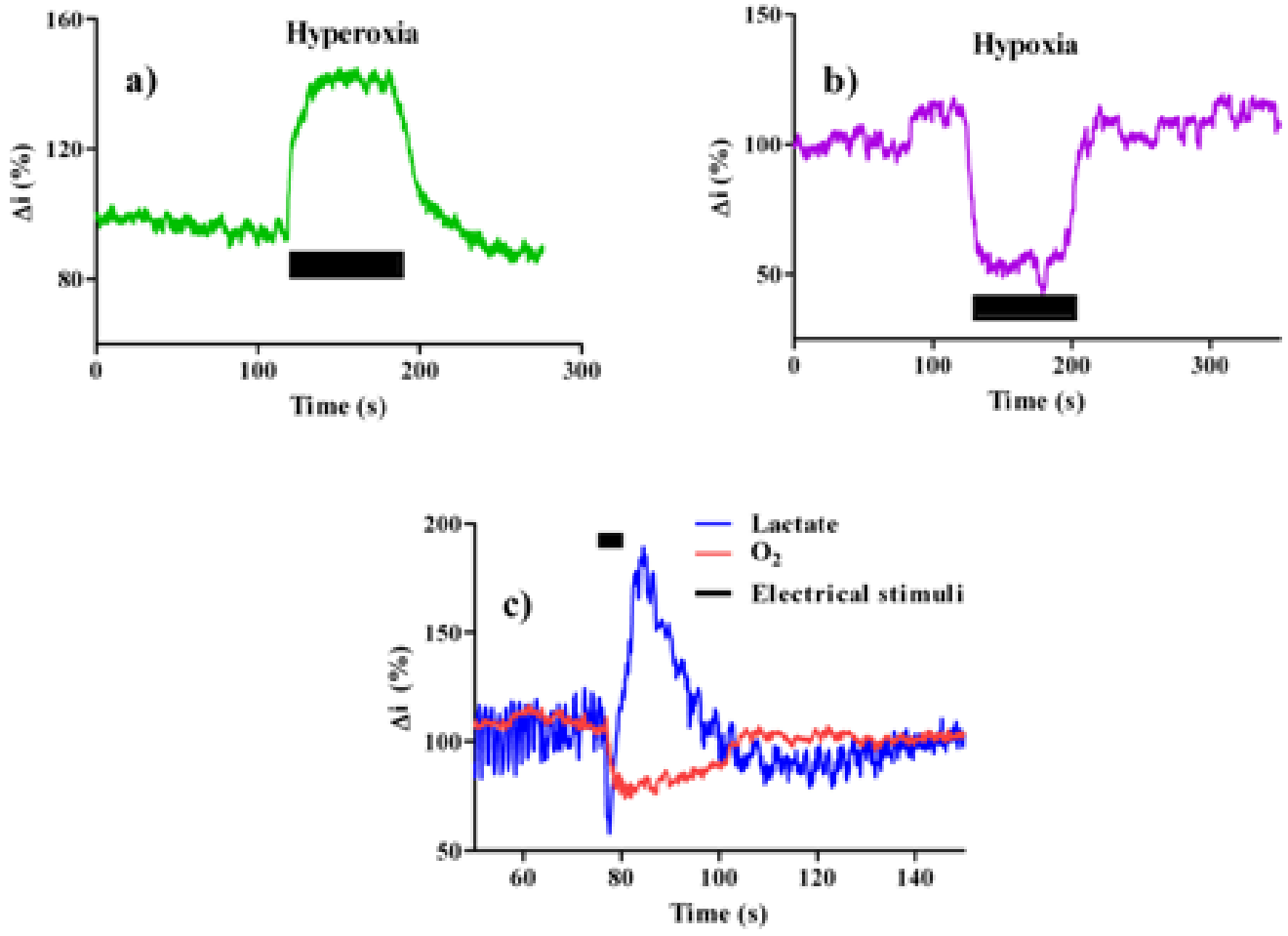

Figure 7. Effect of physiological manipulation of prefrontal cortex dissolved oxygen, monitored using a CFE/PoPD sensor. Exposing the animal briefly to pure oxygen (a), the ECF oxygen concentration promptly increased (~160% of baseline), returning back after restoration of a normal atmosphere. In contrast, exposure to nitrogen (b), induced a short-lasting decline in brain oxygen levels (~50%) which recovered promptly following nitrogen removal. (c) Simultaneous changes in lactate biosensor and oxygen (CFE/PoPD) sensor signals before, during and after electrical stimulation (20 Hz, 5 s) recorded in the prefrontal cortex of an anesthetized rat.

4. CONCLUSIONS

In this study we present a novel lactate microbiosensor based on PB-modified CFEs. This approach allows the detection of H_2O_2 enzymatically generated in the biosensor surface layer at low applied potential (0 V against SCE), instead of the high potential (+0.7 V against SCE) commonly used with the Pt transducers. During construction, each step was studied in detail in order to obtain an optimized configuration determined by functional and biocompatibility needs of neurochemical applications. In this way PB electro-deposition was studied and film properties were characterized using CV, EIS, IR and Vis-UV techniques. After optimizing the protocol to modify the CFEs with this electrocatalytic compound (PB), the next step was its modification with lactate oxidase. In this context, biosensor responses were honed to the special conditions needed for physiological applications such as: sensitivity, selectivity, operational linear range, biocompatibility, *etc*. Finally, an optimized lactate biosensor is presented and some in-vivo results shown to illustrate its application in the study of lactate and oxygen in the brain during neuronal activation.

ACKNOWLEDGMENT
The funds for the development of this device have been provided by the Ministerio de Industria, Turismo y Comercio (TSI-020100-2011-189 and TSI-020100-2010-346) and Ministerio de Ciencia e Innovación (TIN2011-28146 and TIN2008-06867-C02-01/TIN). We thank Dr JL Rodriguez Marrero and J Florez Montaño for help in EIS measurements.

References

1. T.M. Bliss, R.M. Sapolsky, *Brain Res.,* 899 (2001) 134
2. A. K. Bouzier–Sore, M. Merle, P.J. Magistretti, L. Pellerin, *J. Physiol. Paris* 96 (2002) 273
3. L.H. Bergersen, *Neuroscience* 145 (2007) 11
4. L. Hertz, M. Fillenz, *Neurochem. Int*. 34 (1999) 71
5. C.P. Chih, E.L. Roberts, *J. Cerebr. Blood Flow Metab.* 23 (2003) 1263
6. A.K. Bouzier–Sore, P Voisin, P Canioni, P.J. Magistretti, L. Pellerin, *J. Cerebr. Blood Flow Metab*. 23 (2003) 1298
7. T.E. Friedmann, C. Barborka, *J. Biol. Chem.* 141 (1941) 993
8. H. Haljamae, *Intens. Care World* 4 (1987) 118
9. G.A. Brooks, *Fed. Proc.* 45 (1987) 2924
10. Y.B. Hu, G.S. Wilson, *J. Neurochem*. 69 (1997) 1484
11. M.G. Larrabee, *J. Neurochem.* 64 (1995) 1734
12. C.L. Poitry–Yamate, S. Poitry, M. Tsacopoulos, *J. Neurosci.* 15 (1995) 5179
13. A. Schurr, J.J. Miller, R.S. Payne, B.M. Rigor, *J. Neurosci.* 19 (1999) 34
14. L. Pellerin, P,J. Magistretti, *Proc. Nat. Acad. Sci. USA* 91(1994) 10625
15. M. Tsacopoulos, P.J. Magistretti, *J. Neurosci.* 16 (1996) 877
16. A.K. Bouzier–Sore, P. Voisin, V. Bouchaud, E. Bezancon, J.M. Franconi, L. Pellerin, *Euro. J. Neurosci.* 24 (2006) 1687
17. Y. Itoh, T. Esaki, K. Shimoji, M. Cook, M.J. Law, E. Kaufman, L. Sokoloff, *Proc. Natl. Acad. Sci. USA* 100 (2003) 4879
18. L. Pellerin, G. Pellegri, P.G. Bittar, Y. Charnay, C. Bouras, J.L. Martin, N. Stella, P.J. Magistretti, *Dev. Neurosci.* 20 (1998) 291

19. C.P. Chih, P. Lipton, E.L. Roberts, *Trends Neurosci*. 24 (2001) 573
20. G.A. Dienel, L. Hertz, *J. Neurosci. Res.* 66 (2001) 824
21. J. Korf, J. *Cereb. Blood. Flow Metab*. 26 (2006) 1584.
22. A. Schurr, *J. Cereb. Blood Flow Metab.* 26 (2006) 142
23. D.A. Jones, J. Ros, H. Landolt, M. Fillenz, M.G. Boutelle, *J. Neurochem.* 75 (2000) 1703
24. T. Yao, T. Yano, Y. Nanjyo, H. Nishino, *Anal. Sci.* 19 (2003) 61
25. Y. Dong, L. Wang, D. Shangguan, X. Yu, R. Zhao, H. Han, G. Liu, *Neurochem. Int.* 43 (2003) 67
26. R.D. O'Neill, G. Rocchitta, C.P. McMahon, P.A. Serra, J.P. Lowry, T*rends Anal. Chem.* 27 (2008) 78
27. J.B. Gramsbergen, J. Skjøth–Rasmussen, C. Rasmussen, K.L. Lambertsen, *J. Neurosci. Meth.* 140 (2004) 93
28. T. Yao, G. Okano, *Anal. Sci.* 24 (2008) 1469
29. M.C Parkin., S.E. Hopwood, D.A. Jones, P. Hashemi, H. Landolt, M. Fabricius, M. Lauritzen, M.G. Boutelle, A.J. Strong, *J. Cereb. Blood Flow Metab.* 25 (2005) 402
30. R.D. O'Neill, J.L. Gonzalez–Mora, M.G. Boutelle, D.E. Ormonde, J.P. Lowry, A. Duff, B. Fumero, M. Fillenz, M. Mas, *J. Neurochem.* 57 (1991) 22
31. R.D. O'Neill, J.P. Lowry, M. Mas, *Crit. Rev. Neurobiol.* 12 (1998) 69
32. P. Salazar, M. Martín, R. Roche, R.D. O'Neill, J.L. González–Mora, *Electrochim. Acta* 55 (2010) 6476
33. P. Salazar, M. Martín, R. Roche, J.L. González–Mora, R.D. O'Neill, *Biosens. Bioelectron.* 26 (2010) 748
34. P. Salazar, R.D. O'Neill, M. Martín, R. Roche, J.L. González–Mora, *Sensors Act. B–Chem.* 152 (2011) 137
35. R. Roche, P. Salazar, M. Martín, F. Marcano, J.L. González–Mora, J. *Neurosci. Meth.* 202 (2011) 192
36. G. Paxinos, C. Watson, *The Rat Brain in Stereotaxic Coordinates*, Academic Press, Sydney (1986)
37. F. Ricci, G. Palleschi, *Biosens. Bioelectron*. 21 (2005) 389
38. K. Itaya, N. Shoji, I. Uchida, J. *Am. Chem. Soc.* 106 (1984) 3423
39. J.J. García–Jareño, J.J. Navarro, A.F. Roig, H. Scholl, F. Vicente, *Electrochim. Acta* 40 (1995) 1113
40. A. Goux, J. Ghanbaja. A. Walcarius, *J. Mater. Sci.* 44 (2009) 6601
41. M. Zhou, L. Shang, B. Li, L. Huang, S.J. *Dong, Biosens. Bioelectron.* 24 (2008) 442
42. Y. Liu, X. Qu, H. Guo, H. Chen, B. Liu, S. Dong, *Biosens. Bioelectron.* 21 (2006) 2195
43. I.L. Mattos, L. Gorton, T. Laurell, A. Malinauskas, A.A. Karyakin, *Talanta* 52 (2000) 791
44. I.L. Mattos, L. Gorton, T. Ruzgas, *Biosens. Bioelectron.* 18 (2003) 193
45. J.D. Qiu, H.Z. Peng, R.P. Liang, J. Li, X.H. Xia, *Langmuir* 23 (2007) 2133
46. P.J. Kulesza, S. Zamponi, M.A. Malik, K. Miecznikowski, M. Berrettoni, R. Marassi, *J. Solid State Electrochem*. 1 (1997) 88
47. S.A. Agnihotry, P. Singh, A. G. Joshi, D.P. Singh, K.N. Sood, S.M. Shivaprasad, *Electrochim. Acta* 51 (2006) 4291
48. J.D. Breccia, M.M. Andersson, R. Hatti–Kaul, *Biochim. Biophys. Acta* 1570 (2002) 165
49. S.A. Rothwell, S.J. Killoran. R.D. O'Neill, *Sensors* 10 (2010) 6439
50. S.S. El Atrash, R.D. O'Neill, *Electrochim. Acta* 40 (1995) 2791
51. M. Demestre, M. Boutelle, M. Fillenz, *J. Physiol*. 499 (1997) 825
52. N.F. Shram, L.I. Netchiporouk, C. Martelet, N. Jaffrezic–Renault, C. Bonnet, R. Cespuglio, *Anal. Chem*. 70 (1998) 2618
53. R.D. O'Neill, *Analyst* 118 (1993) 433
54. R. Garjonnyte, Y. Yigzaw, R. Meskys, A. Malinauskas, L. Gorton, *Sensors Act. B–Chem.* 79 (2001) 33
55. N.G. Patel, A. Erlenkötter, K. Cammann, G.–C. Chemnitius, *Sensors Act. B–Chem.* 67 (2000)134

56. A. Ges, F. Baudenbache, *Biosens. Bioelectron.* 26 (2010) 828
57. J. Haccoun, B. Piro, V. Noël, M.C. Pham, *Bioelectrochemistry* 68 (2006) 218
58. L. Cheng–Li, S. Cheng–Ling, C. Lai–Kwan, *Anal. Chem.* 79 (2007) 3757
59. A. Poscia, D. Messeri, D. Moscone, F. Ricci, F. Valgimigli, *Biosens. Bioelectron.* 20 (2005) 2244
60. S.A.M. Marzouk, V.V. Cosofret, R.P. Buck, H. Yang, W.E. Cascio, S.S.M. Hassan, Talanta 44 (1997) 1527
61. N. Shram, L. Netchiporouk, R. Cespuglio, *Eur. J. Neurosci.* 16 (2002) 461
62. J.J. Burmeister, M. Palmer, G.A. Gerhardt, *Biosens. Bioelectron.* 20 (2005) 1772
63. J.C Goodman, A.B Valadka, S.P.Gopinath, M. Cormio, C.S. Robertson, *J. Neurotrauma* 13 (1996)549
64. M.L. Hitchman, *Measurement of dissolved oxygen*; John Wiley, New York (1978)
65. F.B. Bolger, J.P. Lowry, *Sensors* 5 (2005) 473

10.-Anexo II: Otras publicaciones

Pese a que se han empleado seis publicaciones en el compendio de la presente tesis, no quería dejar pasar la oportunidad de añadir otras dos que no han sido incluidas por distintos motivos: la 1ª por no llegar a los criterios de inclusión y la 2ª por estar en estos momentos en proceso de redacción.

Sin embargo, creo que su inclusión como material anexo termina de completar y dar forma a la tesis. En ellas se muestra una aplicación inmediata de los microbiosensores de glucosa en el análisis neurometabólico, realizando estudios hemodinámicos simultáneos. Por otro lado, en la otra publicación se introducen mejoras en el diseño propuesto, prestando especial atención a las limitaciones estequiométricas del oxígeno "déficit de oxígeno".

psalazar

Journal of Neuroscience Methods 202 (2011) 192–198

Contents lists available at ScienceDirect

Journal of Neuroscience Methods

journal homepage: www.elsevier.com/locate/jneumeth

Simultaneous measurements of glucose, oxyhemoglobin and deoxyhemoglobin in exposed rat cortex

R. Roche*, P. Salazar, M. Martín, F. Marcano, J.L. González-Mora

Neurochemistry and Neuroimaging Group, Faculty of Medicine, University of La Laguna, Campus de Ofra s/n, 38071 Tenerife, Spain

ARTICLE INFO

Article history:
Received 15 December 2010
Received in revised form 23 June 2011
Accepted 5 July 2011

Keywords:
Glucose biosensor
Optical imaging
Hemoglobin
Neurovascular coupling
Oxidative brain metabolism
Exposed rat cortex

ABSTRACT

The present work addresses the simultaneous monitoring of hemoglobin and glucose consumption in rat somatosensory cortex in vivo. We propose a method which combines two techniques: 2-dimensional optical imaging and an amperometric microbiosensor. The mounted setup optimizes the space in the cranial window so that three micro-electrodes can be inserted: glucose microbiosensor, sentinel and stimulating electrode as well as the holder to manipulate the optical fiber. Additionally, a tool based on graphical user interface programming has been developed to visualize a two-dimension spectral map of oxy-, deoxy- and total hemoglobin, HbO_2, HbR and HbT respectively, in the cortex. Our results showed a good sensitivity, selectivity and spatial resolution for both methods. Relevant hemodynamic responses had a common central focus (at the site of the stimulus) which later segregated to other vascular compartments. A good linear relationship between extracellular glucose concentration and HbO_2 values during brain activation after local electrical stimulation was observed for electrochemical and optical recordings (R^2 values were over 0.94). Time courses between glucose and HbO_2 signals showed a temporal delay ranging from 1 s to 2 s, suggesting that both variables are not always coupled. The temporal mismatching reported here, provides in vivo evidence that supports a neuronal hypothesis: cerebral blow flow and oxidative metabolism are driven in parallel by neural activity – rather than a concatenation of events ('in-series' events) occurring at sites of neuronal activation.

1. Introduction

The human brain has a high-energy requirement. The brain consumes almost 20% of the global resting metabolism although it constitutes only 2% of body weight, (Sokoloff, 1960). The glucose consumption rate increases no more than ~50% when the brain responds to external stimuli, and the increases in oxygen consumption are even lower (Shulman et al., 2001; Giove et al., 2003). These energy requirements and accompanying hemodynamic responses form the basis of most current neuroimaging approaches (e.g., fMRI and PET) used for functional mapping in the brain. However, interpretation of these macroscopic signals in terms of the underlying microscopic neurovascular physiology remains a great challenge. In order to overcome this difficulty, we propose here, using two in vivo techniques simultaneously: optical imaging (González-Mora et al., 2002) and an amperometric biosensor device (Salazar et al., 2010a,b,c) to measure hemoglobin and glucose concentrations in the rat brain cortex. Both techniques have been improved and adapted in our laboratory for use in small animals offering a good temporal and spatial resolution.

Biosensors are based on the detection of any electroactive metabolite that is generated (e.g., H_2O_2) or consumed (e.g., O_2) during enzyme reaction. Biosensors offer a variety of advantages over classical techniques for neurochemical monitoring: high spatial and temporal resolution; good selectivity; ease of implementation; amenability to miniaturization; rapid response time; etc. We have developed a glucose biosensor, using a carbon fiber substrate, (Salazar et al., 2010a,b,c) with significantly smaller dimensions and a low working potential, which has significant advantages for in vivo monitoring and is free of common biological interference (Salazar et al., 2010a,b).

On the other hand, optical imaging is a technique that detects changes in blow flood by simply imaging the exposed cortex under optical illumination (Hernández et al., 2009). This is possible because oxy- and deoxyhemoglobin (HbO_2 and HbR) are chromophores that exhibit markedly different absorption spectra in the near-infrared region (Sfareni et al., 1997; Wray et al., 1988), for wavelengths typically in the range of 650–950 nm. Although this technique is one of the simplest in the field of neuroimaging, calculation of hemoglobin concentration is not simple because optical imaging is affected by physiological noise (breathing, heart-rate,

* Corresponding author at: Dra. Rossany Roche. Laboratorio de Neuroquímica y Neuroimagen, Departamento de Fisiología, Facultad de Medicina, Campus de Ciencias de La Salud, Universidad de La Laguna, 38071, Santa Cruz de Tenerife, Spain. Tel.: +34 922 319363; fax: +34 922 319397.
E-mail addresses: rossanyroche@gmail.com, rroche@ull.es (R. Roche).

0165-0270/$ – see front matter © 2011 Elsevier B.V. All rights reserved.
doi:10.1016/j.jneumeth.2011.07.003

head movement, etc.). In Section 2.2 we describe the procedure we use in our laboratory to obtain and analyze relevant optical data from the exposed rat cortex.

Finally, this work tries to test the capabilities of our proposed method to study different aspects of the relationship between oxygen/glucose supplies during neurovascular coupling by detecting the temporal and spatial characteristic of hemoglobin state and extracellular glucose concentration. Furthermore, this work attempts to propose the use of micro-biosensors for quasi real-time measurement of glucose associated to optical imaging as a valid approach for the elucidation of the mechanisms of energy supply and utilization in the brain.

2. Material and methods

2.1. Glucose biosensor

2.1.1. Reagents and solutions

The enzyme glucose oxidase (Gox) from *Aspergillus niger* (EC 1.1.3.4, Type VII-S), purchased as a lyophilized powder, and glutaraldehyde 25% (Glut) were obtained from Sigma–Aldrich (St. Louis, MO, USA), and stored at −21 °C until use. Bovine serum albumin (BSA, fractionV) was also obtained from Sigma–Aldrich. All chemicals, including o-phenylenediamine (o-PD), glucose, polyethyleneimine (PEI), KCl, $FeCl_3$, $K_3[Fe(CN)_6]$, HCl (35%, w/w), H_2O_2 (30%, w/v), Nafion (5 wt.% in a mixture of lower aliphatic alcohols and water), phosphate buffer saline (PBS, pH 7.4 containing 0.1 M NaCl) were obtained from Sigma–Aldrich and used as supplied. PBS stock solutions were prepared in doubly distilled water (18.2 MΩ cm, Millipore-Q), and stored at 4 °C when not in use. Stock 125 mM solutions of glucose were prepared in water, left for 24 h at room temperature to allow equilibration of the anomers, and then stored at 4 °C. The PEI solution used was prepared by dissolving PEI at 5%, w/v in H_2O. The cross-linking solution was prepared in PBS with 1%, w/v of BSA and 0.1%, w/v of Glut. Monomer solution (300 mM o-PD) was prepared using 48.6 mg of o-PD and 7.5 mg of BSA in 1.5 mL of N2-saturated PBS and sonicated for 15 min (McAteer and O'Neill, 1996). A 300 U/mL solution of Gox was prepared by dissolving 3.7 mg in 2 mL of PBS. Carbon fibers (8 μm diameter), single-barrel glass capillaries, and 250 μm internal diameter Teflon-coated copper wire was obtained from Word Precision Instruments Inc. (Sarasota, FL, USA), and silver epoxy paint was supplied by Sigma–Aldrich.

2.1.2. Glucose biosensor

Carbon fiber electrodes (CFEs: 8 μm diameter, 500 μm length) were constructed by modifying our previous method (Salazar et al., 2010a,b). Briefly: carbon fibers (diameter 8 μm, 20–50 mm in length) were attached to Teflon-coated copper wire (diameter 250 μm), using high purity silver paint, and dried for 1 h at 80 °C. The PB layer was then electro-deposited using cyclic voltammetric (CV) methodology, applying 3 cyclic scans within the limits of −0.2 to 0.4 V at scan rate of 0.1 V/s in a fresh solution containing 1.5 mM $K_3[Fe(CN)_6]$ and 1.5 mM $FeCl_3$ in 0.1 M KCl and 0.1 M HCl. These CFE/PBs were cleaned in doubly-distilled water and activated by applying another 50 cycles of electrolyte solution (0.1 M KCl and 0.1 M HCl), using the same protocol. Before use, the CFE/PBs were cleaned again in doubly-distilled water for several seconds. Finally, the PB film was tempered at 100 °C for 1 h. The next step was to immobilize the Gox using the following protocol: 15 fast immersions in PEI solution and a drying period (5 min); 30 fast immersions in the Gox solution; and 15 fast immersions in the cross-linking solution (BSA/Glut). After the immobilization step, all biosensors were cured for 1 h.

2.1.3. Sentinel

A sentinel electrode has been developed to check non-specific reactions in the background media. Fabrication protocol was the same as described above for glucose biosensor, however Gox was not added.

2.1.4. Assembled

After curing, the glucose biosensor and sentinel electrode were inserted into the pulled single-barrel glass capillary tube under a microscope, leaving 500 μm of the carbon fibers protruding at the pulled end. At the stem end of the capillary tube, the copper wire was fixed by casting with non-conducting epoxy glue; the modified carbon fibers were also sealed into the capillary mouth, using non-conductive epoxy glue. Finally, an interference-rejection film of PoPD/BSA was electropolymerized over the glucose biosensor and sentinel (McAteer and O'Neill, 1996). Electro-polymerization of PoPD was performed with a standard three-electrode setup; a custom-made Ag/AgCl/saturated KCl reference was used as the reference electrode and platinum wire as the auxiliary electrode. The electro-polymerization was driven at a constant potential (+0.75 V) for 20–25 min. After the fabrication procedure of the biosensors and their sentinels (blank sensor) were completed, they were cleaned in doubly-distilled water, stored overnight at 4 °C in a refrigerator, and used the next day. When not in use, both sensors were stored again at 4 °C in a refrigerator in dry conditions.

2.1.5. Instrumentation and software for acquiring amperometric data

Carbon fiber modifications and experiments were computer controlled with data-acquisition software EChem™ for cyclic voltammetry and Chart™ for constant potential applied. The data-acquisition system used was e-Corder 401 from EDAQPty Ltd. (Denistone East, Australia) and a low-noise and high-sensitivity potentiostat, Quadstat (EDAQ). The linear and non-linear regression analyses were performed using the graphical software package Prism (ver. 5.00 Graph Pad Software).

2.2. Optical imaging

2.2.1. Setup

In order to obtain optical data in our experiments, a fiberscope from PENTAX Medical Company (Montvale, NJ, USA) was optically adapted to illuminate the cortex with a filter free high intensity halogen illuminator (FO-150, Chiu Technical Corporation, Kings Park, NY, USA) and to collect images in a cooled charge-coupled device (iXonEM+ 885 EMCCD Camera, ANDOR™, South Windsor, CT, USA). An optosplit from CAIRN Research Ltd. (Faversham, Kent, UK) coupled to the camera can record images simultaneously at two different optical wavelengths: 687 ± 5 nm and 835 ± 5 nm. Images were acquired at 1.00× magnification, 5 frames/s and 512 × 512 pixel array and stored on a desktop computer using ANDOR IQ software. The fibroscope was positioned in the center of the holder to visualize the location of all implanted electrodes (see Fig. 1 for more detail). The sentinel and the microbiosensor were positioned as close to the center of activation as possible, avoiding the pial and dural vessels. The sentinel, microbiosensor and stimulating electrodes were carefully positioned so that the distance between the two sensors and bipolar electrode was less than 100 μm. The main advantage of using this setup is that this optimized the space for the insertion of three electrodes and the fiber at the same time (Fig. 1).

2.2.2. Analysis of optical data

Processing of images was performed after their capture (off-line), by using our user friendly home-made software: Metcalculator. Metcalculator was programmed using Matlab Guide® (v 7.9.0) and allows users to load the dark data (*Idark*), the reference

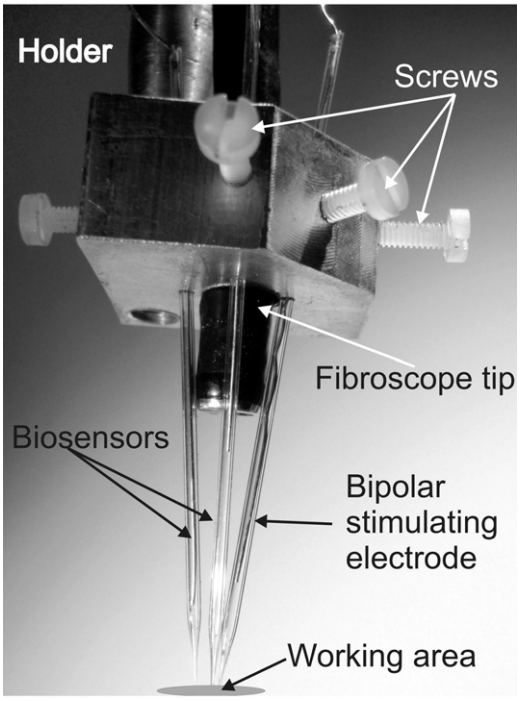

Fig. 1. Photograph of the experimental setup showing the metallic holder for the optic fiber (fibroscope tip) located in the center and the electrodes surrounding the tip. Please note that the microbiosensors are orientated in such a way so that they nearly meet at the tip where the electrodes are implanted.

data (*Iref*) and the resting image data (*Ibasal*) for each experimental essay. In order to reach a higher processing speed, the user can reduce the data by choosing a region of interest (ROI). In this case, any sub-array and any number of frames can be set. Optical density for each pixel was obtained by the following equation: $O.D = -\log((I - Idark)/Iref)$.

This formula was applied to both experimental data (I) and resting data (*Ibasal*). The values of intensity data (*Idark*, *Iref*, *Ibasal* and I) were previously filtered with a spatial filter to smooth the borders, shadows and whites of the images. Afterwards, O.D data was filtered with a Gaussian low-pass filter at 0.8 Hz to remove all artifacts and physiological noise. Relative concentrations of HbR and HbO_2 were calculated from these pre-processing O.D data by solving Eq. (1).

$$\begin{bmatrix} \Delta HbO_2 \\ \Delta HbR \end{bmatrix} = \begin{bmatrix} \alpha^{\lambda 1}_{HbO_2} & \alpha^{\lambda 1}_{HbR} \\ \alpha^{\lambda 2}_{HbO_2} & \alpha^{\lambda 2}_{HbR} \end{bmatrix} \cdot \begin{bmatrix} O.D^{\lambda 1}_{I} - O.D^{\lambda 1}_{Ibasal} \\ O.D^{\lambda 2}_{I} - O.D^{\lambda 2}_{Ibasal} \end{bmatrix} \quad (1)$$

Although we have used the absorption coefficient values ($\alpha^{\lambda}{}_{i}$) reported by Prahl (1998) in our results, these can be set by the user.

On the other hand, the splitter used here can simultaneously acquire images at two wavelengths, which makes it possible to apply Eq. (1) to our collected data and to calculate HbO_2, HbR and HbT values for the whole images. Spectral maps in two dimensions (2D), resulting from correlating a color-map matrix and these values, are useful for analyzing ROIs contained in the cranial window and for establishing comparison criteria and well contrasted contours.

3. Experiments

3.1. In vitro experiments to calibrate the microbiosensor

All in vitro experiments were performed in a 25 mL glass cell at 21 °C, using a standard three-electrode set-up with a commercial saturated calomel electrode (SCE) (CRISON Instrument S.A., Alella, Barcelona, Spain) as the reference and platinum wire as the auxiliary electrode. The optimized applied potential for amperometric studies was 0.0 V against SCE [30,31]. Glucose calibrations were performed in quiescent air-saturated PBS (following stabilization of the background current for 30 min) by adding aliquots of glucose stock solution (0.25 M) to the electrochemical cell. After the addition of glucose aliquots, the solution was stirred for 10 s and then left to reach the steady-state current.

3.2. In vivo

These experiments were conducted with eight male rats of ~350 g (Sprague–Dawley) in accordance with the European Communities Council Directive of 1986 (86/609/EEC) regarding the care and use of animals for experimental procedures, and adequate measures were taken to minimize pain and discomfort. After being anesthetized with urethane (1.5 g/kg), the animal's head was immobilized in a stereotaxic frame and its body temperature maintained at 37 °C with a heating blanket. A midline scalp incision was made to expose the bone over the parietal cortex of one hemisphere. The bone over the hemisphere to be imaged was carefully removed with a dental drill. Agar solution 1%, w/v was applied to increase the stability against physiological noise and the translucency of the area. In order to measure prefrontal cortex glucose, the microbiosensors were implanted according to Paxinos and Watson coordinates: A/P +2.7 from bregma, M/L +1.2 and D/V −0.5 from dura (Dixon et al., 2002). The Ag/AgCl reference electrode and platinum auxiliary electrode were placed over the skull near the prefrontal cortex, and the skull kept wet with saline-soaked pads. Electrical stimulation was provided by an S-8800 Grass model and a bipolar electrode made with two pointed carbon fibers (30 μm diameter; Word Precision Instruments Inc., Sarasota, FL, USA) mounted in a two-barrel glass capillary, and separated by ~100 μm. One stimulation trial consisted of 140 s of recording. Electrical Stimulus was set as follows: 1 s, 0.15 mA, 0.9 ms current pulse. Neural activity was varied by modulating the stimulation frequency (20, 30 and 40 Hz). One stimulus was delivered 20 s after the start of each trial. The trial was repeated 10 times with a 60 s rest interval.

4. Results and discussion

Fig. 2A, shows the spectral map superimposed over the real image obtained at 20 Hz and at 0–1–2–3–5 and 10 s after onset of electrical stimulation. Fig. 2C includes the relative positions of the stimulating electrode, glucose biosensor and their sentinel. The circular area is the cerebral region studied by the optic fibers and the yellow color represents the spectral map superimposed (activated area) 4 s after electrical stimulation. Fig. 2B shows HbT recorded versus time in an activated area (magenta) and non-activated area (blue) for comparison. No changes were detected in non-activated ROIs (no yellow spectral map). This result agrees with the results of Sheth and co-workers where relevant hemodynamic responses have a common central focus which later segregates to other vascular compartments.

Changes in extra-cellular fluid (ECF) of glucose, in the same groups of rats, were measured by a glucose microbiosensor (CFE/PB/Nafion/PEI/Gox/PoPD) after the electrical stimulation (Fig. 3A). Similar recordings were carried out with a blank sensor (without Gox) very close (less than 100 μm) to the glucose microbiosensor (see Fig. 3B). After electrical stimulus, the glucose decreased to 15–20% below the basal levels depending on the frequency used. In contrast to the HbT and HbO_2 results (see Fig. 4 or more details), the application of local stimuli at 20, 30 and 40 Hz

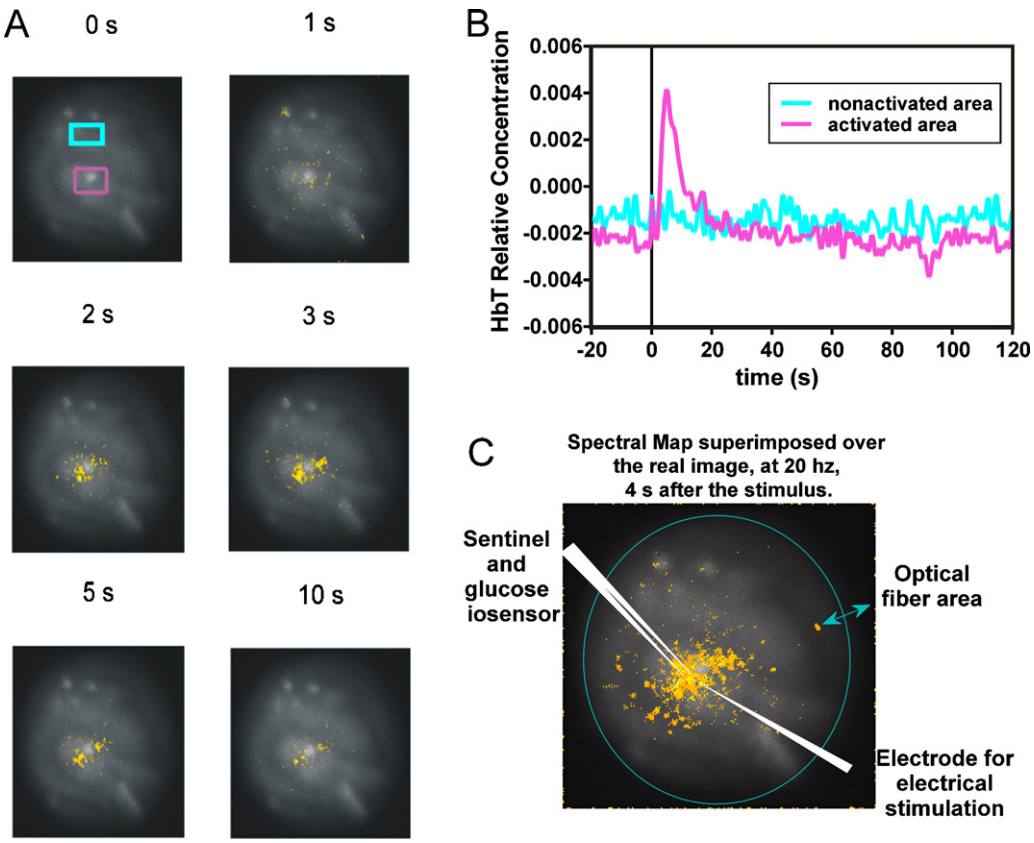

Fig. 2. (A) Hemodynamic optical imaging showing two ROIs, one very close to the bipolar electrical stimulating electrode (activated area) and the other 1 mm away (deactivated area). The images show the HbT following stimulus onset ($t = 0$) with the above described ROIs. Time (in seconds) relative to stimulus onset is indicated above the images. (B) The graph shows the HbT concentration recorded in both ROIs. (C) Relative positions of the stimulating electrode, glucose biosensor and its sentinel.

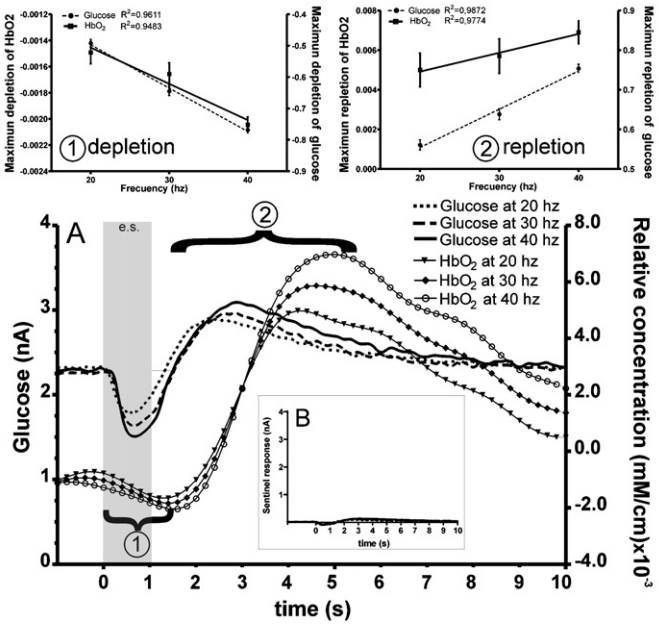

Fig. 3. (A) Glucose and HbO_2 recorded for 10 s in the active area where the microbiosensor for glucose was implanted. The shadow bar shows where the electrical stimulation occurred. The hemodynamic changes start about 2 s after the end of stimulation. The increase of glucose levels start during stimulation and reach the maximum before HbO_2. Insets 1 and 2: curves showing the close relationship between the maximum depletion and repletion amplitude of glucose and HbO_2 at different frequencies of stimulation. (B) Typical recordings showing the responses registered with the blank sensor microbiosensor (without Gox) after local electrical stimulation.

produced a decrease of the glucose current but the signal of glucose started to increase before the end of the stimuli. This typical result has been observed by us (Salazar et al., 2010b,c) and other authors (Dixon et al., 2002; Silver and Erecińska, 1994). Since extracellular concentration of glucose is the product of the rate of sugar delivery from capillaries across the blood–brain barrier and the rate of utilization by cells (Cremer JE et al., 1981; Hawkins et al., 1983; Cunningham et al., 1986; Robinson and Rapoport, 1986; Furler et al., 1991), the glucose decrease observed here could probably be explained by the physiological consumption of glucose caused by the neuronal activation.

After this short decrease, the glucose current began to rise and reached a peak 30% above the basal levels (see Fig. 3A) 3 s after the onset of the stimulus. The glucose recordings returned to basal levels in 12 ± 3 s depending on the frequency of stimuli. Fig. 3B shows the response of the blank sensors (sentinels) after electrical stimulation that only had a brief artifact. As regards the performance of the glucose biosensor, the inset shows the small changes experienced by the sentinel (0.1 nA) in comparison to the high sensitivity of the glucose sensor proving that interferences and other chemicals such as hydrogen peroxide did not influence our measurements.

Similar behavior on maximum depletion (1) and repletion (2) amplitude of glucose and HbO_2 were observed versus used frequencies, see Fig. 3, inset 1 and inset 2. Two blocks (1 and 2) can be observed in Fig. 3A to clarify the behavior of these variables (glucose and HbO_2 state). The first block (1), called depletion, includes the electrical stimulation period and 1 s after the end of the stimulation when the glucose signal reached the basal levels. The second block (2), includes the increase of glucose and HbO_2 concentration in ECF after electrical stimulation and is called repletion. The depletion

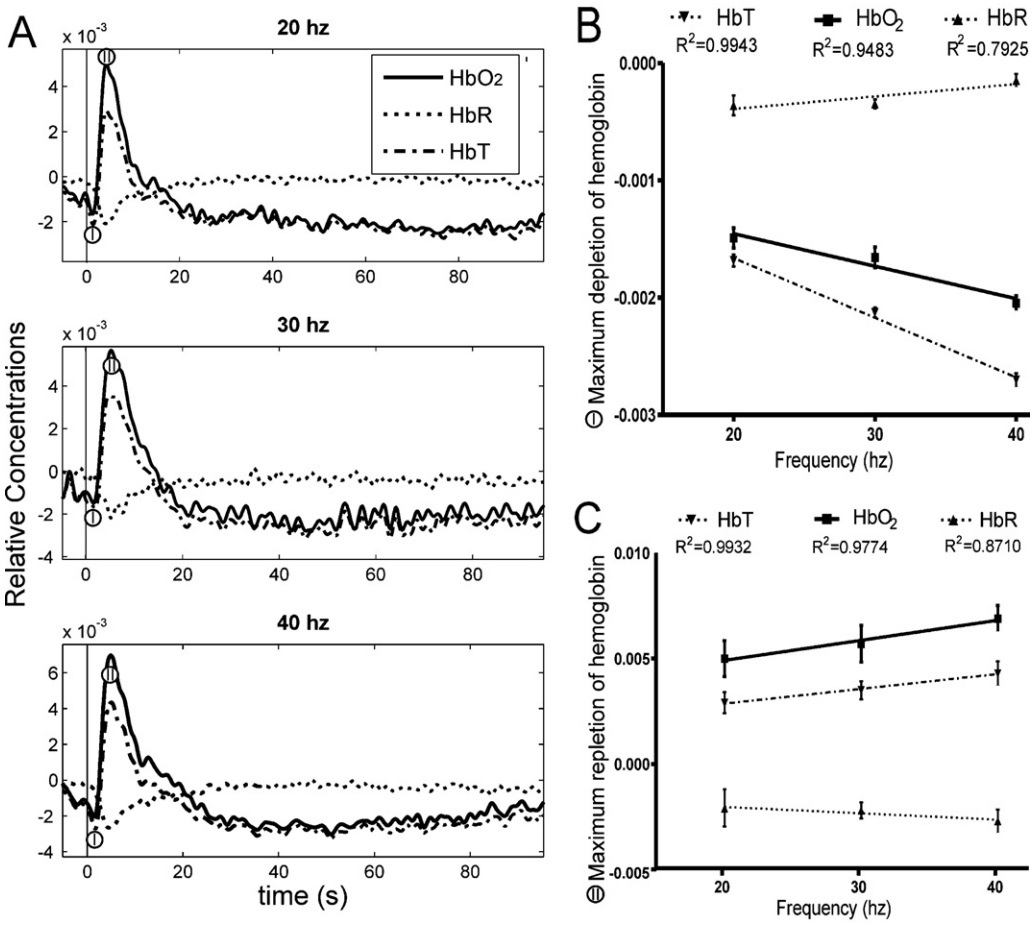

Fig. 4. (A) Hemodynamic time courses. The time course of functional changes in HbO_2, HbR and HbT for 20, 30 and 40 Hz obtained from a selected ROI. The recordings shown are averaged over the eight rats. Maximum depletion (I) and repletion (II) of HbO_2 and HbT decrease/increase linearly with the electrical stimulation frequency (B and C). A transient decrease in HbO_2 ('initial dip') was observed in the group averaged data.

period corresponds with the very well identified change in BOLD signal in response to brief stimuli called "initial dip" (Buxton, 2001; Frostig et al., 1990).

The behavior of both molecules is shown at the top Fig. 3. Glucose and HbO_2 decrease/increase linearly with the frequency (R^2 values are over 0.94 showing a high goodness of the linear regression) during the depletion/repletion period.

The very similar change in HbO_2 in the same direction as glucose, as is shown in Fig. 3 parts 1 and 2, agrees with the metabolic hypothesis that assumes a direct link between cellular energy state and the regulation of blood flow (Zonta et al., 2003; Gordon et al., 2008).

Fig. 4 depicts more detailed results obtained from optical imaging technique. Fig. 4A shows HbO_2, HbR and HbT measurements monitored over a period of 130 s after electrical stimulation of 1 s at 20, 30 and 40 Hz. The local electrical stimuli caused an increase in HbO_2 and HbT concentration with the maximum 5 s after the onset of electrical stimulus and returned to base line levels within 15–20 s after the end of electrical stimulation.

The maximum decrease/increase after electrical stimulation of HbO_2, and HbT during the depletion/repletion period was very linear with the frequency of stimulation (Fig. 4B and C, respectively). HbR increased/decreased linearly with a very moderate slope to the frequency used and the minimum recorded from the onset of electrical stimulation was also at 5 s. The recovery of the basal levels was recorded 20 s after the beginning of the stimuli.

Regarding the temporal evolution experienced by both molecules, our results report that, after electrical stimulation, changes in glucose are detected before hemodynamics changes (see Fig. 3A). Specifically, during depletion period, glucose levels decrease ≈1 s before HbO_2 levels and during repletion period, glucose levels reach the maximum ≈2 s before HbO_2.

There are different reasons which could explain the observed temporal delay of 1–2 s between glucose and HbO_2. One of them could be the fast transport rate attributed to glucose into the brain, since, according to Barros et al. (2007); a glucose molecule will traverse a distance of 20 μm in only 400 ms. Then, different temporal dynamics between glucose and HbO_2 (see Fig. 4A) might be expected.

Another possible explanation for this delay could be linked to a temporal gap between the vasodilatation and the renewal of blood in the capillary bed due to the complexity of the vascular and neural net (Paulson et al., 2010).

Furthermore, the low value of uncoupling between both variables observed here, the increase of glucose levels started to return at basal levels when the vasodilatation (hemodynamic changes) started to increase, could lead one to think that the glucose comes from a compartment other than the blood stream. Evidence from a number of sources suggests that this compartment is astrocytes (Tsacopoulos and Magistretti, 1996; Magistretti and Pellerin, 1999), since they have a small store of glycogen with a rapid turnover rate (Dixon et al., 2002). Additionally, other authors (In-Young et al., 2001a,b) have found that when brain extracellular glucose decreases approaching to zero, CBF sharply increases and brain glycogen degradation begins.

Although this last result does not fit in with the generally accepted idea (Villringer and Dirnagl, 1995) that the energy metabolism dynamic occurring at sites of neuronal activation can be considered as a concatenation of events ('in-series' events), where active neurons liberate signals producing an increase of CBF which afterwards provides energy substrates (e.g., glucose), the reasons explained above support the argument that blood flow and glucose use are not always coupled. In fact, it is possible that uncoupling of CBF and energy metabolism suggests the existence of alternative pathways that use a variety of metabolites such as lactate, H^+ or adenosine to mediate the neurovascular coupling (Magistretti and Pellerin, 1999). Besides which, as far as our results are concerned, it is possible to hypothesize that the observed depletion in brain glucose level must activate homeostatic mechanisms, such as increase in blood flow, also suggested by other authors (Van Harreveld and Ochs, 1957; Leniger-Follert, 1979) and/or enhancement of transport (Gjedde et al., 1981) because the reduction is rapidly followed by a transient overshoot after which the glucose level returns to its original value.

This hypothesis is coherent with recent evidence of mismatching between CBF and cerebral metabolic rate of oxygen ($CMRO_2$) found by Leithner and co-workers. They report the surprising finding that pharmacological inhibition of vasoactive agents reduced CBF responses without affecting $CMRO_2$, which suggests that the oxygen delivered through blood flow serves as a safety mechanism of protection against hypoxia or pathological conditions rather than to increase oxidative metabolism (Leithner et al., 2010).

Moreover, Lindauer and co-workers reported that despite using hyperbaric hyperoxygenation to prevent hemoglobin deoxygenation, hemodynamic and neuronal responses remained unaltered after electrical forepaw stimulation or cortical spreading depression supporting the view that oxygen dissolved in tissue rather than oxygen transported by the vascular net activates oxidative metabolism.

The independence between CBF and neuronal responses found in these works (Leithner et al., 2010; Lindauer et al., 2010) together with the time lag between glucose and HbO_2 signals reported here, support the 'neuronal' hypothesis: the neuron-astrocyte ensemble communicates the energetic demand to the vasculature and modulates changes in CBF in an feed-forward manner (Lindauer et al., 2010; Buxton, 2010) by involving multiple vasoactive messengers such as neurotransmitters, nitric oxide, epoxyeicosatrienoic acids, potassium ions and other intermediaries (Cauli, 2010).

Finally, although the application of spectroscopic analysis to two-dimensional optical imaging data has been used before by other authors (Devor et al., 2003, Paulson et al., 2010; Sheth and Prakash, 2009), this report is the first to extend previous findings by combining measurements of glucose levels in CFS in real-time using microbiosensors to critically assess spatiotemporal characteristics of hemodynamic responses. Our results suggest that functional hemodynamic changes in HbO_2 are very similar to glucose levels after local electrical stimulation of the rat brain, but the temporal time course of both are very different, the glucose kinetic (short and rapid decrease and posterior increase) takes place before hemodynamic changes. This result creates a significant challenge for interpreting blood oxygenation level dependent signal (BOLD signal) which is the basis of some neuroimaging approaches (e.g., fMRI), since CBF and oxidative metabolism seem to be driven in parallel by neural activity – rather than a serial connection with neural activity, as is discussed by Buxton (2010).

5. Conclusions

We have demonstrated that the two in vivo techniques performed in this work can be combined and used to quantify hemoglobin and glucose concentration. Besides which, we have successfully tested the performance of our setup to record signals at a satisfactory temporal and spatial resolution. On the other hand, we developed software (Metcalculator) for 2-dimensional optical imaging, which could be an interesting tool for studying hemodynamics and brain metabolism. Future works will be focused on analyzing the data in real time and on properly integrating a more sophisticated filter design tool aimed at removing physiological noise.

Finally, the existence of the uncoupling between CBF and glucose use found here means that it is now necessary to design new experiments to obtain a better understanding of the interactions between the metabolites and the hemodynamic involved in the neurovascular coupling mechanism. Therefore, new lines of future research will be devoted to simultaneously using two additional biosensors, also developed in our laboratory, to detect lactate and glutamate.

Conflict of interest statement

The authors declare no conflict of interest.

Acknowledgements

The funds for the development of this work had been promoted by the following national public projects: ULLAPD-08/01 granted by the Agencia Canaria de Investigación, Innovación y Sociedad de la Información, Ministerio de Industria, Turismo y Comercio (Proyecto AVANZA) TSI-020100-2008-337 and Ministerio de Ciencia e Innovación (Proyecto CICYT) TIN2008-06867-C02-01/TIN.

References

Barros LF, Bittner CX, Loaiza A, Porras OH. A quantitative overview of glucose dynamics in the gliovascular unit. Glia 2007;55(12):1222–37.
Buxton RB. Interpreting oxygenation-based neuroimaging signals: the importance and the challenge of understanding brain oxygen metabolism. Frontiers in Neuroenergetics 2010;2:8.
Buxton RB. The elusive initial dip. NeuroImage 2001;13:953–8.
Cauli B, Hamel E. Revisiting the role of neurons in neurovascular coupling. Frontiers in Neuroenergetics 2010;2:9.
Cremer JE, Ray DE, Sarna GS, Cunningham V. A study of the kinetic behavior of glucose based on simultaneous estimates of influx and phosphorylation in brain regions of rats in different physiological states. Brain Research 1981;22(1):331–42.
Cunningham VJ, Hargreaves RJ, Pelling D, Moorhouse SR. Regional blood–brain glucose transfer in the rat: a novel double-membrane kinetic analysis. Journal of Cerebral Blood Flow and Metabolism 1986;6(3):305–14.
Devor A, Dunn AK, Andermann ML, Ulbert I, Boas DA, Dale AM. Neuron coupling of total hemoglobin concentration, oxygenation, and neural activity in rat somatosensory cortex. Proceedings of the National Academy of Sciences of the United States of America 2003;39(2):353–9.
Dixon BM, Lowry JP, O'Neill RD. Characterization in vitro and in vivo of the oxygen dependence of an enzyme/polymer biosensor for monitoring brain glucose. Journal of Neuroscience Methods 2002;19(2):135–42.
Frostig RD, Lieke EE, Ts'o DY, Grinvald A. Cortical functional architecture and local coupling between neuronal activity and the microcirculation revealed by in vivo high-resolution optical imaging of intrinsic signals. Proceedings of the National Academy of Sciences of the United States of America 1990;87(16):6082–6.
Furler SM, Jenkins AB, Storlien LH, Kraegen EW. In vivo location of the rate-limiting step of hexose uptake in muscle and brain tissue of rats. American Journal of Physiology 1991;261(3):E337–47.
Giove F, Mangia S, Bianciardi M, Garreffa G, Di Salle F, Morrone R, Maraviglia B. The physiology and metabolism of neuronal activation: in vivo studies by NMR and other methods. Magnetic Resonance Imaging 2003;21:1283–93.
Gjedde A, Hansen AJ, Quistorff B. Blood–brain glucose transfer in spreading depression. Journal of Neurochemistry 1981;37(4):807–12.
González-Mora JL, Martín FA, Rojas-Díaz D, Hernández S, Ramos-Pérez I, Rodríguez VD, Castellano MA. In vivo spectroscopy: a novel approach for simultaneously estimating nitric oxide and hemodynamic parameters in the rat brain. Journal of Neuroscience Methods 2002;119:151–61.
Gordon GR, Choi HB, Rungta RL, Ellis-Davies GC, MacVicar BA. Brain metabolism dictates the polarity of astrocyte control over arterioles. Nature 2008;456(7223):745–9.
Hawkins RA, Mans AM, Davis DW, Hibbard LS, Lu DM. Glucose availability to individual cerebral structures is correlated to glucose metabolism. Journal of Neurochemistry 1983;40(4):1013–8.

Hernández SE, Rodríguez VD, Pérez J, Martín FA, Castellano MA, Gonzalez-Mora JL. Diffuse reflectance spectroscopy characterization of hemoglobin and intralipid solutions: in vitro measurements with continuous variation of absorption and scattering. Journal of Biomedical Optics 2009;14:1–22.

In-Young C, Sang-Pil L, Seong-Gi K, Rolf G. Relationship between glucose/glycogen metabolism and CBF during insulin-induced hypoglycemia in vivo. Annual Meeting Proceedings of the International Society for Magnetic Resonance in Medicine 2001a;9:492.

In-Young C, Sang-Pil L, Seong-Gi K, Rolf G. In vivo measurements of brain glucose transport using the reversible Michaelis–Menten model and simultaneous measurements of cerebral blood flow changes during hypoglycemia. Journal of Cerebral Blood Flow and Metabolism 2001b;21:653–63.

Leithner C, Royl G, Offenhauser N, Füchtemeier M, Kohl-Bareis M, Villringer A, Dirnagl U, Lindauer U. Pharmacological uncoupling of activation induced increases in CBF and $CMRO_2$. Journal of Cerebral Blood Flow & Metabolism 2010;30(2):311–22.

Leniger-Follert E, Hossmann KA. Simultaneous measurements of microflow and evoked potentials in the somatomotor cortex of the cat brain during specific sensory activation. Pflügers Archiv European Journal of Physiology 1979;380(1):85–9.

Lindauer U, Leithner C, Kaasch H, Rohrer B, Foddis M, Füchtemeier M, Offenhauser N, Steinbrink J, Royl G, Kohl-Bareis M, Dirnagl U. Neurovascular coupling in rat brain operates independent of hemoglobin deoxygenation. Journal of Cerebral Blood Flow & Metabolism 2010;30(4):757–68.

Magistretti PJ, Pellerin L. Cellular mechanisms of brain energy metabolism and their relevance to functional brain imaging. Philosophical Transactions of the Royal Society B: Biological Sciences 1999;354(1387):1155–63.

McAteer K, O'Neill RD. Strategies for decreasing ascorbate interference at glucose oxidase-modified poly(o-phenylenediamine)-coated electrodes. Analyst 1996;121:773–7.

Paulson OB, Hasselbalch SG, Rostrup E, Knudsen GM, Pelligrino D. Cerebral blood flow response to functional activation. Journal of Cerebral Blood Flow & Metabolism 2010;30:2–14.

Prahl SA. Tabulated Molar Extinction Coefficient for Hemoglobin in Water, http://omlc.ogi.edu/spectra/hemoglobin/summary.html.1998.

Robinson PJ, Rapoport SI. Glucose transport and metabolism in the brain. American Journal of Physiology 1986;250(1):R127–36.

Salazar P, Martín M, Roche R, González-Mora JL, O'Neill RD. Microbiosensors for glucose based on Prussian Blue modified carbon fiber electrodes for in vivo monitoring in the central nervous system. Biosensors and Bioelectronics 2010a;26:748–53.

Salazar P, Martín M, Roche R, O'Neill RD, González-Mora JL. Prussian Blue-modified microelectrodes for selective transduction in enzyme-based amperometricmicrobiosensors for in vivo neurochemical monitoring. Electrochimica Acta 2010b;55:6476–84.

Salazar P, O'Neill RD, Martín M, Roche R, González-Mora JL. Amperometric glucose microbiosensor based on Prussian Blue modified carbon fiber electrode for physiological applications. Sensors and Actuators B: Chemical 2010c: 1–27.

Sfareni R, Boffi A, Quaresima V, Ferrari M. Near infrared absorption spectra of human deoxy- and oxyhaemoglobin in the temperature range 20–40 °C. Biochimica et Biophysica Acta 1997;1340(2):165–9.

Sheth SA, Prakash N, Michael Guiou M, Toga AW. Validation and visualization of two-dimensional optical spectroscopic imaging of cerebral hemodynamics. NeuroImage 2009;47:T36–43.

Shulman RG, Hyder F, Rothman DL. Lactate efflux and the neuroenergetic basis of brain function. NMR in Biomedicine 2001;14:389–96.

Silver IA, Erecińska M. Extracellular glucose concentration in mammalian brain: continuous monitoring of changes during increased neuronal activity and upon limitation in oxygen supply in normo- hypo-, and hyperglycemic animals. Journal of Neuroscience 1994;14(8):5068–76.

Sokoloff L. The metabolism of the central nervous system in vivo. In: Field J, Magoun HW, Hall VE, editors. Handbook of physiology. Section I. Neurophysiology, vol. 3. Washington, DC: American Physiological Society; 1960. p. 1843–64.

Tsacopoulos M, Magistretti PJ. Metabolic coupling between glia and neurons. Journal of Neuroscience 1996;16(3):877–85.

Van Harreveld A, Ochs S. Electrical and vascular concomitants of spreading depression. American Journal of Physiology 1957;189(1):159–66.

Villringer A, Dirnagl U. Coupling of brain activity and cerebral blood flow: basis of functional neuroimaging. Cerebrovascular and Brain Metabolism Reviews 1995;7(3):240–76.

Wray S, Cope M, Delpy DT, Wyatt JS, Reynolds EO. Characterization of the near infrared absorption spectra of cytochrome aa3 and haemoglobin for the noninvasive monitoring of cerebral oxygenation. Biochimica et Biophysica Acta 1988;933(1):184–92.

Zonta M, Angulo MC, Gobbo S, Rosengarten B, Hossmann KA, Pozzan T, Carmignoto G. Neuron-to-astrocyte signaling is central to the dynamic control of brain microcirculation. Nature Neuroscience 2003;6:43–50.

The use of fluorocarbons to mitigate the "oxygen deficit" in glucose microbiosensors for the neuroscience: an in vitro approach.

Salazar P[1,], Martín M[1,2], O'Neill RD[3], Roche R[1] and González-Mora JL[1]*

[1]*Neurochemistry and Neuroimaging group, Faculty of Medicine, University of La Laguna, Tenerife, Spain.*
[2]*Atlántica Biomédica SL, Tenerife, Spain.*
[3]*UCD School of Chemistry and Chemical Biology, University College Dublin, Belfield, Dublin 4, Ireland.*

Abstract

First generation of amperometric glucose biosensors are the most commonly used method for glucose detection in the neuroscience. The so-called oxygen deficit, which means that the biosensor response depends on the O_2 concentration, is a common problem for all first-generation biosensors. This is an important issue in neurophysiological studies because the mean O_2 concentration in brain ECF has been reported to be close to 50 µM. In the present work we use different fluorocarbons oils such as Nafion and H700 to mitigate the oxygen deficit of our previous glucose biosensor designs. These fluorocarbon-derived materials display a remarkable solubility for O_2, and act as oxygen reservoirs supporting the enzymatic reaction at very low O_2 concentration. We present different biosensor configurations and study, step by step, each biosensor configuration, evaluating its oxygen dependence Finally, Nafion and H700-modified biosensors presented a remarkable oxygen tolerance in the physiological glucose range concentration without the decrease significantively the enzymatic loading.

Keywords: Glucose biosensor, oxygen deficit, Fluorocarbon oil, Nafion, H700.

1. Introduction:

Amperometric glucose biosensors are now the most commonly used method for glucose detection because of its many advantages, such as simplicity and speed. These devices have been employed in several areas of science, especially in the neurosciences. Where such devices must be adapted to special requirements such as: low dimensions, high selectivity and sensitivity, low co-sustrate concentration, short time response, etc. The overall enzymatic process for glucose oxidase (*Gox*), that is similar for many oxidases, may be written as equations 1 and 2, where FAD and $FADH_2$ are the oxidized and reduced forms, respectively, of the prosthetic group, flavin adenine dinucleotide [1]. Equation 3 represents the electrochemical measurement of the H_2O_2 generated during the reaction of oxido-reductase enzymes (see eq. 2), and in first generation devices is generally carried out amperometrically, either directly on the substrate surface at relatively high applied potentials or catalytically at lower potentials.

β-D-glucose + Gox/FAD → D - glucono-δ-lactone + Gox/$FADH_2$ **[eq. 1]**

Gox/$FADH_2$ + O_2 → Gox/FAD +H_2O_2 **[eq. 2]**

H_2O_2 → O_2 + $2H^+$ + $2e^-$ **[eq. 3]**

The so-called *oxygen deficit*, which means that the biosensor response depends on the O_2 concentration (see eq. 2) is a common problem for all first-generation biosensors [2]. This is an important issue in neurophysiological studies because the mean O_2 concentration in brain ECF has been reported to be close to 50 µM (five times lower than aerated solutions), and this level can fluctuate significantly under physiological conditions and with pharmacological intervention [3].

Different approaches have been employed to solve this O_2 dependence. Thus, second and third biosensor generations appeared during last decades. Nevertheless, first generation biosensors are still preferred for many researches for its easy implementation, stability, short time response, etc. Attempts to overcome this problem in first generation biosensors include: (1) the study of different electrode geometries; (2) inclusion of a diffusion barrier to increase O_2/substrate permeation ratio; (3) optimization of the enzymatic loading, and so the biosensor's sensitivity and linear range; (4) the use of oxygen-rich polymers (fluorocarbon-derived materials) as internal oxygen supply.

Fluorocarbon-derived materials display a remarkable solubility for O_2, and they have been used, for example, in carbon paste electrodes as an oxygen reservoir [2]. The internal flux of O_2 can support the enzymatic reaction for extended periods, even in O_2-free media. Although this approach has been used in macrobiosensor design, studies in the microbiosensor field are very limited.

Our group has been working in recent years to implement microbiosensors based on Prussian Blue-modified carbon fiber electrodes (CFEs) with low dimensions (~10 µm diameter) for use in physiological studies. Previous works showed the excellent properties of our glucose biosensors during *in vitro* and i*n vivo* experiments. Nevertheless, O_2 dependence had not been studied before. This work presents our first results using common fluorocarbon polymers such as Nafion and H700 as an internal O_2 source for our previous microbiosensor designs [4].

2. Materials and methods

2.1 Reagents and solutions

The enzyme glucose oxidase (*Gox*) from *Aspergillus niger* (EC 1.1.3.4, Type VII-S), purchased as a lyophilized powder, and glutaraldehyde 25% (Glut) were obtained from Sigma Chemical Co., and stored at –21 ºC until use. Bovine serum albumin (BSA, fraction V) was also obtained from Sigma. All chemicals, including *o*-phenylenediamine (o-PD), glucose, polyethyleneimine (PEI), KCl, $FeCl_3$, $K_3[Fe(CN)_6]$, HCl (35%w/w), H_2O_2 (30% w/v), Nafion (5 wt% in a mixture of lower aliphatic alcohols and water), Halocarbon oil (H700) and phosphate buffer saline (PBS, pH 7.4 containing 0.1M NaCl) were obtained from Sigma and used as supplied. PBS stock solutions were prepared in doubly distilled water (Millipore-Q), and stored at 4 °C when not in use. A stock 250 mM solution of glucose were prepared in water, left for 24 h at room temperature to allow equilibration of the anomers, and then stored at 4 ºC. The PEI and H700 solutions used were prepared by dissolving PEI and H700 at 5% w/v in H_2O. The cross-linking solution was prepared in PBS with 1% w/v of BSA and 0.1% w/v of Glut. Monomer solution of 300 mM o-PD was prepared using 48.6 mg of o-PD and 7.5 mg of BSA in 1.5 mL of N_2-saturated PBS and sonicated for 15 min. A 300 U/mL solution of Gox was prepared by dissolving 3.7 mg in 2 mL of PBS. Carbon fibers (8 µm diameter), glass capillaries, and 250 µm internal diameter Teflon-coated copper wires were obtained from Word Precision Instruments Inc., and silver epoxy paint was supplied by Sigma. N_2 (high grade, O_2 < 2 ppm) was supplied by Air Liquide.

2.2 Micro-biosensor construction based on CFE/PB

Carbon fiber electrodes (CFEs) were constructed and modified with Prussian Blue (PB) as described previously [4]. When PB/CFEs were ready to use, the next step

was to immobilize the Gox, using the following protocol: 15 fast immersions in Nafion or H700 solution and a drying period of 30 min; 15 fast immersions in PEI solution and a drying period (15 min); *n* fast immersions in Gox (300 U/mL) and a drying period (5 min); and 15 fast immersions in the cross-linking solution (BSA/glutaraldehyde). After the immobilization step, all biosensors were cured for 1 h at 37 ºC, and finally an interference-rejection film of poly-o-phenylenediamine (PoPD/BSA) was electropolymerized over the biosensor. In order to compare the beneficial effect of Nafion and H700, different configurations were checked by changing the main steps in the fabrication.

2.3 Amperometric experiments

All calibrations were done in a 25 mL glass cell at 21 °C, using a standard three-electrode set-up with a commercial saturated calomel electrode (SCE) (CRISON Instrument S.A.) as the reference and platinum wire as the auxiliary electrode. The applied potential for amperometric studies was 0.0 V against SCE. Glucose calibrations were performed in quiescent air-saturated or nitrogen-saturated PBS (following stabilization of the background current for 15 min) by adding aliquots of glucose stock solution (0.25 M) to the electrochemical cell. After the addition of glucose aliquots, the solutions were stirred for 5 s and then left to reach the steady-state current. To measure oxygen dependence, several biosensors were stabilized (during continuous air bubbling) in a voltammetric gas cell with 50 ml PBS at different glucose concentration. After that N_2 was bubbled, at the same bubble rate, and the glucose current change registered over time. To relate these results with O_2 concentration, the latter was sensed by using an unmodified CFE poised at – 650 mV against SCE.

2.4 Instrumentation and software

Experiments were computer controlled with data-acquisition software EChem™ for CV and Chart™ for CPA. The data-acquisition system used was e-Corder 401 (EDAQ) and a low-noise and high-sensitivity potentiostat, Quadstat (EDAQ). The linear and non-linear regression analyses were performed using the graphical software package Prism (ver. 5.00 GraphPad Software). To electro-deposit and activate the PB, a custom-made Ag/AgCl/saturated KCl reference electrode and platinum wire auxiliary electrode were used.

3. Results and discussion:

One of the most important parameters in biosensor design is its substrate sensitivity. However, for biosensors, excessive sensitivity may carry two significant problems: (1) short linear range; and (2) high cofactor consumption (eq. 2). In order to check the oxygen dependence of our previous glucose biosensors, we constructed and calibrated different biosensor configurations both in aerated and in de-aerated solution. ***Figure 1*** shows responses of a glucose biosensor with a high sensitivity (1.07 nA/mM) calibrated under these two conditions. The effect of de-aeration (or, more realistically, low O_2 concentration) is clear when the retained response (RR%, the percentage difference between these two conditions) is computed. Even at low glucose concentrations, RR% (green) was ~70%, showing a significant stoichiometric limitation.

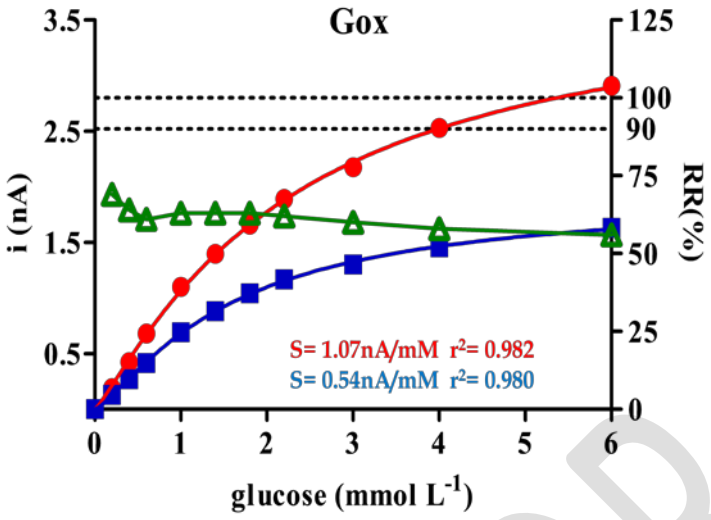

Figure 1.- Calibration curves for glucose biosensor (Gox) in aerated (*red*) and de-aerated (*blue*) solutions. Retained response (RR%) was computed as the percentage difference between these two conditions (*green*). Sensitivity was computed in the range of 0-2 mM glucose.

The addition of a diffusive membrane (such as PoPD) on top of the biosensor to enhance the glucose/O_2 ratio is commonly used [1]. The main effect of this diffusion barrier was to decrease the sensitivity to the target analyte (to compare see ***Figure 1*** and ***Figure 2a***). Different configurations, with different sensitivities were studied (***Figure 2a, b, c***). Although RR% was improved, it did not reach an acceptable value (RR% ≥ 90) in the physiological glucose concentration range for brain ECF (0.5 – 2 mM) (***Figure 2a*** and ***Figure 2b***). Finally, with this approach, only when glucose sensitivity was reduced to ~0.17 nA/mM (***Figure 2c***), RR% reached an acceptable value in a relevant glucose concentration range (0 – 3 mM).

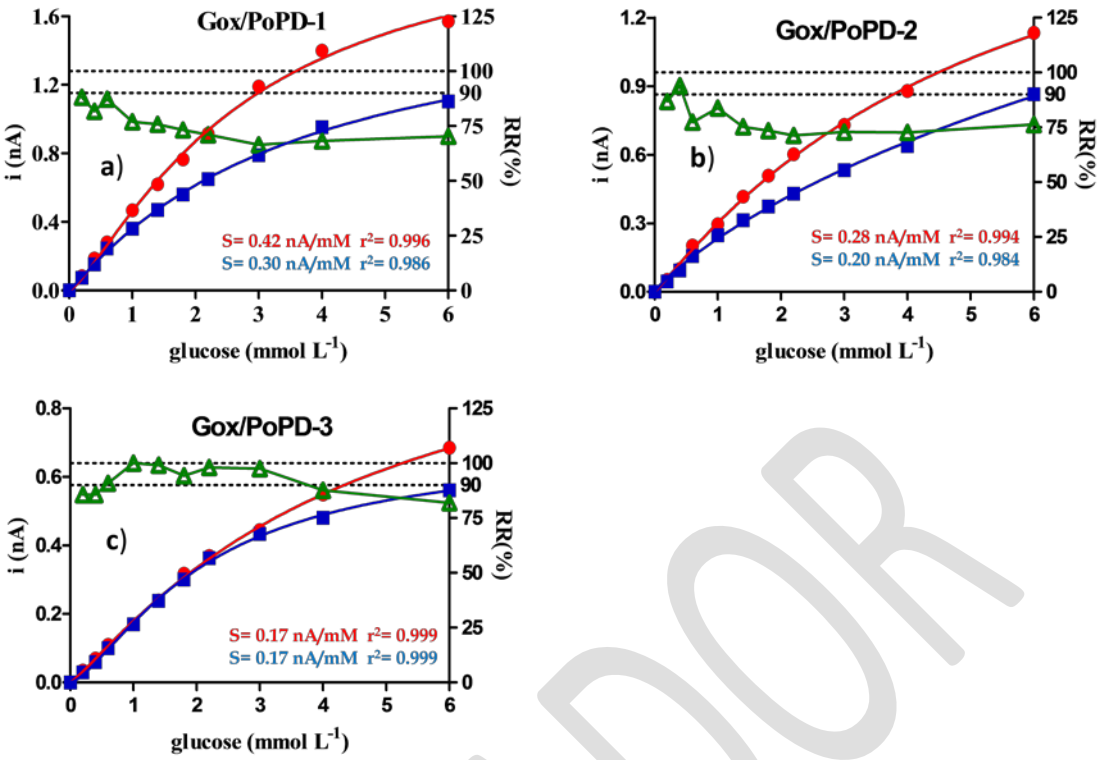

Figure 2.- Calibration curves for glucose biosensor configurations (Gox/PoPD) with different enzymatic loading and sensitivity in aerated (*red*) and de-aerated (*blue*) solutions. Retained response (RR%) was computed as the percentage difference between these two conditions (*green*). Sensitivity was computed in the range of 0-2 mM glucose

In order to show the utility of Nafion to solve the O_2 problem, we used this polymer during biosensor construction, the PoPD film being retained as an effective permselective barrier. Two different biosensors with glucose sensitivity of 1.09 (***Figure 3a***) and 0.5 nA/mM (***Figure 3b***), values similar to the previous designs in ***Figure 1*** and ***2a*** respectively, were tested. The beneficial effects of Nafion were evident: the more sensitive biosensor displayed an acceptable RR% value at a concentration up to 1 mM glucose (data not shown). Even better, the other biosensor (***Figure 1c***), with a sufficient sensitivity for in-vivo studies, was free of a significant oxygen deficit up to 3 mM glucose.

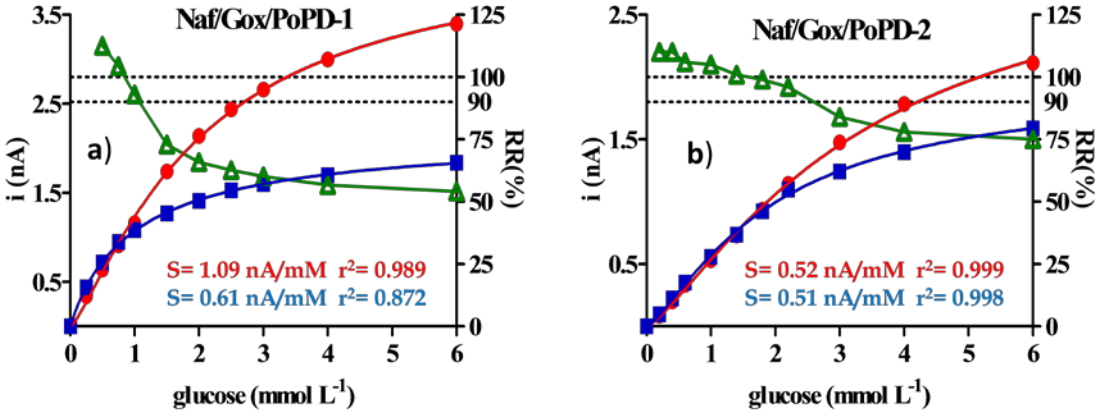

Figure 3.- Calibration curves for glucose biosensor configurations (Naf/Gox/PoPD), with different enzymatic loading and sensitivity in aerated (*red*) and de-aerated (*blue*) solutions. Retained response (RR%) was computed as the percentage difference between these two conditions (*green*). Sensitivity was computed in the range of 0-2 mM glucose

More detailed studies were carried out under dynamic conditions (***Figure 4a***), using different biosensor configurations. These experiments consisted of changing the O_2 concentration (*bubbling with N_2 or air*) at different glucose concentrations. In this way, biosensor oxygen dependence was quantified as $K_M(O_2)$ defined by eq. (3)

$$\mathbf{J_{Gluc} = J_{max} / (1 + K_M(O_2)/[O_2])} \qquad \mathbf{(eq.\ 3)}$$

$K_M(O_2)$ value of 11 ± 2 µM (mean ± SD) in the brain ECF glucose range (0.5 – 2 mM); meanwhile, at higher glucose levels (5 – 10 mM), the $K_M(O_2)$ value was 31 ± 8 µM. The smaller the value of $K_M(O_2)$, the lower the oxygen dependence because higher oxygen affinity leads to oxygen saturation at lower pO_2, thereby reducing biosensor dependency at higher pO_2 levels. These data reveal that our optimized configuration is adequate for applications in neurophysiology where oxygen levels may fluctuate in a range of 30 – 80 µM under non-extreme (*i.e.*, normoxic) conditions.

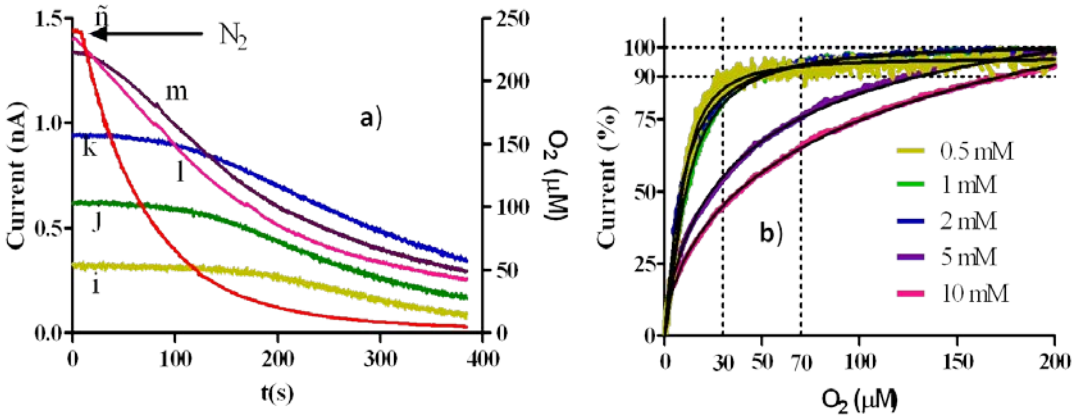

Figure 4.- a) Glucose biosensor response for Naf/Gox/PoPD-2 configuration at different glucose concentration (**i**:0.5 mM; **j**:1 mM, **k**:2 mM, **l**:5 mM; **m**:10 mM) against oxygen concentration (**ñ**) **b)** Normalized glucose–oxygen correlation plots for these five concentrations.

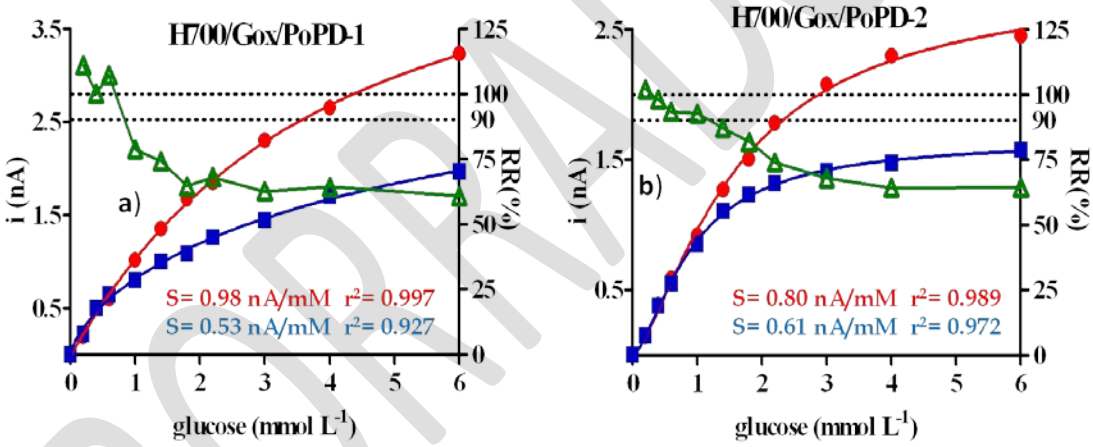

Figure 5.- Calibration curves for glucose biosensor configurations (H700/Gox/PoPD), with different enzymatic loading and sensitivity in aerated (*red*) and de-aerated (*blue*) solutions. Retained response (RR%) was computed as the percentage difference between these two conditions (*green*). Sensitivity was computed in the range of 0-2 mM glucose.

During the present study we carried out preliminary tests on other fluorocarbon oils as an internal source of oxygen to solve the oxygen deficit problem (***Figure 5a***). H700 displayed promising behavior in this respect, showing good oxygen tolerance, even for biosensors with higher glucose sensitivity (***Figure 5b***). These alternative fluorocarbons will be explored more systematically in future investigations.

Acknowledgement

The funds for the development of this device have been provided by subprograma INNCORPORA and FEDER (INC-TU-2011-1621), Ministerio de Industria, Turismo y Comercio (TSI-020100-2011-189 and TSI-020100-2010-346); Ministerio de Ciencia e Investigación (TIN2011-28146).

References

1) McMahon CP, Killoran SJ, O'Neill RD (2005) Design variations of a polymer–enzyme composite biosensor for glucose: Enhanced analyte sensitivity without increased oxygen dependence. *Journal of Electroanalytical Chemistry* **580**: 193–202.

2) Wang J, Lu F (1998) Oxygen-Rich Oxidase Enzyme Electrodes for Operation in Oxygen-Free Solutions. *Journal of American Chemistry Society* **120**: 1048–1050.

3) Dixon BM, Lowry JP, O'Neill RD (2002) Characterization in vitro and in vivo of the oxygen dependence of an enzyme/polymer biosensor for monitoring brain glucose. Journal of Neuroscience Methods **119**: 135–142.

4) Salazar P, O'Neill RD, Martín M, Roche R, González Mora JL (2011) Amperometric glucose microbiosensor based on a Prussian Blue modified carbon fiber electrode for physiological applications. *Sensors and Actuators B* **152**: 137–143.

BIBLIOGRAFÍA

11.- Bibliografía

Abad A, Montoya A. Production of monoclonal antibodies for carbaryl from a hapten preserving the carbamate group. J. Agric. Food Chem. 42 (1994) 1818-1823.

Abbaspour A, Kamyabi MA. Electrochemical formation of Prussian blue films with a single ferricyanide solution on gold electrode.J. Electroanal. Chem. 584 (2005) 117–123.

Anderson JM. Mechanisms of inflammation and infection with implanted devices. Cardiovasc. Pathol. 2 (1993) 33S–41S.

Andreescu S, Magearu V, Lougarre A, Fournier D, Marty JL. Immobilization of enzymes on screen-printed sensors via an histidine tail. Application to the detection of pesticides using modified cholinesterase. Anal. Lett. 34 (2001) 529–540.

Andreescu S, Marty JL. Twenty years research in cholinesterase biosensors: from basic research to practical applications. Biomol. Eng. 23 (2006) 1-15.

Antiochia R, Gorton L. Development of a carbon nanotube paste electrode osmium polymer-mediated for determination of glucose in alcoholic beverages. Biosens. Bioelectron. 22 (2007) 2611–2617.

Araque A, Parpura V, Sanzgiri RP, Haydon PG. Tripartite synapses: glia, the unacknowledged partner. Trends Neurosci 22 (1999) 208–215.

Arya SK, Datta M, Malhotra BD. Recent advances in cholesterol biosensor. Biosens. Bioelectron. 23 (2008) 1083–1100.

Avshalumov MV, Chen BT, Marshall SP, Peña DM, Rice ME. Glutamate-dependent inhibition of dopamine release in striatum is mediated by a new diffusible messenger, H2O2. J Neurosci. 23 (2003) 2744 –2750.

Baldwin SA, Lienhard GE. Purification and reconstitution of glucose transporter from human erythrocytes. Methods Enzymol. 174 (1989) 39–50.

Ballerstadt R, Schultz JS. A fluorescence affinity hollow fiber sensor for continuous transdermal glucose monitoring. Anal. Chem. 72 (2000) 4185–4192.

Barrett D, Shumake J, Jones D, Gonzalez-Lima F. Metabolic mapping of mouse brain activity after extinction of a conditioned emotional response. J. Neurosci. 23 (2003) 5740–5749.

Bazzu G, Puggioni GM, Dedola, Calia G, Rocchitta G, Migheli R, Desole MS, Lowry JP, O'Neill RD, Serra PA. Real-time monitoring of brain tissue oxygen using a miniaturized biotelemetric device implanted in freely-moving rats Anal. Chem. 81 (2009) 2235-2241.

Benveniste H, Drejer J, Schousboe A, Diemer NH. Regional cerebral glucose phosphorylation and blood flow after insertion of a microdialysis fiber through the dorsal hippocampus in the rat. J. Neurochem. 49 (1987) 729-734.

Benveniste H, Hüttemeier PC. Microdialysis-theory and application. Progr. Neurobiol. 35 (1990) 35 195-215.

Berezhetskyy AL, Sosovska OF, Durrieu C, Chovelon JM, Dzyadevych SV, Tran-Minh C. Alkaline phosphatase conductometric biosensor for heavy-metal ions determination. ITBM-RBM 29 (2008) 136–140.

Bergersen LH. Is lactate food for neurons? Comparison of monocarboxylate transporter subtypes in brain and muscle, Neuroscience 145 (2007) 11-19.

Bermúdez V, Bermúdez F, Arraiz N, Leal E, Linares S, Mengual E, Valdelamar L, Rodríguez M, Seyfi H, Amell A, Carrillo M, Silva C, Acosta A, Añez J, Andara C, Angulo V, Martins G. Biología molecular de los transportadores de glucosa: clasificación, estructura y distribución. AVFT 26 (2007) 76-86.

Bito L, Davson H, Levin E, Murray M, Snider N. The concentrations of free amino acids and other electrolytes in cerebrospinal fluid, in vivo dialysate of brain, and blood plasma of the dog. J. Neurochem. 13 (1966) 1057-1067.

Bliss TM, Sapolsky RM, Interactions among glucose, lactate and adenosine regulate energy substrate utilization in hippocampal cultures, Brain Res. 899 (2001) 134-141.

Bolger FB, Lowry JP. Brain Tissue Oxygen: In Vivo Monitoring with Carbon Paste Electrodes. Sensors 5 (2005) 473-487.

Bondy CA, Lee CY, Zhou J Ontogeny and cellular distribution of brain glucose transporter gene expression. Mol Cell Neurosci 3 (1992) 305–313.

Borland LM, Guoyue S, Yang H, Michael AC. Voltammetric study of extracellular dopamine near microdialysis probes acutely implanted in the striatum of the anesthetized rat. J. Neurosci. Meth. 146 (2005) 149-158.

Bouzier-Sore AK, Merle M, Magistretti PJ, Pellerin L. Feeding active neurons: (re)emergence of a nursing role for astrocytes, J. Physiol. Paris 96 (2002), 273-282.

Bouzier-Sore AK, Voisin P, Canioni P, Magistretti PJ. and L. Pellerin, Lactate is a preferential oxidative energy substrate over glucose for neurons in culture, J. Cerebr. Blood Flow Metab. 23 (2003) 1298–1306.

Bradbury MWB. The blood-brain barrier. Experimental Physiology 78(1993) 453-472.

Breccia JD, Andersson MM, Hatti–Kaul R. The role of poly(ethyleneimine) in stabilization against metal-catalyzed oxidation of proteins: a case study with lactate dehydrogenase. Biochim. Biophys. Acta 1570 (2002) 165–173.

Brooks GA. Lactate production under fully aerobic conditions: the lactate shuttle during rest and exercise. Fed. Proc. 45 (1987) 2924–2929.

Bucur B, Danet AF, Marty JL. Versatile method of cholinesterase immobilization via affinity bonds using concanavalin A applied to the construction of a screen-printed biosensor. Biosens. Bioelectron. 20 (2004) 217–225.

Burmeister JJ, Palmer M, Gerhardt GA.L-lactate measures in brain tissue with ceramic-based multisite microelectrodes. Biosens Bioelectron. 20 (2005) 1772-1779.

Buser HJ, Schwarzenbach D, Petter W. Ludi A. The crystal structure of Prussian Blue: Fe4[Fe(CN)6]3 ×H2O. Inorg. Chem. 16 (1977) 2704–2710.

Cano M, Ávila JL, Mayén M, Mena ML, Pingarrón M, Rodríguez-Amaro R. A new, third generation, PVC/TTF–TCNQ composite amperometric biosensor for glucose determination. J. Electroanal. Chem. 615 (2008) 69-74.

Cao L. Carrier-bound immobilized enzymes—principles, applications and design. Wiley-VCH 2005.

Castillo J, Gáspár S,. Leth S, Niculescu, Mortari A, Bontidean I, Soukharev V, Dorneanu SA, Ryabov AD, Csöregi E. Biosensors for life quality design, development and applications. Sens. Actuators B 102 (2004) 179–194.

Cerdan S, Rodrigues T B, Sierra A, Benito M, Fonseca L L, Fonseca CP, García-Martín M L. The redox switch/redox coupling hypothesis. Neurochem. Int. 48 (2006) 523–530.

Chapman RG, Ostuni E, Liang MN, Meluleni G, Kim E,Yan L, Pier G, Warren HS, Whitesides GM. Polymeric thin films that resist the adsorption of proteins and the adhesion of bacteria. Langmuir 17 (2001) 1225-1233.

Chaubey A, Malhotra BD. Mediated biosensors. Biosens. Bioelectron. 17 (2002) 441-456.

Chaubey A, Pande KK, Singh VS, Malhotra BD. Co-immobilization of lactate oxidase and lactate dehydrogenase on conducting polyaniline films. Anal. Chim. Acta 407 (2000) 97-103.

Cheer JF, Wassum KM, Heien MLAV, Phillips PEM, Wightman RM. Cannabinoids enhance subsecond dopamine release in the Nucleus Accumbens of awake rats. J. Neurosci. 24 (2004) 4393-4400**.**

Chi Q, Dong S. Amperometric biosensors based on the immobilization of oxidases in a Prussian Blue film by electrochemical codeposition. Anal. Chim. Acta 310 (1995) 429–436.

Chiba K, Ohsaka T, Ohnuki Y, Oyama N. Electrochemical preparation of a ladder polymer containing phenazine rings. J Electroanal. Chem. 219 (1987) 117-124.

Chih CP, Roberts EL. Energy substrates for neurons during neural activity: a critical Review of the Astrocyte-Neuron Lactate Shuttle Hypothesis J. Cerebr. Blood Flow Metab. 23 (2003) 1263–1281.

Choeri C, Staines W, Miki T, Seino S, Messier C. Glucose transporter plasticity during memory processing. Neuroscience 130 (2005) 591–600.

Choi HN, Kim MA, Lee W-Y. Amperometric glucose biosensor based on sol–gel derived metal oxide/Nafion composite films. Anal. Chim. Acta 537 (2005) 179–187.

Choi MFM. Progress in enzyme-based biosensors using optical transducers. Microchim. Acta 148 (2004) 107–132.

Chumbimuni-Torres KY, Dai Z, Rubinova N, Xiang Y, Pretsch E, Wang J, Bakker E. Potentiometric biosensing of proteins with ultrasensitive ion-selective microelectrodes and nanoparticle labels. J. Am. Chem. Soc. 128 (2006) 13676-13677.

Chumbimuni-Torres KY, Wang J. Nanoparticle-induced potentiometric biosensing of NADH at copper ion-selective electrodes. Analyst 134 (2009) 1614-1617.

Clark Jr LC, Misrahy G, Fox RP. Chronically implanted polarographic electrodes. J. Appl. Physiol. 13 (1958) 85–91.

Clark LC Jr, Lyons C. Studies of a glassy carbon electrode for brain polarography with observations on the effect of carbonic anhydrase inhibition. Ala. J. Med. Sci. 4 (1965) 353-359.

Clark LC, Lyons C. Electrode system for continuous monitoring in cardiovascular surgery. Ann. N. Y. Acad. Sci. 102 (1962) 29-45.

Clarke DD, Sokoloff L. Circulation and energy metabolism of the brain. (en) Basic neurochemistry:molecular, cellular, and medical aspects, 6th Ed. Lippincott-Raven, Philadelphia (1999) 637–669 .

Colliver TL, Pyott SJ, Achalabun M, Ewing AG. VMAT-Mediated changes in quantal size and vesicular volume. J. Neurosci. 20 (2000) 5276–5282.

Cremer JE, Cunningham VJ, Pardridge WM, Braun LD, Oldendort WH. Kinetic of blood-brain barrier transport of pyruvate, lactate and glucose in the suckling, weaking and adult rats. J. Neurochem. 33 (1979) 439-445.

Cremer JE. Substrate utilization and brain development. J. Cereb. Blood Flow Metab. 2(1982) 394–407.

Delgado JMR, DeFeudis FV, Roth RH, Ryugo OK, Mitruka BM**.** Dialytrode for long term intracerebral perfusion in awake monkeys. Arch. Int. Pharmacodyn. Ther. 198 (1972) 9-21.

Delvaux M, Demoustier-Champagne S. Immobilisation of glucose oxidase within metallic nanotubes arrays for application to enzyme biosensors. Biosens Bioelectron 18 (2003) 943–951.

Demchenko AV, Melnik VG, Starodub NF. Thermal biosensor for detecting nonylphenol in the environment. Ukr. Biokhim. Zh. 79 (2007) 212-215.

Demestre M, Boutelle M, Fillenz M. Stimulated release of lactate in freely moving rats is dependent on the uptake of glutamate. J. Physiol. 499 (1997) 825–32.

Divis C. Ethanol oxidation by an Acetobacter xylinum microbial electrode. Ann. of Microbiol. 126A (1975) 175-186

Dixon BM, Lowry JP, O'Neill RD. Characterization in vitro and in vivo of the oxygen dependence of an enzyme/polymer biosensor for monitoring brain glucose. J.Neurosci. Methods 119 (2002) 135-142.

Doege H, Schürmann A, Bahrenberg G, Brauers A & Joost HG. GLUT8, a novel member of the sugar transport facilitator family with glucose transport activity. Journal of Biological Chemistry 275 (2000) 16275–16280.

D'Orazio P. Biosensors in clinical chemistry - 2011 update. Clin. Chim. Acta 412 (2011) 1749-1761.

D'Orazio P. Biosensors in clinical chemistry. Clin. Chim. Acta 334 (2003) 41-69.

Dostal A, Meyer B, Scholz F, Schroder U, Bond AM, Marken F, Shaw SJ. Electrochemical study of microcrystalline solid Prussian Blue particles mechanically attached to graphite and gold electrodes: electrochemically induced lattice reconstruction. J. Phys. Chem. 99 (1995) 2096–2103.

Duncan, JF, Wrigley, PWR. The electronic structure of the iron atoms in complex iron cyanides. J. Chem. Soc. (1963) 1120–1125.

Dwyer D S, Vannucci S J, Simpson, I A. Expression, regulation and functional role of glucose transporters (GLUTs) in brain. Int. Rev. Neurobiol. 51 (2002) 159–188.

Ellis D, Eckhoff M, Neff VD. Electrochromism in the mixed valence hexacyanides. 1. Voltammetric and spectral studies of the oxidation and reduction of thin films of Prussian Blue. J. Phys. Chem. 85 (1981)1225–1231.

Farrell CL, Pardridge WM. Blood–brain barrier glucose transporter is asymmetrically distributed on brain capillary endothelial lumenal and ablumenal membranes: an electron microscopic immunogold study. Proc. Natl. Acad. Sci. USA 88 (1991) 5779–5783.

Feldman BJ, Murray RW. Electron diffusion in wet and dry Prussian Blue films on interdigitated array electrodes. Inorg. Chem. 26 (1987) 1702–1708.

Ferreira L, Ramos M, Dordick J, Gil M. Influence of different silica derivatives in the immobilization and stabilization of a Bacillus licheniformis protease (Subtilisin Carlsberg). J. Mol. Catalysis B 21 (2003) 189–199.

Ferri T, Maida S, Poscia A, Santucci R. A Glucose Biosensor Based on Electro-Enzyme Catalyzed Oxidation of Glucose Using a HRP-GOD Layered Assembly. Electroanalysis 13 (2001) 1198-1202.

Fillenz M, Lowry JP.The relation between local cerebral blood flow and extracellular glucose concentration in rat striatum. Exp. Physiol. 83 (1998) 233-238.

Fiorito PA, Córdoba de Torresi I. Optimized multilayer oxalate biosensor. Talanta 62 (2004) 649–654.

Fiorito PA, Córdoba de Torresi SI. Glucose Amperometric Biosensor Based on the Co-immobilization of Glucose Oxidase (GOx) and Ferrocene in Poly(pyrrole) Generated from Ethanol / Water Mixtures. J. Braz. Chem. Soc. 12 (2001) 729-733.

Fox PT, Raichle M, Mintun M, Dence C. Nonoxidative glucose consumption during focal physiologic neuronal activity. Science 241 (1988) 462−464.

Fox PT, Raichle ME. Focal physiological uncoupling of cerebral blood flow and oxidative metabolism during somatosensory stimulation in human subjects. Proc Natl Acad Sci USA 83 (1986) 1140–1144.

Fox SI. Fisiología Humana 7ª ed. McGraw-Hill, Madrid (2004).

Fritzen-García MB, Oliveira IRWZ, Zanetti-Ramos BG, Fatibello-Filho O, Soldi V, Pasa AA, et al. Carbon paste electrode modified with pine kernel peroxidase immobilized on pegylated polyurethane nanoparticles. Sens. Actuators B 139 (2009) 570–575.

Frost M, Meyerhoff ME. In Vivo Chemical Sensors: Tackling Biocompatibility Anal. Chem. 78 (2006) 7371-7377.

Fumero B, Guadalupe T, Valladares F, Mora F, O'Neill RD, Mas M, González-Mora JL. Fixed versus removable microdialysis probes for in vivo neurochemical analysis: implications for behavioral studies. J. Neurochem. 63 (1994) 1407–1415.

Gallardo-Soto AM, Jaffari SA, Bone S. Characterisation and optimisation of AC conductimetric biosensors. Biosens. Bioelectron. 16 (2001) 23-29.

García-Jareño A, Navarro-Laboulais J, Vicente F. Electrochemical study of Nafion membranes/Prussian Blue films on ITO electrodes. Electrochim. Acta 41 (1996) 2675–2682.

García-Jareño JJ, Sanmatias A, Navarro-Laboulais J, Vicente F. The role of potassium and hydrogen ions in the Prussian Blue–Everitt's salt process. Electrochim. Acta 44 (1998) 395–405.

Garguilo M. Amperometric microsensors for monitoring choline in the extracellular fluid of brain. J. Neurosci. Methods 70 (1996) 73–82.

Garjonyte R, Malinauskas A. Amperometric glucose biosensor based on glucose oxidase immobilized in poly(o-phenylenediamine) layer. Sens. Actuators B 56 (1999a) 85-92.

Garjonyte R, Malinauskas A. Amperometric glucose biosensors based on Prussian Blue and polyaniline glucose oxidase modified electrodes. Biosens. Bioelectron. 15 (2000b) 445–451.

Garjonyte R, Malinauskas A. Glucose biosensor based on glucose oxidase immobilized in electropolymerized polypyrrole and poly(*o*-phenylenediammine) films on a Prussian Blue-modified electrode. Sens. Actuators B 63 (2000a) 122–128.

Garjonyte R, Malinauskas A. Operational stability of amperometric hydrogen peroxide sensors, based on ferrous and copper hexacyanoferrates. Sens. Actuators B 56 (1999b) 93–97.

Garjonyte R, Yigzaw Y, Meskys R, Malinauskas A, Gorton L. Prussian-Blue and lactate oxidase-based amperometric biosensor for lactic acid. Sens. Actuators B 79 (2001) 33–38.

Garnett MC. Gene-delivery systems using cationic polymers**.** Crit. Rev. Ther. Drug Carr. Syst. 16 (1999) 147-207.

Gerhardt GA, Oke AF, Nagy G, Moghaddam B, Adams RN. Nafion-coated electrodes with high selectivity for CNS electrochemistry. Brain Research 290 (1984) 390-395.

Gifford R, Batchelor MM, Lee Y, Gokulrangan G, Meyerhoff ME, Wilson GSJ. Mediation of in vivo glucose sensor inflammatory response via nitric oxide release Biomed. Mater. Res. 75A (2005) 755-766.

Giménez-Romero D, Agrisuelas J, García-Jareño JJ, Gregori J, Gabrielli C, Perrot H, Vicente F. Electromechanical Phase Transition in Hexacyanometallate Nanostructure (Prussian Blue) J. Am. Chem,. Soc. 129 (2007) 7121-7126.

Godet C, Boujtita M, El Murr N. Direct electron transfer involving a large protein: glucose oxidase. New J. Chem. 23 (1999) 795-797.

Gogol EV, Evtugyn GA, Marty JL, Budnikov HC, Winter VG. Amperometric biosensors based on nafion coated screen-printed electrodes for the determination of cholinesterase inhibitors. Talanta (53) 2000 379–389.

Gonon FG, Fombarlet CM, Buda MJ, Pujol JF. Electrochemical treatment of pyrolytic carbon fiber electrodes. Anal. Chem. 53 (1981) 1386–1389.

González-Mora JL, Guadalupe T, Fumero Blas, Mas M. Mathematical resolution of mixed in vivo voltammetry signals. Models, algorithm, equipment, assessment by simultaneous microdialysis sampling. J. Neurosci. Methods 39 (1991) 231-244.

González-Mora JL, Guadalupe T, Mas M. In vivo voltammetry study of the modulatory action of prolactin on the mesolimbic dopaminergic system. Brain Res. Bull. 25 (1990) 729–733.

González-Mora JL, Maidment NT, Guadalupe T, Mas M. Postmortem dopamine dynamics assessed by voltammetry and microdialysis. Brain Res. Bull. 23 (1989) 323–327.

González-Mora JL, Sánchez-Bruno JA, Mas M. Concurrent on-line analysis of striatal ascorbate, dopamine and dihydroxyphenylacetic acid concentrations by in vivo voltammetry. Neuroscience Letters.86 (1988) 61-66.

Goodman JC, Valadka AB, Gopinath SP, Cormio M, Robertson CS. Lactate and excitatory amino acids measured by microdialysis are decreased by pentobarbital coma in head-injured patients. J. Neurotrauma 13 (1996) 549–556.

Grieshaber D, MacKenzie R, Vörös J, Reimhult E. Electrochemical Biosensors - Sensor Principles and Architectures. Sensors 8 (2008) 1400-1458.

Guadalupe T, González-Mora JL, Fumero B, MAs M. Voltammetric monitoring of brain extracellular levels of serotonin, 5-hydroxyindoleacetic acid and uric acid as assessed by simultaneous microdialysis. J. Neurosci. Methods 45 (1992) 59-64.

Guan JG, Miao YQ, Chen JR. Prussian Blue modified amperometric FIA biosensor: one step immunoassay for α-fetoprotein. Biosens. Bioelectron. 19 (2004) 789–794.

Guerrieri A, Lattanzio V, Palmisano F, Zambonin P. Electrosynthesized poly(pyrrole)/ poly(2-naphthol) bilayer membrane as an effective anti-interference layer for simultaneous determination of acethylcholine and choline by a dual electrode amperometric biosensor. Biosens. Bioelectron. 21 (2006) 1710–1718.

Guilbault G., Lubrano G. An enzyme electrode for the amperometric determination of glucose Anal. Chim. Acta 64 (1973) 439-455.

Guyton AC, Hall JE. Tratado de fisiología médica 12ª Ed. Elsevier, Barcelona (2011).

Habermüller K, Mosbach M, Schuhmann W. Electron-transfer mechanisms in amperometric biosensors. Fresenius J. Anal. Chem. 366 (2000) 560–568.

Haghighi B, Varma S, Alizadeh ShFM, Yigzaw Y, Gorton L. Prussian Blue modified glassy carbon electrodes-study on operational stability and its application as a sucrose biosensor. Talanta 64 (2004) 3–12.

Haljamae H. Lactate metabolism. Intens. Care World 4 (1987) 118–121.

Hamai M, Minokoshi Y, Shimazu T. L-Glutamate and insulin enhance glycogen synthesis in cultured astrocytes from the rat brain through different intracellular mechanisms. J. Neurochem. 73 (1999) 400–407.

Harik SI, Kalaria RN, Andersson L, Lundahl P, Perry G. Immunocytochemical localization of the erythroid glucose transporter: abundance in tissues with barrier functions. J. Neurosci. 10 (1990) 3862–72.

Hashimoto T, Hussien R, Cho HS, Kaufer D, Brooks GA. Evidence for the mitochondrial lactate oxidation complex in rat neurons: demonstration of an essential component of brain lactate shuttles. PLoS One 3 (2008) 1-8.

Hermanson GT, Mallia AK, Smith PK. Immobilized affinity ligand techniques. San Diego: Academic Press 1992.

Herren F, Fisher P, Ludi A, Halg W. Neutron diffraction study of Prussian Blue, Fe4[Fe(CN)6]3 ×H2O. Location of water molecules and long-range magnetic order. Inorg. Chem. 19 (1980) 956–959.

Hertz L, Fillenz M, Does the mystery of the extra glucose during CNS activation reflect glutamate synthesis? Neurochem. Int. 34 (1999) 71-75.

Hu YB, Wilson GS. A temporary local energy pool coupled to neuronal activity: fluctuations of extracellular lactate levels in rat brain monitored with rapid-response enzyme-based sensor. J. Neurochem. 69 (1997) 1484−1490.

Itaya K, Akahoshi H, Toshima S. Electrochemistry of Prussian Blue modified electrodes: an electrochemical preparation method. J. Electrochem. Soc. 129 (1982a) 1498–1500.

Itaya K, Ataka T, Toshima S, Shinohara T. Electrochemistry of Prussian Blue. An in situ Moessabauer effect measurement. J. Phys. Chem. 86 (1982c) 2415–2418.

Itaya K, Ataka T, Toshima S. Spectroelectrochemistry and electrochemical preparation method of Prussian Blue modified electrodes. J. Am. Chem. Soc. 104 (1982b) 4767–4772.

Itaya K, Shoj N, Uchida I, Catalysis of the reduction of molecular oxygen to water at Prussian Blue modified electrodes. J. Am. Chem. Soc. 106 (1984a) 3423–3429.

Itaya K, Uchida I, Neff VD. Electrochemistry of polynuclear transition metal cyanides: Prussian Blue and its analogues. Acc. Chem. Res. 19(1986) 162–168.

Itaya K, Uchida, I, Toshima, S, De la Rue RM. Photoelectrochemical studies of Prussian Blue on n-type semiconductor (N-TiO2). J. Electrochem. Soc. (1984b) 131, 2086–2092.

Jiang W, Yuan R, Chai YQ, Yin B. Amperometric immunosensor based on multiwalled carbon nanotubes/Prussian blue/nanogold-modified electrode for determination of α-fetoprotein. Anal Biochem. 407(2010) 65-71.

Joost HG, Bell GI, Best JD, Birnbaum MJ, Charron MJ, Chen YT, Doege H, James DE, Lodish HF, Moley KH, Moley JF, Mueckler M, Rogers S, Schurmann A, Seino S, Thorens B. Nomenclature of the GLUT/SLC2A family of sugar/polyol transport facilitators. Am J Physiol Endocrinol Metab 282(2002) 974–976.

Joost HG, Thorens B . The extended GLUT-family of sugar/polyol transport facilitators: nomenclature, sequence characteristics, and potential function of its novel members. Molecular Membrane Biology 18 (2001) 247–256.

Karyakin AA Karyakina EE. Prussian Blue-based "artificial peroxidase" as a transducer for hydrogen peroxide detection. Application to Biosensors. Sens. Actuators B 57 (1999) 268–273.

Karyakin AA, Chaplin M. Polypyrrole Prussian Blue films with controlled level of doping: codeposition of polypyrrole and Prussian Blue. J. Electroanal. Chem. 56(1994) 85–92.

Karyakin AA, Gitelmacher OV, Karyakina EE. Prussian Bluebased first-generation biosensor. A sensitive amperometric electrode for glucose. Anal. Chem. 67 (1995) 2419–2423.

Karyakin AA, Karyakina EE, Gorton L. Amperometric biosensor for glutamate using Prussian Blue-based 'artificial peroxidase' as a transducer for hydrogen peroxide. Anal. Chem. 72 (2000) 1720–1723.

Karyakin AA, Karyakina EE, Gorton L. Prussian-Blue based amperometric biosensors in flow-injection analysis. Talanta 43 (1996) 1597–1606.

Karyakin AA, Karyakina EE, Gorton L. The electrocatalytic activity of Prussian Blue in hydrogen peroxide reduction studied using a wall-jet cell with continuous flow. J. Electroanal. Chem. 456 (1998) 97–104.

Karyakin AA, Kotelnikova EA, Lukachova LV, Karyakina EE, Wang J. Optimal environment for glucose oxidase in perfluorosulfonated ionomer membranes: improvement of first-generation biosensors. Anal Chem. 74 (2002) 1597-1603.

Karyakin AA. Prussian Blue and its analogues: electrochemistry and analytical applications. Electroanalysis 13 (2001) 813–819.

Kasai N, Jimbo Y, Niwa O, Matsue T, Torimitsu K. Real-time multisite observation of glutamate release in rat hippocampal slices. Neurosci. Lett. 304 (2001) 112-116.

Kasai N, Jimbo Y, Torimitsu K. Electrochemical monitoring of glutamate release at multiple positions in a rat hippocampal slice. Anal. Sci. 18 (2002) 1325-1327.

Kaul S, Faiman MD, Lunte CE. Determination of GABA, glutamate, dopamine and carbamathione in brain microdialysis samples by micellar electrokinetic chromatography and laser-induced fluorescence (MEKC-LIF).Anal. Methods 3 (2011) 1514-1520.

Keggin JF, Miles FD. Structures and formulae of the Prussian Blues and related compounds. Nature 137 (1936) 577–578.

Khan AS, Michael AC. Invasive consequences of using micro-electrodes and microdialysis probes in the brain. Tr. Anal. Chem. 22 (2003) 503-508.

Killoran SJ, O'Neill RD. Characterization of permselective coatings electrosynthesized on Pt-Ir from the three phenylenediamine isomers for biosensor applications. Electrochim. Acta 53 (2008) 7303-7312.

Killoran SJ, Rai DK, O'Neill RD. Comparison of phenylenediamine isomers for the synthesis of permselective biosensor polymers for neurochemical analysis. J. Neurochem. 102 (2007) 196-197

Kissinger PT, Hart JB, Adams RN. Voltammetry in brain tissue: a new neurophysiological measurement. Brain Res. 55 (1973) 209-213.

Koncki R, Lenarczuk T, Radomska A, Glab S. Optical biosensors based on Prussian Blue films. Analyst 126 (2001) 1080–1085.

Koncki, R. Chemical sensors and biosensors based on Prussian Blues. Crit. Rev. Anal. Chem. 32 (2002) 79–96.

Kong T, Chen Y, Ye Y, Zhang K,Wang Z,Wang X. An amperometric glucose biosensor based on the immobilization of glucose oxidase on the ZnO nanotubes. Sens. Actuators B Chem. 138 (2009) 344–350.

Kozminski KD, Gutman DA, Davila V, Sulzer D, Ewing AG. Voltammetric and pharmacological characterization of dopamine release from single exocytotic events at rat pheochromocytoma (PC12) cells. Anal. Chem. 70 (1998) 3123–3130.

Kraft A. On the discovery and history of Prussian Blue. Bull. Hist. Chem. 33 (2008) 61-67.

Kreutz C, Lorgen J, Graewe B, Bargon J, Yoshida M, Fresco ZM, Frechet JMJ. High frequency quartz micro balances: a promising path to enhanced sensitivity of gravimetric sensors. Sensors 6 (2006) 335-340.

Kulagina NV, Shankar L, Michael AC. Monitoring glutamate and ascorbate in the extracellular space of brain tissue with electrochemical microsensors. Anal. Chem. 71 (1999) 5093-5100.

Kulys J, Laurinavicius V, Pesliakiene M, Gureviciene V. Metabolite determination in foodstuffs by enzyme analyzers. Biotechnol. Appl. Biochem. 11 (1989) 149-154.

Lammers F, Scheper T. Thermal biosensors in biotechnology. Adv. Biochem. Eng. Biotechnol. 64 (1999) 35-67.

Langer JJ, Filipiak M, Kecinska J, Jasnowska J, Wlodarczak J, Buladowski B. Polyaniline biosensor for choline determination. Surf. Sci. 573 (2004) 140–145.

Larrabee MG. Lactate metabolism and its effects on glucose metabolism in an excised neural tissue. J. Neurochem. 64 (1995) 1734−1741.

Lehninger AL, Nelson DL, Cox MM. Lehninger principles of biochemistry. New York: W.H. Freeman (2005).

Lemire J, Mailloux RJ, Appanna VD Mitochondrial Lactate Dehydrogenase Is Involved in Oxidative-Energy Metabolism in Human Astrocytoma Cells (CCF-STTG1). PLoS One 3 (2008) 1-10.

Leypoldt JK, Gough DA. Model of a two-substrate enzyme electrode for glucose, Anal. Chem. 56 (1984) 2896–2904.

Li G, Wang Y, Xu H. A Hydrogen Peroxide Sensor Prepared by Electropolymerization of Pyrrole Based on Screen Printed Carbon Paste Electrodes. Sensors 7 (2007) 239–250.

Li J, Peng T, Peng Y. A cholesterol biosensor based on entrapment of cholesterol oxidase in a silicic sol-gel matrix at a Prussian Blue modified elctrode. Electroanalysis 15 (2003) 1031–1037.

Li L, Qinglin Sheng Q, Zheng J, Zhang H. Facile and controllable preparation of glucose biosensor based on Prussian blue nanoparticles hybrid composites. Bioelectrochemistry 74 (2008) 170-175.

Li XG, Huang MR, Duan W. Novel multifunctional polymers from aromatic diamines by oxidative polymerizations. Chem. Rev. 102 (2002) 2925–3030.

Liu H, Yu R, Peng K, Zhao H, Li L, Wu X.A Signal-Amplified Electrochemical Immunosensor Based on Prussian Blue and Pt Hollow Nanospheres as Matrix. Electroanalysis 22 (2010) 2577 – 2586

Liu SN, Yin YJ, Cai CX. Immobilization and characterization of glucose oxidase on single-walled carbon nanotubes and its application to sensing glucose. Chin. J. Chem. 25 (2007) 439–447.

Loaiza A, Porras OH, Barros LF. Glutamate triggers rapid glucose transport stimulation in astrocytes as evidenced by realtime confocal microscopy. J. Neurosci. 23 (2003) 7337–7342.

Loaiza OA, Campuzano S, Guzmán-Vázquez de Prada A, Pedrero M, Pingarrón JM. Amperometric DNA quantification based on the use of peroxidase-mercaptopropionic acid-modified gold electrodes. Sens. Actuators B 132 (2008) 250-257

Loaiza OA, Campuzano S, Pedrero M, Pingarrón JM. DNA sensor based on an Escherichia coli lac Z gene probe immobilization at self-assembled monolayers-modified gold electrodes Talanta 73 (2007) 838-844.

Lönnroth P, Jansson PA, Smith U. A microdialysis method allowing characterization of intercellular water space in humans. Am. J. Physiol. 253 (1987) 228–231.

López MA, Ortega F. Domínguez E, Katakis I. Electrochemical immunosensor for the detection of atrazine. J. Mol. Recogn. 11 (1998) 178-181.

López MA, Ortega F. Inmunosensores: herramientas analíticas con un gran potencial de futuro. Schironia 1 (2002) 52-60.

López-Bayghen E, Ortega A. Células gliales y actividad sináptica: control traduccional del acople metabólico. Rev. Neurol. 50 (2010) 607-615.

López-Bayghen E, Rosas S, Castelán F, Ortega A. Cerebellar Bergmann glia: an important model to study neuron-glia interactions. Neuron Glia Biol. 3 (2007) 155-167.

Louilot A, González-Mora JL, Guadalupe T, Mas M. Sex-related olfatory stimuli induce a selective increase in dopamine release in the nucleus accumbens of male rats. a voltammetric study. Brain Res. 553(1991) 313-317.

Lowe AG, Walmsley AR. The kinetics of glucose transport in human red blood cells. Biochim. Biophys. Acta 857 (1986)146–54.

Lowry JP, Boutelle MG, O'Neill RD, Fillenz M. Characterization of carbon paste electrodes in vitro for simultaneous amperometric measurement of changes in oxygen and ascorbic acid concentrations in vivo. Analyst 121 (1996) 761-766.

Lowry JP, Demestre M, Fillenz M. Relation between cerebral blood flow and extracellular glucose in rat striatum during mild hypoxia and hyperoxia. Dev. Neurosci. 20 (1998) 52-58.

Ludi A, Gudel HU. Structural chemistry of polynuclear transition metal cyanides. Struct. Bond. 14 (1973) 1–22.

Lukachova LV, Kotel'nikova EA, D'Ottavi D, Shkerin EA, Karyakina EE, Moscone D, Palleschi G, Curulli A, Karyakin AA. Electrosynthesis of poly-*o*-diaminobenzene on the Prussian Blue modified electrodes for improvement of hydrogen peroxide transducer characteristics. Bioelectrochemistry 55 (2002) 145–148.

Lukachova LV, Kotel'nikova EA, D'Ottavi D, Shkerin EA, Karyakina EE, Moscone D, Palleschi G, Curulli A, Karyakin AA. Nonconducting polymers on Prussian Blue modified electrodes: improvement of selectivity and stability of the advanced H2O2 transducer. IEE Sens. J. 3 (2003) 326–332.

Luo P, Liu Y, Xie GM, Xiong XL, Deng SX, Song FZ. Determination of serum alcohol using a disposable biosensor. Forensic. Sci. Int. 179 (2008) 192–198.

Magistretti PJ, Pellerin L, Rothman DL, Shulman RG. Energy on demand. Science 283 (1999b) 496–497.

Magistretti PJ, Pellerin L. Cellular bases of brain energy metabolism and their relevance to functional brain imaging: evidence for a prominent role of astrocytes. Cereb. Cortex 6 (1996) 50–61.

Magistretti PJ, Pellerin L. Cellular mechanisms of brain energy metabolism and their relevance to functional brain imaging. Philos. Trans. R. Soc. Lond. B Biol. Sci. 354 (1999a) 1155–1163.

Magner E. Trends in electrochemical biosensors. Analyst 123 (1998) 1967–1970.

Maher F, Davies-Hill TM, Simpson IA. Substrate specificity and kinetic parameters of GLUT3 in rat cerebellar granule neurons. Biochem J 315 (1996) 827–31.

Maher F, Simpson IA. The GLUT3 glucose transporter is the predominant isoform in primary cultured neurons: assessment by biosynthetic and photoaffinity labelling. Biochem. J. 301(1994) 379–384.

Maher F, Vannucci SJ, Simpson IA. Glucose transporter isoforms in brain: absence of GLUT3 from the blood-brain barrier. J Cereb Blood Flow Metab 13(1993)342–345.

Malinski T, Taha Z. Nitric oxide release from a single cell measured in situ by a porphyrinic-based microsensor. Nature 358 (1992) 676-678.

Manclús JJ, Abad A, Lebedev MY, Mojarrad F, Micková B, Mercader JV, Primo J, Miranda MA, Montoya A. Development of a monoclonal immunoassay selective for chlorinated cyclodiene insecticides. J. Agric. Food Chem. 52 (2004) 2776-2784.

Mansouri S, Schultz JS. A miniature optical glucose sensor based on affinity binding. Biotechnology 2 (1984) 885–890.

Mao F, Mano N, Heller A. Long tethers binding redox centers to polymer backbones enhances electron transport in enzyme "wiring" hydrogels. J. Am. Chem. Soc. 125 (2003) 4951-4957.

Marcus RA, Sutin N. Electron transfers in chemistry and biology Biochim. Biophys. Acta 811 (1985)265–322.

Marcus RA. Electron Transfer Reactions in Chemistry: Theory and Experiment (Nobel Lecture). Angew. Chem. Int. Ed. English 32 (1993) 1111–1121.

Martínez-Paredes G, González-García MB, Costa-García A. Genosensor for detection of four pneumoniae bacteria using gold nanostructured screen-printed carbon electrodes as transducers. Sens. Actuators B 149 (2010) 329-335.

Marvin JS, Hellinga HW. Engineering biosensors by introducing fluorescent allosteric signal transducers: construction of a novel glucose sensor. J. Am. Chem. Soc. 120 (1998) 7–11.

Mas M, Fumero B, González-Mora JL. Voltammetric and microdialysis monitoring of brain monoamine neurotransmitter release during sociosexual interactions. Behav. Brain Res. 71 (1995b) 69-79.

Mas M, Fumero B, O'Neil RD, González-Mora JL. Fixed versus removable microdialysis cannulae for in vivo neurochemical analysis: implications for behavioral studies. J. Neurochem. 64 (1995a) 1899-1900.

Mas M, González-Mora JL, Louilot A, Solé C, Guadalupe T. Increased dopamine release in the nucleus accumbens of copulating male rats as evidenced by in vivo voltammetry. Neurosci. Lett.110 (1990) 303-308.

Mas M, González-Mora JL, Sanchez-Bruno A. Numerical methods for the analysis of in vivo voltammetry signals. J. Neurosci. Meth. 29 (1989) 303.

Mason MJ. Determination of glucose, sucrose, lactose, and ethanol in foods and beverages, using immobilized enzyme electrodes. Assoc. Anal. Chem. 66 (1988) 981-984.

Mateo C, Palomo JM, Fernandez-Lorente G, Guisan JM, Fernandez-Lafuente R. Improvement of enzyme activity, stability and selectivity via immobilization techniques. Enzyme Microb. Technol. 40 (2007) 1451–63.

Mathebe NGR, Morrin A, Iwuoha EI. Electrochemistry and scanning electron microscopy of polyaniline/peroxidase-based biosensor. Talanta 64 (2004) 115–120.

Mathews CK, van Holde KE, Ahern KG. Biochemistry (3 ed.) Prentice Hall (1999).

Mazeikiene R, Malinauskas A. The stability of poly(o-phenylenediamine) as an electrode material. Synth. Met. 128 (2002) 121–125.

McKenna M.C., Gruetter R., Sonnewald U., Waagepetersen H.S., Schousboe A. Energy Metabolism of the Brain (en) Basic Neurochemistry: Molecular, cellular and medical aspects, 7ª ed., Elsevier Academic Press. (2006) 531-557.

McMahon C P, Rocchitta G, Kirwan S M, Killoran SJ, Serra PA, Lowry JP, O'Neill RD. Oxygen tolerance of an implantable polymer/enzyme composite glutamate biosensor displaying polycation-enhanced substrate sensitivity. Biosens. Bioelectron. 22 (2007) 466-1473.

McMahon CP, Killoran SJ, O'Neill RD. Design variations of a polymer-enzyme composite biosensor for glucose: Enhanced analyte sensitivity without increased oxygen dependence. J. Electroanal. Chem. 580 (2005) 193-202.

McMahon CP, O'Neill RD. Polymer-enzyme composite biosensor with high glutamate sensitivity and low oxygen dependence. Anal. Chem. 77 (2005)1196-1199.

McMahon CP, Rocchitta G, Serra PA, Kirwan SM, Lowry JP, O'Neill RD. Control of the oxygen dependence of an implantable polymer/enzyme composite biosensor for glutamate. Anal. Chem. 78 (2006) 2352-2359.

McNay EC, McCarty RC, Gold PE. Fluctuations in brain glucose concentration during behavioral testing: dissociations between brain areas and between brain and blood, Neurobiol. Learn. Mem. 75 (2001) 325–337.

Medina, J. M. The role of lactate as an energy substrate for the brain during the early neonatal period. Biol. Neonate 48 (1985) 237–244.

Mehrvar M, Abdi M. Recent developments, characteristics, and potential applications of electrochemical biosensors. Anal. Sci. 20 (2004) 1113–1126.

Minteer SD. Enzyme stabilization and immobilization: methods and protocols. Methods in molecular biology. Humana Press 2011.

Mitala M. Improving the performance of electrochemical microsensors based on enzymes entrapped in a redox hydrogel. Anal.Chim. Acta 556 (2006) 326–332.

Mortimer RJ, Rosseinsky DR. Electrochemical polychromicity in iron hexacyanoferrate films, and a new film form of ferric ferricyanide. J. Electroanal. Chem. 151 (1983) 133–147.

Mortimer RJ, Rosseinsky DR. Iron hexacyanoferrate films: spectroelectrochemical distinction and electrodeposition sequence of "soluble" (K+-containing) and "insoluble" (K+-free) Prussian Blue, and composition changes in polyelectrochromic switching. J. Chem. Soc. Dalton Trans. (1984) 2059–2062.

Moscone D, D'Ottavi D, Compagnon, D, Palleschi G, Amine A. Construction and analytical characterization of Prussian Blue based carbon paste electrodes and their assembly as oxidase enzyme sensors. Anal. Chem. 73 (2001) 2529–2535.

Moscone D, Mascini M. Microdialysis and glucose biosensor for in vivo monitoring.Ann. Biol. Clin. 50 (1992) 323-327.

Moussy F, Harrison DJ, O'Brien DW, Rajotte RV. Performance of subcutaneously implanted needle-type glucose sensors employing a novel trilayer coating. Anal. Chem. 65 (1993) 2072-2077.

Murr R, Berger S, Schürer L, Peter K, Baethmann A. A novel, remote-controlled suspension device for brain tissue pO2 measurements with multiwire surface electrodes. Pflugers Arch. 426 (1994) 348-350.

Nagamatsu S, Sawa H, Kamada K, Nakamichi Y, Yoshimoto K, Hoshino T Neuron-specific glucose transporter (NSGT): CNS distribution of GLUT3 rat glucose transporter (RGT3) in rat central neurons. FEBS Lett. 334 (1993) 289–295.

Nair PK, Buerk DG, Halsey JH. Comparisons of oxygen metabolism and tissue pO2 in cortex and hippocampus of gerbil brain. Stroke 18 (1987) 616-622

Neff VD. Electrochemical oxidation and reduction of thin films of Prussian Blue. J. Electrochem. Soc. 125 (1978) 886–887.

Nehlig A. Brain uptake and metabolism of ketone bodies in animal models. Prostaglandins Leukot. Essent. Fatty Acids 70 (2004) 265–275.

Odaci D, Telefoncu A, Timur S. Pyranose oxidase biosensor based on carbon nanotube (CNT)-modified carbon paste electrodes. Sens. Actuators B 132 (2008) 159–165.

Oh BK, Robbines ME, Nablo BJ, Schoenfisch MH. Miniaturized glucose biosensor modified with a nitric oxide-releasing xerogel microarray. Biosen. Bioelectron. 21 (2005) 749-757.

Ohzuku T, Sawai K, Hurai T. On a homogeneous electrochemical reaction of Prussian Blue/Everitt's salt system. J. Electrochem. Soc. 132 (1985) 2828–2834.

Oldenziel WH, Dijkstra G, Cremers TIFH, Westerink BHC. In vivo monitoring of extracellular glutamate in the brain with a microsensor. Brain Res. 118 (2006) 34-42.

Oldenziel WH, Zeyden van der M, Dijkstra G, Ghijsen WEJM, Karst H, Cremers TIFH, Westerink BHC. Monitoring extracellular glutamate in hippocampal slices with a microsensor. J. Neurosci. Meth. 160 (2007) 37–44.

O'Neill RD, Fillenz M, Albery WJ, Goddard NJ.The monitoring of ascorbate and monoamine transmitter metabolites in the striatum of unanaesthetised rats using microprocessor-based voltammetry. Neuroscience 9 (1983) 87-93.

O'Neill RD, Fillenz M. Detection of homovanillic acid in vivo using microcomputer-controlled voltammetry: simultaneous monitoring of rat motor activity and striatal dopamine release. Neuroscience. 14 (1985) 753-63.

O'Neill RD, González-Mora JL, Boutelle MG, Ormonde DE, Lowry JP, Duff A, Fumero B, Fillenz M, Mas M. Anomalously high concentrations of brain extracellular uric acid detected with chronically implanted probes: implications for in vivo sampling techniques. J. Neurochem. 57 (1991) 22–29.

O'Neill RD, Grunewald RA, Fillenz M, Albery WJ. Linear sweep voltammetry with carbon paste electrodes in the rat striatum. Neuroscience 7 (1982) 1945-1954.

O'Neill RD, Lowry JP, Mas M. Monitoring brain chemistry in vivo: voltammetric techniques, sensors and behavioral applications. Crit. Rev. Neurobiol. 12 (1998) 69-127.

O'Neill RD, Lowry JP, Rocchitta G, McMahon CP, Serra PA, Designing sensitive and selective polymer/enzyme composite biosensors for brain monitoring in vivo, Trends Anal. Chem. 27 (2008) 78–88.

O'Neill RD. Uric acid levels and dopamine transmission in rat striatum: diurnal changes and effects of drugs. Brain Res. 507 (1990) 267-272.

Ortiz M, Torréns M, Alakulppi N, Strömbom L, Fragoso A, O'Sullivan CK. Amperometric supramolecular genosensor self-assembled on cyclodextrin-modified surfaces Electrochem. Commun. 13 (2011) 578-581.

Palmisano F, Zambonin PG, Centonze D. Amperometric biosensors based on electrosynthesised polymeric films. Fres. J. Anal. Chem. 366 (2000) 586-601.

Paxinos G, Watson C, The Rat Brain in Stereotaxic Coordinates, Academic Press, Sydney 1986.

Pei J, Tian F, Thundat T. Glucose biosensor based on the microcantilever. Anal. Chem. 76 (2004) 292–297.

Pellerin L, Magistretti PJ. Sweet sixteen for ANLS. J Cereb Blood Flow Metab. (2011) doi:10.1038/jcbfm.2011.149

Pellerin L, Magistretti PJ. Glutamate uptake into astrocytes stimulates aerobic glycolysis: a mechanism coupling neuronal activity to glucose utilization. Proc. Nat. Acad. Sci. USA 91 (1994) 10625−10629**.**

Pellerin L, Magistretti PJ. Glutamate uptake stimulates Na+/K+-ATPase activity in astrocytes via activation of a distinct subunit highly sensitive to ouabain. J. Neurochem. 69(1997) 2132–2137.

Pellerin L, Pellegri G, Bittar PG, Charnay Y, Bouras C, Martin JL, Stella N, Magistretti PJ. Evidence supporting the existence of an activity-dependent astrocyte-neuron lactate shuttle. Dev. Neurosci. 20 (1998) 291–299.

Pellerin L. How Astrocytes Feed Hungry Neurons. Molecular Neurobiology 32 (2005) 59-72.

Pellerin L. Lactate as a pivotal element in neuron-glia metabolic cooperation. Neurochem. Int. 43 (2003) 331-338.

Pérez Escoda MT. Diseño y síntesis de péptidos para el diagnóstico de la infección por virus de la hepatitis G (GBV-C/HGV). Universidad de Barcelona, Facultad de Farmacia, tesis doctoral (2007).

Pickup JC, Hussain F, Evans ND, Rolinski OJ, Birch D. Fluorescence-based glucose sensors. Biosens. Bioelectron. 20 (2005) 2555–2565.

Pohanka M, Pavlis O, Skladal P. Diagnosis of tularemia using piezoelectric biosensor technology. Talanta 71 (2007) 981-985.

Pohanka M, Skladal P. Piezoelectric immunosensor for Francisella tularensis detection using immunoglobulin M in a limiting dilution. Anal. Lett. 2005, 38, 411-422.

Poitry-Yamate CL, Poitry S, Tsacopoulos M. Lactate released by Muller glial cells is metabolized by photoreceptors from mammalian retina. J. Neurosci. 15 (1995) 5179−5191.

Ponchon JL, Cespuglio R, Gonon F, Jouvet M, Pujol JF. Normal pulse polarography with carbon fiber electrodes for in vitro and in vivo determination of catecholamines. Anal. Chem. 51 (1979) 1483-1486.

Porras OH, Loaiza A, Barros LF. Glutamate mediates acute glucose transport inhibition in hippocampal neurons. J. Neurosci. 24 (2004) 9669–9673.

Pothos EN, Larsen KE, Krantz DE, Liu Y, Haycock JW, Setlik W, Gershon MD, Edwards RH, Sulzer D. Synaptic vesicle transporter expression regulates vesicle phenotype and quantal size. J Neurosci 20 (2000) 7297–7306.

Prodromidis MI, Karayannis MI. Enzyme Based Amperometric Biosensors for Food Analysis. Electroanal. 14 (2002) 241-261.

Puig-Lleixa C, Jimenez C, Bartroli J. Acrylated polyurethane Ð photopolymeric membrane for amperometric glucose biosensor construction. Sens. Actuators B 72 (2001) 56–62.

Qian JM, Suo AL, Yao Y, Jina ZH. Polyelectrolyte-stabilized glucose biosensor based on woodceramics as electrodeClin. Biochem. 37 (2004) 155–161.

Quinn CA, Connor RE, Heller A. Biocompatible, glucose-permeable hydrogel for in situ coating of implantable biosensors. Biomaterials 18 *(*1997) 1665-1670.

Rajan KP, Neff VD. Electrochromism in the mixed valence hexacyanides. 2. Kinetics of the reduction of Ruthenium Purple and Prussian Blue. J. Phys. Chem. 86 (1982) 4361–4368.

Ramanathan K, Rank M, Svitel J, Dzgoev A, Danielsson B. The development and applications of thermal biosensors for bioprocess monitoring. Trends Biotechnol. 17 (1999) 499-505.

Ramírez BG, Rodrigues T B, Violante I R, Cruz F, Fonseca L L, Ballesteros P, Castro MM, García-Martín ML, Cerdán S. Kinetic properties of the redox switch/redox coupling mechanism as determined in primary cultures of cortical neurons and astrocytes from rat brain. J. Neurosci. Res. 85 (2007) 3244–3253.

Ramos M, del Arco A, Pardo B, Martínez-Serrano AM, Martínez-Morales JR, Kobayashi K, Yasuda T, Bogónez E, Bovolenta P, Saheki T, Satrústegui J. Developmental changes in the Ca2+-regulated mitochondrial aspartate-glutamate carrier aralar1 in brain and prominent expression in the spinal cord. Dev. Brain Res. 143(2003) 33–46.

Ramsay G. Commercial Biosensors: Applications to clinical, bioprocess, and environmental samples. (Ed. Ramsay G.) New York: John Willey& Sons, 1998.

Rayner DV, Thomas ME, Trayhurn P. Glucose transporters (GLUTs 1–4) and their mRNAs in regions of the rat brain: insulin-sensitive transporter expression in the cerebellum. Canadian Journal of Physiology and Pharmacology 72 (1994) 476–479.

Reichert WM, Sharkawy AA. Handbook of Biomaterials Evaluation: Scientific, Technical, and Clinical Testing of Implant Materials vol. 28. Taylor and Francis, Philadelphia, (1999) 439–460.

Ricci F, Amine A, Palleschi G, Moscone D. Prussian Blue based screen printed biosensors with improved characteristics of long-term lifetime and pH stability. Biosens. Bioelectron. 18 (2003*a*) 165–174.

Ricci F, Amine A, Tuta CS, Ciucu AA, Lucarelli F, Palleschi G, Moscone D. Prussian Blue and enzyme bulk modified screen printed electrodes for hydrogen peroxide and glucose determination with improved storage and operational stability. Anal. Chim. Acta 485 (2003*b*) 111–120.

Ricci F, Caprio F, Poscia A, Valgimigli F, Messeri D, Lepori E, Dall'Oglio G, Palleschi G, Moscone D. Toward continuous glucose monitoring with planar modified biosensors and microdialysis. Study of temperature, oxygen dependence and in vivo experiment. Biosens Bioelectron. 22 (2007) 2032-2039.

Ricci F, Goncalves C, Amine A, Gorton L, Palleschi G, Moscone D. Electroanalytical study of Prussian Blue modified glassy carbon paste electrodes. Electroanalysis 15 (14) (2003c) 1204–1211.

Ricci F, Palleschi G. Sensor and biosensor preparation, optimisation and applications of Prussian Blue modified electrodes. Biosen. Bioelectron. 21 (2005) 389–407.

Roach PC, Ramsden DK, Hughes J, Williams P. Development of a conductimetric biosensor using immobilised Rhodococcus ruber whole cells for the detection and quantification of acrylonitrile. Biosens Bioelectron. 19 (2003) 73-78.

Robin, MB, Day P. Mixed valence chemistry—a survey and classification. (en) Emelus HJ, Sharpe AG (Eds.): Advances in Inorganic Chemistry and Radiochemistry Academic Press, New York 10 (1967) 247–422.

Robinson DL, Venton B J, Heien MLAV, Wightman RM. Detecting subsecond dopamine release with fast-scan cyclic voltammetry in vivo." Clin. Chem. 49 (2003) 1763-1773.

Rodrigues TB, López-Larrubia P, Cerdán S. Redox dependence and compartmentation of [13C] pyruvate in the brain of deuterated rats bearing implanted C6 gliomas J. Neurochem. 109 (2009) 237–245.

Rothwell S.A. and O'Neill R.D. Effects of applied potential on the mass of non-conducting poly(ortho-phenylenediamine) electro-deposited on EQCM electrodes: comparison with biosensor selectivity parameters. Phys. Chem. Chem. Phy. 13 (2011) 5413-5421.

Rothwell SA, Killoran SJ, Neville EM, Crotty AM, O'Neill RD. Poly(o-phenylenediamine) electrosynthesized in the absence of added background electrolyte provides a new permselectivity benchmark for biosensor applications. Electrochem.Commun. 10 (2008) 1078-1081.

Rothwell SA, Kinsella ME, Zain ZM, Serra PA, Rocchitta G, Lowry JP, O'Neill RD. Contributions by a novel edge effect to the permselectivity of an electrosynthesized polymer for microbiosensor applications. Anal. Chem. 81 (2009) 3911-3918.

Rothwell SA, McMahon CP, O'Neill RD. Effects of polymerization potential on the permselectivity of poly(o-phenylenediamine) coatings deposited on Pt-Ir electrodes for biosensor applications. Electrochim. Acta 55 (2010) 1051-1060.

Rubianes MD, Rivas GA. Carbon nanotubes paste electrodes. Electrochem. Commun. 5 (2003) 689–694.

Russell RJ, Pischko MV, Gefrides GC, McShane MJ, Coté GL. A fluorescence-based glucose biosensor using concanavalin A and dextran encapsulated in a poly(ethylene glycol) hydrogel. Anal. Chem. 71 (1999) 3126–3132.

Ruzgas T, Csöregi E, Emneus J, Gorton L, Marko-Varga G. Peroxidase-modified electrodes: Fundamentals and application. Anal. Chim. Acta 330 (1996) 123-138.

Ryabov AD, Amon A, Gorbatova RK, Ryabova ES, Gnedenko BB. Mechanism of a "jumping off" ferricenium in glucose oxidase-d-glucose-ferrocene micellar electrochemical systems. J.Phys. Chem. 99 (1995) 14072–14077.

Ryabova ES, Goral VN, Csöregi E, Matthiasson B, Ryabov AD. Coordinative approach to mediate electron transfer: ruthenium complexed to native glucose oxidase. Angew. Chem. Int. Ed. Engl. 38 (1999) 38 804-807.

Sassolas A, Blum LJ, Leca-Bouvier BD. Immobilization strategies to develop enzymatic biosensors. Biotechnol. Adv. 30 (2012) 489–511

Schuhmann W, Wohlschläger H, Lammert R, Schmidt HL, Löffler U, Wiemhöfer AD, Göpel W. Pyrrole, a new possibility for covalent binding of oxidoreductases to electrode surfaces as a base for stable biosensors. Sens. Actuators B 1 (1990) 537-541.

Schurr A, Miller JJ, Payne RS, Rigor BM. An increase in lactate output by brain tissue serves to meet the energy needs of glutamate-activated neurons. J. Neurosci. 19 (1999) 34−39.

Schurr A, Payne RS, Miller JJ, Rigor BM. Brain lactate, not glucose, fuels the recovery of synaptic function from hypoxia upon reoxygenation: an in vitro study. Brain Res. 744 (1997a) 105–111.

Schurr A, Payne RS. Lactate, not pyruvate, is neuronal aerobic glycolysis end product: an in vitro electrophysiological study. Neuroscience 147 (2007) 613–619.

Schurr A, Payne, RS, Miller JJ, Rigor BM,. Glia are the main source of lactate utilized by neurons for recovery of function post-hypoxia. Brain Res. 774 (1997b) 221–224.

Schurr A. Lactate: the ultimate cerebral oxidative energy substrate? J Cereb. Blood Flow Metab. 26(2006) 142–152.

Senthil Kumar SM, K. Chandrasekara Pillai K. Cetyltrimethyl ammonium bromide surfactant-assisted morphological and electrochemical changes in electrochemically prepared nanoclustered iron(III) hexacyanoferrate J. Electroanal. Chem. 589 (2006*b*) 167-175.

Senthil Kumar SM, K. Chandrasekara Pillai K. Compositional changes in unusually stabilized Prussian blue by CTAB surfactant: Application to electrocatalytic reduction of H2O2. Electrochem. Commun. 8 (2006*a*) 621-626.

Serrá MR, Díaz J, de Sande ML. Fisioterapia en neurología, sistema respiratorio y aparato cardiovascular. Elsevier, Barcelona (2005).

Shao Z, Li Y, Yang Q, Wang J, Li G. A novel electrochemical method to detect cell surface carbohydrates and target cells. Anal. Bioana.l Chem. 398 7-8 (2010) 2963–2967.

Sharp T, Maidment NT, Brazell M, Zetterstrom T, Bennett GW, Ungerstedt U, Mardsden CA. Parallel changes in voltammetric oxidation peaks and extracellular monoamine metabolites in rat striatum in vivo. Neurosci. Lett. Suppl. 14 (1983) 340.

Shin JH, Marxer HSM, Schoenfisch MH. Nitric oxide-releasing sol-gel particle/polyurethane glucose biosensor. Anal. Chem. 76 (2004) 4543-4549.

Shram NF, Netchiporouk LI, Martelet C, Jaffrezic–Renault N, Bonnet C, Cespuglio R. In vivo voltammetric detection of rat brain l-lactate with carbon fiber microelectrodes coated with l-lactate oxidase. Anal. Chem. 70 (1998) 2618–2622.

Siesjo BK. Utilisation of substrates by brain tissues. (*en*) Brain energy metabolism. New York: Wiley (1978) 101−130.

Simpson IA, Carruthers A, Vannucci SJ. Supply and demand in cerebral energy metabolism: the role of nutrient transporters. J. Cerebr. Blood F. Met. 27 (2007) 1766–1791.

Skladal P. Piezoelectric quartz crystal sensors applied for bioanalytical assays and characterization of affinity interactions. J. Braz. Chem. Soc. 14 (2003) 491-502.

Sokoloff L, Reivich M, Kennedy C, Des Rosiers MH, Patlak CS, Pettigrew KD, Sakurada O, Shinohara M. The [14C]deoxyglucose method for the measurement of local cerebral glucose utilization: theory, procedure, and normal values in the conscious and anesthetized albino rat. J. Neurochem. 28 (1977**)** 897–916.

Sokoloff L. Metabolism of the central nervous system in vivo. *(en)* Handbook of Physiology. Section 1 Neurophysiology. Williams and Wilkins, Washington DC. vol. 3 (1960) 1843–1864.

Steinkuhl R, Sundermeier C, Hinkers H, Dumschat C, Cammann K, Knoll M. Microdialysis system for continuous glucose monitoring. Sens. Actuators B 33 (1996) 19-24.

Stilwell D, Park, KH, Miles MH. Electrochemical studies of the factors influencing the cycle stability of Prussian Blue films. J. Appl. Electrochem. 22 (1992) 325–331.

Stuber GD, Roitman MF, Phillips PE, Carelli RM, Wightman RM. Rapid dopamine signaling in the nucleus accumbens during contingent and noncontingent cocaine administration. Neuropsychopharmacol. 30 (2005b) 853–863.

Stuber GD, Wightman RM, Carelli RM. Extinction of cocaine self-administration reveals functionally and temporally distinct dopaminergic signals in the nucleus accumbens. Neuron. 46 (2005a) 661–669.

Tabernero A, Vicario C, Medina JM. Lactate spares glucose as a metabolic fuel in neurons and astrocytes from primary culture. Neurosci. Res. 26 (1996) 369–376.

Takahashi S, Driscoll BF, Law MJ, Sokoloff L. Role of sodium and potassium ions in regulation of glucose metabolism in cultured astroglia. Proc. Natl. Acad. Sci. U.S.A. 92 (1995) 4616–4620.

Thévenot DR, Toth K, Durst RA, Wilson GS. Electrochemical Biosensors: Recommended Definitions and Classification. Biosens. Bioelectron. 16 (2001) 121–131.

Thévenot DR, Toth K, Durst RA, Wilson GS. Electrochemical Biosensors: Recommended Definitions and Classification. Pure Appl. Chem. 71 (1999) 2333-2348.

Tseng TF, Yang YL, Chuang MC, Lou SL, Galik M, Flechsig GU, Wang J. Thermally Stable Improved First-Generation Glucose Biosensors based on Nafion/Glucose-Oxidase Modified Heated Electrodes. Electrochem commun. 11 (2009)1819-1822.

Ungerstedt U, Pycock C. Functional correlates of dopamine neurotransmission. Bull. Schweiz Akad. Med. Wis., 30 (1974) 44-55.

Ungerstedt U. Microdialysis: principles and applications for studies in animals and man. J. Int. Med. 230 (1991) 365-373.

Updike SJ and Hicks GP. The enzyme electrode. Nature 214 (1967) 986-988.

Vannucci S J, Simpson I A. Developmental switch in brain nutrient transporter expression in the rat. Am. J. Physiol. Endocrinol. Metab. 285(2003) E1127–E1134.

Vannucci SJ, Clark RR, Koehler-Stec E, Li K, Smith CB, Davies P, Maher F, Simpson IA Glucose transporter expression in brain: relationship to cerebral glucose utilization. Dev Neurosci 20 (1998) 369 –379.

Vannucci SJ, Maher F, Simpson IA Glucose transporter proteins in brain: delivery of glucose to neurons and glia. Glia 21 (1997) 2–21.

Vidal JC, Espuelas J, García-Ruiz E, Castillo JR. Amperometric cholesterol biosensors based on the elctropolymerisation of pyrrole and the electrocatalytic effect of Prussian-Blue layers helped with self-assembled monolayers. Biosens. Bioelectron. 64 (2004) 655–664.

Vittal R, Gomathi H, Kim KJ. Beneficial role of surfactants in electrochemistry and in the modification of electrodes Adv. Colloid. Interfac. 119 (2006) 55.

Vittal R, Gomathi H, Prabhakara Rao G. Influence of a cationic surfactant on the modification of electrodes with nickel hexacyanoferrate surface films. Electrochim. Acta 45 (2000) 2083.

Vittal R, Gomathi H, Prabhakara Rao H. Derivatised nickel and cobalt oxide modified electrodes: effect of surfactant. J. Electroanal. Chem. 497 (2001) 47-54.

Vittal R, Jayalakshm M, Gomathi H, Prabhakara Rao G. J. Surfactant promoted enhancement in electrochemical and electrochromic properties of films of Prussian Blue and its analogs. Electrochem. Soc. 146 (1999) 786-793.

Vittal R, Kim KJ, Gomathi H, Yegnaraman V. CTAB-promoted Prussian Blue-modified electrode and its cation transport characteristics for K+, Na+, Li+, and NH4+ ions. J. Phys. Chem. B 112 (2008) 1149-1156.

Wang G, Zhang G, Huang H, Wang L. Graphene-Prussian blue/gold nanoparticles based electrochemical immunoassay of carcinoembryonic antigen. Anal. Methods 3 (2011), 2082-2087

Wang J, Chen L, Chatrathi MP. Evaluation of different fluorocarbon oils for their internal oxygen supply in glucose microsensors operated under oxygen-deficit conditions Anal. Chim. Acta 411 (2000a) 187–192.

Wang J, Chen L, Hocevar SB, Ogorevc B. One-step electropolymeric co-immobilization of glucose oxidase and heparin for amperometric biosensing of glucose. Analyst 125 (2000b) 125, 1431-1434.

Wang J, Li S, Moa JW, Porter J, Musameh MM, Dasgupta PK. Oxygen-independent poly(dimethylsiloxane)-based carbon-paste glucose biosensors .Biosens. Bioelectron. 17 (2002) 999–1003.

Wang J, Lu F. Oxygen-Rich Oxidase Enzyme Electrodes for Operation in Oxygen-Free Solutions. J. Am. Chem. Soc. 120 (1998) 1048–1050.

Wang J, Mo JW, Li S, Porter J. Comparison of oxygen-rich and mediator-based glucose-oxidase carbon-paste electrodes. Anal. Chim. Acta 441 (2001) 183–189.

Wang J, Wang L, Di J, Tu Y. Electrodeposition of gold nanoparticles on indium/tin oxide electrode for fabrication of a disposable hydrogen peroxide biosensor. Talanta 77 (2009) 1454–1459.

Wang J. Analytical Electrochemistry (2 ed.) John Wiley & Sons (2000c).

Wang J. Electrochemical Glucose Biosensors Chem. Rev. 108 (2008) 814-825.

Wang J. Glucose biosensors: 40 years of advances and challenges. Electroanal. 13 (2001) 983–988.

Wang Y, Chen Q, Zeng X. Potentiometric biosensor for studying hydroquinone cytotoxicity in vitro. Biosens. Bioelectron. 25 (2010) 1356-1362.

Wightman RM, May LJ, Michael AC.Detection of dopamine dynamics in the brain. Anal. Chem. 60 (1988) 769A–779A.

Williams DF. A model for biocompatibility and its evaluation. J. Biomed. Eng. 11 (1989) 185–191.

Wilson GS, Gifford R. Biosensors for real-time in vivo measurements. Biosens. Bioelectron. 20 (2005) 2388–2403.

Wilson MS. Electrochemical immunosensors for the simultaneous detection of two tumor markers. Anal. Chem. 77 (2005) 1496–1502.

Wood IS, Trayhurn P, Glucose transporters (GLUT and SGLT): expanded families of sugar transport proteins. British Journal of Nutrition 89 (2003) 3–9.

Wu H, Olier R, Jaffrezic-Renault N, Clechet P, Nyamsi A, Martelet C. Covalent immobilization of glucose ocidase onto graphitic electrodes. Electrochimica Acta 39 (1994) 327–331.

Xi F, Gao J, Wang J, Wang Z. Discrimination and detection of bacteria with alabel-freeimpedimetric biosensor based on self-assembled lectin monolayer. J. Electroanal. Chem. 656 (2001) 252-257.

Xiao Y, Patolsky F, Katz E, Hainfeld JF, Willner I. "Plugging into enzymes": Nanowiring of redox enzymes by a gold nanoparticle. Science 299 (2003) 1877-1881.

Xu L, Zhu Y, Tang L, Yang X, Li C. Dendrimer-encapsulated Pt nanoparticles /polyaniline nanofibers for glucose detection. J. Appl. Polym. Sci. 109 (2008) 1802–1807.

Xue Y, Ding L, Lei J, Ju H. A simple electrochemical lectin-probe for in situ homogeneous cytosensing and facile evaluation of cell surface glycan. Biosens. Bioelectron. 26 (2010) 169–174.

Yano J. Electrochemical and structural studies on soluble and conducting polymer from *o*-phenylenediamine. J. Polym Sci. 33 (1995) 2435–2441.

Yáñez-Sedeño P, Pingarrón JM. Microelectrodos: nuevas posibilidades de la Electroquímica analítica. An. R. Soc. Esp. Quím. 4 (2001) 19-28.

Yao T, Yano T. On-line microdialysis assay of l-lactate and pyruvate in vitro and in vivo by a flow-injection system with a dual enzyme electrode. Talanta 63 (2004) 771-775.

Yonemori Y, Takahashi E, Ren H, Hayashi T, Endo H. Biosensor system for continuous glucose monitoring in fish. Anal. Chim. Acta. 633 (2009) 90–96.

Yu J S, Liao H X, Gerdon A E, Huffman B, Scearce RM, McAdams M, Alam SM, Popernack PM, Sullivan NJ, Wright D, Cliffel DE, Nabel GJ, Haynes BF. Detection of Ebola virus envelope using monoclonal and polyclonal antibodies in ELISA, surface plasmon resonance and a quartz crystal microbalance immunosensor. J. Virol. Methods 137 (2006) 219-228.

Zauner A, Bullock R, Di X, Young HF. Brain oxygen, CO2, pH, and temperature monitoring: evaluation in the feline brain. Neurosurgery 37 (1995) 1168-1176.

Zhang J, Luo A, Liu P, Wei S, Wang G, Wei S. Detection of organophosphorus pesticides using potentiometric enzymatic membrane biosensor based on methylcellulose immobilization. Anal. Sci. 25 (2009a) 511-515.

Zhang M, Liu K, Xiang L, Lin Y, Su L, Mao L. Carbon nanotube-modified carbon fiber microelectrodes for in vivo voltammetric measurement of ascorbic acid in rat brain. Anal. Chem. 79 (2007) 6559-6565.

Zhang Z, Xia S, Leonard D, Jaffrezic-Renault N, Zhang J, Bessueille F, Goepfert Y, Wang X, Chen L, Zhu Z, Zhao J, Almeida MG, Silveira CM. A novel nitrite biosensor based on conductometric electrode modified with cytochrome c reductase composite membrane. Biosens. Bioelectron. 24 (2009b) 1574–1579.

Zhou F, Zhu X, Castellani RJ, Stimmelmayr R, Perry G, Smith MA, Drew KL. Hibernation, a model of neuroprotection. Am. J. Pathol. 158 (2001) 2145-2151.